University of Southampton
FACULTY OF PHYSICAL SCIENCES AND ENGINEERING
ELECTRONICS AND COMPUTER SCIENCE

Buffer-Aided Multihop Wireless Communications

by

Chen Dong
BSc. MEng.

A thesis submitted for the degree of
Doctor of Philosophy at the University of Southampton

January 2014

SUPERVISOR: *Professor Lajos Hanzo*
Dipl Ing, M.Sc, Ph.D, FIEEE, FRAEng, FIET, DSc
Chair in Communications, Signal Processing and Control Group
SUPERVISOR: *Professor Lie-Liang Yang*
BEng MEng PhD, SMIEEE, FIET
Communications, Signal Processing and Control Group
School of Electronics and Computer Science
University of Southampton
Southampton SO17 1BJ
United Kingdom

UNIVERSITY OF SOUTHAMPTON

ABSTRACT

Faculty of Physical Sciences and Engineering
School of Electronics and Computer Science

A thesis submitted for the degree of
Doctor of Philosophy at the University of Southampton

Buffer-Aided Multihop Wireless Communications

by Chen Dong

In this thesis, we propose a suite of buffer-aided transmission schemes designed for a multihop link or for a three-node network by exploiting the characteristics of buffer-aided transmissions. Our objective is to improve the end-to-end BER, outage probability, throughput and energy dissipation.

Specifically, we firstly proposed and studied a buffer-aided multihop link (MHL), where all the relay nodes (RNs) are assumed to have buffers for temporarily storing their received packets. Hence, the RNs are operated under the so-called store-and-forward (SF) relaying scheme. As a benefit of storing packets at the RNs, during each time-slot (TS), the best hop having the highest signal-to-noise ratio (SNR) can be activated from the set of those hops that have packets awaiting transmission in the buffer. A packet is then transmitted over the best hop. This hop-selection procedure is reminiscent of selection (SC) diversity, which is referred to here as multi-hop diversity (MHD), when assuming that each hop experiences both propagation pathloss and independent identically distributed (i.i.d) flat Rayleigh fading. In order to make the channel activation practical, a MAC layer implementation is proposed and several closed-form formulas are derived for its characterization.

Then we studied the buffer-aided multihop link, when assuming that each hop experiences both propagation pathloss and independent non-identically distributed (i.n.i.d) flat Nakagami-m fading. Both BPSK as well as M-ary quadrature amplitude modulation (MQAM) are employed. During each TS, the MHD scheme activates the specific hop's transmission, whose signal-to-noise ratio (SNR) cumulative distribution function (CDF) gives the highest ordinate value amongst all the available hops. The next packet is then transmitted over the selected hop. This CDF-aware MHD scheme is suitable for operation in the scenarios, where the different hops may have different length, hence resulting in different average SNRs, and/or experience different types of fading. This MHD scheme is also capable of achieving the maximum attainable diversity gain provided by the independent fading experienced by the different hops.

Then the benefits of adaptive modulation are exploited, where the number of bits transmitted in each TS is affected both by the channel quality and the buffer fullness. During each TS, the criterion used for activating a specific hop is that of transmitting the highest number of bits (packets). When more than one hops are capable of transmitting the same number of bits, the particular hop having the highest channel quality (reliability) is activated. Hence we refer to this regime as the Maximum Throughput Adaptive Rate Transmission (MTART) scheme. Additionally, a new MAC layer protocol is proposed for implementing our MTART management.

Finally, we propose and study a routing scheme, namely the Buffer-aided Opportunistic Routing (BOR) scheme, which combines the benefits both opportunistic routing and MHD transmission. It is conceived for the transmission of information in a Buffer-aided Three-node Network (B3NN) composed of a Source Node (SN), a buffer-aided Relay Node (RN) and a Destination Node (DN). When applying opportunistic routing, each packet is transmitted from SN to DN either directly or indirectly via a RN based on the instantaneous channel quality. When applying MHD transmission, the RN is capable of temporarily storing the received packets, which facilitates transmission over three links, namely the SR, RD and SD links. In this network, the three channels define a 3D channel probability space (CPS), which is divided into four regions representing the activation-region of the three channels and an outage region. Then the instantaneous channel quality values map to a specific point in this 3D channel space. The BOR scheme relies on the position of this point to select the most appropriate channel in the 3D CPS for its transmission.

In comparison to the benchmark schemes considered in the literature, the BER, the OP, throughput and/or energy dissipation of our proposed systems are significantly improved.

Declaration of Authorship

I, **Chen Dong**, declare that the thesis entitled **Buffer-Aided Multihop Wireless Communications** and the work presented in it are my own and has been generated by me as the result of my own original research. I confirm that:

- This work was done wholly or mainly while in candidature for a research degree at this University;
- Where any part of this thesis has previously been submitted for a degree or any other qualification at this University or any other institution, this has been clearly stated;
- Where I have consulted the published work of others, this is always clearly attributed;
- Where I have quoted from the work of others, the source is always given. With the exception of such quotations, this thesis is entirely my own work;
- I have acknowledged all main sources of help;
- Where the thesis is based on work done by myself jointly with others, I have made clear exactly what was done by others and what I have contributed myself;
- Parts of this work have been published.

Signed: .....

Date: .....

Acknowledgements

I would like to express my appreciation to my supervisor Professor Lajos Hanzo for his outstanding supervision and support throughout my research. His constant inspiration, unfailing encouragement and the altitude of research have greatly benefited me. Especially, his diligence, endless energy and inclusion deserve my sincere respect.

Moreover, I wish to thank my second supervisor Prof. Lie-liang Yang for his patient and professional guidance. At the earlier stage of my PhD study, he gave me a basic scope of the research, an analysis-based research method and he guild me to think about the impact of the buffer in wireless communication system. I may not complete this thesis without those with him. I am very grateful for his careful teaching.

I also appreciate the unconditional support from my parents. Both of them are retired and I am the their single child. Day and night, we had telephone chats every other day on average. Apart from my parents, my wife Guanxing Li gave me endless love.

I also appreciate the help from the other staffs of the communication group, Professor Sheng Chen, Dr. Soon Xin Ng, Dr Robert Maunder, Dr El-Hajjar Mohammed and Dr. Rong Zhang, Dr. Jing zuo, Yongkai Huo, Chuan Zhu, Chao Xu, Dr. Li Li, Xin Zuo, Dr. Shaoshi Yang, Tao Wang, Dr. Fucheng Yang, Dr. Dandan Liang, Jiao Feng, K.T.K Cheung, Kadir, Dr. Shuai Wang, Dr. Hong Chen, Dr. Jiayi Zhang and another Dr. JiayiZhang, Dr. Li Wang, Dr. G. Salman, Dr. Liang Li, Dr. Hung Viet Nguyen, Dr. Hoang Anh Ngo, Dr. S. Sugiura, Dr. Du Yang, Dr. Muhammad Fasih Uddin Butt, Dr. Chong Xu, Dr. Xinyi Xu, Dr. Wang Yao, Dr. Lingkun Kong, Prof. Gan Liu, Dr. B. Choi, Prof. Qinghai Yang, Dr. Haiping Huang, Peichang Zhang, Junyi Jiang, Fan Jin, Wenbo Zhang, Wei Liang, Hua Sun, Ning Zheng, Xuan Li, Meng Cheng, Dr. Hui Zhang, Jia Shi, Jie Hu, Y. Halil, Ping Yang, Bo Zhang, Hongming Zhang, A. J. Aljohani, Zunaira Babar, Varghese Antony Thomas, Dr. Jiankang Zhang. Many thanks to all roommates for their help and friendship throughout my PhD study, Di Lin and Rui Zhang, Li Shen and Yunhao Wu, Chenfei Lu, Mu Yang and Chunjia Han, He Song, Jing Zhang, Jiajun Liang and another Jiajun Liang, Qi Zhou, Yuwei Zhang, Junyu Ou, Tao Li. Special thanks to Mr. J. Park for his outstanding language teaching. The financial support of the China-UK Scholarship Council and of ECS are gratefully acknowledged.

Contents

List of Publications

Journal papers

1. **Chen Dong**, Lie-Liang Yang, Lajos Hanzo, "Multi-Hop Diversity Aided Multi-Hop Communications: A Cumulative Distribution Function Aware Approach", *IEEE Transactions on Communications*, IEEE Transactions on Communications, vol.61, pp.4486-4499, Nov. 2013
2. **Chen Dong**, Lie-Liang Yang, Lajos Hanzo, "Performance Analysis of Multihop-Diversity-Aided Multihop Links", *IEEE Transactions on Vehicular Technology*, vol.61, no.6, pp.2504-2516, July 2012
3. **Chen Dong**, Lie-Liang Yang, Lajos Hanzo, "Adaptive Modulation for Multihop Communications Exploiting Multihop Diversity", *Submitted to IEEE Transactions on Wireless Communications*, (Major Revision).
4. **Chen Dong**, Jing Zuo, Lie-Liang Yang, Soon Xin Ng, Lajos Hanzo, "Minimum Average End-to-end Packet Energy Dissipation of a Buffer-Aided Three-Node Network", , (to be submitted).
5. Jing Zuo, **Chen Dong**, Viet Nguyen Hung, Soon Xin Ng, Lie-Liang Yang, Lajos Hanzo, "Energy-Efficient Routing in Ad Hoc Networks Relying on Channel State Information and Limited MAC Retransmissions", *IEEE Transactions on Communications*, , vol.62, no.2, pp.522-535, February 2014.
6. Jia Shi, **Chen Dong**, Lie-Liang Yang, "Performance of Two-Hop Communication Links with Multiple Relay Nodes: Nakagami/Gamma-Aproximation Approaches", *EURASIP Journal on Wireless Communications and Networking*, Accepted.
7. Xiaojie Ju, **Chen Dong**, Lie-Liang Yang, Youguang Zhang, "Intercell Interference Modelling in the Uplink Cellular Networks", *to be submitted.*
8. Jing Zuo, **Chen Dong**, Soon Xin Ng, Lie-Liang Yang, Lajos Hanzo, "Cross-Layer Aided Routing Design for in Ad Hoc Networks", *to be submitted.*
9. Bo Zhang, **Chen Dong**, Jing Lei, Mohammed El-Hajjar, Lie-Liang Yang and Lajos Hanzo, "Buffer-Aided Relaying for Multi-user Uplink: Outage Analysis and Power Allocation", *to be submitted.*
10. Ateeq Ur Rehman, **Chen Dong**, Lie-Liang Yang and Lajos Hanzo, "Performance of cognitive Go-Back-N Hybrid Automatic Repeat reQuest", *to be submitted.*
11. **Chen Dong**, Jing Zuo, Lie-Liang Yang, Soon Xin Ng, Lajos Hanzo, "Survey of Delay-Tolerant Buffer-Aided Wireless Networks", *to be submitted.*

Conference papers

1. **Chen Dong**, Lie-Liang Yang, Lajos Hanzo, "Multihop Diversity for Fading Mitigation in Multihop Wireless Networks", *Proceedings of IEEE Vehicular Technology Conference (VTC) Fall*, 5-8 Sept. 2011.
2. **Chen Dong**, Lie-Liang Yang, Jing Zuo, Soon Xin Ng, Lajos Hanzo, "Maximum Throughput Adaptive Rate Transmission Scheme for Multihop Diversity Aided Multihop Links", *Accepted by ICC 2014*.
3. **Chen Dong**, Jing Zuo, Lie-Liang Yang, Yongkai Huo, Soon Xin Ng, Lajos Hanzo, "Energy-Efficient Buffer-Aided Relaying Relying on Non-Linear Channel Probability Space Division", *Accepted by WCNC 2014*.
4. Jing Zuo, **Chen Dong**, Soon Xin Ng, Lie-Liang Yang, Lajos Hanzo, "Energy-Efficient Routing in Ad Hoc Networks Relying on Channel State Information and Limited MAC Retransmissions", *Proceedings of IEEE Vehicular Technology Conference (VTC) Fall*, 5-8 Sept. 2011.
5. Lie-Liang Yang, **Chen Dong**, Lajos Hanzo, "Multihop Diversity - A Precious Source of Fading Mitigation in Multihop Wireless Networks", *Proceedings of IEEE Global Communications Conference (GLOBECOM)*, 5-9 Dec. December 2011.
6. Peichang Zhang, Sheng Chen, **Chen Dong**, Li Li, Lajos Hanzo, "Norm-Based Joint Transmit/Receive Antenna Selection Aided and Two-Tier Channel Estimation Assisted STSK Systems", *Accepted by ICC 2014*.
7. **Chen Dong**, Jing Zuo, Lie-Liang Yang, Yongkai Huo, Soon Xin Ng, Lajos Hanzo, "Buffer-Aided Opportunistic Routing Design with Linear Channel Probability Space Division for Relay-Aided Networks.", *submitted to VTC-fall 2014*.

List of Symbols

C	Capacity of a specific channel.
C^{cql}	Channel-quality.
$C_{\{\widehat{\boldsymbol{r}}\}}$	Capacity based on an existing transmission state $\{\widehat{\boldsymbol{r}}\}$.
d	Distance between two nodes.
$\boldsymbol{D}$	State distance matrix.
E_b	End-to-end energy per bit.
E_{ffe}	A compensation parameter in channel probability space based nonlinear channel activation.
$\mathcal{E}$	Instantaneous energy dissipation.
$\bar{\mathcal{E}}$	average energy dissipation.
$\boldsymbol{E}$	Constellation-point to constellation-point error matrix.
$E_{SD\{SD\ SR\}}$	Energy dissipation of the SD hop when both the SD and the SR hops are available, etc.
$\mathcal{F}$	A unified expression of probability, energy dissipation and capacity.
$F_{m_l}(\gamma_l)$	SNR CDF ordinate values of the lth hop with Nakagami-m factor m_l.
h	Channel amplitude.
l	A specific hop's index in a multihop link.
L	Total number of hops in a multihop link.
m_l	Nakagami-m factor m_l.
$\boldsymbol{M}$	A matrix storing the intermediate probabilities, when we calculate the PMF of delay.
P_{1TS}^{suc}	The probability of successfully receiving the packet from the source node in the first TS.
$\boldsymbol{p}$	Transmission probability of the constellations.
$\boldsymbol{P_d}$	The PMF of delay.
$P_e(m)$	Exact BER with diversity order m.
$P_{H,ber\{\widehat{\boldsymbol{r}}\}(\gamma)}$	Single-hop BER of the MHLs employing the MTART scheme.

$P_{L,e}$	Lower-bound of the single hop BER.
$P_{L,E}$	Lower-bound of the end-to-end BER.
$P_{L,O}$	Single hop lower-bound of the outage probability.
P_m	Probability of the event that m out of the L hops can transmit.
P_{M_r}	Single-hop BER formula of MQAM/BPSK stream transmitted over an AWGN channel.
P_O	End-to-end lower-bound of the outage probability.
P_{out}	Outage probability.
$P_{out\{\widehat{\boldsymbol{r}}\}}$	Outage probability based on an existing transmissio state $\{\widehat{\boldsymbol{r}}\}$.
$P_{SD\{SD\ SR\}}$	Activation probability of the SD hop, when both the SD and the SR hops are available, etc.
$P_{\{\widehat{\boldsymbol{r}}\}}(\gamma)$	The PDF of the selected channel SNR, when the potential rate of the channels is $\{\widehat{\boldsymbol{r}}\}$.
$P_{\boldsymbol{\pi}}$	Steady-state probabilities of each state.
$Q(x)$	Gaussian Q function.
$\widehat{r_i}$	Potential rate of the ith hop.
$\widehat{\boldsymbol{r}}$	Potential rate of all the hops.
$r^l_{\gamma_i}$	Corresponding transmission rate, when the channel quality of the lth hop is γ_i.
S	Buffer state.
S_i^{cql}	Number of channel-quality levels.
$\boldsymbol{T}$	Buffer transition matrix.
T_{hi}	Threshold of activating the ith channel.
$T_{h\widehat{r_i}}$	Lower boundary of the potential rate region of the ith hop.
$T^l_{h\gamma_i}, T^l_{h\gamma_i \oplus 1}$	Region constrained by these two thresholds, when the channel quality of the lth hop is γ_i.
$x, \boldsymbol{x}$	Transmitted signal.
$y, \boldsymbol{y}$	Received signal.
α	Pathloss exponent.
γ	Channel SNR after selection.
γ_b	Received average SNR per bit.
γ_h	Average SNR per hop.
γ_l	Instantaneous channel SNR for the lth hop.
γ_T, γ_{Th}	Threshold of SNR for different modulation schemes.
σ^2	The variance of noise.
τ	The PMF of delay.
$\bar{\tau}$	The average delay.
$\lvert \bullet \rvert$	The number of logical '1' value in $\lvert \bullet \rvert$.

ΔS	A small square in channel probability space.
$\oplus$	The plus in subscript.
Φ	End-to-end throughput.

Chapter 1

Introduction

1.1 Motivation

The first *ad hoc* networks were conceived by the Defense Advanced Research Project Agency (DARPA) [1] in the 1970s, which motivated further research on decentralized self-organized networks [2]. The most important benefit of ad hoc networks is their distinctively flexible nature.

The discussions in this thesis touch upon three design aspects. The first is the deployment of the nodes and their connectivity, as discussed in Section 1.2. The second aspect is related to the hardware of the nodes in the system, such as the number of antennas, their buffer size, etc. The third aspect is related to the specific transmission scheme, which should be carefully designed based on the above-mentioned other two aspects and it is typically implemented in software. Hence, Chapters 2 to 5 rely on their own hardware assumptions and transmission schemes. In the next section, the connectivity of the nodes is discussed.

1.2 The Structure and the Physical Layer of Ad Hoc Networks

Given the rich literature of ad hoc networks [2,3], it is a challenge to classify the vast plethora of schemes relying on diverse assumptions. Nonetheless, we may propose the simple classification seen in Table 1.1. The associated system models are introduced in this chapter, followed by the corresponding literature.

1.2.1 Direct Transmission

The classic direct transmission is based on the simple system model shown in Fig. 1.1. Let us commence our discourse with a historic perspective on the expressions

Table 1.1: The classification of *ad hoc* networks.

Model	Single/Multi- Source Node (SN) Destination Node (DN)	Figure	Description
Direct	Single	1.1	Only one SN and one DN.
Link	Single	1.2	An L hop link. The data is transmitted from SN to DN via RNs sequentially.
Lattice Network	Single	1.3,1.4	Every node has a fixed hop index.
	Multi	1.5,1.6	
Ad Hoc Network	Single	1.11,1.7	The hop index of each node is unfixed.
	Multi	1.8,1.9,1.10	

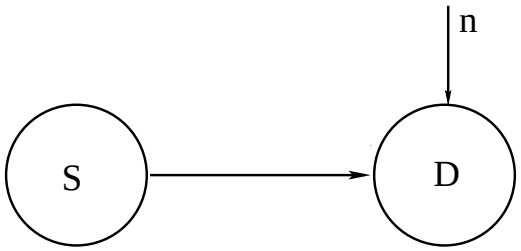

Figure 1.1: General system model of a single-hop wireless link. Transmission takes place from the SN to the DN and n represents noise. The detailed discussions of the figures presented will be portrayed in this section.

of the BER/outage probability in a fading channel. Then, a range of modulation schemes as well as coding and diversity-combining techniques are discussed.

1.2.2 BER and Outage Probability Expressions

In direct transmission, the most important performance metrics are the Bit Error Ratio (BER) and the outage probability (OP). In this section, we only discuss these expressions in the case of single input single output (SISO) systems. The research related to multiple input multiple output (MIMO) schemes will be discussed in the context of the associated diversity combining techniques in Section 1.2.3. In order to highlight the evolution of the BER/OP evaluation techniques, let us look back over the past 20 years. There are two main types of expressions used for BER/OP evaluation, relying on either the triangle function or on series expressions.

The triangle expression was introduced in 1991, when Craig expressed the Q function as an integral of the triangle function $Q(x)=\frac{1}{\pi}\int_0^{\frac{\pi}{2}}\exp(-\frac{x^2}{2sin^2(\Phi)})d\Phi$ [4](9). This expression provided researchers with an alternative choice, when deriving the BER

formulas for fading channels, especially for those convenient cases, when the moment-generating function (MGF) is known. Craig's classic paper is cited in numerous papers and books, such as [5] and [6]. Later, Simon expressed the two-dimensional Gaussian Q function in form of a single-fold integral in [7]. He then also extended his own formulation to the product of up to four Q functions in [8]. As a further advance, Beaulieu explained in [9] that there is no simple expression for the product of a higher number of Gaussian Q functions.

Let us now focus our attention on the family of series-expansion based techniques, such as the Generalized hypergeometric function [10](9.14.1) F, the Meijer-G function [10](9.301) G and the Fox-H function [11] function H. All of them are single-variable functions containing a single-fold infinite series or the sum of single-fold infinite series. Moreover, some papers/books allude to the multi-variable F (Lauricella function, [10](9.19)) and to the multi-variable H function [12], such as [13]. Theoretically, an r-variable H-functions can be expressed as an r-fold infinite series or as the sum of some r-fold infinite series. However, in [14], the G function relying on two variables is calculated as a double-fold complex valued integral. With these mathematical tools in mind, we can now proceed to look at the history of the BER/outage evaluation. At the early stages of development researchers typically considered the Rayleigh fading channel. Based on this assumption, the expression of BER/outage probability of diversity-combining techniques can be obtained in closed-form without relying on the F, G or H functions.

This situation changed with the introduction of the Nakagami-m fading channel. An important milestone was set by Eng and Milstein [15] in 1995, since they found the BER expression for transmission over Nakagami-m fading channels by using the F function where m is either a non-integer parameter [15](A8) or an integer parameter [15](A13). Later, this work was extended to Nakagami-m fading channels combined with lognormal shadowing in [16], where the BER expression involved the Laplace approximation [17] of the F function [10](9.14.1). By the end of the 20th century, Alouini found the BER expressions for transmission over Nakagami-m, Nakagami-n and Nakagami-q channels [5]. The first appearance of the single-variable G- and H-function may be traced back to [18], where the discussions are still based on the classic Rayleigh channel. Later Aalo, Piboongungon and Iskander found the BER expression of the generalized Gamma-distributed channel in [19]. The first generalized BER expressions derived for fading channels relying on the H function can be found in [20,21], albeit there is no journal version of these seminal contributions. In 2006, the authors of [22] provided the performance analysis of digital communications systems for transmission over generalized-K fading channels, based on the channels

characterized in [23]. In 2007, Yacoub modelled the channel either as the summation of numerous zero-mean or non-zero-mean variables in [24], which can be viewed as another interpretation of the family of Nakagami-n and Nakagami-q channels. Later, Di Renzo conceived a unified framework based on the non-central moments of different channels in [25]. In 2010, Di Renzo also derived a formula for linking the MGF and the capacity in [26]. As a further substantial advance, in 2012 Yilmaz and Alouini summarized the features of 24 different types of channels and expressed all of them by a H-function, namely by the Gamma-Shadowed Generalized Nakagami-m Fading channel [27]. In the same paper, Di Renzo's formula linking the MGF and the capacity has been updated for the sake of characterizing both the maximal ratio combining (MRC) and the equal gain combining (EGC) operation of the received signal.

Let us now focus our attention on the approximation of the Gaussian Q-function. Karagiannidis provided a convenient approximation of the Gaussian Q-function in [28]. He then further streamlined the expressions in [29]. Although, the expression in [28](6) is tight, it contains e^{-x}, which is inconvenient for further derivation. Then his discussions were extended to the Marcum-Q function in [29] which is a more generalized function. Although there are numerous papers trying to find a closed-form approximation of the various Q-functions, there is only a single contribution [30], which succeeded in providing a series-based approximation. However, even this paper stopped that of providing a closed-form formula.

Finally, the definition of a closed-form formula is discussed. The original interpretation of a closed-form formula requires an expression without an infinite integral or an infinite summation. Although the F, G and H functions are often considered to be in closed-form in recent research, in reality, they are constituted by infinite series. Another important formula is constituted by $\int_0^{\infty} f(x)dx = \int_0^{\frac{\pi}{2}} f[\arctan(t)]d \cdot \arctan(t)$, which changes the infinite integral to a finite integral as proposed in [31]. Recently, some papers expressed their results based on a single integral as orthogonal polynomial-type series [27, 32]. Although this representation is not in a closed-form, its evaluation is convenient, fast, accurate and hence practical.

1.2.3 Diversity Combining

The family of diversity combining techniques rapidly developed during the last decade of the 20th century. The most important basic combining techniques are selection combining (SC), switch selective combining (SSC), MRC and EGC [33]. Apart from the basic combining techniques [34], a generalized selection combining (GSC) combining technique was also proposed [35]. Finally, the relationship between diversity

Table 1.2: Major contributions on the BER, OP, channel PDFs and the Q function.

Year	Authors	Contribution
1991	Craig [4]	The $Q(x) = \frac{1}{\pi}\int_0^{\frac{\pi}{2}} \exp(-\frac{x^2}{2sin^2(\Phi)})d\Phi$ function is expressed by a finite integral.
1995	Eng and Milstein [15]	The BER over Nakagami-m fading channel is expressed by the F function [10](9.14.1).
1998	Simon [7]	The product of two Q functions is expressed by a single integral.
1999	Alouini and Goldsmith [5]	The BER expression over Nakagami-m, Nakagami-n and Nakagami-q channels is provided.
2001	Huo and Alouini [18]	First applied the G [10](9.301) and H [11] functions in the wireless field.
2002	Simon [8]	The product of upto four Q function is expresseds by a single integral.
2004	Shankar [23]	The generalized-K fading channel is proposed.
2004	Kung, Simon and Biglieri [20, 21]	The generalized fading distribution is expressed by the H-function.
2005	Aalo *et al.* [19]	The BER expression for generalized Gamma channels.
2006	Bithas *et al.* [22]	The BER performance of generalized-K distributed channels.
2007	Yacoub [24]	Proposed $\kappa - \mu$ and $\eta - \mu$ channels.
2007	Karagiannidis [28]	A tight approximation of the Gaussian-Q function.
2009	Di Renzo *et al.* [25]	Non-central moments of different channels.
2010	Di Renzo *et al.* [26]	A formula linking the MGF and capacity.
2011	Farhadi *et al.* [31]	Expressed infinite integral of MGF as a finite integral based on the triangle function.
2011	Ansari *et al.* [14]	The first paper relying on the G or H functions of two variables.
2012	Yilmaz and Alouini [27]	Summarized 24 types of channels and expressed all of them by a H function.
2012	Shi [30]	A tight approximation of the Gaussian-Q function.
2012 2013	Yilmaz and Di Renzo [27, 32]	The results based on a single integral are expressed as orthogonal polynomial-type series.

combining and the achievable capacity was unveiled in [36].

Alouini characterized the BER of both SC and MRC in [37]. Equations (14)-(20) are the most cited aspect of [37]. These equations expressed the product of the incomplete gamma function in closed-form, when m is an integer. Formula (16) of [37] is similar to Hahn's work [38], but more convenient. This formula can also be found in [39]. From 2005 onwards some more generalized channel models surfaced, which were characterized by the Meijer-G function. The authors of [40] derived both the SSC BER and the achievable spectral efficiency for transmission over Generalized Gamma (GG) channels. The MRC, SC, SSC, EGC based BER expressions dervied for Generalized-K channels are studied in [41]. Later, the authors of [42] considered both switch diversity and adaptive modulation. The sum of Gamma-Gamma distributions was found in [43]. The $\eta - \mu$ fading channels exhibiting correlation and relying on MRC were studied in [44]. Apart from these achievements, Chen and Laneman combined the signal at the bit level after a hard-desision in [45], which led to the follow-on paper [46].

In 1995, Eng, Kong and Milstein proposed a so-called Generalized Selection Combining (GSC) technique in [35], where the receiver was capable of accumulating the SNR generated from different channels, until the required threshold was exceeded. The channel model in [35] was the classic Rayleigh fading channel. Then Ma [47] extended the results of [35] to uncorrelated Nakagami-m channels. Later, Mallik and Win extended these results to correlated Nakagami-m channels [48]. Moreover, Karagiannidis, Zogas and Kotsopoulos derived the (PDF) of the SC-aided Multivariate Nakagami-m channel with the aid of Green's matrix approximation in [49]. In 2006, Yang [50] proposed the exact BER formula for GSC. Then Bithas, Sagias and Mathiopoulos extended GSC for transmission over GG channel [51]. Furthermore, the authors of [52] jointly considered GSC, power allocation and adaptive modulation. In 2009, the authors of [53] discussed a correlated Nakagami-m channel, albeit their results were only accurate for MRC. The bivariate generalized-K channel was proposed by Bithas, Sagias and Mathiopoulos in [54], where BER expressions were provided for EGC/MRC. Furthermore, the authors of [55, 56] discussed the distribution of the nth largest variable amongst L random variables and its application in GSC. Additionally, the authors of [57] discussed the GSC in the presence of self-interference. Recently, Beaulieu and Hemachandra [58] extended the results of [48] to scenarios, when the channel was characterized by a correlated channel matrix.

Alouini and Goldsmith also discussed the capacity improvements achieved with the aid of both SC and MRC in [36]. Ten years later, this work was extended to Generalized-Gamma (GG) channel by Bithas [59]. A classic paper related to the

capacity of MIMO systems is [60]. Actually, the capacity that may be achieved for a given channel matrix is determined by the associated eigenvalues. The generalized-Gamma channel-related version of [36] is [59].

1.2.4 Adaptive Modulation and Coding

Hayes proposed the concept of adaptive modulation as early as 1968 [61]. However, it was not until the 1990s that the concept became sufficiently mature for practical exploitation. Webb and Steele [62] conceived the variable rate QAM concept, while Goldsmith and Chua [63] extended it to variable-rate, variable-power (MQAM). Adaptive modulation was also advocated in a cellular system by Qiu and Chawla [64].

The earliest discussions related to arbitrary constellations used in an adaptive modulation context can be found in [65]. However, in practice, either the classic square MQAM or star-QAM [66] may be preferred. Jeong *et al.* [67] then extended the results to (MPSK) communicating in Nakagami-m/Rician channels [68].

Based on the near-instantaneous channel conditions, the system maps the input bits to different modulation and/or coding schemes, hence this regime is referred to as Adaptive Modulation and Coding (AMC). Adaptive modulation aided transmissions over Nakagami-m channels is systematically discussed in the work of Alouini and Goldsmith in [69], while Choi *et al.* [70] characterized adaptive modulation in conjunction with MRC and Space-Time Block Coding (STBC), when communicating over Nakagami-m channels. The achievable throughput was maximized by finding the optimal switching threshold of different modulation schemes.

Although the BER performance achieved without channel coding has been lavishly studied, only a very few papers discussed the achievable performance of packet-by-packet transmissions [71–75]. Liu, Zhou and Giannakis [71] characterized the relationship between the SNR and the Packet Error Ratio (PER) in conjunction with AMC and the High Performance Radio LAN (HIPERLAN/2) standard [76]. Later, the associated queuing effects were taken into account at the data link layer in [72], while Kwon and Cho [73] discussed the SNR-PER relationship of AMC using truncated ARQ. Then the same authors discussed the associated resource allocation in [74]. Ramis and Femenias [75] extended the results of [71] with the aid of ARQ, while Aniba and Aissa [77] jointly considered adaptive modulation, packet combining, ARQ, MIMO and STBC for communicating over Nakgami-m channels.

In 2007, Yang, Belhaj and Alouini combined adaptive modulation with GSC in [78]. Later, Ko *et al.* [79] extended [78] to an adaptive modulation aided system

relying on MRC, while Gjendemsjo *et al.* [80] extended the concept of [78] to an adaptive modulation assisted system using both GSC and power control.

1.2.5 DS-CDMA

In 1995, Eng and Milstein [15] discussed the performance of coherent direct-sequence CDMA (DS-CDMA). Then, Hara and Prasad [81] compared the BER performance, when of DS-CDMA to multicarrier CDMA (MC-CDMA). Later in 2002, Cheng and Beaulieu [82] characterized the exact BER performance communicating in Rayleigh channels while Yang and Hanzo [83] discussed the BER performance of multicarrier DS-CDMA communicating in Nakagami-m channels. Lastly, asynchronous DS-CDMA was considered by Liu and Hanzo [84]. This work was then extended to MC-DS-CDMA by Smida, Hanzo and Affes in [85].

1.2.6 Multihop Link

A multihop link is shown in Fig. 1.2, which consists of a source node (SN), a destination node (DN) and $(L-1)$ relay nodes (RNs). The data is transmitted from the SN to the DN via RNs sequentially. The distance and the fading distribution of the channel between each pair of the adjacent nodes is typically different.

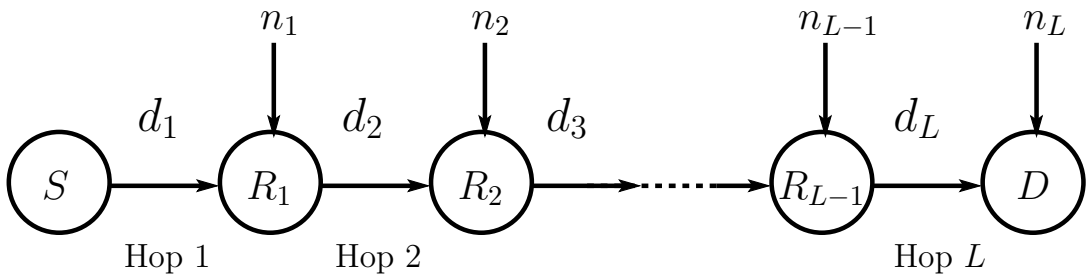

Figure 1.2: System model of a multi-hop wireless link having hops of different length, where the SN sends messages to the DN via $(L-1)$ intermediate RNs.

It is widely known that there are two basic relaying techniques: Decode (Detection)-and-Forward (DF), and Amplify-and-Forward (AF). A challenging problem is to find an equivalent End-to-End (E2E) SNR based on the SNR of each hop. Hasna and Alouini [86] provided one of the most important results in the field of multihop links stating that $1+\frac{1}{\gamma_{eq}} = \prod_{i=1}^{L}(1+\frac{1}{\gamma_i})$ [86](Eq. 2), where γ_i is the instantaneous SNR in the ith hop and γ_{eq} is the E2E equivalent SNR. For the sake of simplicity in some cases, $\gamma_{eq} = \left[\sum_{i=1}^{L}\frac{1}{\gamma_i}\right]^{-1}$ was adopted [86](Eq. 4) which was accurate in the high SNR region. The same authors also published another paper [87] for quantifying the E2E BER, when the E2E MGF were known. They also extended their work to the Nakagami-m channel [88]. The benefits of a low-complexity fixed-gain relay were

studied in [88, 89], while those of power allocation were discussed in [90]. Karagiannidis extended the discussion of the harmonic mean from two hops to L hops in [91], while Waqar *et al.* [92] conceived a unified framework for the ergodic capacity for transmission over generalized fading channels. Afterwards, Trigui *et al.* [93] provided a unified framework for expressing the capacity/BER/outage probability of a SISO multihop link using AF relaying for transmission over generalized fading channels with the aid of the Lauricella functions [10](9.19). Recently, Yilmaz, Tabassum and Alouini [94] analyzed the Higher Order Statistics (HOS) of the channel capacity for a SISO multihop link using AF relaying for transmission over generalized fading channels. The Average Outage Duration (AoD) is obtain with the aid of the MGF of end-to-end SNR and an axuiliary function [94](4).

MIMO-aided relays were widely studied [95–106]. For example, the outage probability of a MIMO-aided relay was investigated in [95]. In [96] it was assumed that both the user and the relay have a single antenna, whilst the base station has multiple antennas. Sulyman *et al.* [97] quantified the capacity of MIMO-aided spatial multiplexing for multi-hop relaying aided single links. The analysis of beamforming provided in [98] was extended to a dual-hop scenario in [99, 100]. The capacity of multihop relaying invoking both adaptive rate and power allocation for transmission over Nakagami-m channels was discussed in [101], which extended the results of [36] to a more complex scenario. A MIMO-assisted Ultra-Wide-Band (UWB) system relying on dual-hop relaying and outdated channel side information (CSI) was analyzed in [102]. Xu and Hua designed transmit-precoding matrices for two-way MIMO-assisted relays in [103]. Meanwhile, Vaze and Heath quantified the capacity of a two-way MIMO relay in [104]. Transmissions over a correlated dual-hop MIMO relay channel, whilst relying on both transmit antenna selection and MRC reception were considered in [105]. This work was extended from Rayleigh channels to Nakagami-m channels in [106].

In general it is difficult to analyze the performance attained with the aid of channel coding. Nonetheless, Lee and Kim analyzed the achievable BER performance of a two-hop scenario in conjunction with orthogonal space-time block code (OSTBC) [107]. Similar investigations can also be found in [108].

The management of buffer control combined with AMC in the Media Access Control (MAC) layer was considered in [109] and [110]. The authors of [111] analyzed the simplest two-hop scenario in terms of several metrics. Specifically, Equation (16) characterized the steady-state probability distribution of the buffer fullness.

Following [13], the authors of [112] considered the realistic scenario of bidirectional

transmissions over Nakagami-m channels. You, Chen and Li [113] included network coding in two-way relaying using the classic DF protocol and characterized the MAC layer.

Mehta *et al.* [114] investigated the benefits of both rateless codes and of buffering at the relay. They considered two hops and M relays. The SN transmitted rateless codes [115], until at least one relay successfully decoded the message.

As a further development, in [116] non-identical Nakagami-m channel were considered for each hop. Finally, Morgado *et al.* [117] characterized the E2E performance, when the performance of every single hop was different, while the routing aspects were considered in [118].

1.2.7 Multihop Lattice Networks with One Source and One Destination

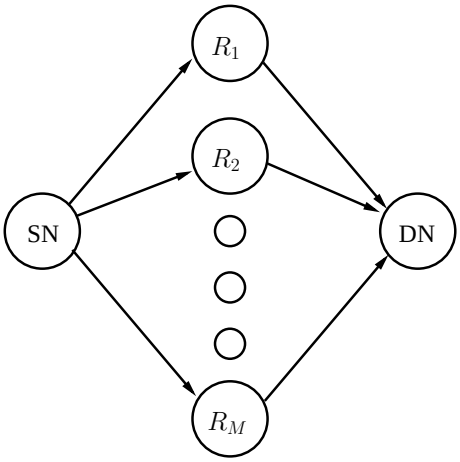

Figure 1.3: System model of a two-hop MHLN, where the SN transmits messages to the DN via M relays.

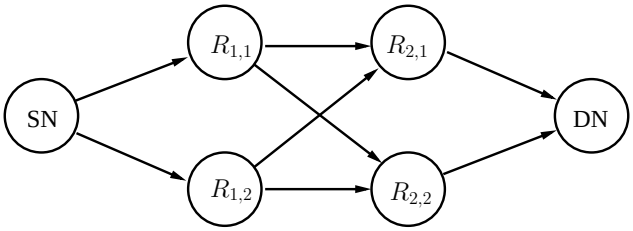

Figure 1.4: System model of a three-hop MHLN, where the SN transmits messages to the DN via two intermediate hops and there are two relay nodes in each hop.

Let us now define the concept of Multihop Lattice Networks (MHLN), where each RN is aware of its own hop index in the route. The packets will be transmitted from a node with hop index l to a node with hop index $(l+1)$ and its transmission from the SN to the DN requires L hops, as shown in Fig. 1.3, regardless of the specific

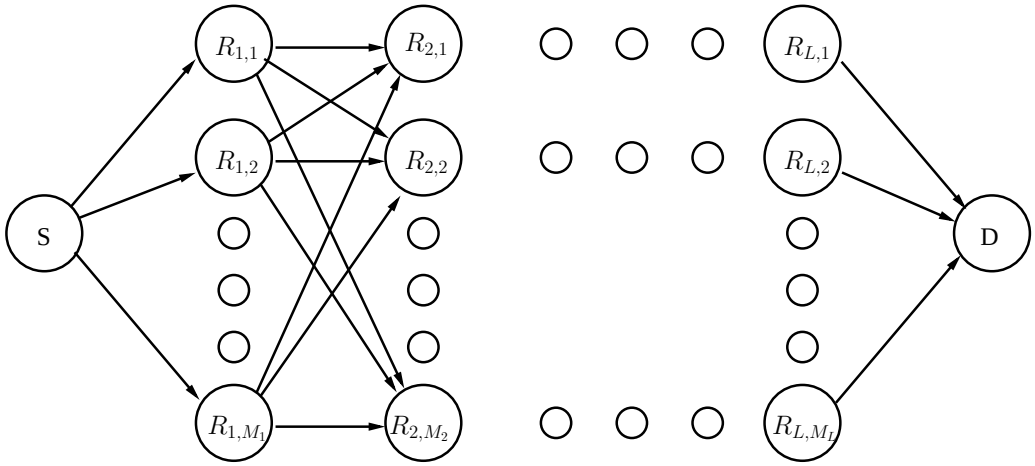

Figure 1.5: System model of a multi-hop lattice network, where the SN transmits messages to the DN via $(L+1)$ intermediate hops and there are M_l nodes in lth hop.

route. In this figure, M relays with hop index one are employed between the SN and DN, hence any packet reaching the DN requires two transmissions.

Another example is shown in Fig. 1.4, which portrays a three-hop MHLN, where the SN sends its messages to the DN via two intermediate hops and there are two RNs in each hop. Finally, Fig. 1.5 portrays the generalized L-hop model relying on M_l relays during the lth hop.

For the simplest case considered in Fig. 1.3, the authors of [119] considered an outage-optimal AF or DF relaying scheme. Gui, Dai and Cimini combined the lattice network model of Fig. 1.5 and the routing techniques in [120], while Wubben [121] characterized lattice networks relying on both power allocation and adaptive modulation. Pan, Ekici and Feng [122] analyzed the Asymptotical Relative Diversity Order (ARDO) and the corresponding performance communicating over log-normal channels. AF relaying-aided lattice networks were considered in [123]. Li *et al.* [124] elaborated on the cooperation of relays having outdated CSI under the assumption that either only outdated CSIs are available or both outdated CSIs and statistical channel information are available. Liu and Kim [125] assumed that there are M relays and two hops associated with outdated CSI, where an AF relaying scheme was used.

Bidirctional relaying was combined with adaptive modulation in [126], while the authors of [127] claimed that their technique of selecting a specific relay was capable of approaching the Mth-order diversity gain with the aid of M relays. Both the authors of [127] of [128] quantified the performance erosion imposed by outdated CSI.

1.2.8 Multihop Lattice Networks with Multiple Sources and Destinations

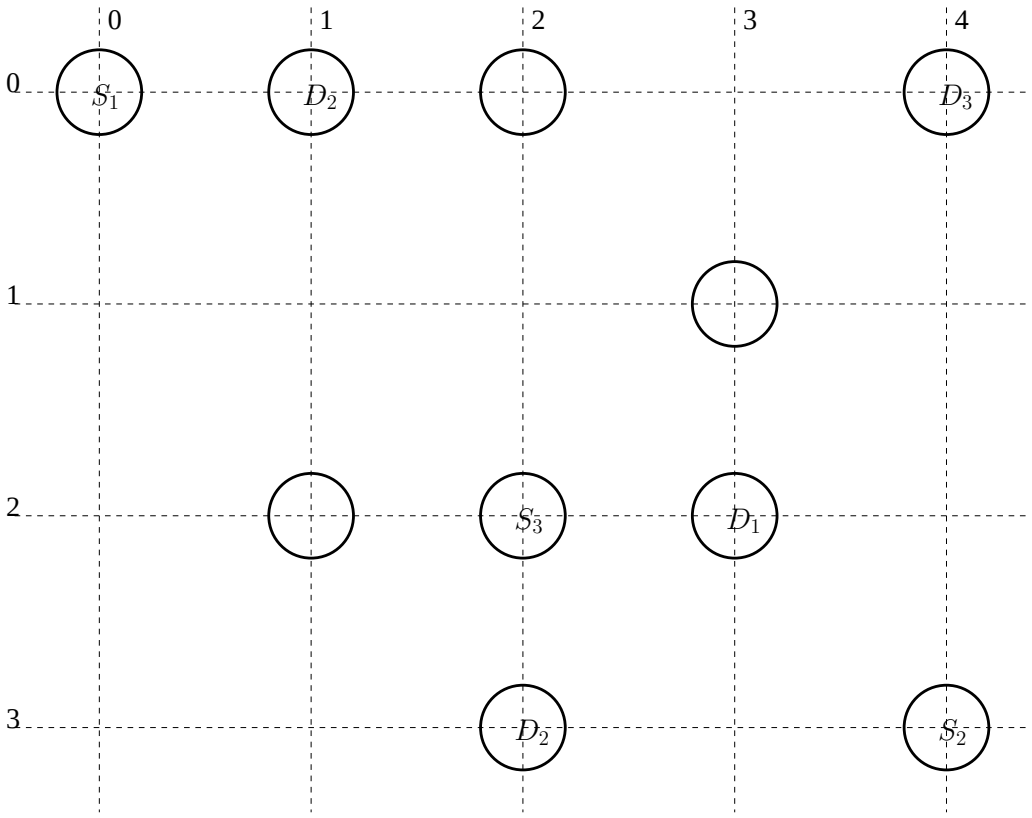

Figure 1.6: System model of a multi-hop lattice networks supporting multiple sources and destinations. The number of SNs may be different from the number of DNs. In this figure, S_1 and S_3 have the corresponding destinations of D_1 and D_3, while S_2 has two destinations, namely D_2 located at either $(0, 1)$ or at $(3, 2)$.

A MHLN may have more than one pair of SNs and DNs. Furthermore, one SN or DN may have more than one corresponding DN or SN. However, the hop index of a relay node associated with a pair of SN-DN is fixed. As an example shown in Fig. 1.6, there are three SNs and four corresponding DNs in this figure. Then the nodes S_i, D_i may act as a RN for the data transmitted from S_j to D_j, when $i \neq j$.

In their seminal contribution, Xie and Kumar [129] discussed multihop lattice networks supporting multiple sources and destinations. Sengupta *et al.* [130] researched a network relying on multiple sources and destinations as well as on network coding.

In classic BS-aided cellular networks, the RNs assist the base station (BS) in communicating with the users. Typically, there is a strong direct link between the BS and the users. Cooperation may occur between two BSs, or between two relays or a relay and a BS. Oyman [131] studied the RN-BS cooperation and the associated spectrum allocation issues in a single cell. As a further advance, Zhang *et al.* [132] analyzed the BER, outage probability and the diversity order of AF, DF as well as

of selective DF. Ding *et al.* [133] investigated a scenario associated with multiple sources and relays transmitting to a single destination. The outage probability was calculated for both AF and DF relaying. Zhang *et al.* [134] conceived a scheduling scheme for multiple sources and relays supporting a single destination. The authors of [135] researched the scenario of a single-BS multi-relay aided multi-user network. Their analysis showed that a diversity order of $(M + N)$ may be achieved with the aid of AF relaying, where M was the number of users and N was the number of relays.

1.2.9 Multihop Networks with One Source and One Destination

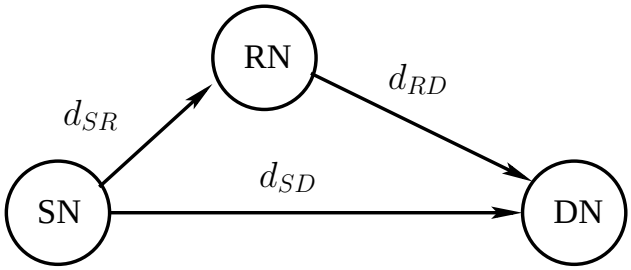

Figure 1.7: A simple three-node model. The source can transmit its data to the destination both directly and via the RN. The distance between the pairs of nodes are d_{SD}, d_{SR}, d_{RD}.

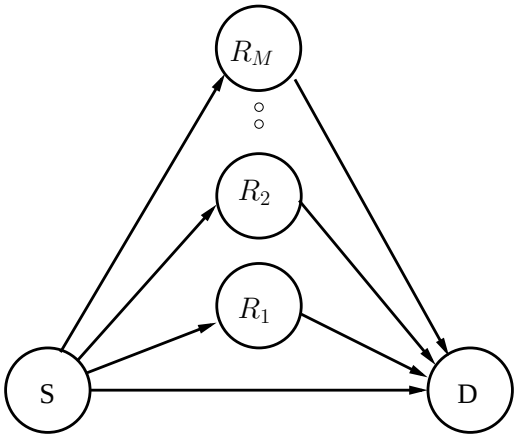

Figure 1.8: System model of an M relay MHN, where the SN sends messages to the DN via M relays or directly. All the relays have the same hop index, which means that the relays cannot communicate with each other.

Multihop networks may be defined on the basis of having at least one node, which has a routing-dependent hop index. This definition leads to two sub-categories. In category 1 only the SN has a routing-dependent hop index. In most practical case, it is assumed that the SN is capable of directly communicating with the DN, as shown in both Fig. 1.7 and Fig. 1.8. In Category 2 at least one RN has a routing

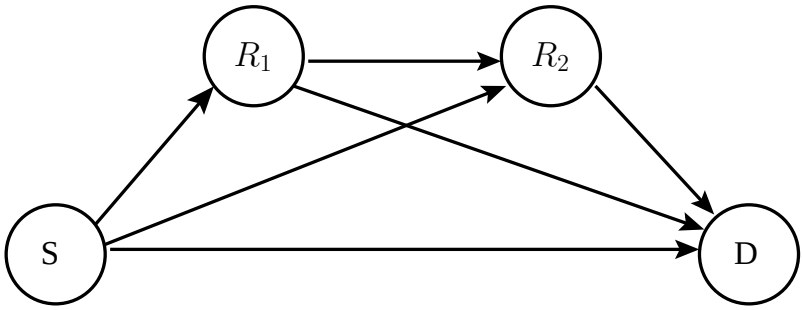

Figure 1.9: System model of a four-node MHN, where the SN sends messages to the DN via two relays. The relays are allowed to communicate with each other.

dependent hop index. Normally, it is assumed that all RNs and the SN have a routing-dependent hop index, as shown in Fig. 1.9. Usually, the receive set[1] of each RN and SN is predetermined for this type of network. Note that Fig. 1.7 represents the only example belonging to both categories due to having a single RN.

Fig. 1.7 portrays one of the classical models. Ng and Yu [136] incorporated a number of novel elements into this model, namely the relay selection technique, the relaying-strategy as well as the power allocation (PA) and reformulated the associated cross-layer operation problem as an optimization problem. Fareed and Uysal proposed a relay-position selection for an STBC-assisted scheme in [137]. Further improvements were proposed in [138, 139], which explored the benefits of STBC. The average receive SNR was taken into account in [140], which effectively represented the distance, because in ad hoc networks typically no power-control is used. This paper also discussed several relaying models relying on the instantaneous channel condition. Lee *et al.* [141] combined the benefits of ARQ, PA as well as DF relaying and quantified how the ARQ reduced the outage probability. Then Ropokis *et al.* [142] considered the attainable successful decoding probability at the relay node under the idealized simplifying assumption that no channel coding is applied. Different modulation schemes combined with DF relaying were discussed in [143]. Benjillali *et al.* [144] considered two different relaying schemes and the Bit-Interleaved Coded Modulation (BICM) assisted capacity was quantified.

Xia, Fan, Thompson and Poor designed an attractive MAC layer for a three-node relay network benefitting from having a buffer [145]. Onat *et al.* [146] provided the BER analysis of relay-aided cooperation, while the authors of [147] analyzed the modulation-mode switching thresholds of adaptive modulation.

A new node model was proposed in [148], where M relays were located between

[1]Receive Set of node i: all nodes which are qualified to receive the data from node i form the receive set of node i.

the SN and the DN, but the SN was also capable of directly communicating with the DN. Two specific cases were considered, namely when all relay nodes actively participated in relaying or only the best relay node using the AF protocol has been considered. The benefits of power control on both the achievable throughput and on the outage probability were quantified. The Symbol Error Ratio (SER) analysis of the same system model was provided in [149]. The outage probability of DF relaying was derived by Beaulieu and Hu in [150], while the attainable BER was studied by Lee and Kim in [151]. The same system relying on MIMO-aided DF relaying was considered by Adinoyi and Yanikomeroglu in [152]. In [153], Ikki and Ahmad extended the model of [150] from the Rayleigh channels to the more general family of Nakagami-m channels in the context of DF relaying and both the BER as well as the outage probability were analyzed. Similar results can also be found in [154].

1.2.10 Multihop Networks with Multiple Sources and Destinations

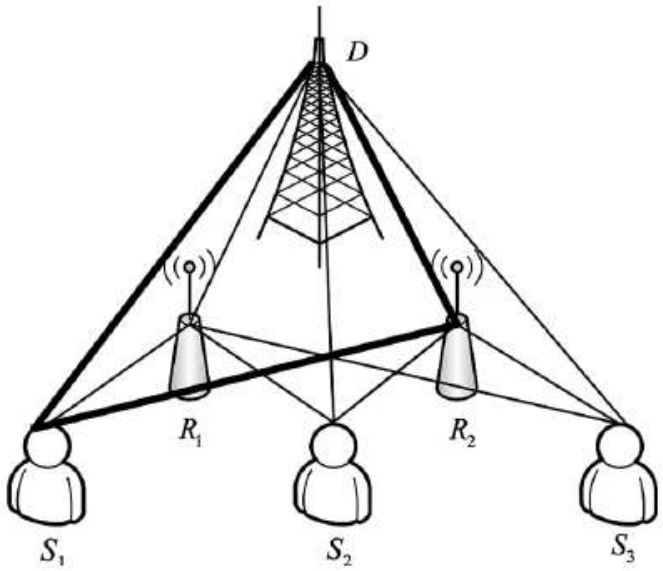

Figure 1.10: An ad hoc network supporting multiple SNs, multiple RNs and a single DN. The DN can receive the signal both directly from SN or via the RNs. Multi-user detection can be applied at the DN of this model.© [135]

The final ad hoc model considered here is constituted by the multihop network supporting both multiple SNs and DNs as shown in Fig. 1.10 , where the multiple-SNs transmit their data to the single DN either via the RNs or directly. This model is also often applied in the research of cellular networks [135]. As the most sophisticated scenario, Fig. 1.11 shows a network having multiple sources, destinations and hops.

Both the physical layer related papers [155, 156] and the upper layer based contributions [157] discussed the behavior of the network supporting multiple sources and

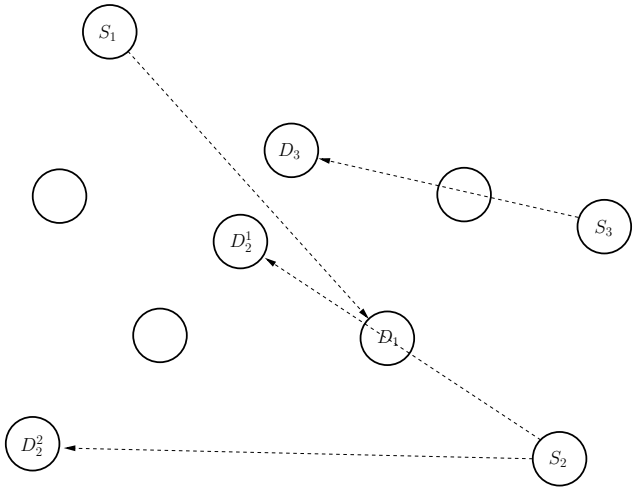

Figure 1.11: System model of a multi-hop network having multiple sources and destinations. The number of SNs may be different from the number of DNs. In this figure, S_1 and S_3 have the corresponding destinations of D_1 and D_3, while the S_2 has two destinations, namely D_2^1 and D_2^2.

destinations. However, the upper layer based papers are beyond the scope of this chapter.

The capacity of wireless networks was evaluated in [158]. Then Grossglauser and Tse [159] claimed that the per-user throughput may actually be increased when the nodes were mobile rather than fixed. Gupta and Kumar [160] were the first authors to consider the family of lattice networks. In 2003, a series of papers was published on the subject of cooperative diversity by Sendonaris, Erkip, Aazhang [161, 162] as well as by Laneman, Tse and Wornell [163].

Beneficial power allocation was proposed for a network supporting multiple sources, relays and destinations in [155], while the authors of [156] proposed a range of deployment concepts for fixed relays. Then Ibrahim *et al.* [164] put forward and answered a pair of fundamental questions: *When to cooperate? Whom to cooperate with?*. Farhadi and Beaulieu extended the results of [165] and in [166] they found the most beneficial DF RN position. In 2012, Maric, Goldsmith and Medard [167] discussed the design of networks supporting multiple sources and destinations relying on network coding. They also considered AF relaying in the high-SNR region [167].

1.3 Thesis Outline and Novel Contributions

1.3.1 Novel Contribution

The thesis is based on the publications [168–171]. The novel contributions of this thesis are listed as follows:

Contribution 1 [168]: A novel buffer-aided multihop transmission scheme has been proposed and investigated. The corresponding MAC layer protocol has also been conceived. The BER, outage probability and delay of MHLs have been analyzed and a range of formulas have been obtained, when assuming that BPSK signals are transmitted over all the hops, which experience i.i.d Rayleigh fading. Our analysis and performance results show that exploiting the independent fading of multiple hops results in a significant diversity gain. Given an L-hop link, the MHD scheme is capable of achieving an Lth order diversity, when each RN has a buffer of sufficient size and data blocks of sufficiently large size are transmitted. It can be shown that the maximum achievable MHD may be approached, when each RN has a moderate buffer size. The MHD scheme significantly outperforms the conventional multi-hop transmission arrangement in terms of the BER/outage performance, when sufficiently large buffers are considered.

Contribution 2 [169]: The performance of MHLs employing the MHD scheme was investigated, when communicating over Nakagami-m fading channels. Given a time-slot (TS), the MHD scheme activates a specific hop from the set of the all available hops based on the values given by their CDFs. Both accurate and approximate expressions were derived for the end-to-end BER as well as for the outage probability of BPSK/MQAM signals. Furthermore, our MHD scheme is capable of achieving the maximum achievable diversity gain provided by the independent fading experienced by different hops.

Contribution 3 [170]: Adaptive modulation assisted buffer-aided transmissions were conceived and investigated. A new transmission scheme namely the Maximum Throughput Adaptive Rate Transmission (MTART) scheme is proposed. A matching MAC layer protocol is also proposed for implementing our MTART. The bit error ratio (BER), the outage probability (OP), the throughput as well as the bandwidth-efficiency of the MTART scheme is analyzed. Our results demonstrate that our MRART regime has the potential of significantly outperforming conventional adaptive modulation. Naturally, the OP is improved by the buffering scheme advocated at the cost of an increased delay. Finally, the distribution of the end-to-end packet delay is characterized.

Contribution 4 [171]: A Buffer-aided Opportunistic Routing (BOR) scheme is proposed for a three-node network. Furthermore, the three-dimensional (3D) Transmission Activation Probability Space (TAPS) formed by the associated three channels is conceived. Both the energy consumption and the outage probability (OP) are investigated for transmission in this network. The results show that when the system is operated at $0.4 packet/TS$, the energy consumption is

reduced by as much as 24.8% to 77.6% when compared to four other state-of-the-art benchmark schemes. Furthermore, the OP is reduced by 89.6%, when compared to conventional opportunistic routing. Finally, the packet delay of the BOR scheme is studied.

1.3.2 Outline of the Thesis

In this section we provide an overview of the remainder of this thesis. As described in Section 1.3.1, the proposed buffer-aided transmission is capable of reducing both the BER and the outage probability as well as the energy consumption. Let us now highlight the outline of this thesis, which is portrayed in Figure 1.12.

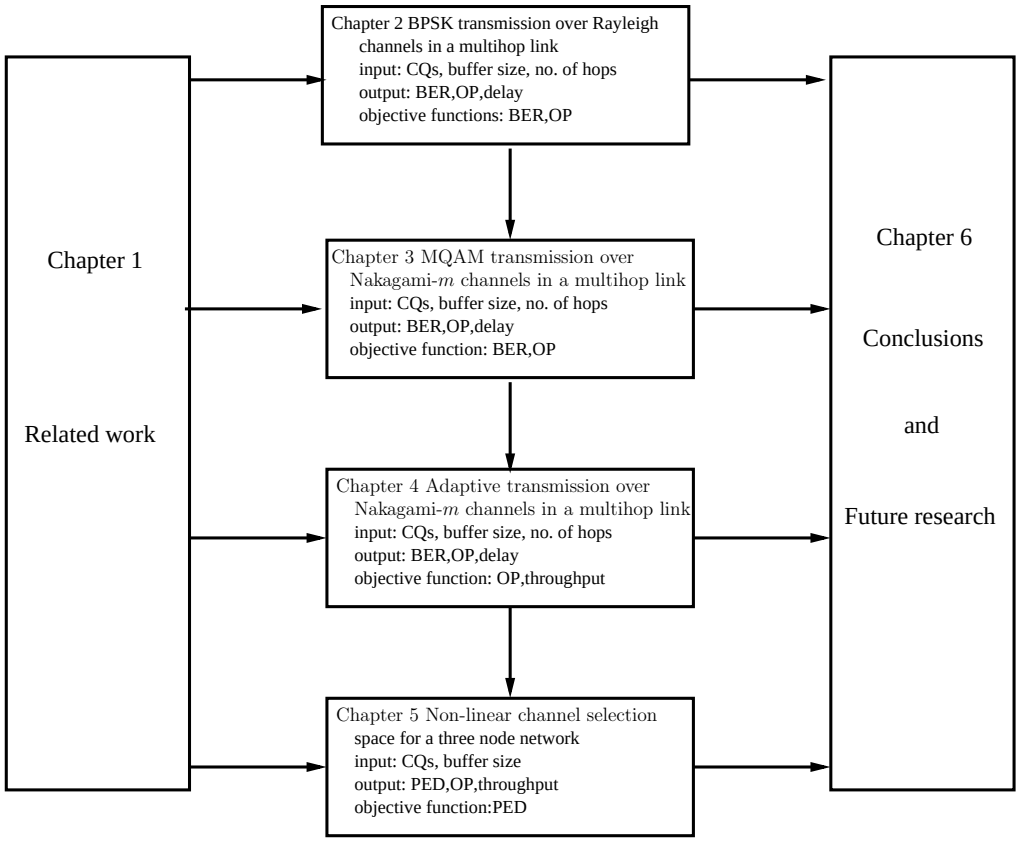

Figure 1.12: Organization of the thesis. CQ: channel quality. BER: Bit error ratio. OP: outage probability. PED: packet energy consumption.

Chapter 2: A multi-hop transmission scheme is proposed in Section 2.1, where the relay nodes of a multi-hop link are assumed to have buffers for temporarily storing their received packets. Then in Section 2.2, we assume that each hop experiences both propagation pathloss and independent identically distributed (i.i.d) flat Rayleigh fading. As a benefit of storing packets at the RNs, during each TS, the hop having the highest signal-to-noise ratio (SNR), can be activated from the set of those hops that have packets awaiting transmission in

their buffer. A packet is then transmitted over the best hop. After introducing the related MAC layer implementation in Section 2.3, the system's BER/outage probability performance analysis is provided in Section 2.4. It is shown that this hop-activation procedure is reminiscent of selection (SC) diversity, which is referred to here as multi-hop diversity (MHD). Then, the BER, OP, diversity order and the performance of the MAC layer is characterized in Section 2.5. Section 2.6 concludes this chapter.

Chapter 3: The concept of multihop diversity is applied to MQAM transmission over non-independent identically distributed (i.n.i.d) flat Nakagami-m channel. A cumulative distribution functions (CDFs) based channel selection method is proposed in Section 3.1. Then in Section 3.3 the exact BER and OP are evaluated. An approximate expression is derived, which assists us in finding the distribution of how many packets are stored in the buffer, when the buffer size and/or the number of hops is large. It is shown in Section 3.3.4 that this hop-activation procedure is also reminiscent of the MHD regime of Chapter 2. Then, a number of results, including the BER and OP are obtained in Section 3.4. Finally, the conclusions of this chapter are provided in Section 3.5.

Chapter 4: The adaptive modulation is invoked for buffer-aided transmission. The number of bits in each time slot is affected both by the channel quality and the buffer fullness. During each time-slot (TS), the criterion used for activating a specific hop is that of transmitting the highest number of bits (packets). When more than one hops are capable of transmitting the same number of bits, the particular hop having the highest channel quality (reliability) is activated. After introducing this new concept in Section 4.1, a specific MAC layer protocol is proposed in Section 4.3 for implementing the new transmission scheme. In the same Section, we refer to this regime as the Maximum Throughput Adaptive Rate Transmission (MTART) scheme, which is analyzed for transmission over the i.i.d Nakagami-m fading channels in Section 4.4 and 4.5. Then in Section 4.6, the theoretical expression of the BER, OP, capacity, throughput as well as the delay-PMF are confirmed by our simulation. Finally, Section 4.7 offers our conclusion.

Chapter 5: The Buffer-aided Opportunistic Routing (BOR) concept is proposed in Section 5.1, which combines the benefits of both opportunistic routing [172] and of MHD-aided transmissions [168]. This principle was conceived for a Buffer-aided Three-node Network (B3NN) composed of a SN, a buffer-aided RN and a DN. As mentioned in Section 5.2, when applying opportunistic routing, each packet is transmitted from the SN to the DN either directly or indirectly via the

RN, depending on the instantaneous channel qualities. In MHD assisted transmission, the RN is capable of temporarily storing the received packets, which facilitates the flexible selection of the channels. A matching MAC layer protocol is provided in Section 5.3 for implementing this transmission scheme. Section 5.4 describes the channel selection criterion used in our simulations. From Section 5.5 to Section 5.8, the concept of the three-dimensional (3D) Transmission Activation Probability Space (TAPS), the channel activation philosophy and the PMF of the packet delay are discussed, respectively. In Section 5.9, we constructed a three-node network for investigating the energy consumption, OP and the PMF of the delay. Section 5.10 summaries the findings of this chapter.

Chapter 6: Section 6.1 summarizes the entire thesis. Then, Section 6.2 provides design guidelines and finally we suggest future research ideas in Section 6.3.

Chapter 2

Buffer Aided Multi-Hop BPSK Links for Rayleigh Channels

In Chapter 1, we reviewed the state-of-the-art. In this chapter, a multi-hop transmission scheme is proposed and studied, where all the relay nodes (RNs) of a multi-hop link (MHL) are assumed to have buffers for temporarily storing their received packets. Hence, the RNs are operated under the so-called Store-and-Forward (SF) relaying scheme. As a benefit of storing packets at the RNs, during each time-slot (TS), the best hop typically has the highest signal-to-noise ratio (SNR), which can be activated from the set of those hops that have packets awaiting transmission in the buffer. A packet is then transmitted over the best hop. This hop-activation procedure is reminiscent of selection (SC) diversity, which is referred to here as multi-hop diversity (MHD). In this chapter, we investigate both the bit error and outage probability as well as the delay performance of the MHD scheme, when assuming that each hop experiences both propagation pathloss and independent identically distributed (i.i.d) flat Rayleigh fading. The (MAC) layer implementation and several closed-form formulas are derived. Both numerical and simulation results are provided for characterizing the achievable performance of the MHD scheme. Our performance results show that relying on multiple hops has the potential of providing a significant diversity gain, which may be exploited for enhancing the reliability of wireless multi-hop communications.

2.1 Introduction

In wireless multi-hop communications, a source node (SN) sends information to a corresponding destination node (DN) via intermediate relay nodes (RNs), which results

in a range of advantages over conventional single-hop communications. These advantages may include an improved energy-efficiency and extended coverage, improved link performance, enhanced throughput, simplicity and high-flexibility of network planning, etc. [110, 121, 173]. Owing to their advantages, multi-hop communications have drawn a lot of attention and have been investigated from different perspectives [86–88, 91, 96, 110, 121, 173–176].

In the context of multi-hop links (MHLs), it has typically been assumed that information is transmitted from the SN to the DN one node by one node successively, without any store-and-wait stage at the intermediate RNs [87, 174, 175]. For convenience of description, we refer to this scheme as the conventional multi-hop transmission scheme in our forthcoming discourse. In this conventional multi-hop scheme, information is transmitted over a single hop during its scheduled time-slot (TS) regardless of its link quality quantified, for example, by its signal-to-noise ratio. Hence, the overall reliability of a MHL is dominated by that of the poorest hop and a route outage occurs, once an outage is encountered in any of the invoked hops. As a result, the route error/outage performance of a MHL usually degrades or remains the same in the best case, as the number of hops increases. In order to improve the performance of MHLs, novel signaling schemes have been proposed [110, 173, 177], which require the nodes to have a store-and-wait capability. For example, in [173, 177], Adaptive Modulation and Coding (AMC) combined with automatic repeat request (ARQ) schemes has been invoked in cooperative decode-and-forward (DF) communications. Very recently, the authors of [110] have employed AMC for dual-hop cooperative communications relying on a regenerative RN, where the AMC mode of both the hops may be configured independently.

In this chapter, we view the independently fading multiple hops of MHLs as an adaptively configurable resource that may be exploited for achieving diversity. This diversity is achieved by assuming that every node of a MHL has a buffer for temporarily storing the packets received. In contrast to the conventional multi-hop transmission schemes, where a hop is forced to transmit during its scheduled TS regardless of its reliability, our proposed scheme activats the highest-quality hop from the set of hops having packets in their buffers to send. Hence, our multi-hop transmission scheme is reminiscent of selection (SC) diversity, which is referred to here as multi-hop diversity (MHD). In this chapter, we analyze the characteristics and achievable performance of the MHLs supported by MHD. For simplicity, we assume that information is transmitted hop-by-hop using binary-phase shift-keying (BPSK) modulation. The bit error and outage probability as well as the delay performance of the MHD scheme are investigated, when assuming that each hop experiences both

propagation pathloss and independent identically distributed flat Rayleigh fading. We analyze in detail the bit error ratio (BER), the outage probability, the achievable diversity order (DO), the probability mass function (PMF) of the delay as well as the average and maximum delay. Both numerical and simulation results are provided for characterizing the achievable performance of the MHD scheme. The impact of both the number of hops and the buffer size of RNs on the performance of the MHD scheme is addressed. Our BER/outage performance results demonstrate that independently fading multiple hops have the potential of providing a significant diversity gain for improving the reliability of multi-hop communications. The achievable error/outage performance may be improved, as the buffer size increases and/or the number of hops of a link increases. However, given the total number of hops of a MHL, the maximum attainable MHD may be approached, provided that each of the RNs has a sufficiently large buffer size.

Naturally, due to the store-and-wait characteristics of the RNs, the above-mentioned error/outage performance improvement is obtained at the cost of an increased delay. In this chapter, we study both the *block delay* and the *packet delay*. The block delay is defined as the time required for a block of packets generated by the SN to reach the DN. By contrast, the packet delay is the time required for delivering a specific packet from the SN to the DN, when assuming that there is an infinite number of packets to transmit. Our studies show that for a sufficiently large amount of data, the MHD scheme on average does not have to strike an explicit trade-off between the delay tolerated and the achievable error/outage performance. Our studies show that both our MHD scheme and the conventional multi-hop transmission scheme [178] use exactly the same number of TSs to deliver a block of packets, yielding the same block delay. This is because our MHD scheme transmits one packet over one hop per TS, identically to the conventional multi-hop transmission scheme. By contrast, the packet delay is a random variable, distributed in a range bounded by the minimum and maximum packet delays. However, for an L-hop link, the MHD scheme delivers on average one packet per L TSs to the DN, while the conventional multi-hop scheme delivers exactly one packet per L TSs to the DN.

Note that the terminology of MHD has also been used in [166]. However, the MHD considered in [166] and that defined in this chapter have an entirely different meaning. In [166], it is assumed that a receiving node can receive replicas of the same signals from several other nodes. In this case, MHD is attained at the receiving node by combining the signals received from the different nodes transmitting the same information. Therefore, the MHD in [166] is obtained by multipath combining.

By contrast, the MHD in this chapter belongs to the category of SC diversity. Furthermore, in [166] the RNs do not use a buffer to store packets, hence the signals are transmitted hop-by-hop based on the conventional multi-hop transmission scheme.

The remainder of this chapter is organized as follows. The next two sections present the system model and the implementation of the system. Section 2.4 analyzes both the BER and outage probabilities, as well as the delay imposed. In Section 2.5, we provide our numerical and simulation results. Finally, our conclusions are offered in Section 2.6.

2.2 System Model of Multi-Hop Links

The system model under consideration is a typical multi-hop wireless link [175, 178], which is shown in Fig. 2.1. The MHL consists of $(L+1)$ nodes, a SN S (node 0),

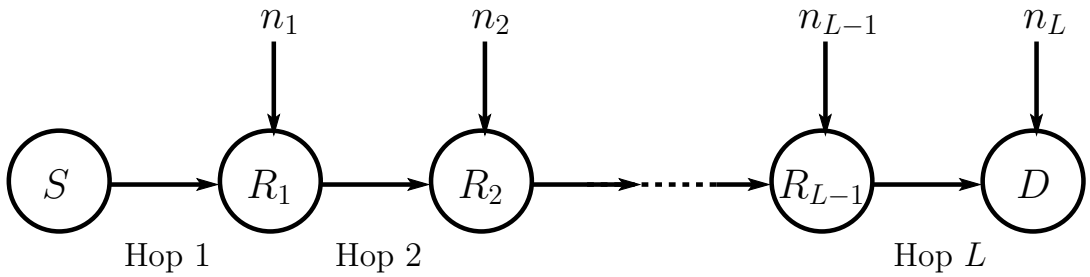

Figure 2.1: System model for a multi-hop wireless link, where source node S sends messages to destination node D via $(L-1)$ intermediate relay nodes.

$(L-1)$ RNs $R_1, R_2, \ldots, R_{L-1}$ and a DN D (node L). The distance from the SN S to the DN D is normalized to $D_{SD} = 1$. For simplicity, we assume that every hop spans the same distance, expressed as $d = D_{SD}/L = 1/L$. The SN S sends information to the DN D via L hops with the aid of the $(L-1)$ RNs. At the RNs, the classic decode-and-forward (DF) protocol is employed for relaying the signals. For convenience, we denote the symbol transmitted by node 0 as x_0 and its estimate at the DN D of node L by $x_L = \hat{x}_0$, while the symbol estimated at the lth RN by x_l, $l = 1, \ldots, L-1$. At packet level, they are correspondingly represented by $\boldsymbol{x}_0$, $\boldsymbol{x}_l$, $l = 1, \ldots, L-1$, and $\boldsymbol{x}_L = \hat{\boldsymbol{x}}_0$. We assume baseband BPSK modulation and that x_l assumes the values of $+1$ or -1 with equal probability. In this chapter, we assume that the signals are transmitted on the basis of TSs having a duration of T seconds. In addition to propagation pathloss, the channels of the L hops are assumed to experience independent block-based flat Rayleigh fading, where the complex-valued fading envelope of a hop remains constant within a TS, but is independently faded for different TSs. The pathloss is assumed to follow the exponential law of $d^{-\alpha}$, where α is the pathloss exponent, having a value between 2 to 6, typically. We assume

that the total energy per bit transmitted from the SN S to the DN D is $E_b = 1$ unit, regardless of the number of hops per MHL. This one unit of energy is uniformly assigned to the L hops of the MHL. Hence, the energy required for transmitting one bit over a hop is $1/L$ units. Based on the above settings, when the $(l-1)$st node transmits a packet $\boldsymbol{x}_{l-1}$, the observations received by node l can be expressed as

$$\boldsymbol{y}_l = \sqrt{\gamma_h} h_l \boldsymbol{x}_{l-1} + \boldsymbol{n}_l, \ l = 1, 2, \ldots, L \tag{2.1}$$

where h_l represents the fast fading channel gain of the lth hop from node $(l-1)$ to node l, while $\boldsymbol{n}_l$ is the Gaussian noise added at node l. The fast-fading channel gain h_l obeys the Rayleigh distribution with a mean of one and the average receive SNR is γ_h. The noise samples in $\boldsymbol{n}_l$, $l = 1, \ldots, L$, obey the complex Gaussian distribution with zero mean and a common variance of $\sigma^2 = 1/(2\gamma_b)$ per dimension, where γ_b denotes the received average SNR per bit, when the SN directly sends signals to the DN over a single hop spanning a distance of $D_{SD} = 1$ using one unit of energy. Based on the above definitions, the average receive SNR of the lth hop is then given by $\gamma_h = L^{\alpha-1}\gamma_b$. Explicitly, the average SNR per hop increases, as the number of hops of a MHL increases, which results in a power gain.

Table 2.1: Example of a five-hop link.

TS i	Buffer [2 4 3 5]	Channel SNR [0.2 0.8 1.2 1.1 0.7]	Channel 3 is activated
TS i+1	Buffer [2 3 4 5]	Channel SNR [0.7 1.2 0.5 0.4 0.3]	Channel 2 is activated
TS i+2	Buffer [1 4 3 5]	Channel SNR [1.2 1.4 1.1 0.3 0.9]	Channel 2 is activated
TS i+3	Buffer [0 5 3 5]	Channel SNR [0.2 1.3 0.8 0.8 1.5]	Channel 5 is activated
TS i+4	Buffer [0 5 3 4]	Channel SNR [0.6 1.9 0.8 1.2 1.1]	Channel 4 is activated
TS i+5	Buffer [0 5 2 5]	Channel SNR [1.4 0.5 0.9 1.1 1.1]	Channel 1 is activated
TS i+6	Buffer [1 5 3 5]	Channel SNR [0.2 1.3 0.8 0.8 1.5]	Channel 5 is activated
TS i+7	Buffer [0 6 3 4]	...	...

As mentioned in Section 2.1, the channel having the highest instantaneous channel quality is activated. However, since the channel conditions and interference patterns are random, they cannot be predicted. Let us assume that there is a five-hop link where every RN can store upto 8 packets. Since we have five hops, apart from the source and destination node, there are four relay nodes and a total of five channels, as shown in Fig. 2.1. We also assume that at time slot (TS) i, there are [2 4 3 5] packets in the buffer of the RN [1 2 3 4]. Let us assume that the instantaneous channel SNRs are [0.2 0.8 1.2 1.1 0.7]. The third channel has the highest SNR as detailed in Table 2.1, hence Channel 3 is activated. At TS $(i+4)$ time, the second channel is the best one, but no packet are stored in the buffer of the first relay, hence the second best channel, namely Channel 4 is activated.

In this chapter, we investigate both the achievable BER and outage performance as well as the delay characteristics of MHLs employing our MHD scheme, where the following assumptions are adopted:

- The SN always has packets to send, hence the MHL operates in its steady state.
- Both the SN S and DN D can store an infinite number of packets. By contrast, each of the $(L-1)$ RNs can only store at most B packets.
- The fading processes of the L hops of a MHL are independent, while the fading of a given hop remains constant within a packet duration, but it is independently faded from one packet to another.
- There is a central control unit (CCU), which evaluates and exploits the global knowledge about the channels of the L hops. Based on the global channel knowledge of the L hops within a given TS, the CCU decides which of the L nodes, i.e. nodes $0, 1, \ldots, L-1$, is allowed to transmit and then informs the corresponding receive node without a delay and without errors.

Among those hops having at least one packet stored in the buffer awaiting transmission, the CCU first decides as to which one is the most reliable hop according to the instantaneous SNR values of $\{\gamma_l\}$. Then, one packet is transmitted over the most reliable hop using a TS. According to this strategy, the packets are transmitted obeying the classic time-division principles. Hence transmitting a packet from the SN S to the DN D requires L TSs.

In next section, a MAC layer protocol is conceived for supporting the system's operation.

2.3 MAC Protocol for Supporting Multihop Diversity

In the previous section, we assumed that based on the global channel-quality knowledge of all the hops the CCU makes the decisions on which node is allowed to transmit. In practice, however, it is a challenge to realize such an ideal CCU, especially, when distributed ad-hoc networks are considered. Therefore, we have to design protocols for efficiently exchanging the relative information over multihop links, so that those hops are activated that require the least resources.

Our protocol is based on the following assumptions. Consider the L-hop link shown in Fig. 2.1, where the nodes are indexed from the SN to DN as node 0, node 1 ... node L, and each of the L nodes knows its own index, which indicates its relative position within the link. We assume that the transmission range of a node is at most one hop, i.e. a node can only communicate with its pair of adjacent nodes. However, we assume that a node, say node $(k-1)$ is always able to receive the request for

transmission (RFT) signal from node k. The interference range of a node is assumed to be at most two hops, implying that a transmitted signal may affect upto five consecutive nodes of the link, including the one transmitting from the middle one of the five. We assume that a single-hop channel within the transmission range is divided into S_i^{cql} number of channel-quality levels, namely $C_0^{cql}, C_1^{cql}, \ldots, C_{S_i^{cql}-1}^{cql}$ with $C_{S_i^{cql}-1}^{cql}$ being the highest, while a two-hop channel within the interference range is divided into two states, namely 'interfered (1)' or 'uninterfered (0)'. Furthermore, the link-quality between node i and node j is denoted by $C_{i,j}^{cql}$. In Fig. 2.2 to Fig. 2.10, the circles represent nodes, while the numbers between/on the nodes represent the link-quality and interference, respectively.

We also assume that node $(k-1)$ can always receive the RFT signal from node k. This assumption is reasonable since a) the RFT signal is typically transmitted at a high power and b) the protocol prefers the more reliable hops, which implies that the hops to be activated are the more reliable hops of the MHL. Furthermore, for the signal RFT and CFT (Clear For Transmission is the response to RFT which will be detailed later.) , the error-resistance binary signalling has to be used. By contrast, $\log_2(S_i^{cql})$ bits are required for distinguishing the S_i^{cql} number of channel qualities.

In order to activate the most appropriate hop from the set of L hops for transmission, our proposed protocol has the following three stages of operations. a) The first stage uses five symbol durations for the $(L+1)$ nodes to broadcast their channel-quality estimation pilots, in order to assist their adjacent (one hop) and interfering (two hops) nodes in estimating the qualities of the corresponding channels. b) The second stage uses four symbol durations for identifying the specific nodes whose buffers are either full or empty. c) Finally, during the third stage, the most appropriate hops are activated. We will shows that this stage may require a variable number of symbol durations. To elaborate a little further, the operations associated with the above-mentioned three stages are described as follows.

Stage 1 (Channel state Identification): Again, this stage requires five symbol durations. Within the ith, $i = 0, 1, 2, 3, 4$, symbol duration, the nodes having position index obeying $(i + 5j)$, $j = 0, 1, \ldots$ and $i + 5j \leq L$, broadcast their pilot signals. After receiving the pilot signal, the two adjacent nodes of a transmitting node estimate the corresponding channel-quality and classify it into one of the S_i^{cql} levels. Specifically, for node k, the quality of the channel between node $(k-1)$ and node k is expressed as $C_{k-1,k}^{cql}$, while that of the channel from node k to node $(k+1)$ is as $C_{k,k+1}^{cql}$, both of which belong to $\{C_0, C_1, \ldots, C_{S_i^{cql}-1}\}$. If the two nodes within the interference range receive the pilot signal, they set the interference flag to logical one. Otherwise it is set to zero.

Stage 2 (Buffer state Identification): This stage requires four symbol durations to make the adjacent nodes aware of whether a node's buffer is full or empty since the nodes having a full buffer cannot act as receiving nodes, while nodes having an empty buffer cannot be the transmit nodes. In detail, within the ith, $i = 0, 1, 2, 3$, symbol duration, a node having a position index of $(i + 4j)$, $j = 0, 1, \ldots,$ and $i + 4j \leq L$, broadcasts 1, if its buffer is full, and broadcasts -1, if its buffer is empty. Otherwise, if the node's buffer is neither full nor empty, it remains inactive and transmits no signal. After four symbol durations, every node has been informed of the buffer states of its two neighbour nodes. If the buffer of node $(k-1)$ is empty, node k changes the channel quality level of the hop spanning from node $(k-1)$ to node k to logical 0, indicating that the hop is unavailable. By contrast, if the buffer of node $(k+1)$ is full, node k changes the channel quality level of the hop between node k and node $(k+1)$ to logical 0.

Following Stage 2, we can see that the buffer states of the $(L-1)$ RNs are embedded into the channel states of the L hops.

Stage 3 (Activation of desired hops): The number of symbol durations required by this stage is a variable, but it is at most $(L \times S_i^{cql})$ symbol durations. The specific hop having the highest channel quality has the priority to transmit. Secondly, for two hops at the same channel quality level, the hop related to a transmit node having a higher position index has the priority over the lower position index. Additionally, the hops having a logically zero channel state will not be activated. For convenience, we define four node states, namely *transmitting* (T), *receiving* (R), *waiting* (W) and *unknown* (X). Furthermore, since both the transmit and receive nodes of a hop exploit the channel quality knowledge of the hop, the hop may be classified either by the transmit node or by the receive node. In our protocol described below, a hop activated for transmission will be activated by the corresponding receive node. In Fig. 2.2 to Fig. 2.10, we use arrow to express the RFT signal is broadcast from potential receiver. In these figures, the states of each node are also displayed.

Let us distinguish the symbol durations as $0, 1, \ldots, (L \times S_i^{cql} - 1)$. Initially, all the nodes are in state X. A given receive node, such as node k, $k = 1, 2, \ldots, L$[1], may use one of the symbol durations satisfying $L(C_{S_i^{cql}} - 1 - i) + (L - k)$ for $i = (C_{S_i^{cql}} - 1), (C_{S_i^{cql}} - 2), \ldots, 1, 0$. However, the decision whether the kth receive node is allowed to receive from the kth hop is also dependent on the activities of its neighbour nodes. Specifically, given the channel quality of $C_{k-1,k}^{cql} \in \{C_0^{cql}, C_1^{cql}, \ldots, C_{S_i^{cql}}^{cql} - 1\}$ of the kth hop, the kth node is only allowed to receive over the kth hop using the symbol duration indexed by $L(C_{S_i^{cql}} - 1 - C_{k-1,k}) + L - k$, if it is in the state of X.

[1]Recall that, the L hops are numbered as hop 1, hop 2, ... L.

Otherwise, it takes no action within this symbol duration, i.e. if it is in one of the states T, R, or W.

Let us assume that the kth node declares ownership of the kth hop by sending a RFT signal to its neighbor nodes, namely nodes to $(k-3)$, $(k-2)$, $(k-1)$, $(k+1)$ and $(k+2)$. Then, the neighbour nodes as well as node k take the following actions :

- Node $(k-1)$: After receiving the RFT control message sent by node k, it changes its state to T, provided that it is allowed. Furthermore, node $(k-1)$ responds to the RFT a signal by sending a CFT message, within the next symbol duration. However, if node $(k-1)$ happens to be in the state W and unable to respond to the RFT because it is in the interference range of another transmission, it remains silent.
- Node $(k-2)$: If it receives the RFT control message from node k within the current symbol duration or the CFT from node $(k-1)$ within the next symbol duration, it changes its state to W. Otherwise, it takes no action and hence remains in its current state.
- Node $(k-3)$: If it receives the CFT from node $(k-1)$ within the next symbol duration, it changes its state to W. Otherwise, it takes no action and remains in its current state.
- Node $(k+1)$: It takes the same actions as that stated for node $(k-2)$.
- Node $(k+2)$: If it receives the RFT control message from node k within the current symbol duration, it changes its state to W. Otherwise, it takes no action and remains in its current state.
- Node k: Finally, if node k receives the CFT from node $(k-1)$ within the next symbol duration, it changes its state to R. Otherwise, if it receives no response from node $(k-1)$, indicating that node $(k-1)$ is not free to transmit, it retransmits a RFT control message within the following symbol duration and remains in state X. Correspondingly, nodes $(k-2)$, $(k+1)$ and $(k+2)$ return to state X, if previously they have changed their states to W.

Following the above operations, provided that a link can be successfully constructed between node $(k-1)$ and node k, which is confirmed by the fact that node $(k-1)$ sends a CFT to node k, then node $(k-1)$ can start transmitting its data to node k, immediately after it transmitted the CFT. Simultaneously, the other nodes (except for the SN) that are in state X continue the above activation process, until all of them change their states to W, T or R, or the maximum search duration of $(L \times S_i^{cql})$ is reached.

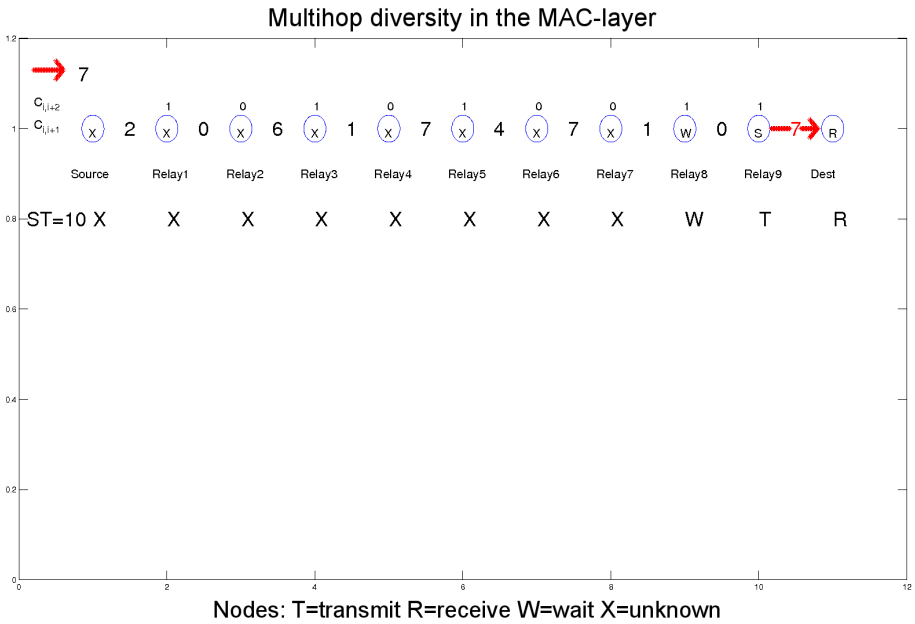

Figure 2.2: An example of the MAC layer process for a ten-hop MHL having a SN, nine RNs and one DN. The channel quality between each pair of adjacent nodes is shown in the middle of them while the channel quality between node i and node $(i+2)$, $i = 0, 1, \ldots, 8$ is shown at the top of node $(i+1)$. ST means Symbol Time (Symbol Duration). Stage 3 starts from $ST = 10$. In the 10th ST, if the channel quality of the 10th hop is "7". Node 10 broadcast the RFT. In this figure, the DN broadcasts the RFT and both Relay 9 and Relay 8 receive the RFT. Hence Relay 9 sets its state to "T", while Relay 8 sets its state to "W".

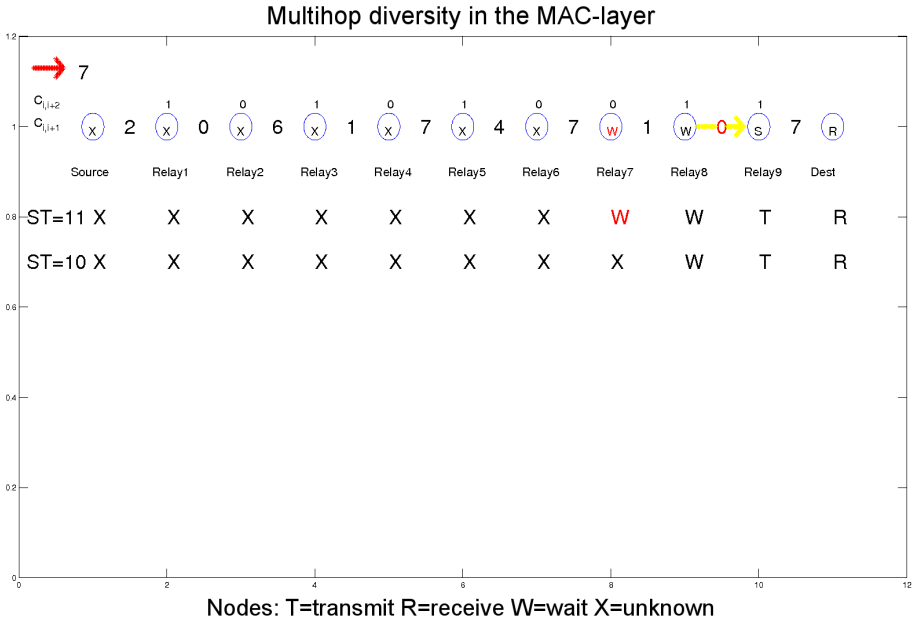

Figure 2.3: Following the MAC layer's operation from Fig. 2.2, Relay 9 which received the RFT at $ST = 10$ responds with the CFT message at $ST = 11$. Once Relay 8 received this CFT messaage, it sets its state to "W".

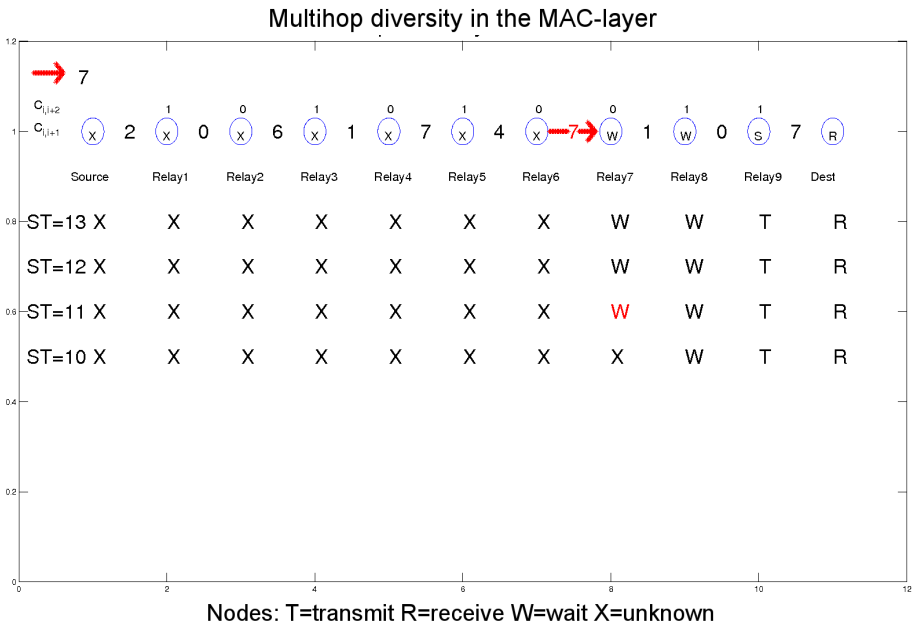

Figure 2.4: Following on from Fig. 2.3, Relay 7 satisfies the position condition and channel quality condition for broadcasting the RFT. However the state of Relay 7 had been set to "W". Therefore, no action is taken during this ST.

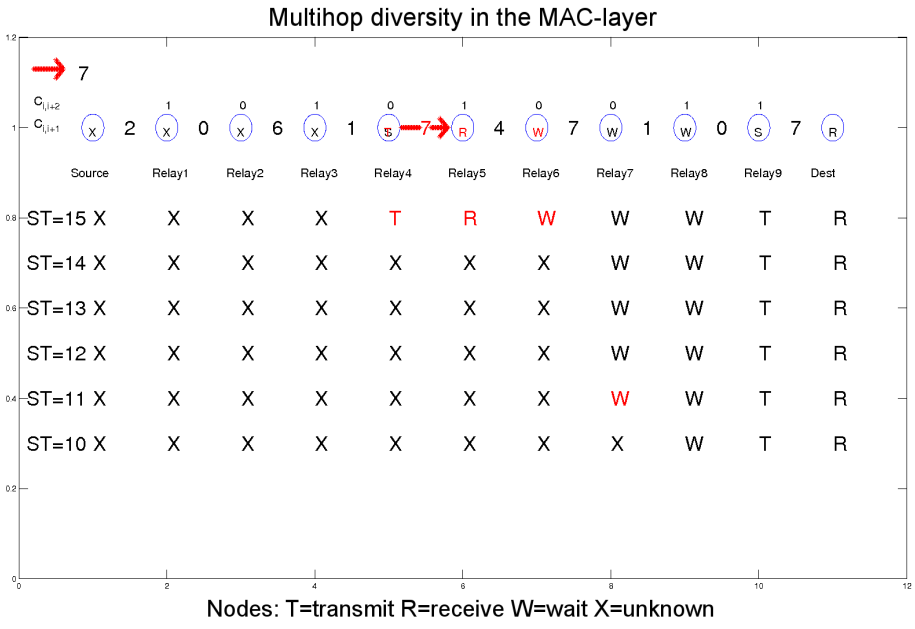

Figure 2.5: Following on from Fig. 2.4, Relay 5 satisfies both the position, and the channel quality as well as the state condition to broadcast the RFT. Hence, Relay 5 sets its state to Receive, i.e to "R" while Relay 4 sets its state to Transmit, "T". The channel quality between Relay 5 and Relay 3 is "0", therefore Relay 3 does not receive the broadcast message from Relay 5.

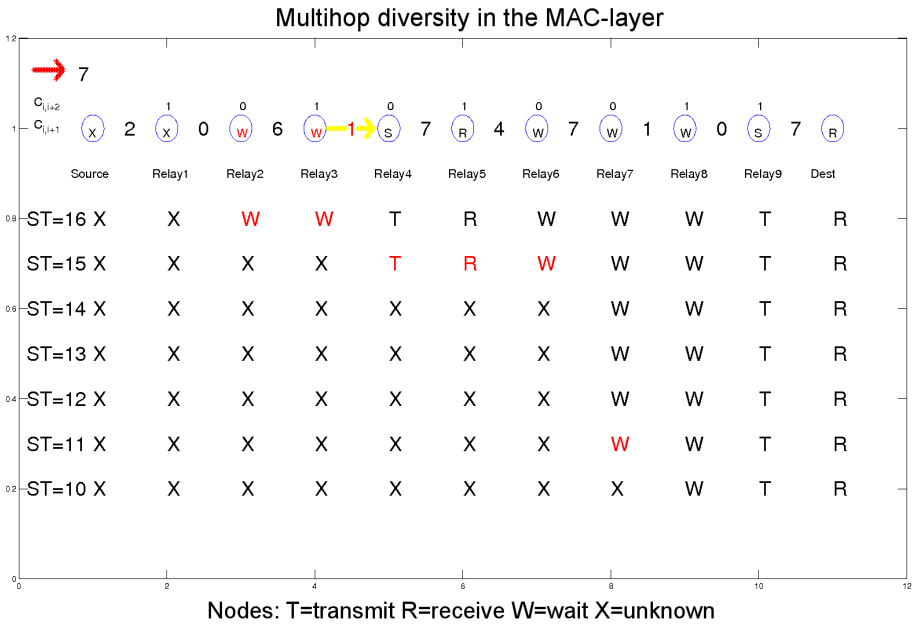

Figure 2.6: Following on from Fig. 2.5, Relay 4 has received the RFT at $ST = 15$ and responds with a CFT at $ST = 16$. Both Relay 3 and Relay 2 received this CFT, hence they set their state to Wait, "W".

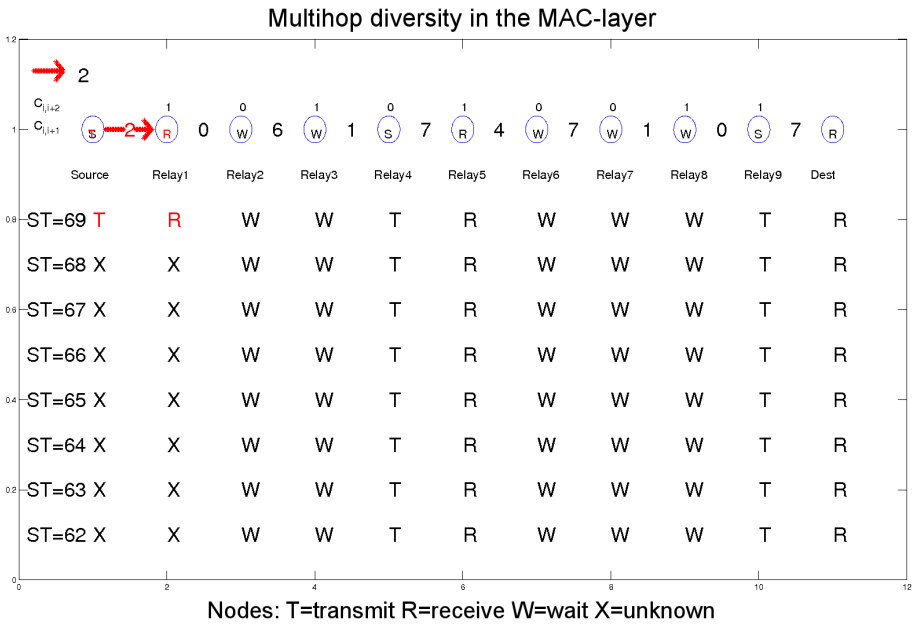

Figure 2.7: Following on from Fig. 2.6, the third transmission is set up at $ST = 69$, because the channel quality between SN and Relay 1 is "2".

Let us consider an illustrative example of the process invoked in the MAC layer. We consider a ten-hop MHL having a Source, nine RNs and a DN. The channel quality related to each pair of adjacent nodes is shown between them ($S_i^{cql} = 8$, from "7" to "0"), while the channel quality between node i and node $(i+2)$, $i = 0, 1, \ldots, 8$ is shown at the top of node $(i + 1)$ ("0" or "1") of Fig. 2.2, where ST represents the symbol time (symbol duration). Stage 3 of the activation process starts from $ST = 10$. In Fig. 2.2 to Fig. 2.5, the channel quality experienced at the instant of broadcasting the RFT message is shown at the top left corner of each figure. Moreover, the specific position index of the node for a specific ST is shown in the link. If a node satisfies both the channel quality condition and position condition, but the state of this node is unknown, it is denoted by "X", it will broadcast the RFT message and sets its state to receive, as denoted by "R". In Fig. 2.2, the DN satisfies both the channel, as well as the position and buffer state conditions, hence it broadcasts the RFT control message. Both Relay 9 and Relay 8 receive the RFT and hence they change their states. Explicitly, Relay 9 sets its state to "T" while Relay 8 sets its state to "W" in Fig. 2.2. Observe in Fig. 2.3that , Relay 9 received the RFT at $ST = 10$ responses with the CFT at $ST = 11$. When Relay 8 received this CFT, it sets its state to "W". Then, as seen in Fig. 2.4, Relay 7 satisfies the position condition and the channel quality condition in order to broadcast RFT. However, the state of Relay 7 had been set to "W". Therefore, no action occurs in this ST. In Fig. 2.5, Relay 5 satisfies both the position and the channel quality as well as the state condition to broadcast the RFT. Hence, Relay 5 sets its state to "R" while Relay 4 sets its state to "T". The channel quality between Relay 5 and Relay 3 is "0", therefore Relay 3 does not receive the broadcast message from Relay 5. In Fig. 2.6, Relay 4 received the RFT at $ST = 15$ and responses the CFT at $ST = 16$. Both Relay 3 and Relay 2 received this CFT and hence they set their state to "W". In Fig. 2.7, the third transmission is set up at $ST = 69$ when the channel quality between the SN and Relay 1 is "2". More explicitly, the channel quality decreased by one level per 10 STs, hence there are 50 STs during the channel quality reduction from "7" to "3". The position condition is stated from the 10th hop outward and the position condition decreases one per ST. Hence 10 more STs are required. The time delay encountered during State 1 and State 2 is 9STs, hence the total delay becomes $9 + 50 + 10 = 69$STs.

The examples seen in Fig. 2.8 to Fig. 2.10 represent the scenario associated with the hidden terminal problem. To elaborate a little further, the hidden terminal problem occurs when a potential transmitter/receiver tries to set up a transmission session aimed at a potential receiver/transmitter, but the potential receiver/transmitter may

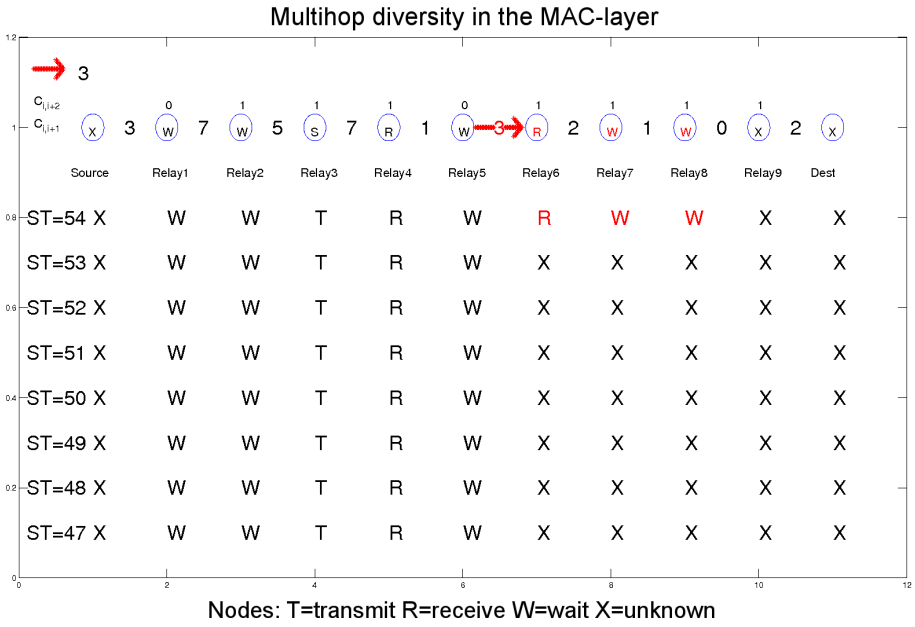

Figure 2.8: Another example that shows the hidden terminal problem and the corresponding solution. Before $ST = 54$, a transmission from Relay 3 to Relay 4 had been set up and the state of Relay 5 had been set to Wait, "W". However, Relay 6 did know the transmission from Relay 3 to Relay 4. At $ST = 54$, all conditions of broadcasting the RFT from Relay 6 are satisfied, hence Relay 6 broadcasts the RFT and changes its state to Receive, "R". However, the Relay 5 remains its state "W". Both Relay 7 and Relay 8 received the RFT and hence they set their state to "W".

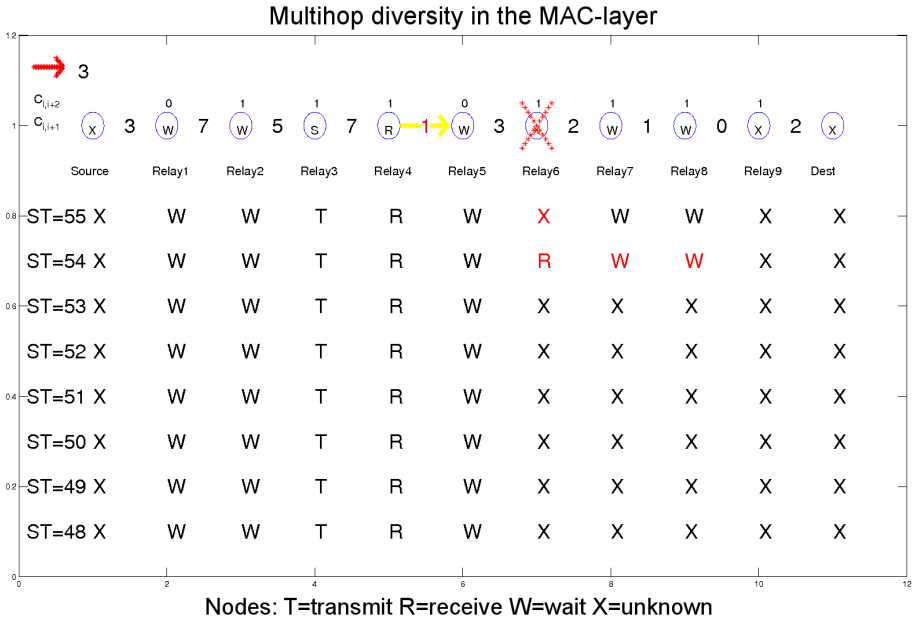

Figure 2.9: Following on from Fig. 2.8, Relay 6 did not receive any response from Relay 5 and Relay 6 realized that Relay 5 was not in the unknown state "X", hence Relay 6 sets its state back to "X" and retransmits the RFT.

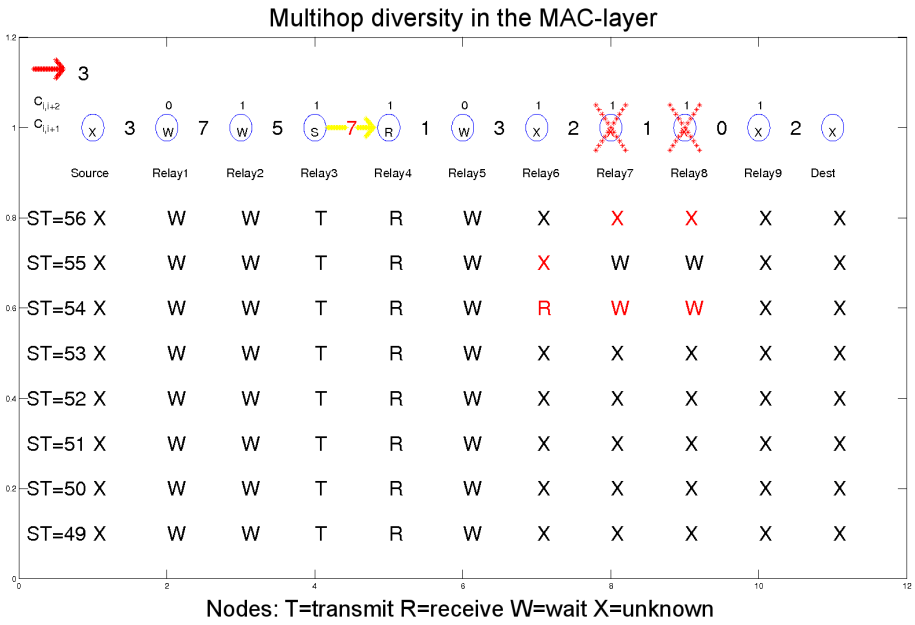

Figure 2.10: Following on from Fig. 2.9, Relay 7 and Relay 8 received the retransmitted RFT and changes their states back to unknown, "X".

not able to respond which may cause a conflict. Let us consider, for example, when the potential transmission is requested by the receiver, but there is no response from the potential transmitter, which is a specific manifestation of the hidden terminal problem. Another detailed example of the hidden terminal problem is provided in Fig. 2.8-Fig. 2.10. In Fig. 2.8, an existing transmission session in progress from Relay 3 to Relay 4 had been set up and the state of Relay 5 had been set to "W". However, Relay 6 did not receive any response from Relay 5. In Fig. 2.8 at $ST = 54$, all required conditions of enabling the broadcast at the RFT from Relay 6 are satisfied. Hence Relay 6 broadcasts the RFT and changes its state to "R". However, Relay 5 remains in state "W". Both Relay 7 and Relay 8 received the RFT and hence set their state to "W". In Fig. 2.9, Relay 6 did not receive any response from Relay 5 or Relay 6, hence it realized that Relay 5 was not in the unknown state "X". Therefore, Relay 6 set its state back to "X" and retransmits the RFT. In Fig. 2.10, Relay 7 and Relay 8 received the retransmitted RFT and changes their states back to "X".

In summery, our protocol has the following characteristics:

- Even though the maximum time required for the third stage is $(L \times S_i^{cql})$ symbol durations, the activation process is completed, once all the receive nodes, including $R_1, R_2, \ldots, D$, change their states from X to the states W, T and R.
- Due to the fading of wireless channels and owing to our specific assumptions characterizing the interference range, after the activation process, several hops might be transmitting their data simultaneously, especially, when a relatively

long MHL is considered. These active hops definitely include the best hop, but not necessarily, for example, the second best hop, because the second best hop might be within the interference range of the best hop. Hence, in order to guarantee a BER below the required target, a channel quality threshold may be used.

- The above strategy may result in outage, but also equips us with a degree of freedom for striking a trade-off between the achievable throughput and the BER performance. Furthermore, the search time required by the third stage may be reduced, since only the channel having a quality above the threshold has to be considered.

Again, the activation process duration is a variable. However, commencing from Stage 1 of the search process, the average delay required for the best hop to commence transmitting data can be analyzed. Let the L hops have the same probability of $p = 1/S_i^{cql}$ to be at any of the S_i^{cql} channel-quality levels. Furthermore, let the required channel-quality threshold be C_{th}^{cql}. Then, this average delay may be expressed as

$$A_{d1} = A_0 + \sum_{i=C_{th}}^{C_{S_i^{cql}}-1} \sum_{l=1}^{L} p[(i+1)p]^{l-1}(ip)^{L-l}[(S_i^{cql} - i - 1)L + L - l + 2], \tag{2.2}$$

where the constant A_0 is contributed by the first two stages[2], which is equal to 8 for $L = 4$ and 9 for $L \geq 5$. In (2.2), the term p represents the probability that the lth hop is the best hop with its channel quality level of i, while the term $[(i+1)p]^{l-1}$ is the probability that the $(l-1)$ hops ahead of hop l have channel-quality levels not higher than level i. Furthermore, the third term $(ip)^{L-l}$ is the probability that the channel-quality levels of the $(L-l)$ hops behind hop l are lower than level i and, finally, the last term of $[(S_i^{cql} - i - 1)L + L - l + 2]$ in (2.2) is the number of symbol durations required for the best hop to commence data transmission.

As an example, when we have $S_i^{cql} = 10$, $L = 8$ and $C_{th}^{cql} = 0$, the average delay imposed by completing the configuration of the best hop is about $A_{d1} \approx 19$ symbol durations. By contrast, the maximum is 89 symbols, which is significantly higher than 19.

Above a protocol has been designed for general MHLs. For specific cases, such as two-hop and three-hop MHLs, specific protocols can be designed, in order to reduce

[2] $L = 2, 3$ will be discussed later.

the search duration. Below we state the strategies conceived for these two specific cases.

Two-hop case - In this scenario, the MHL has a single RN, which can act as the CCU. Specifically, the best hop may be activated as follows. Within the first symbol duration, the SN broadcasts the channel-quality estimation pilot, while in the second symbol duration, the DN broadcasts the same pilot. At this point, the RN exploits the channel knowledge of both the SN-RN as well as of RN-DN channels and hence it can make an informed activation. During the third symbol duration, the RN transmits a RFT signal, if it chooses the first hop, while it sends a CFT signal, if it activates the second hop. Data transmission starts from the fourth symbol duration. Therefore, the full activation process requires three symbol durations.

Three-hop case - In this case, there are two RNs, R_1 and R_2. In detail, the activation process is operated as follows. At Stage 1, four symbol durations are used for sending the pilots, in order to decide the channel quality levels of the three hops. At Stage 2, the two RNs use two symbol durations to signal their buffer states to each other. At Stage 3, if there is an outage between R_1 and R_2, i.e. if R_1 and R_2 are unable to receive signals from each other, then, during the seventh symbol duration, R_1 sends a RFT to S, while R_2 sends a CFT to D. In this case, data transmission start from the eighth symbol duration over the first and the third hops , if the corresponding channel quality levels are sufficiently high. By contrast, if there is no outage between R_1 and R_2, then, all the receive nodes skip the seventh symbol duration. Then, R_2 conveys the channel quality level of the third hop to R_1 within the eighth symbol duration, consequently, R_1 has the channel quality level information of all the three hops and hence it acts as the CCU. During the ninth symbol duration, provided that the first hop is the best one, R_1 send a RFT to S and the first hop starts transmitting data from the tenth symbol duration. If the second hop is the best one, then R_1 sends a CFT to R_2 and the second hop starts data transmission from the tenth symbol duration. By contrast, if the third hop is the best one, R_1 remains silent within the ninth symbol duration. After realizing that the third hop is the best, node R_2 sends a CFT to D within the tenth symbol duration, and data transmission over the third hop commences at the 11th symbol duration. Hence, identifying the best hop of a three-hop MHL requires at most 10 symbol durations.

In the next section, the performance of MHLs is analyzed under our idealized assumptions interpreted for the CCU.

2.4 Performance Analysis

In this section, we first derive the BER and outage probability expressions of the MHD scheme. Both the lower-bounds and near exact formulas are derived. Then, the diversity order of the MHD scheme is analyzed. Furthermore, the formulas of the delay's PMF, as well as the average and maximum delay expressions are derived.

Based on Fig. 2.1 and on the operational principles of the MHD described in Section 2.2, we can now infer that if every RN has a buffer of size of B packets, the following events may occur. 1) Firstly, the buffer of a RN may be empty at some instants. In this case, this RN cannot be the transmit node, since it has no data to transmit. 2) Secondly, the buffer of a RN may be full at some instants. Then, this RN cannot be the receive node, since it cannot accept further packets. In these cases, the CCU has to choose a hop for transmission from a reduced set of hops, which results in an increased Bit Error Ratio (BER) and outage probability due to the reduced single-selective diversity gain. Therefore, our lower-bounds of the BER and outage probability are derived by relaxing the above-mentioned constraints and assuming that each RN has an unlimited buffer size and that a node always has packets to transmit. By contrast, for near exact analysis of the BER and outage probability, the above-mentioned constraints are considered. Below we first derive both the lower-bound BER and the near exact BER expressions.

2.4.1 Bit Error Ratio

2.4.1.1 Lower-Bound Bit Error Ratio

In order to derive the lower-bound BER, we first derive the single-hop BER, $P_{L,e}$, under the assumptions that every RN has an infinite buffer and that a node always has packets prepared to send. Then, the lower-bound of the end-to-end BER, $P_{L,E}$, of the MHL is derived. The subscript 'L' in $P_{L,e}$ and $P_{L,E}$ stands for the lower-bound.

Considering a TS, when the SNR is given by γ, the conditional BER of BPSK modulation is given by [179]

$$P_{L,e}(\gamma) = Q\left(\sqrt{2\gamma}\right), \tag{2.3}$$

where $Q(x)$ is the Gaussian Q-function. According to the principles described in Section 2.2, during a TS, the hop with the highest SNR is chosen for transmitting a packet. Hence, the SNR γ in (2.3) is given by

$$\gamma = \max\{\gamma_1, \gamma_2, \ldots, \gamma_L\}, \tag{2.4}$$

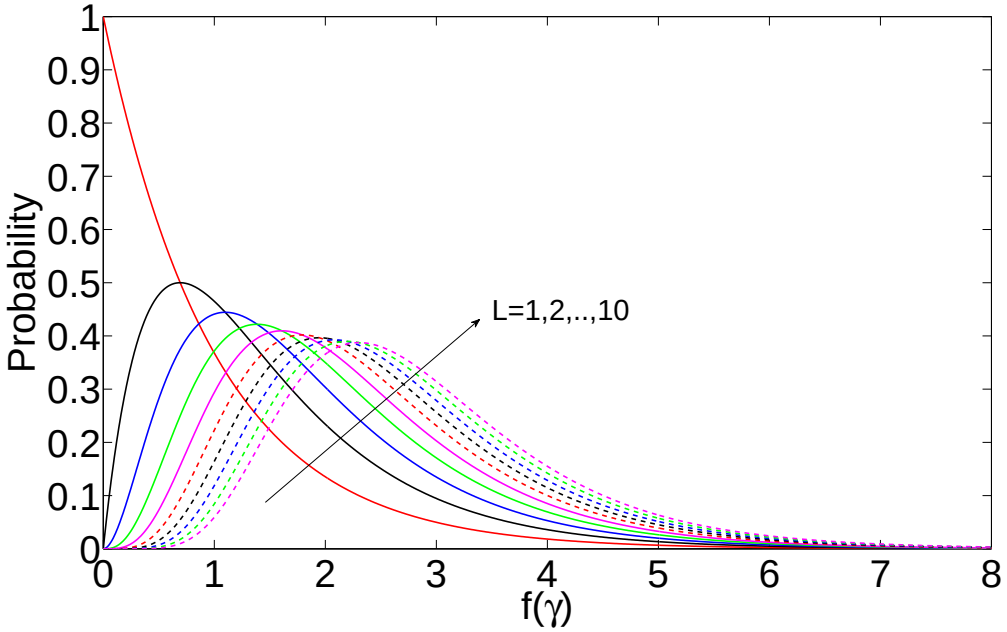

Figure 2.11: The channel qualities of $f(\gamma)$ for various L values. All curves are generated based on (2.5). It is clearly seen that the channel quality is better, when L is higher.

where $\gamma_l = L^{\alpha-1}|h_l|^2\gamma_b$ is the SNR of the lth hop within the TS considered. Let $\gamma_l = |h_l|^2\gamma_h$, where $\gamma_h = L^{\alpha-1}\gamma_b$ denotes the average SNR of a hop. Then, the probability density function (PDF) of γ_l may be readily found, which is $f(\gamma_l) = \gamma_h^{-1}e^{-\gamma_l/\gamma_h}$, $l = 1, \ldots, L$. Furthermore, the PDF of γ defined in (2.4) may be expressed as [33]

$$\begin{aligned} f(\gamma) &= \frac{d}{d\gamma}\left[\int_0^{\gamma} f(\gamma_l)d\gamma_l\right]^L \\ &= \frac{L}{\gamma_h}\exp\left(-\frac{\gamma}{\gamma_h}\right)\left[1-\exp\left(-\frac{\gamma}{\gamma_h}\right)\right]^{L-1}. \end{aligned} \tag{2.5}$$

Based on the above equation, the channel qualities of $f(\gamma)$ associated with various L values are shown in Fig. 2.11. The average single-hop BER $P_{L,e}$ can be obtained by weighing each specific SNR-dependent BER with the probability of this SNR represented by the SNR-PDF of (2.3) and then averaging - i.e integrating it - over the legitimate SNR range, yielding

$$P_{L,e} = \int_0^{\infty} P_{L,e}(\gamma)f(\gamma)d\gamma. \tag{2.6}$$

Upon substituting both (2.3) associated with the Q-function and (2.5) into the above equation, with the aid of (5A.11) in [33]or Appendix in this Chapter, the single-hop

lower-bound BER is given by

$$P_{L,e} = \frac{1}{2}\sum_{l=0}^{L}(-1)^l \binom{L}{l}\sqrt{\frac{\gamma_h}{l+\gamma_h}}. \tag{2.7}$$

Having obtained the single-hop lower-bound BER $P_{L,e}$, the lower-bound end-to-end BER $P_{L,E}$ may be obtained with the aid of the following approach. Let $P_{L,C}(l-1)$ and $P_{L,E}(l-1)$, where we have $l = 1, \ldots, L$, be the correct and erroneous detection probabilities, respectively, after detection at the $(l-1)$st RN. Explicitly, we have $P_{L,C}(0) = 1$, $P_{L,E}(0) = 0$, and $P_{L,C}(l-1) = 1 - P_{L,E}(l-1)$. Then, the correct and erroneous detection probabilities, $P_{L,C}(l)$ and $P_{L,E}(l)$, after detection at the lth RN can be expressed in matrix form as

$$\begin{bmatrix} P_{L,C}(l) \\ P_{L,E}(l) \end{bmatrix} = \begin{bmatrix} 1-P_{L,e} & P_{L,e} \\ P_{L,e} & 1-P_{L,e} \end{bmatrix} \begin{bmatrix} P_{L,C}(l-1) \\ P_{L,E}(l-1) \end{bmatrix}. \tag{2.8}$$

Hence, the correct and erroneous end-to-end detection probabilities $P_{L,C}$ and $P_{L,E}$ may be obtained in a recursive manner as

$$\begin{aligned} \begin{bmatrix} P_{L,C} \\ P_{L,E} \end{bmatrix} &= \begin{bmatrix} P_{L,C}(L) \\ P_{L,E}(L) \end{bmatrix} = \begin{bmatrix} 1-P_{L,e} & P_{L,e} \\ P_{L,e} & 1-P_{L,e} \end{bmatrix} \begin{bmatrix} P_{L,C}(L-1) \\ P_{L,E}(L-1) \end{bmatrix} \\ &= \begin{bmatrix} 1-P_{L,e} & P_{L,e} \\ P_{L,e} & 1-P_{L,e} \end{bmatrix}^L \begin{bmatrix} P_{L,C}(0) \\ P_{L,E}(0) \end{bmatrix} \\ &= \begin{bmatrix} 1-P_{L,e} & P_{L,e} \\ P_{L,e} & 1-P_{L,e} \end{bmatrix}^L \begin{bmatrix} 1 \\ 0 \end{bmatrix}. \end{aligned} \tag{2.9}$$

In (2.9), the matrix containing $P_{L,e}$ may be decomposed with the aid of eigen-analysis [180], yielding

$$\begin{aligned} \boldsymbol{M} &= \begin{bmatrix} 1-P_{L,e} & P_{L,e} \\ P_{L,e} & 1-P_{L,e} \end{bmatrix} \\ &= \frac{1}{\sqrt{2}} \begin{bmatrix} 1 & 1 \\ 1 & -1 \end{bmatrix} \begin{bmatrix} 1 & 0 \\ 0 & 1-2P_{L,e} \end{bmatrix} \frac{1}{\sqrt{2}} \begin{bmatrix} 1 & 1 \\ 1 & -1 \end{bmatrix}. \end{aligned} \tag{2.10}$$

where $\lambda_1 = 1$ and $\lambda_2 = 1 - 2P_{L,e}$ are two eigenvalues of $\boldsymbol{M}$, while $\frac{1}{\sqrt{2}}\begin{bmatrix} 1 & 1 \\ 1 & -1 \end{bmatrix}$ is a corresponding orthonormal matrix. Upon substituting (2.10) into (2.9), we can

readily obtain the lower-bound end-to-end BER expression, which is

$$P_{L,E} = \frac{1}{2} - \frac{1}{2}\left(1 - 2P_{L,e}\right)^L \tag{2.11}$$

$$= \frac{1}{2} - \sum_{n=0}^{L} (-1)^n \binom{L}{n} 2^{n-1} P_{L,e}^n, \tag{2.12}$$

where the single-hop lower-bound BER $P_{L,e}$ is given by (2.7).

Note that, for RNs operating without buffers, we can readily show that the BER or the approximate BER of an L-hop link can also be expressed as in (2.11) or (2.24) upon replacing $P_{L,e}$ by $P_e = (1 - \sqrt{\gamma_h/(1+\gamma_h)})/2$, which is the BER of a BPSK scheme communicating over iid Rayleigh fading channels [179].

2.4.1.2 Near Exact Bit Error Ratio

When deriving the near exact BER of the MHD scheme, we have to consider the constraint that the L-hop link is forced to choose the best one from the set of m hops in order to send its information, when $(L-m)$ out of the L hops do not have information to transmit. This happens either when some of the transmit nodes' buffers are empty or when some of the receive nodes' buffers are full. In this case, based on (2.7), the BER is given by

$$P_e(m) = \frac{1}{2} - \frac{m}{2} \sum_{l=0}^{m-1} \frac{(-1)^l}{l+1} \binom{m-1}{l} \sqrt{\frac{\gamma_h}{l+1+\gamma_h}}, \tag{2.13}$$

where $m = 1, \ldots . L$. Let us express $P_m,\ m = 1, \ldots, L$, namely the probability of the event that m out of the L hops can transmit. Then, the average BER of the L-hop link may be formulated as

$$P_e = \sum_{m=1}^{L} P_m P_e(m). \tag{2.14}$$

Hence, what we need for the evaluation of P_e is first to find all the probabilities $\{P_m\}$, which may be derived by realizing that the packet transmissions over an L-hop link based on the MHD scheme obey a Markov process.

Let us assume that the buffer size of every RN is B packets. Let the number of packets that the RNs $R_1, R_2, \ldots, R_{L-1}$ store be $b_1, b_2, \ldots, b_{L-1}$, where $b_l = 0, 1, \ldots, B$. Then, the states of the L-hop link can be defined in terms of the number of packets

stored in the buffers of the $(L-1)$ RNs as

$$S_i = \left[b_1^{(i)}, b_2^{(i)}, \ldots, b_{L-1}^{(i)}\right]^T, i = 0, 1, \ldots, N-1, \tag{2.15}$$

where $b_l^{(i)}$ denotes the number of packets stored by the lth RN, when the L-hop link is in state i and $N = (B+1)^{L-1}$ is the total number of states, which constitute the set $\mathcal{S} = \{S_0, S_1, \ldots, S_{N-1}\}$. For example, let us consider a three-hop link having the parameters of $L = 3$ and $B = 2$. Then, there are in total $N = 3^2 = 9$ states, which form the set

$$\begin{aligned}\mathcal{S} = \big\{&S_0 = [0,0]^T, S_1 = [0,1]^T, S_2 = [0,2]^T,\\ &S_3 = [1,0]^T, S_4 = [1,1]^T, S_5 = [1,2]^T,\\ &S_6 = [2,0]^T, S_7 = [2,1]^T, S_8 = [2,2]^T\big\}.\end{aligned}$$

From the N states, a state transition matrix denoted by $\boldsymbol{T}$ can be populated by the state transition probabilities $\{P_{ij} = P(s(t+1) = S_j | s(t) = S_i),\ i, j = 0, 1, \ldots, N-1\}$. Specifically, the state transition matrix of the above example is given by

$$\boldsymbol{T} = \begin{bmatrix} 0 & 0 & 0 & 1 & 0 & 0 & 0 & 0 & 0 \\ 1/2 & 0 & 0 & 0 & 1/2 & 0 & 0 & 0 & 0 \\ 0 & 1/2 & 0 & 0 & 0 & 1/2 & 0 & 0 & 0 \\ 0 & 1/2 & 0 & 0 & 0 & 0 & 1/2 & 0 & 0 \\ 0 & 0 & 1/3 & 1/3 & 0 & 0 & 0 & 1/3 & 0 \\ 0 & 0 & 0 & 0 & 1/2 & 0 & 0 & 0 & 1/2 \\ 0 & 0 & 0 & 0 & 1 & 0 & 0 & 0 & 0 \\ 0 & 0 & 0 & 0 & 0 & 1/2 & 1/2 & 0 & 0 \\ 0 & 0 & 0 & 0 & 0 & 0 & 0 & 1 & 0 \end{bmatrix}. \tag{2.16}$$

We can see from this example that although the transition matrix $\boldsymbol{T}$ may be large, it can be formed easily. A possible algorithm for constructing the matrix $\boldsymbol{T}$ can be formulated as follows:

1. The $(B+1)^{L-1} \times (B+1)^{L-1}$ matrix $\boldsymbol{T}$ is first initialized with zero elements.
2. For row i, $i = 0, 1, \ldots, (B+1)^{L-1} - 1$, which corresponds to the ith state $S_i = \left[b_1^{(i)}, b_2^{(i)}, \ldots, b_{L-1}^{(i)}\right]^T$, the following operations are executed:
   - If $b_1^{(i)} + 1 \leq B$, the column corresponding to the output state $\left[b_1^{(i)} + 1, b_2^{(i)}, \ldots, b_{L-1}^{(i)}\right]^T$ is set to one;

- For $l = 1, 2, \ldots, L-2$, if $b_l^{(i)} - 1 \geq 0$ and $b_{l+1}^{(i)} + 1 \leq B$, the column corresponding to the output state $\left[b_1^{(i)}, \ldots, b_l^{(i)} - 1, b_{l+1}^i + 1, \ldots, b_{L-1}^{(i)}\right]^T$ is set to one;
- If $b_{L-1}^{(i)} - 1 \geq 0$, the column corresponding to the output state $\left[b_1^{(i)}, b_2^{(i)}, \ldots, b_{L-1}^{(i)} - 1\right]^T$ is set to one.

3. Each of the rows is divided by the number of ones in the row.

The state transition matrix $\boldsymbol{T}$ has the following properties:

- Matrix $\boldsymbol{T}$ is a sparse matrix. Every row has at most L number of non-zero elements, while the remaining at least $[(B+1)^{L-1} - L]$ elements are zero;
- The sum of the probabilities in each row is one;
- The number of non-zero elements in a row represents the number of hops that may be chosen by the CCU for transmission.

Having obtained the state transition matrix $\boldsymbol{T}$, the steady-state probabilities can be computed by the formula [181]

$$P_{\boldsymbol{\pi}} = \boldsymbol{T}^T P_{\boldsymbol{\pi}}, \tag{2.17}$$

where we have $P_{\boldsymbol{\pi}} = \left[P_{\pi_0}, P_{\pi_1}, \ldots, P_{\pi_{(B+1)^{L-1}-1}}\right]^T$, and P_{π_i} is the steady-state probability that the L-hop link is in state S_i [110]. The steady-state probability of a state is the expected of value the probability of this specific state in system. The knowledge of the steady-state probability of every state allows us to determine the PMF of a buffer. Equation (4.27) shows that $P_{\boldsymbol{\pi}}$ is the right eigenvector of the matrix $\boldsymbol{T}^T$ corresponding to an eigenvalue of one. Therefore, $P_{\boldsymbol{\pi}}$ can be derived with the aid of classic methods conceived for solving the corresponding eigenvalue problem [182].

Given $P_{\boldsymbol{\pi}}$, we can now compute the probability P_m, $m = 1, 2, \ldots, L$, by adding those entries in $P_{\boldsymbol{\pi}}$, which correspond to the specific rows of $\boldsymbol{T}$ that have m nonzero entries. Finally, given $\{P_m\}$, the near exact (or steady-state) BER of the L-hop link employing the MHD scheme can be evaluated using (2.14). Let us now analyze the outage probability.

2.4.2 Outage Probability

2.4.2.1 Lower-Bound Outage Probability

The outage probability is the probability of the event that the maximal SNR of *all* the L hops is lower than a pre-set threshold. When this event occurs, either no data is transmitted on the MHL in order to guarantee the required reliability, or the BER

becomes higher than a predicted value, if data is still transmitted. Given a threshold γ_T, the lower-bound outage probability is given by

$$P_{L,O} = \int_0^{\gamma_T} f(\gamma) d\gamma. \tag{2.18}$$

When substituting (2.5) into this equation, we can readily obtain

$$P_{L,O} = \left[1 - \exp\left(-\frac{\gamma_T}{\gamma_h}\right)\right]^L = \sum_{l=0}^{L} (-1)^l \binom{L}{l} \exp\left(-\frac{l\gamma_T}{\gamma_h}\right), \tag{2.19}$$

which is simply the probability that each of the L hops has an SNR lower than γ_T.

In contrast to the above MHD scheme, an outage occurs in the conventional L-hop transmission scheme, when a single one out of the L hops has an SNR below the threshold γ_T. Therefore, the outage probability can be expressed as

$$P_O = 1 - [P(\gamma_l > \gamma_T)]^L = 1 - \left[\int_{\gamma_T}^{\infty} f(\gamma_l) d\gamma_l\right]^L. \tag{2.20}$$

After substituting the PDF of $f(\gamma_l)$ into this equation, we obtain the BER of the conventional L-hop transmission scheme as

$$P_O = 1 - \exp\left(-\frac{L\gamma_T}{\gamma_h}\right). \tag{2.21}$$

2.4.2.2 Near Exact Outage Probability

From the derivation of (2.19), we can infer that, if m out of the L-hops are available for transmission, the conditional outage probability is given by

$$P_O(m) = \left[1 - \exp\left(-\frac{\gamma_T}{\gamma_h}\right)\right]^m, \ m = 1, 2, \ldots, L. \tag{2.22}$$

Consequently, the near exact (or steady-state) outage probability of the L-hop link may be expressed as

$$P_O = \sum_{m=1}^{L} P_m P_O(m), \tag{2.23}$$

where $\{P_m\}$ are the probabilities derived in Section 2.4.1.2.

2.4.3 Diversity Order

In this subsection, we analyze the achievable single selective diversity order of an L-hop MHL using the MHD scheme. Our analysis is based on (2.11) or (2.19) and (2.21).

Firstly, from a BER respective, we can immediately infer from (2.11) that we have

$$P_{L,E} \approx LP_{L,e}, \tag{2.24}$$

when $P_{L,e}$ is sufficiently low.

In more detail, after substituting (2.7) into (2.11), and considering that $\gamma_h \to \infty$, which results in $P_{L,e} \to 0$, we obtain

$$P_{L,E} \approx LP_{L,e} = \frac{L}{2}\sum_{l=0}^{L}(-1)^l\binom{L}{l}\sqrt{1-\frac{l}{l+\gamma_h}}. \tag{2.25}$$

After expanding $\sqrt{1-l/(l+\gamma_h)}$ in (2.25) using the formula (1.112.3) of [10] and ignoring the terms corresponding to $k > L$, the above equation may be written as

$$P_{L,E} \approx \frac{L}{2}\sum_{k=0}^{L}c_k\sum_{l=0}^{L}(-1)^l\binom{L}{l}\left(\frac{l}{\gamma_h}\right)^k, \tag{2.26}$$

where $c_0 = 1$, $c_1 = -1/2$ and, for $k \geq 2$, $c_k = (-1)^k(2k-3)!!/(2k)!!$. In (2.26), it can be shown that we have $\sum_{l=0}^{L}(-1)^l\binom{L}{l}(l/\gamma_h)^k = 0$ for any $k < L$. Hence, when $\gamma_h \to \infty$, the end-to-end BER of the L-hop MHL is given by

$$\begin{aligned} P_{L,E} &\approx \frac{Lc_L}{2}\sum_{l=0}^{L}(-1)^l\binom{L}{l}\left(\frac{l}{\gamma_h}\right)^L \\ &= \begin{cases} \frac{L}{4\gamma_h}, & \text{when } L=1 \\ \frac{(2L-3)!!}{(2L)!!}\frac{L!}{2}\frac{L}{\gamma_h^L}, & \text{when } L \geq 2 \end{cases} \end{aligned} \tag{2.27}$$

Explicitly, the end-to-end BER decays as a function of $1/\gamma_h^L$, explicitly indicating that the diversity order achieved by the MHD-aided L-hop link is L.

Secondly, from an outage probability respective, we can readily show that

$$\lim_{\gamma_h\to\infty}\frac{\log(P_{L,O})}{\log(P_O)} = L. \tag{2.28}$$

This suggests that, if the SNR γ_h per hop is high, the outage probability of the

MHD-based L-hop scheme decreases L times faster than that of the conventional L-hop transmission scheme. This property also explains that the MHD-based L-hop transmission scheme is capable of achieving an Lth-order diversity.

Above we have analyzed both the BER and outage probability of MHLs based on our proposed MHD scheme, where the RNs employ buffers for storing packets. Furthermore, the diversity order achieved by the MHD-based MHLs was analyzed, demonstrating that an Lth-order diversity may be attainable by a MHD-assisted L-hop link, when each hop experiences independent fading. Therefore, the MHD-based multi-hop transmission scheme outperforms the conventional multi-hop transmission scheme in terms of both its BER and outage performance. However, in our MHD-assisted MHLs, the RNs are required to have buffers for temporarily storing packets, which introduces transmission delay. Therefore, in the following subsection, we analyze the delay experienced by the MHD-assisted MHLs.

2.4.4 Transmission Delay

The transmission delay considered here is the time required for the end-to-end delivery of a packet or a block of packets from the SN to the DN, which are termed here as the *packet delay* or *block delay*. Explicitly, when the conventional multi-hop transmission scheme is used, the packet delay introduced by an L-hop link is L TSs, when one TS is required for transmitting a single packet over one hop. In the proposed MHD scheme, a single packet is delivered across a single hop during a TS, as in the conventional multi-hop transmission scheme. Hence, when transmitting a block of M packets, the total number of TSs required by both the conventional and by our MHD-aided multi-hop transmission scheme is the same, namely LM TSs. In other words, the block delay generated by both of the above-mentioned multi-hop transmission schemes is the same. Furthermore, since M packets are delivered from the SN to the DN within ML TSs, the SN transmits one packet per L TSs on average, while the DN receives one packet per L TSs on average. However, under the MHD scheme, a packet may be delivered in L TSs or stay in the MHL for a long time. Therefore, the packet delay, i.e. the time required for a packet to travels through the MHL, is a variable that is distributed in a range bounded by the minimum and maximum packet delays. Below, we analyze both the minimum and maximum packet delay, the PMF of packet delay as well as the average packet delay of the MHD-aided MHLs.

Let us first consider transmitting a packet over an L-hop link, one hop per TS. Then, the minimum delay of a MHD-aided L-hop link is $\tau_m^{(D)} = L$ TSs.

Secondly, for a MHD-aided L-hop link where each RN has a buffer of size B, the maximum delay of a packet, referred to as the *test packet*, is evaluated by jointly observing the following events: All the buffers 'in front' of the test packet are full after the SN sends the test packet to RN 1, and all the buffers 'behind' the test packet are entirely filled before RN $(L-1)$ sends the test packet to the DN. The time required for these operations is detailed as follows.

1. Sending the test packet from the SN to RN 1 - This operation requires one TS. (Fig. 2.12, from (a) to (b))
2. Transmitting all the packets stored in front of the test packet - In this case, RN 1 stores $(B-1)$ packets, while each of the remaining $(L-2)$ RNs stores B packets. For a packet stored at the ith RN, $(L-i)$ TSs are required for transmitting it to the DN. Hence, the total time required for clearing the packets in front of the test packet is $\sum_{i=1}^{L-1} B(L-i)-(L-1)$. (Fig. 2.12, from (b) to (c))
3. Delivering the test packet from RN 1 to RN $(L-1)$ - this process requires $(L-2)$ TSs. (Fig. 2.12, from (c) to (d))
4. Filling all the buffers of the RNs by packets arriving later than the test packet - In this case RN $(L-1)$, requires $(B-1)$ packets, while any of the other RNs requires B packets. Since sending a packet from the SN to RN j requires j TSs, the total time required for this process is $\sum_{j=1}^{L-1} Bj-(L-1)$. (Fig. 2.12, from (d) to (e))
5. Sending the test packet from RN $(L-1)$ to DN - One TS is required. (Fig. 2.12, from (e) to (f))

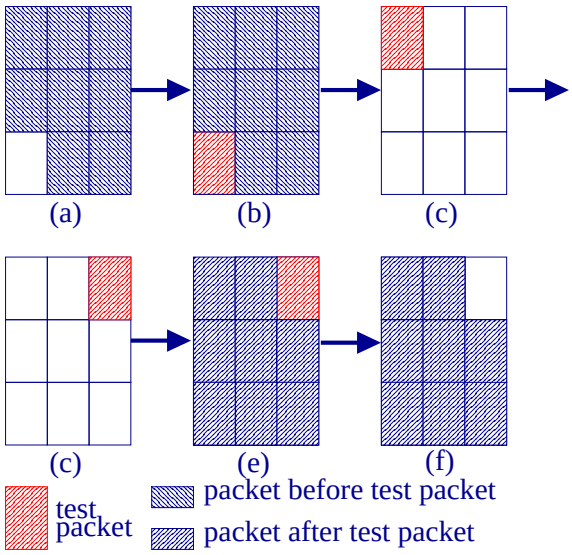

Figure 2.12: An example of determining the maximum delay.

Note that, encountering the above events implies that there should be a high number of packets to transmit. For simplicity, we assume that the SN has an infinite number of packets to transmit. In this case, the maximum packet delay of a MHD-aided L-hop link is then given by

$$\begin{aligned}\tau_M^{(D)} =& 1 + \sum_{i=1}^{L-1} B(L-i) - (L-1) + (L-2) \qquad (2.29)\\ &+ \sum_{j=1}^{L-1} Bj - (L-1) + 1\\ =& BL^2 - BL - L + 2 \ \text{(TSs)}. \qquad (2.30)\end{aligned}$$

Eq. (2.29) shows that the packet delay is linearly related to the buffer size of a RN, but quadratically to the number of hops.

Let us now derive the PMF of the packet delay. For achieving this objective, we first define a so-called *distance matrix*, whose elements represent respectively the number of TSs required for the MHL to change from one state to another. Then, we state that the 'distance' from state S_i to state S_j represents the shortest transport delay between them. For example, the distance between [2 0] and [1 1] is 1TS and the distance between [3 4 5] and [4 3 4] is 2TSs. Considering all the $(B+1)^{L-1}$ possible states as defined in (2.15), we can form an $(B+1)^{L-1} \times (B+1)^{L-1}$-element distance matrix as

$$\boldsymbol{D} = \left[d_{ij}\right]. \qquad (2.31)$$

Specifically, for the example considered for obtaining (2.16), the corresponding (9×9)-element distance matrix is given by

$$\boldsymbol{D} = \begin{bmatrix} 3 & 4 & 5 & 5 & 6 & 7 & 7 & 8 & 9 \\ 5 & 6 & 7 & 7 & 8 & 9 & 9 & 10 & 11 \\ 7 & 8 & 9 & 9 & 10 & 11 & 11 & 12 & 13 \\ 4 & 5 & 6 & 6 & 7 & 8 & 8 & 9 & 10 \\ 6 & 7 & 8 & 8 & 9 & 10 & 10 & 11 & 12 \\ 8 & 9 & 10 & 10 & 11 & 12 & 12 & 13 & 14 \\ 5 & 6 & 7 & 7 & 8 & 9 & 9 & 10 & 11 \\ 7 & 8 & 9 & 9 & 10 & 11 & 11 & 12 & 13 \\ 9 & 10 & 11 & 11 & 12 & 13 & 13 & 14 & 15 \end{bmatrix}. \qquad (2.32)$$

Now, from $\boldsymbol{D}$ of (2.31) we can now construct a range of matrices formulated as

$$\boldsymbol{D}(n) = \left[d_{ij} \wedge n \right], \tag{2.33}$$

where n takes an integer value representing the possible distance between two states, say, S_i and S_j. Furthermore, in (2.33), we have $d_{ij} \wedge n = n$, when $d_{ij} = n$, while $d_{ij} \wedge n = 0$, otherwise.

In Section 2.4.1.2, we have shown that the steady state probabilities of the MHD-aided L-hop link are given in $P_{\boldsymbol{\pi}}$, which may be evaluated from (4.27). Let us use the elements of $P_{\boldsymbol{\Pi}}$ as the diagonal elements to form a diagonal matrix $P_{\boldsymbol{\Pi}} = \text{diag}\{P_{\boldsymbol{\pi}}\}$. Then, given $P_{\boldsymbol{\Pi}}$, the state transition matrix $\boldsymbol{T}$ of (2.16) and the distance matrices $\{\boldsymbol{D}(n)\}$ of (2.33), the probability that the MHL requires d TSs to deliver the test packet from the SN to the DN can be expressed as

$$P(d) = L \times \mathbf{1}^T P_{\boldsymbol{\Pi}}^T \boldsymbol{T}^{(1)} \boldsymbol{T}^{d-2} \boldsymbol{D}(d-2) \boldsymbol{T}^{(L)} \mathbf{1}, \ \tau_m^{(D)} \leq d \leq \tau_M^{(D)}. \tag{2.34}$$

In (2.34), $\boldsymbol{T}^{(1)}$ denotes the transition when the first hop is chosen to send the test packet from the SN to RN 1. The matrix $\boldsymbol{T}^{(1)}$ is obtained from $\boldsymbol{T}$ by setting all the elements to zeros, which do not result in choosing the first hop. Similarly, $\boldsymbol{T}^{(L)}$ represents the transition, when the last hop is chosen to send the test packet from RN $(L-1)$ to the DN, which is obtained from $\boldsymbol{T}$ by setting all the elements to zero, which do not result in choosing the last hop. Once the test packet enters the MHL, $(d-2)$ transitions are involved in delivering the test packet from RN 1 to RN $(L-1)$, which explains the term $\boldsymbol{T}^{d-2}$. In (2.34), the multiplication by $\boldsymbol{D}(d-2)$ represents the transitions having a distance of $(d-2)$ from node 1 to node $(L-1)$, so that the total time required for delivering the test packet from SN to DN is d TSs. Finally, in (2.34), $\mathbf{1}$ denotes an $(B+1)^{L-1}$-length column vector with elements of 1, which is invoked to add together all the probabilities corresponding to using d TSs for delivering the test packet from the SN to the DN. Note that in (2.34) the multiplicative factor L is used for ensuring that the entry probability becomes unity.

The average packet delay can be expressed with the aid of (2.34) as

$$\bar{\tau}^{(D)} = \sum_{d=\tau_m^{(D)}}^{\tau_M^{(D)}} P(d) \times d. \tag{2.35}$$

In the next section, we characterize the performance of the MHD-aided MHLs.

2.5 Performance Results

In this section, we provide a range of numerical and/or simulation results for characterizing the BER, outage probability and delay performance of MHLs, in order to illustrate the effect of both the number of hops L and the buffer size B of RNs on the achievable MHD gain. Note that, the lower bound end-to-end BER and lower-bound outage probability of MHLs were evaluated from Eq. (2.12) and (2.19), respectively. The near exact end-to-end BER and outage probability were evaluated from Eqs. (2.14) and (2.23), respectively. Note furthermore that, in the following figures, γ_b was defined in Section 2.2, which is the received average SNR per bit, when the SN uses one unit of energy to transmit signals directly to the DN.

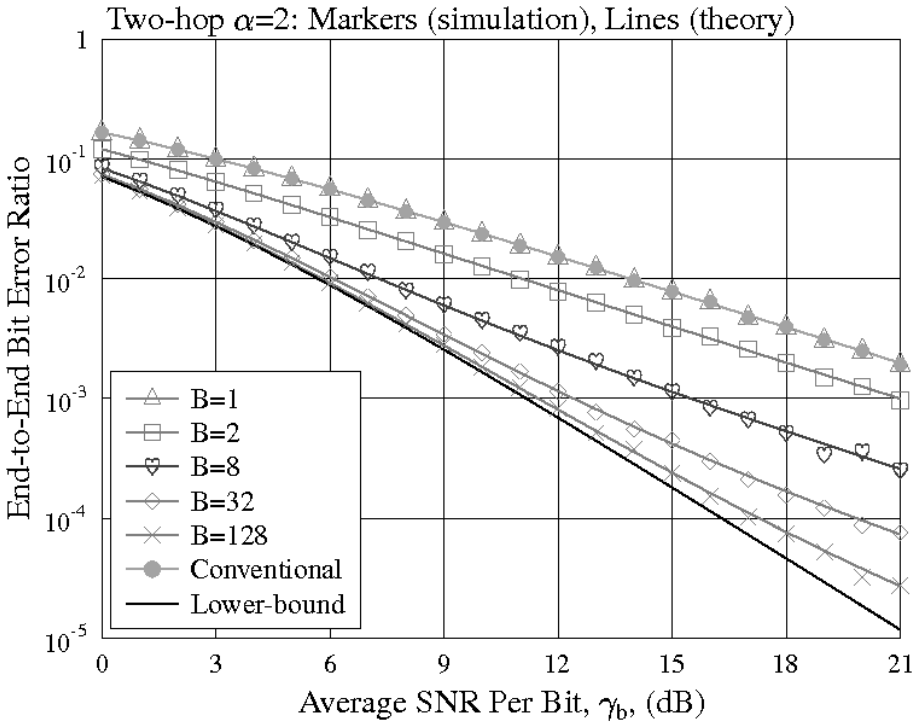

Figure 2.13: BER versus average SNR per hop performance of two-hop links with RNs having various buffer sizes, when communicating over Rayleigh fading channels. The results were evaluated from (2.11), (2.13) and (2.14). The markers represent simulation results while the lines represent theoretical results.

The first set of results characterizes the impact of the buffer size on the end-to-end BER performance. The results are plotted versus the average SNR per bit γ_b, which is actually the equivalent average SNR per bit for a single-hop link. In Figs. 2.13 and 2.14[3], multi-hop scenarios having two and four hops are characterized, respectively. In all these figures, the corresponding lower-bound end-to-end BER is also included. Furthermore, for comparison, the corresponding end-to-end BER of the conventional

[3]Note that, the BER curve when pathloss factor $\alpha = \alpha^\star$ can be obtained by moving the corresponding curve in all figures where $\alpha = 2$ to the right side $10(\alpha^\star - 2)\log 10(L)$dB.

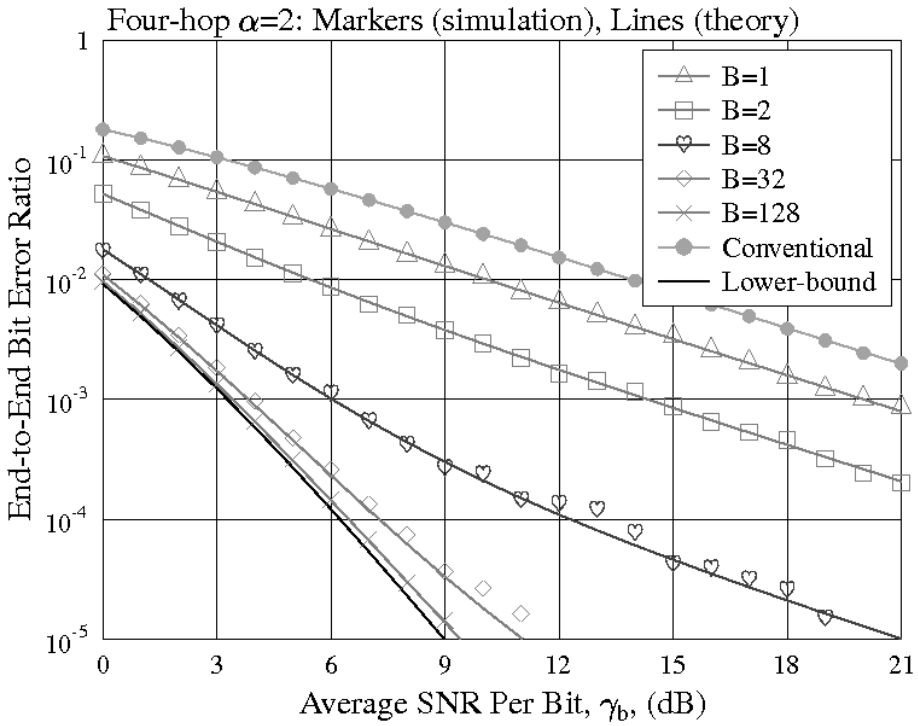

Figure 2.14: BER versus average SNR per hop performance of four-hop links with RNs having various buffer sizes, when communicating over Rayleigh fading channels. The results were evaluated from (2.11), (2.13) and (2.14). The markers represent simulation results while the lines represent theoretical results.

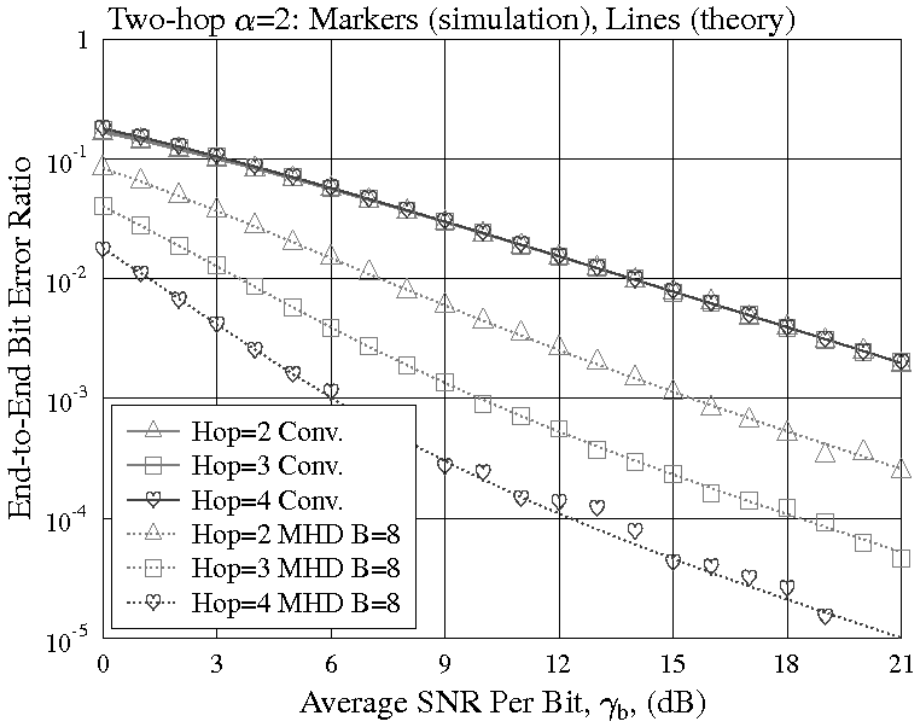

Figure 2.15: BER versus average SNR per hop performance of various number of hops at a buffer size of 'B=8', when communicating over Rayleigh fading channels. The results were evaluated from (2.11), (2.13) and (2.14). The markers represent simulation results while the lines represent theoretical results.

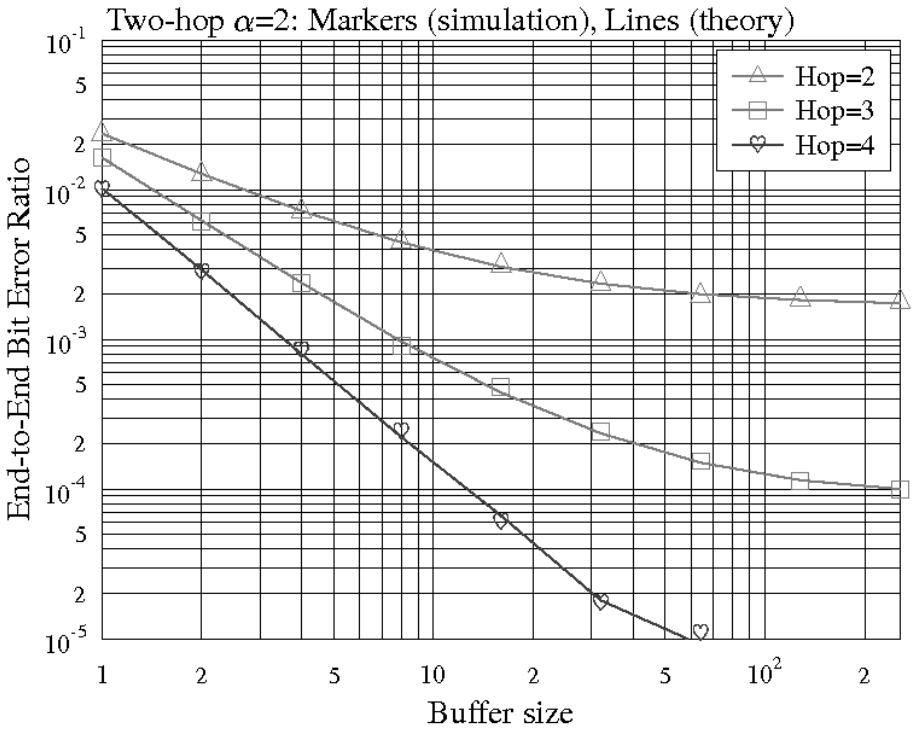

Figure 2.16: BER versus buffer size performance of various number of hop at $\gamma_b = 10dB$, when communicating over Rayleigh fading channels. The results were evaluated from (2.11), (2.13) and (2.14). The markers represent simulation results while the lines represent theoretical results.

multi-hop transmission scheme [175, 178] is shown in Figs. 2.13 and 2.14. Note that for the two-hop link considered in Figs. 2.13, the end-to-end BER of the conventional scheme is the same as that of the MHD scheme marked with '$B = 1$'. Fig. 2.15 shows the impact of the number of hops. The buffer size is '$B = 8$' in MHD. In Fig. 2.16, the impact both of the buffer size and of the number of hops is shown for $\gamma_b = 10dB$. Based on the results of Figures (2.13, 2.14 and 2.15), we may draw the following conclusions.

Firstly, MHD is attainable by equipping each of the RNs (also the SN that was assumed to have an infinite buffer) with a buffer. As expected, the diversity gain improves, as the buffer size of RNs increases, until reaching the lower-bound end-to-end BER corresponding to infinite buffers. Secondly, the lower-bound end-to-end BER may be approached by employing buffers of reasonable size, which depends on the actual SNR. Typically, for the two- and four-hop links considered, using the buffers of size $B = 32$ or 128 packets is capable of achieving most of the attainable MHD. Thirdly, even when the RNs employ small buffers, the achievable MHD may still be significant. Furthermore, when considering four-hop links (≥ 3 actually) MHD is attainable, even when each of the buffers can only store a single packet, i.e., for $B = 1$, as seen in Figs. 2.14. Quantitatively, observe in Fig. 2.14, for $B = 1$, the

MHD scheme proposed in this chapter is capable of yielding an approximately 3 dB performance gain in comparison to the conventional multi-hop transmission scheme.

Note again that the reason for the MHD scheme's ability to significantly outperform the conventional scheme is explicit. In the MHD scheme proposed in this chapter, the end-to-end BER performance improves as the number of hops increases owing to the increased MHD. By contrast, in the conventional multi-hop transmission scheme [175,178], the end-to-end BER performance remains the same regardless the number of hops, since the packets are transmitted from one node to another successively.

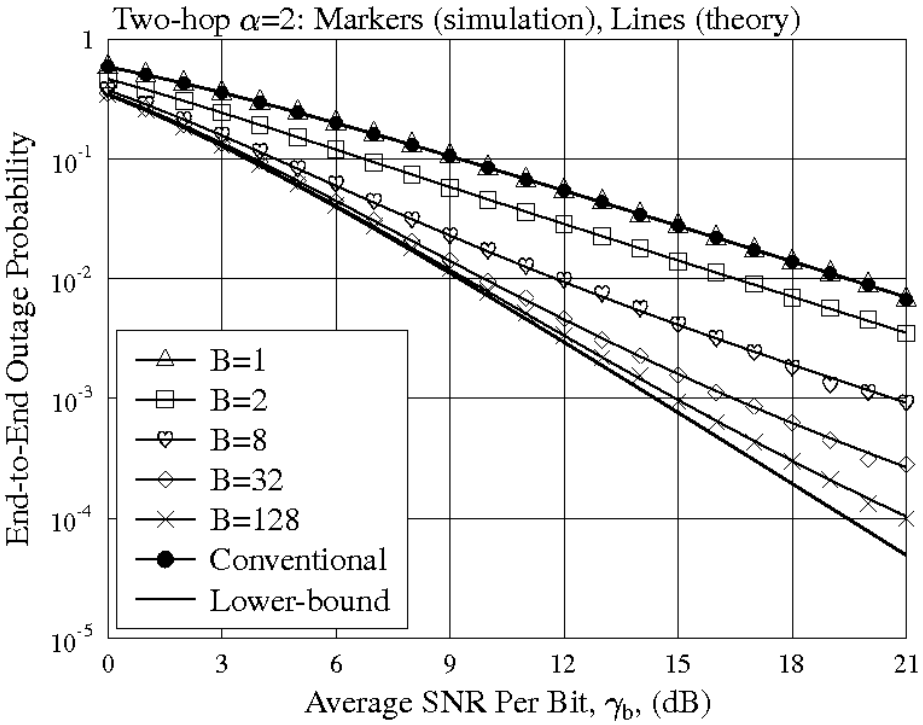

Figure 2.17: Outage probability versus average SNR per hop performance of two-hop links with RNs having various buffer sizes, when communicating over Rayleigh fading channels. The results were evaluated from (2.22) and (2.23). The markers represent simulation results while the lines represent theoretical results.

The second set of results characterizes the outage probability of MHLs, as shown in Figs. 2.17 2.18 2.19 and 2.20 for the $\alpha = 2, 3$ and two- and four-hop links, respectively, when RNs having various buffer sizes are considered. Note that, in our numerical computations and simulations, the threshold γ_T was adjusted to maintain a BER of 0.03 for a single-hop link. This definition is from [70].The corresponding lower-bound outage probability evaluated using (2.19) for the two- and four-hop links, respectively, is also shown in Figs. 2.17 2.18 and 2.19 2.20. Furthermore, the corresponding outage probability of the conventional MHLs is also provided for comparison. Figs. 2.21 and 2.22 compared the impact of both the buffer size and of the

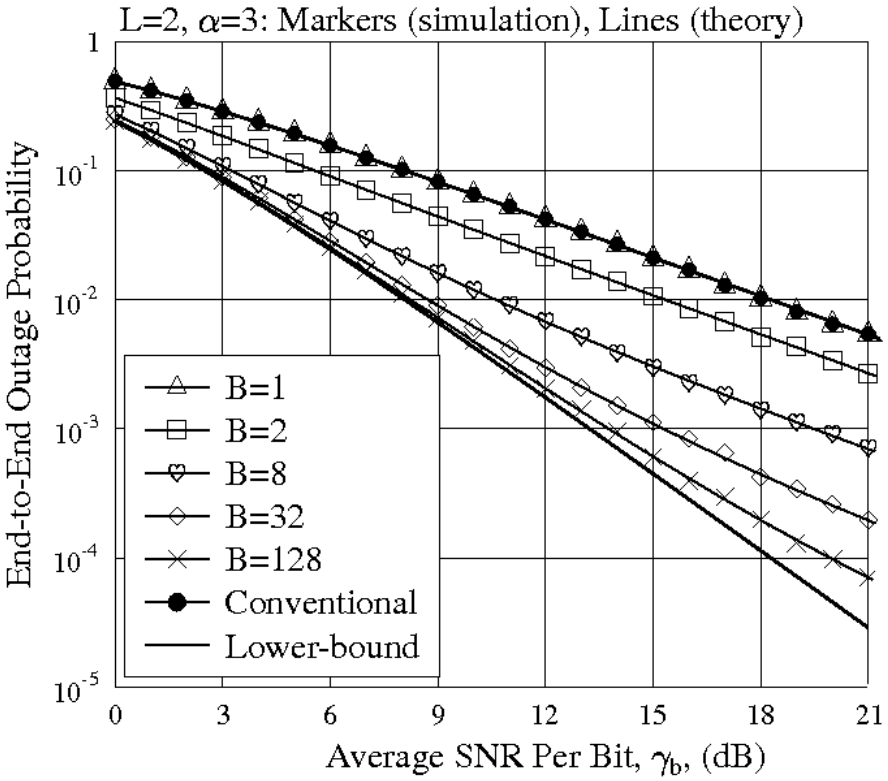

Figure 2.18: Outage probability versus average SNR per hop performance of two-hop links with RNs having various buffer sizes, when communicating over Rayleigh fading channels. The results were evaluated from (2.22) and (2.23). The markers represent simulation results while the lines represent theoretical results.

number of hops on the outage probability. From these results, we can draw similar observations to those drawn from Figs. 2.13, 2.14, 2.16 and 2.21. A significant MHD gain is attainable, when the RNs employ buffers of a sufficiently large size. Hence, the MHD transmission scheme proposed in this chapter outperforms the conventional multi-hop transmission scheme [175, 178].

Fig. 2.23 portrays the achievable diversity order for both an infinite theoretical bound and for finite buffers. The diversity order for infinite buffer is $DO = 2$, however this for any finite buffer is $DO = 1$. This is because if we have no selection diversity, this substantially degrades the BER, as shown in the Appendix of this Chapter.

Fig. 2.24 shows the PMF of packet delay, when MHLs relying $L = 2, 3, 4$ or 8 hops are considered. Note that for the sake of illustrating the results conveniently in a single figure, a similar maximum packet delay of about 100 TSs was stipulated by choosing the corresponding buffer sizes for the different number of hops. As shown in Fig. 2.24, when the number of hops increases, the PMF becomes more symmetric, reminiscent of the shape of the Gaussian or Gamma distribution. Furthermore, when the number of hops increases, the average packet delay increases.

In Fig. 2.25, the average packet delay of the MHD-aided MHLs relaying on $L =$

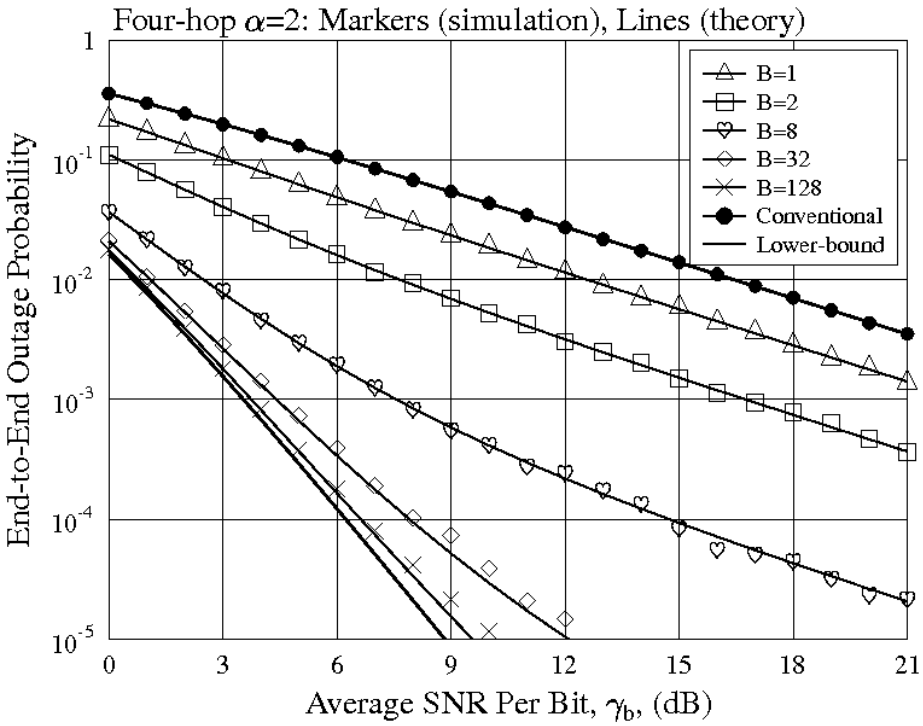

Figure 2.19: Outage probability versus average SNR per hop performance of four-hop links with RNs having various buffer size, when communicating over Rayleigh fading channels. The results were evaluated from (2.22) and (2.23). The markers represent simulation results while the lines represent theoretical results.

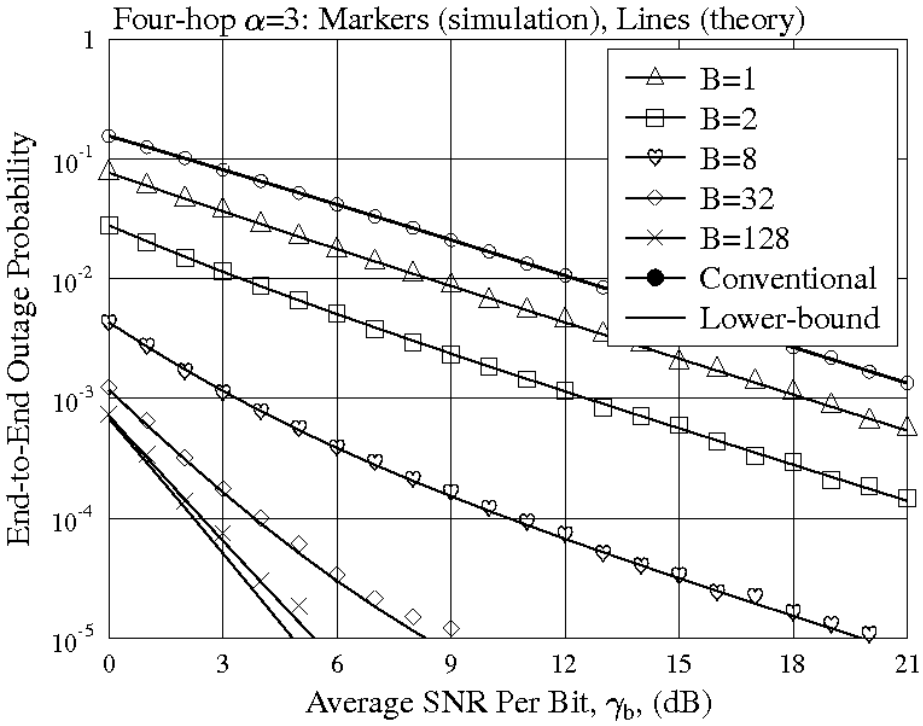

Figure 2.20: Outage probability versus average SNR per hop performance of four-hop links with RNs having various buffer size, when communicating over Rayleigh fading channels. The results were evaluated from (2.22) and (2.23). The markers represent simulation results while the lines represent theoretical results.

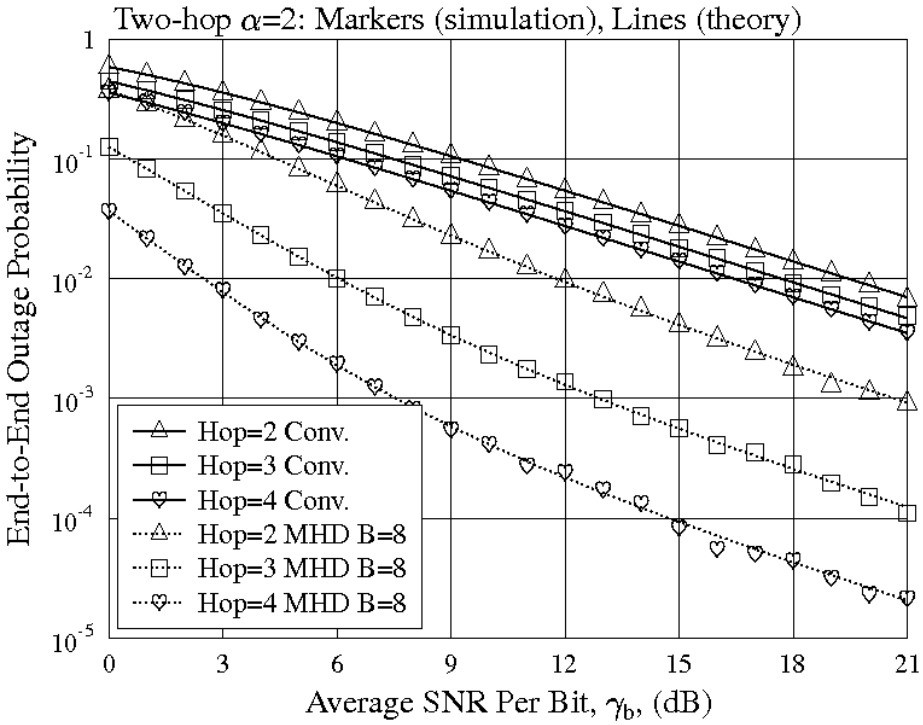

Figure 2.21: Outage probability versus average SNR per hop performance of various hops links with RNs having buffer size '$B = 8$', when communicating over Rayleigh fading channels. The results were evaluated from (2.22) and (2.23). The markers represent simulation results while the lines represent theoretical results.

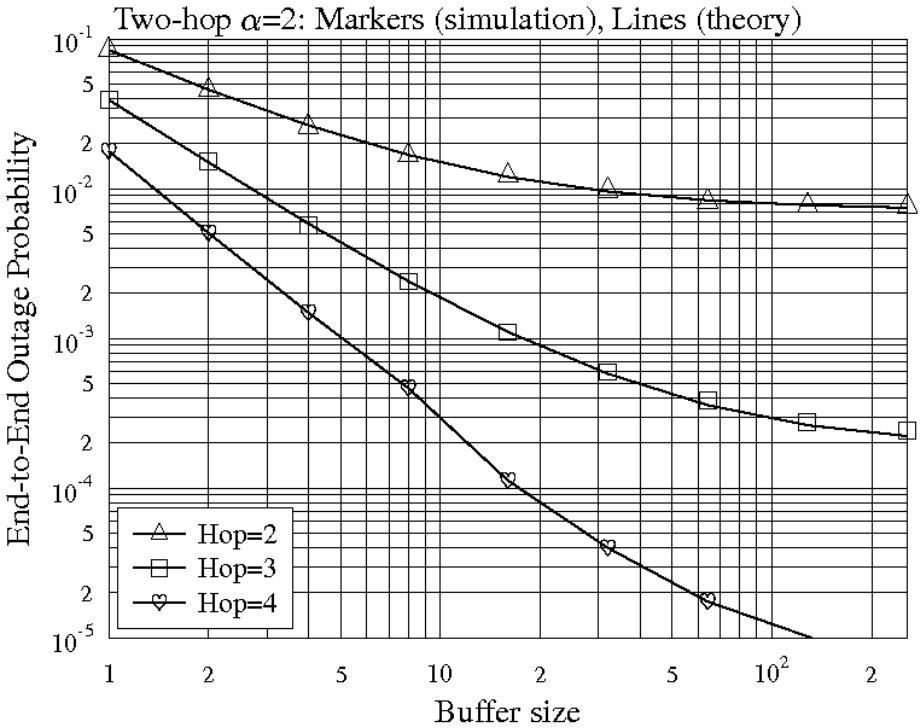

Figure 2.22: Outage probability versus buffer size performance of various number of hop at $\gamma_b = 10dB$, when communicating over Rayleigh fading channels. The results were evaluated from (2.22) and (2.23). The markers represent simulation results while the lines represent theoretical results.

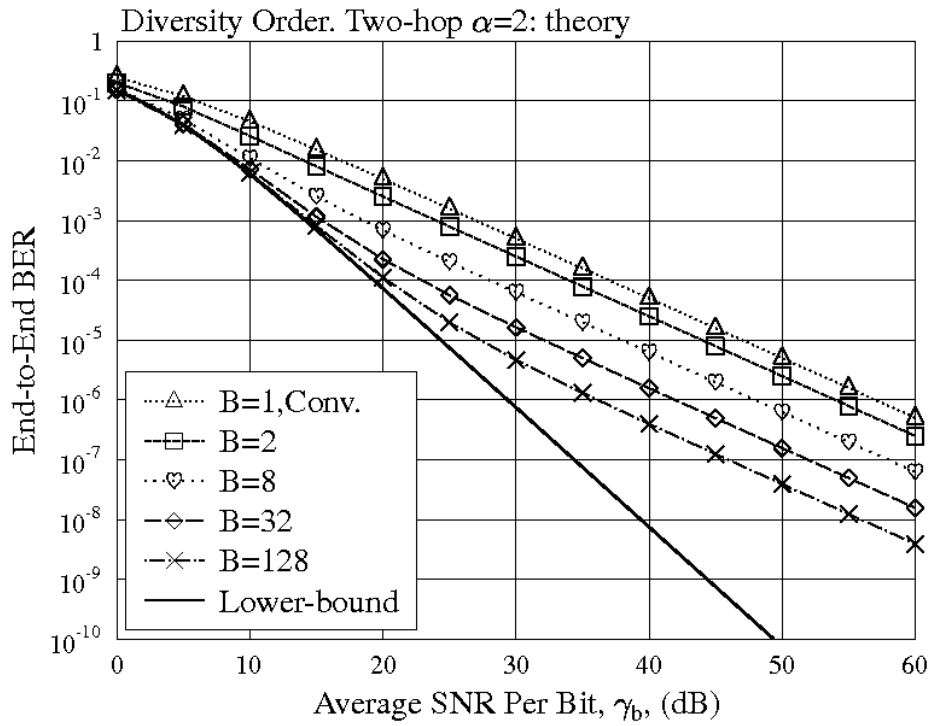

Figure 2.23: This figure shows the diversity order for a two-hop link when $\alpha = 2$. The diversity order for theoretical bound is 2, however the diversity order for any finite buffer is 1. All curves in this figure are generated by theory formula. The results were evaluated from (2.27) and (2.28).

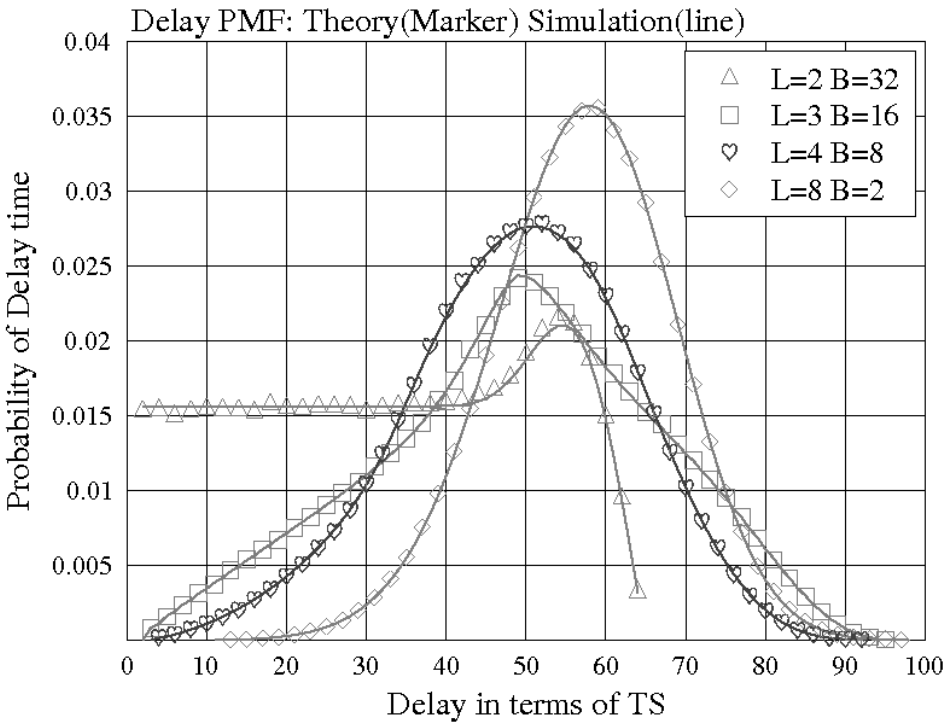

Figure 2.24: The delay's PMF for MHLs having $L = 2, 3, 4$ or 8 hops. The results were evaluated from (2.34). The markers represent simulation results while the lines represent theoretical results.

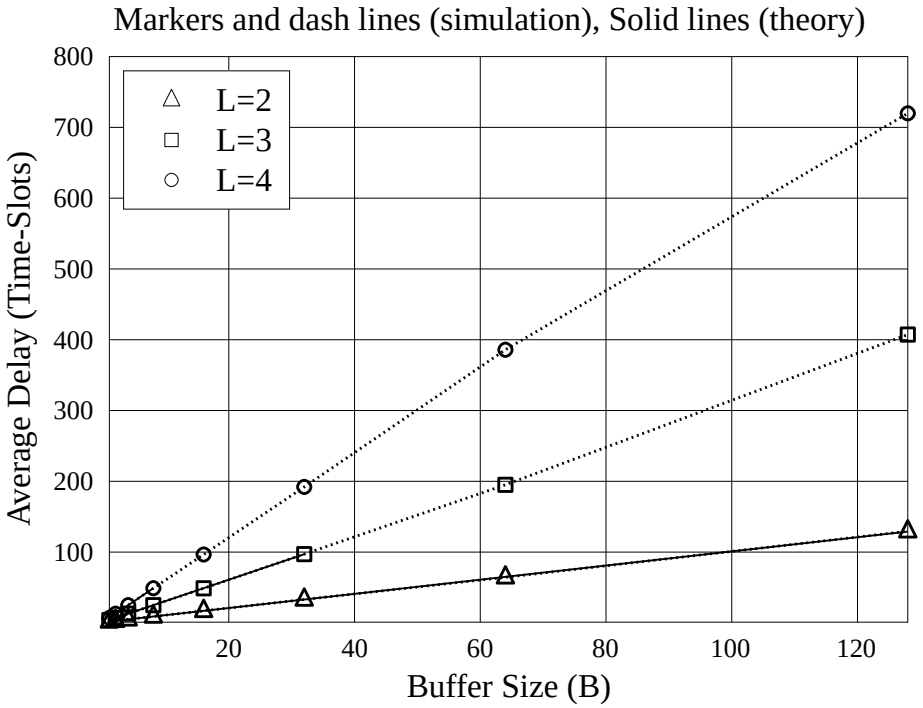

Figure 2.25: Average delay of the MHD-aided MHLs having $L = 2, 3$ or 4 hops, when communicating over independent Rayleigh fading channels. The results were evaluated from (2.34) and (2.35). The markers represent simulation results while the lines represent theoretical results.

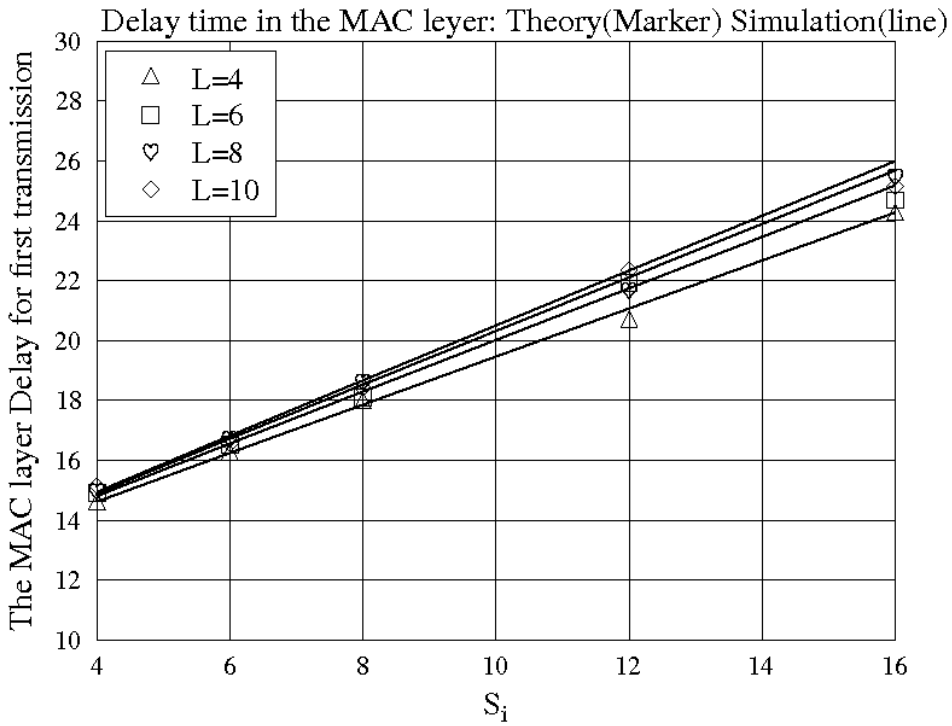

Figure 2.26: Average delay for the first transmission versus S_i^{cql} in the MAC layer. The results were evaluated from (2.2). The markers represent simulation results while the lines represent theoretical results.

2, 3 or 4 hops is depicted. The results illustrate that the average packet delay linearly increases with the RNs' buffer size. Furthermore, as seen in Figs. 2.24 and 2.25, the packet delay may become significantly longer than the time required by the conventional multi-hop scheme to deliver a packet from the SN to the DN. However, we have highlighted in Section 2.4.4 that, given a MHL, the MHD scheme and the conventional multi-hop transmission scheme exhibit the same block delay. This implies that given a block of packets, the number of TSs for the DN to receive all the packets is the same for both the MHD scheme and the conventional multi-hop transmission scheme. The difference between the MHD scheme and the conventional multi-hop transmission scheme is that in the MHD scheme, one packet is received by the DN within L TSs on average, which is in contrast to the conventional multi-hop transmission scheme, where the DN receives exactly one packet per L TSs.

Finally, Fig. 2.26 characterizes the delay of the first transmission in the MAC layer, which increases with S_i^{cql}, while the delay remains roughly the same, regardless the number of hops. Note that the delay of the first transmission is significantly lower than the maximum MAC layer delay. For example, the maximum delay in the MAC layer for $L = 8$ and $S_i^{cql} = 8$ is $S_i^{cql} * L + 9 + 2 = 75$ symbol durations, while the delay of the first transmission is 18.6 symbol duration. If 500 symbols are transmitted in one time slot, the delay of the first transmission becomes $\frac{18.6}{500} = 3.7\%$ of one TS.

2.6 Chapter Conclusions

In this chapter, we have proposed and investigated a MHD scheme and designed a MAC layer protocol for it. The system relied on storing data in the RNs, as evidenced in Section 2.1. In Section 2.3, a decentralized MAC layer protocol was constructed for supporting this buffer-aided transmission. Then, in Section 2.4, the BER, the outage probability and the delay of MHLs have been analyzed and a range of formulas have been obtained, when assuming that BPSK signals are transmitted over all the hops, which experience i.i.d Rayleigh fading. As seen in Fig. 2.13, Fig. 2.14 and Fig. 2.17 - Fig. 2.20, our performance results show that exploiting the independent fading of multiple hops results in a significant diversity gain. Given an L-hop link, the MHD scheme is capable of achieving an Lth order diversity, when each RN has a buffer of sufficient size and data blocks of sufficiently large size are transmitted. It can be shown in these figures that the maximum MHD may be approached, when each RN has a moderate buffer size. The MHD scheme significantly outperforms the conventional multi-hop transmission arrangement in terms of the BER/outage performance, when sufficiently large buffers are considered.

In the context of delay, given an L-hop link, both the MHD scheme and the conventional multi-hop transmission scheme impose the same block delay. In the MHD scheme, the DN receives one packet per L TSs on average. By contrast, when employing the conventional multi-hop transmission scheme, the MHL delivers exactly one packet to the DN per L TSs. However, the MHD scheme may impose significantly longer packet delays than the conventional multi-hop transmission scheme, as evidenced in Fig. 2.24 and Fig. 2.25.

The performance of buffer-aided transmissions was characterized in this Chapter under a range of idealized simplifying assumptions. In the next chapter, the modulation scheme will be extended from BPSK to MQAM and the fading channel model will be the Nakagami-m channel model.

2.7 Appendix

2.7.1 Derivation of $P_{L,e}$ in (2.7)

The derivation of single hop lower bound BER $P_{L,e}$ in (2.7) is

$$
\begin{aligned}
P_{L,e} =& \int_0^\infty Q(\sqrt{2\gamma})\frac{L}{\gamma_h}\exp\left(-\frac{\gamma}{\gamma_h}\right)\left[1-\exp\left(-\frac{\gamma}{\gamma_h}\right)\right]^{L-1}d\gamma \\
=&\frac{L}{\gamma_h}\sum_{l=0}^{L-1}(-1)^l\binom{L-1}{l}\int_0^\infty Q(\sqrt{2\gamma})\exp(-\frac{(l+1)\gamma}{\gamma_h})d\gamma \\
=&\frac{L}{\gamma_h}\sum_{l=0}^{L-1}(-1)^l\binom{L-1}{l}\int_0^\infty Q(\sqrt{2\gamma})\gamma_h\frac{-1}{l+1}d\exp(-\frac{(l+1)\gamma}{\gamma_h}) \\
=&L\sum_{l=0}^{L-1}\frac{(-1)^{l+1}}{l+1}\binom{L-1}{l}\left(Q(\sqrt{2\gamma})\exp(-\frac{(l+1)\gamma}{\gamma_h})|_0^\infty-\int_0^\infty\exp(-\frac{(l+1)\gamma}{\gamma_h})dQ(\sqrt{2\gamma})\right) \\
=&L\sum_{l=0}^{L-1}\frac{(-1)^{l+1}}{l+1}\binom{L-1}{l}\left(\frac{1}{2}-\int_0^\infty\exp(-\frac{(l+1)\gamma}{\gamma_h})\frac{1}{\sqrt{2\pi}}(-1)\exp(\frac{-2\gamma}{2})d\sqrt{2\gamma}\right) \\
=&L\sum_{l=0}^{L-1}\frac{(-1)^{l}}{l+1}\binom{L-1}{l}\left(\frac{1}{2}-\frac{1}{\sqrt{2\pi}}\int_0^\infty\exp(-\gamma\frac{l+1+\gamma_h}{\gamma_h})d\sqrt{2\gamma}\right) \\
\overset{\gamma=t^2}{=}&L\sum_{l=0}^{L-1}\frac{(-1)^{l}}{l+1}\binom{L-1}{l}\left(\frac{1}{2}-\sqrt{2}\sqrt{\frac{\gamma_h}{2(l+1+\gamma_h)}}\right. \\
&\left.\times\underbrace{\left(\frac{1}{\sqrt{2\pi}\sqrt{\frac{\gamma_h}{2(l+1+\gamma_h)}}}\int_0^\infty\exp(-\frac{t^2}{2(\sqrt{\frac{\gamma_h}{2(l+1+\gamma_h)}})^2})dt\right)}_{\text{Positive side of Normal distribution, }\frac{1}{2}}\right) \\
=&\frac{L}{2}\sum_{l=0}^{L-1}\frac{(-1)^{l}}{l+1}\binom{L-1}{l}\left(1-\sqrt{\frac{\gamma_h}{l+1+\gamma_h}}\right) \\
=&\frac{1}{2}\sum_{l=0}^{L}(-1)^l\binom{L}{l}\sqrt{\frac{\gamma_h}{l+\gamma_h}}.
\end{aligned}
\tag{2.36}
$$

Now, we have the close-form express of $P_{L,e}$.

2.7.2 Proof of the Domination of $P_e(1)$ in (2.13) at High SNR

When the SNR is high, the $\sqrt{\frac{\gamma_h}{\gamma_h+1+l}}$ in (2.13) can be approximately expressed as

$$\begin{aligned}\sqrt{\frac{\gamma_h}{\gamma_h+1+l}} \approx & \frac{1}{\sqrt{1+\frac{l+1}{\gamma_h}+\underbrace{\frac{(l+1)^2}{(2\gamma_h)^2}}_{\approx 0}}} \\ =&\frac{1}{1+\frac{l+1}{\gamma_h}} \\ =&1-\frac{1}{2\gamma_h} \end{aligned} \tag{2.37}$$

Then put (2.37) into (2.13), we have

$$\begin{aligned} P_e(m) \approx & \frac{1}{2}-\frac{m}{2}\sum_{l=0}^{m-1}\frac{(-1)^l}{l+1}\binom{m-1}{l}(1-\frac{1}{2\gamma_h}) \\ =&\frac{1}{2}-\frac{m}{2}\sum_{l=0}^{m-1}\frac{(-1)^l}{l+1}\binom{m-1}{l}+\frac{m}{2}\sum_{l=0}^{m-1}\frac{(-1)^l}{l+1}\binom{m-1}{l}\frac{l+1}{2\gamma_h} && (2.38)\\ =&\frac{1}{2}-\frac{1}{2}\sum_{l=0}^{m-1}(-1)^l\frac{m!}{l!(m-l-1)!}+\frac{m}{4\gamma_h}\sum_{l=0}^{m-1}(-1)^l\binom{m-1}{l} && (2.39)\\ =&\frac{1}{2}+\frac{1}{2}\sum_{l=0}^{m}(-1)^l\frac{m!}{l!(m-l)!}-\frac{1}{2}+\frac{1}{4\gamma_h}(1-1)^{m-1} && (2.40)\\ =&\frac{1}{2}+\frac{1}{2}(1-1)^m-\frac{1}{2} && (2.41)\\ =&0+\frac{1}{4\gamma_h}0^{m-1}, && (2.42)\\ & && (2.43)\end{aligned}$$

hence $P_e(m)=0, m>1$ and $P_e(1)=\frac{1}{4\gamma_h}$. Therefore, $P_e(1)$ dominate the P_e which is why the diversity order of no selection diversity order dominate the result in high SNR. As a result, the diversity order for finite buffer is 1 in high SNR regardless the total number of the link.

Chapter 3

Multi-Hop Diversity Aided Multi-Hop QAM Links for Nakagami-m Channels

In Chapter 2, the buffer-aided multihop link of Figure 2.1 was proposed for achieving multihop diversity, where the specific hop having the highest channel SNR was activated. The transmitted signal in Chapter 2 was assumed to be a BPSK signal and the channel experienced independent block-based flat Rayleigh fading. Although this transmission scheme was capable of achieving multihop diversity, in practice each hop's fading distribution is non-identical. Hence, for the sake of solving this problem, in this chapter a cumulative distribution function (CDF) based hop-activation scheme was proposed for guaranteeing that the number of input packets is the same as the number of output packets for each RN, when each hop experienced independent but non-identical distributed (i.n.i.d) flat Nakagami-m fading. Furthermore, the BPSK scheme of Chapter 2 is upgraded to MQAM.

3.1 Introduction

In [168, 183, 184], we have proposed a multihop diversity (MHD) scheme by exploiting the independent fading experienced by the different hops of a MHL. The studies demonstrated that significant performance improvements may be attainable in comparison to the conventional multi-hop transmission scheme. In [168, 183, 184], we assumed that all hops have the same distance and also experience the same fading CDF. Under these assumptions, during each TS, the specific hop having the highest instantaneous SNR was selected from the set of available hops and, then a packet was transmitted over the selected hop. Explicitly, this MHD scheme achieved selection

diversity. Furthermore, all the hops have the same probability to be chosen during a TS, which is desirable for attaining the maximum possible throughput and minimum possible transmission delay.

As a further development of our work in [168, 183, 184], in this chapter, we generalize both the system model and the corresponding MHD scheme studied in [168, 183, 184]. In the context of the system model, we now consider the general MHLs, where different hops may have different distances and may also experience different fading. When selecting a hop for transmission based on the instantaneous SNRs of the hops invoked, as in [168,183,184], it will result in the hops being selected with different probabilities. Explicitly, a hop having a higher average SNR owing to experiencing less severe fading has a higher chance of being activated than a hop having a lower average SNR. Clearly, this is undesirable. In order to circumvent this impediment, while still benefitting from MHD, our MHD scheme proposed in this chapter opts for activating a hop for transmission according to the instantaneous probability values provided by the SNR's cumulative distribution functions (CDFs) of the available hops. To be more specific, let us assume that L hops are available for selection, where we assume having the knowledge of the L Nakagami-m parameters of $m_1, m_2, \ldots, m_L$ and the knowledge of the L SNR values of $\gamma_1, \gamma_2, \ldots, \gamma_L$. Therefore, the SNR CDF ordinate values of $F_{m_l}(\gamma_l),\ l = 1, 2, \ldots, L$, can be calculated. Then, the hop having the highest CDF ordinate value is selected for transmitting a packet within the TS. This way we can avoid granting a higher transmission probability to the links subjected to benign fading. To elaborate a little further, activating always the highest-SNR link would potentially lead to buffer-overflow for the severely fading lower-SNR links. More explanation, it is possible that a higher SNR γ_l actually maps to a lower $F_{m_l}(\gamma_l)$ ordinate value, even if the fading parameter m_l is higher, because the fading is less severe. In this way, it can be shown that all L hops have the same probability to be chosen, regardless of the specific fading parameter m_l experienced by them. Note however that if all hops have the same average SNR and also experience the same fading CDF, implying that all hops have the same SNR CDF, our CDF-assisted MHD scheme proposed in this chapter becomes equivalent to the MHD scheme considered in [168,183,184]. This is, because in this case a higher instantaneous SNR generates a higher CDF value.

In this chapter, we study the performance of the MHLs employing our proposed MHD scheme, when assuming that the different hops may experience different fading CDF modeled by Nakagami-m distributions associated with different fading parameters. We analyze both the BER and outage probability of the MHLs employing M-ary quadrature amplitude modulation (MQAM), when either buffers of limited

or unlimited size are used. We derive both the lower-bound expression and the exact expressions for them. Furthermore, approximation technologies are proposed for the efficient evaluation of both the BER and of the outage probability. Additionally, we demonstrate that our proposed MHD scheme is capable of achieving the full multi-hop diversity. Our performance results demonstrate that the CDF-assisted MHD scheme has the potential of providing a significant diversity gain for improving the reliability of multihop communications, hence both the attainable BER and the outage performance can be enhanced.

Additionally, we noted that, as analyzed in [168], once a SN completes its transmission, an increased buffering-induced delay is imposed, as the RNs need to empty their buffered packets. This process makes the overall delay is higher than that of the conventional multihop transmission scheme [178]. However, for the transmission of a sufficiently large amounts of data, the multihop diversity scheme does not have to strike an explicit trade-off between the delay tolerated and the achievable error/outage performance on average, because the MHD scheme transmits a single packet over a single hop per time-slot, which is identical to the conventional multihop transmission scheme.

The contributions of this chapter are summarized as follows:

1. A CDF-assisted MHD scheme is proposed, which makes use of the multiple hops of a MHL for enhancing the reliability of information delivery over the MHL.

2. The end-to-end BER and end-to-end outage probability of MHLs are analyzed, when the signal is transmitted using MQAM. A range of expressions for both the lower-bound and for the exact BER as well as for the lower-bound and the exact outage probability.

3. An approximate algorithm is provided for evaluating the steady-state probabilities that are required for computing both the end-to-end BER and the end-to-end outage probability.

4. We demonstrate that for an L-hop link, the achievable diversity order is L.

The remainder of this chapter is organized as follows. In the next sections, we present both our system model and the implementation of the MHD scheme. Section 3.3 analyzes both the BER and the outage probabilities. In Section 3.4, we provide our numerical and simulation results. Finally, our conclusions are offered in Section 3.5.

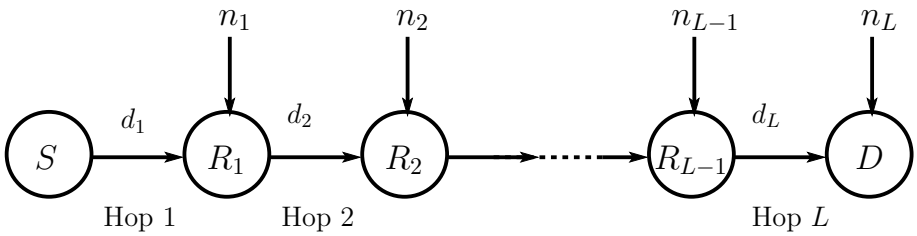

Figure 3.1: System model for a multihop wireless link, where the source S sends messages to the destination D via $(L-1)$ intermediate relays.

3.2 System Model of Multi-Hop Links

The system model under consideration is a typical multi-hop wireless link [175, 178], which is shown in Fig. 3.1. The MHL consists of $(L+1)$ nodes, a SN S (node 0), $(L-1)$ RNs $R_1, R_2, \ldots, R_{L-1}$ and a DN D (node L). The distance of the lth hop between nodes $(l-1)$ and l is $d_l,\ l = 1, \ldots, L$, and the total distance or the distance between SN and DN is $d = \sum_{l=1}^{L} d_l$. The SN S sends its information to the DN D via L hops with the aid of the $(L-1)$ RNs. At the RNs, the classic decode-and-forward (DF) protocol is employed for relaying the signals. For convenience, we denote the symbol transmitted by node 0 as x_0 and its estimate at the DN D of node L by $x_L = \hat{x}_0$, while the symbol estimated at the lth RN by $x_l,\ l = 1, \ldots, L-1$. At packet level, they are correspondingly represented by $\boldsymbol{x}_0$, $\boldsymbol{x}_l,\ l = 1, \ldots, L-1$, and $\boldsymbol{x}_L = \hat{\boldsymbol{x}}_0$. We assume baseband BPSK/MQAM modulation and that the signals are transmitted on the basis of TSs having a duration of T seconds. In addition to propagation pathloss, the channels of the L hops are assumed to experience independent block-based flat Nakagami-m fading, where the complex-valued fading envelope of a hop remains constant within a TS, but it is independently faded for different TSs. Based on the above assumptions, when the $(l-1)$st node transmits a packet $\boldsymbol{x}_{l-1}$, the observations received by node l can be expressed as

$$\boldsymbol{y}_l = h_l \boldsymbol{x}_{l-1} + \boldsymbol{n}_l,\ l = 1, 2, \ldots, L, \tag{3.1}$$

where h_l represents the channel gain of the lth hop from node $(l-1)$ to node l, while $\boldsymbol{n}_l$ denotes the Gaussian noise at node l. When communicating over Nakagami-m fading channels, $|h_l|$ obeys the Nakagami-m distribution with the probability density function (PDF) [185]

$$f_{|h_l|}(y) = \frac{2m_l^{m_l}}{\Gamma(m_l)} y^{2m_l-1} \exp\left(-m_l y^2\right),\ y \geq 0 \tag{3.2}$$

where $\Gamma(\ldots)$ denotes the gamma function [10](8.310.1), $E\left[|h_l|^2\right] = 1$ and m_l is the Nakagami-m fading parameter of the lth hop. As shown in [33], the Nakagami-m fading can be used for modelling of different types of fading channels, which are characterized by the associated fading parameter m. Specifically, the Nakagami-m fading reduces to the Rayleigh fading when $m = 1$, $m \to \infty$ corresponds to the conventional Gaussian scenario, and $m = 1/2$ describes the so-called one-side Gaussian fading, i.e., the worst-case fading condition. The Rician and lognormal distributions can also be closely approximated by the Nakagami distribution in conjunction with values of $m > 1$. In (3.2), the background noise samples in $\boldsymbol{n}_l$ obey the complex Gaussian distribution with zero mean and a variance of $\sigma_l^2 = 1/(2\bar{\gamma}_l)$ per dimension. Here, $\bar{\gamma}_l$ denotes the average SNR of the lth hop, which is dependent on the propagation pathloss experienced by the lth hop.

Let us consider a given TS. The corresponding instantaneous SNR values of the L hops are expressed as $\{\gamma_1, \gamma_2, \ldots, \gamma_L\}$, where $\gamma_l = |h_l|^2\bar{\gamma}_l,\ l = 1, \ldots, L$. Then, given the PDF of $|h_l|$ as shown in (3.2), the PDF and CDF of γ_l can be readily derived, which are

$$f_l(\gamma_l) = \frac{1}{\Gamma(m_l)} \left(\frac{m_l}{\bar{\gamma}_l}\right)^{m_l} \gamma_l^{m_l-1} \exp\left(-\frac{m_l\gamma_l}{\bar{\gamma}_l}\right),\ \gamma_l \geq 0, \tag{3.3}$$

$$F_{m_l}(\gamma_l) = \frac{\gamma(m_l, \frac{m_l\gamma_l}{\bar{\gamma}_l})}{\Gamma(m_l)},\ \gamma_l \geq 0. \tag{3.4}$$

where $\gamma(a, x)$ is the incomplete gamma function [37].

Given the SNRs, $\gamma_1, \gamma_2, \ldots, \gamma_L$, of the L hops within a TS, in our multi-hop transmission scheme, the packets are transmitted over the MHLs based on the following strategy. Among those hops, whose transmitter buffers have packets awaiting transmission and whose receivers are ready for reception, the MHD protocol first decides, which of the L CDFs, $F_{m_1}(\gamma_1), F_{m_2}(\gamma_2), \ldots, F_{m_L}(\gamma_L)$, has the highest value. Then, a packet is transmitted over the specific hop having the highest CDF ordinate value using a TS. Explicitly, according to this strategy, the packets are transmitted following the classic time-division principles, hence transmitting a packet from the SN S to the DN D requires a total of L TSs.

As mentioned in Section 3.1, we have proposed a MHD scheme in [168,184], which selects the specific hop having the highest SNR for transmitting a packet within a TS, which effectively implements selection diversity. In the MHD scheme proposed in [168, 184], we assumed that all the hops have the same average SNR and their channels experience the same fading, implying that the SNRs of all the hops obey the same CDF. Hence, the selection procedure directly based on the SNRs of the L hops

would give each hop the same probability of $1/L$ to be chosen. By contrast, in this chapter, the SNRs of the L hops obey different distributions, which depend on the L parameters m_l, for $l = 1, 2, \ldots, L$. In this case, directly selecting the hop having the highest SNR would result in different activation probabilities for the L links. Again, this is undesirable, since the hops chosen with relatively low probabilities may impose significant delays on the packet delivery, potentially resulting in a low throughput and possible buffer-overflow. Therefore, our proposed MHD scheme activates the specific hop, whose SNR maps to the maximum CDF ordinate value from the set $F_{m_1}(\gamma_1), F_{m_2}(\gamma_2), \ldots, F_{m_L}(\gamma_L)$, so that each hop has the same probability of $1/L$ to be chosen for transmission within a TS.

Let us consider the example of non-identical hop's fading distribution. Assuming the fading parameters of $m = [3\ 2\ 1]$ for these hops and that the average received SNR for all hops is $\gamma_l = 1, l = 1, 2, 3$, the selection criterion based on the CDF ordinate value is given by $max\{F_1(0.5)\ F_2(1.3)\ F_3(0.7)\}$ $=max\{0.19\ 0.73\ 0.5\}$. Therefore the second hop is selected. It is worth nothing that a higher SNR γ_l might actually map to a lower $F_{m_l}(\gamma_l)$ value, if the high-SNR-hop's fading parameter m_l is lower, for example, if we have $F_1(0.5) > F_2(0.6)$.

Given the set of independent CDFs $F_{m_1}(\gamma_1), F_{m_2}(\gamma_2), \ldots, F_{m_L}(\gamma_L)$ corresponding to L hops, the proof that any hop is selected with a probability of $1/L$ is as follows. Let us define a new random variable $X_j = F_{m_j}(\gamma_j)$ as the CDF of γ_j which constitutes our selection criterion. It may be readily shown that X_j are i.i.d for the different hops. In fact, the CDF of X_j is expressed by

$$\begin{aligned} F_{X_j}(x) &= P(X_j <= x) \\ &= P(F_{m_j}(\gamma_j) <= x) \\ &= P(\gamma_j <= F_{m_j}^{-1}(x)) \text{(since the CDF is always an increasing function)} \\ &= F_{m_j}(F_{m_j}^{-1}(x)) \text{(by definition)} \\ &= x \text{ independent of } j, \end{aligned} \tag{3.5}$$

where $F^{-1}(\ldots)$ denotes the inverse function of the CDF $F(\ldots)$. Therefore, X_j are i.i.d (we already know that they are independent). Hence, we can say that the probability of selecting any hop is $\frac{1}{L}$. In addition to the above property, this MHD scheme also has the following pair of desirable properties. Firstly, when the SNRs of all hops have the same CDF, selecting the hop with the maximum SNR from the set $\gamma_1, \gamma_2, \ldots, \gamma_L$ is equivalent to selecting the hop with the maximum CDF value, since this maximum CDF value is generated by the maximum SNR in the set of $\gamma_1, \gamma_2, \ldots, \gamma_L$. Secondly, our forthcoming discourse will demonstrate that similarly to

the MHD scheme of [168,184] the proposed MHD scheme is also capable of achieving full diversity. Based on the above properties, the MHD scheme proposed in this chapter may be viewed as a generalized MHD scheme, which achieves full multihop diversity, while guaranteeing that all hops have the same probability to be activated for transmission.

Note additionally that in [168] a MAC layer protocol was proposed for the implementation of the MHD scheme. This MAC layer protocol can be directly used for the MHD scheme proposed in this chapter, after replacing $\gamma_1, \gamma_2, \ldots, \gamma_L$ of [168] by $F_{m_1}(\gamma_1)$, $F_{m_2}(\gamma_2)$, $\ldots$, $F_{m_L}(\gamma_L)$.

Having described the system model and the MHD scheme, below we focus our attention on the MHLs' performance, including its BER, outage probability as well as diversity order. The main assumptions adopted in our study are summarized as follows:

- The SN always has packets to send, hence the MHL operates in its steady state.
- The DN D can store an infinite number of packets, while the RNs can only store at most B packets.
- The fading processes of the L hops of a MHL are independent, while the fading of a given hop remains constant within a packet duration, but it is independently faded from one packet to another.

3.3 Performance Analysis

In this section, we first derive the lower-bound for the BER of the MHLs conveying BPSK/MQAM baseband signals. Then, the BER for the MHLs relying on the RNs having a buffer size B is analyzed. Similarly, the lower-bound and exact outage probabilities are analyzed in this section. Due to the complexity to evaluate the exact BER and outage probability, when L and B are large, an approximation approach is proposed. Finally, the diversity order of our MHD scheme is derived.

Based on Fig. 3.1 and the operational principles of the MHLs described in Section 3.2, the following events may occur, when every RN has a buffer size of B packets. Firstly, the buffer of a RN may be empty at some instants. In this case, this RN cannot be the transmit node, since it has no packets to transmit. Secondly, the buffer of a RN may be full. Then, this RN cannot act as the receiver node, since its buffer is unable to store further packets. In both of the above cases, a hop has to be chosen for transmission from the resultant reduced set of hops. This results in an increased BER and outage probability due to the associated reduced selection diversity gain, as explained in our forthcoming discourse. Therefore, if we eliminate

the above-mentioned constraints by assuming that every RN has an infinite buffer size, and that all the RNs can always transmit and receive packets, we can obtain the lower-bounds for both the BER and the outage probability of the MHLs. By contrast, when the exact performance analysis is considered, the effects of the finite buffer size have to be considered. In this case, we can carry out the relevant analysis based on the classic Markov chains [110]. Let us first analyze the achievable BER.

3.3.1 Bit Error Ratio Analysis

In this section, the lower-bound single-hop BER for the lth hop, expressed as $P_{Le}^{(l)}$, is analyzed first, when every RN is assumed to have an infinite buffer for storing the received packets and also always have packets prepared for transmission. Then, the end-to-end lower-bound BER, P_{LE}, is derived, where the subscript 'LE' stands for 'lower-bound error rate'. Finally, the near exact single-hop and end-to-end BER are derived, when assuming that the RNs have buffers of finite size.

Based on the operational principles of the MHLs and the identical selection probability of every hop, when the lth hop is activated, the instantaneous SNR of the selected hop obeys

$$f_l^{SC}(\gamma) = \frac{L}{[\Gamma(m_l)]^L}\left(\frac{m_l}{\bar{\gamma}_l}\right)^{m_l}\gamma^{m_l-1}\left[\gamma(m_l,\frac{m_l\gamma}{\bar{\gamma}_l})\right]^{L-1}\exp\left(-\frac{m_l\gamma}{\bar{\gamma}_l}\right), \quad 0\le\gamma<\infty;\ l=1,2,\ldots,L. \tag{3.6}$$

It is interesting to observe from (3.6) that if the lth hop is selected based on our MHD scheme, the PDF of its SNR is independent of the other $(L-1)$ channels. This conditional PDF is identical to that encountered, when the L hops experience the same fading CDF as the lth hop. Furthermore, we can see that (3.6) is in fact the PDF of the maximum SNR selected from the set of SNRs $\{\gamma_1,\gamma_2,\ldots,\gamma_L\}$, when these SNRs obey independent identical distribution (i.i.d) with the PDF and CDF as given by (3.3). Hence, our MHD scheme effectively emulates a selection diversity scheme. The more hops are invoked, the higher the diversity gain becomes and therefore the better the BER performance becomes. Hence, when all the L hops are assumed to be always available for activation, the BER obtained represents the lower-bound of the BER, which justifies the terminology of, lower-bound single-hop BER, and, lower-bound end-to-end BER, used in this chapter.

Given the PDF $f_l^{SC}(\gamma)$, as shown in (3.6), the lower-bound single-hop BER for the lth hop $P_{Le}^{(l)}$ can be derived by first considering the conditional probability $P_{Le}^{(l)}(\gamma)$.

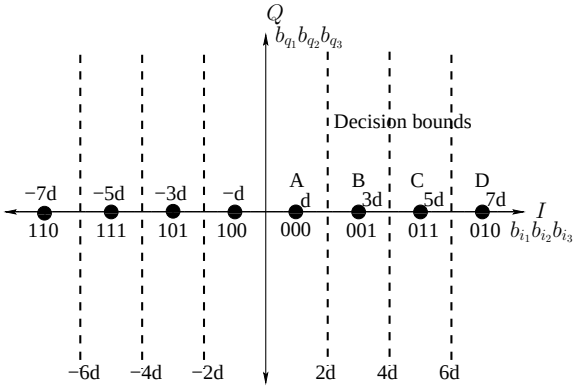

Figure 3.2: IQ-axis mapping of the 64QAM constellation.

It is well-known that the (square) MQAM signal can be decomposed into two independent Pulse Amplitude Modulation (PAM) signals [33,186,187], each of which has the constellation points located at

$$\{\pm d, \pm 3d, \ldots, \pm(\sqrt{M}-1)d\}, \tag{3.7}$$

where $2d$ represents the minimum Euclidean distance of the constellation points. When normalized by the noise's standard deviation σ, we have [33, 186]

$$\frac{d}{\sigma} = \sqrt{\frac{6\gamma}{2(M-1)}}. \tag{3.8}$$

In MQAM, the two component PAM signals have the same error probability and can be treated independently. For example, when the classic Gray coded bit mapping is applied, which is the case considered in this chapter, the 64QAM constellation can be decomposed into (I-)PAM and (Q-)PAM, as shown in Fig. 3.2, where $b_{i1}b_{i2}b_{i3}$ and $b_{q1}b_{q2}b_{q3}$ are the bits conveyed by the I-PAM and Q-PAM, respectively.

Let us specifically consider the I-PAM stream and express the probability P_i that a transmitted signal belongs to the constellation point id, where $i = \pm 1, \ldots, \pm(\sqrt{M}-1)$. Let $P^{(l)}_{\{i,j\}}(\gamma)$ represent the transition probability at the lth hop, which is the probability that the receiver declares that jd is detected, while id was transmitted. Furthermore, let $e_{i,j}$ be the number of different bits between the signal representing the constellation point id and that corresponding to the constellation point jd. Then,

the BER of MQAM can be expressed as[1]

$$P_{Le}^{(l)}(\gamma) = \frac{2}{\log_2 M} \sum_{i=-\sqrt{M}+1}^{\sqrt{M}-1} P_i \left(\sum_{j=-\sqrt{M}+1}^{\sqrt{M}-1} e_{i,j} P_{\{i,j\}}^{(l)}(\gamma) \right). \tag{3.9}$$

Let us define

$$\begin{aligned} \boldsymbol{p} &= \left[P_{-\sqrt{M}+1}, P_{-\sqrt{M}+3}, \ldots, P_{\sqrt{M}-1}\right]^T \\ \boldsymbol{P}_l(\gamma) &= \left[P_{\{i,j\}}^{(l)}(\gamma)\right], \ \boldsymbol{E} = \left[e_{i,j}\right], \ \mathbf{1} = [1, 1, \ldots, 1]^T, \end{aligned} \tag{3.10}$$

where $\boldsymbol{p}$ is an $\sqrt{M}$-length vector, $\mathbf{1}$ is an $\sqrt{M}$-length vector with elements of one, while $\boldsymbol{P}_l(\gamma)$ and $\boldsymbol{E}$ are $(\sqrt{M} \times \sqrt{M})$-element square matrices. Explicitly, let us consider 64QAM as an example which may be considered as a pair of 8-level in-phase and quadrature-phase schemes. Hence there are eight constellation levels in each dimension. The transmission probability of each constellation point has the same probability, therefore we have $\boldsymbol{p} = [P_{-7}\ P_{-5}\ P_{-3}\ P_{-1}\ P_1\ P_3\ P_5\ P_7]^T = [\frac{1}{8}\ \frac{1}{8}\ \frac{1}{8}\ \frac{1}{8}\ \frac{1}{8}\ \frac{1}{8}\ \frac{1}{8}\ \frac{1}{8}]^T$, which is shown in Fig. 3.2. Let us represent the number of different bits, when corrupting symbol i to symbol j by $e_{i,j}$. The matrix $\boldsymbol{E}$ for the 8-level in-phase component is given by

$$\boldsymbol{E} = \begin{bmatrix} TX.bits/RX.bits & 000 & 001 & 010 & 011 & 100 & 101 & 110 & 111 \\ 000 & 0 & 1 & 1 & 2 & 1 & 2 & 2 & 3 \\ 001 & 1 & 0 & 2 & 1 & 2 & 1 & 3 & 2 \\ 010 & 1 & 2 & 0 & 1 & 2 & 3 & 1 & 2 \\ 011 & 2 & 1 & 1 & 0 & 3 & 2 & 2 & 1 \\ 100 & 1 & 2 & 2 & 3 & 0 & 1 & 1 & 2 \\ 101 & 2 & 1 & 3 & 2 & 1 & 0 & 2 & 1 \\ 110 & 2 & 3 & 1 & 2 & 1 & 2 & 0 & 1 \\ 111 & 3 & 2 & 2 & 1 & 2 & 1 & 1 & 0 \end{bmatrix}. \tag{3.11}$$

Let us intuitively interpret the (3.9) step by step.

1) A constellation point i is selected with a probability P_i.

2) The probability of transmitting the constellation point i and receiving j is $P_{i,j}(\gamma)$.

3) There are $e_{i,j}$ bit error's when '2)' occurs.

[1] A detailed example is shown later.

4) Let us hence evaluate $e_{i,j}$ for transmitting ll constellation points and receiving all constellation points. Finally, the BER of a single hop can be obtained. Then, (3.9) can be expressed in a compact form as

$$\begin{aligned} P_{Le}^{(l)}(\gamma) =& \frac{2}{\log_2 M} \boldsymbol{p}^T \left[\boldsymbol{E} \odot \boldsymbol{P}_l(\gamma)\right] \mathbf{1} \\ =& \frac{2}{\log_2 M} \mathbf{1}^T \left[\boldsymbol{E}^T \odot \boldsymbol{P}_l^T(\gamma)\right] \boldsymbol{p}, \end{aligned} \tag{3.12}$$

where $\odot$ represents the Hadamard product [180][2]. Observe that at the right-hand side of (3.12), only $\boldsymbol{P}_l(\gamma)$ is a function of γ. Hence, the average single-hop BER $P_{Le}^{(l)}$ may be obtained by averaging $P_{Le}^{(l)}(\gamma)$ of (3.12) with respect to the PDF of (3.6), which can be expressed as

$$\begin{aligned} P_{Le}^{(l)} =& \int_0^\infty P_{Le}^{(l)}(\gamma) f_l(\gamma) d\gamma \\ =& \frac{2}{\log_2 M} \mathbf{1}^T \left(\boldsymbol{E}^T \odot \int_0^\infty \boldsymbol{P}_l^T(\gamma) f_l^{SC}(\gamma) d\gamma \right) \boldsymbol{p} \\ =& \frac{2}{\log_2 M} \mathbf{1}^T \left(\boldsymbol{E}^T \odot \boldsymbol{P}_l^T \right) \boldsymbol{p}, \end{aligned} \tag{3.13}$$

where $\boldsymbol{P}_l = \left[P_{\{i,j\}}^{(l)}\right]$ with $P_{\{i,j\}}^{(l)}$ denoting the average transition probability from the constellation point i to j, given by

$$P_{\{i,j\}}^{(l)} = \int_0^\infty P_{\{i,j\}}^{(l)}(\gamma) f_l^{SC}(\gamma) d\gamma, \;\; i,j = \pm 1, \pm 3, \ldots, \pm(\sqrt{M}-1). \tag{3.14}$$

Again, $P_{\{i,j\}}^{(l)}(\gamma)$ is the transition probability that the receiver declares the jth constellation point, given that the ith constellation point was transmitted. This probability can be readily derived by referring to Fig. 3.2, which is

$$P_{\{i,j\}}^{(l)}(\gamma) = \begin{cases} Q\left[(|i-j|-1)\frac{d}{\sigma}\right], & \text{when } j = \pm(\sqrt{M}-1) \\ Q\left[(|i-j|-1)\frac{d}{\sigma}\right] - Q\left[(|i-j|+1)\frac{d}{\sigma}\right], & \text{others} \end{cases} \tag{3.15}$$

where $Q(x)$ is the Gaussian Q-function. For example, when 4QAM (QPSK) is employed, we have $d/\sigma = \sqrt{\gamma}$. Hence, the probability transition matrix is expressed with the aid of (3.15) as

$$\boldsymbol{P}(\gamma) = \begin{bmatrix} 1 - Q\left(\sqrt{\gamma}\right) & Q\left(\sqrt{\gamma}\right) \\ Q\left(\sqrt{\gamma}\right) & 1 - Q\left(\sqrt{\gamma}\right) \end{bmatrix}. \tag{3.16}$$

[2]If both matrices $\boldsymbol{A}$ and $\boldsymbol{B}$ are $(m \times n)$-element matrices. The Hadamard product $\boldsymbol{A} \odot \boldsymbol{B}$ is given by $(\boldsymbol{A} \odot \boldsymbol{B})_{i,j} = \boldsymbol{A}_{i,j} \times \boldsymbol{B}_{i,j}$.

Finally, when substituting (3.6), (3.8) as well as (3.15) into (3.14) and completing the integration, $P_{i,j}$ can be expressed as

$$P_{\{i,j\}}^{(l)} = \begin{cases} \bar{Q}_l\left(\sqrt{(|i-j|-1)\bar{\gamma}_l}\right), & \text{when } j = \pm(\sqrt{M}-1) \\ \bar{Q}_l\left(\sqrt{(|i-j|-1)\bar{\gamma}_l}\right) - \bar{Q}_l\left(\sqrt{(|i-j|+1)\bar{\gamma}_l}\right), & \text{others} \end{cases} \tag{3.17}$$

By letting $A_{i,j} = |i-j|-1$ or $A_{i,j} = |i-j|+1$, $\bar{Q}_l\left(\sqrt{A_{i,j}\bar{\gamma}_l}\right)$ in the above equation is given by

$$\begin{aligned} \bar{Q}_l\left(\sqrt{A_{i,j}\bar{\gamma}_l}\right) = &\left(\frac{m_l}{\bar{\gamma}_l}\right)^{m_l} \frac{L}{(\Gamma(m_l))^L} \int_0^\infty Q\left(\sqrt{A_{i,j}\gamma}\right) \gamma^{m_l-1} \\ &\times \left[\gamma\left(m_l, \frac{m_l\gamma}{\bar{\gamma}_l}\right)\right]^{L-1} \exp\left(-\frac{m_l\gamma}{\bar{\gamma}_l}\right) d\gamma. \end{aligned} \tag{3.18}$$

When m_l is an arbitrary non-integer value, we find that it is extremely hard to derive the closed-form solution for the integral in (3.18). By contrast, when m is an integer, a closed-form expression can be derived for (3.18). In this case, firstly, the incomplete gamma function can be expressed as [10](8.352.6)

$$\frac{\gamma(m,x)}{\Gamma(m)} = \left(1 - e^{-x}\sum_{n=0}^{m-1}\frac{x^n}{n!}\right). \tag{3.19}$$

Then, upon substituting (3.19) into (3.18) and after some rearrangement, we arrive at

$$\begin{aligned} \bar{Q}_l\left(\sqrt{A_{i,j}\bar{\gamma}_l}\right) = &\left(\frac{m_l}{\bar{\gamma}_l}\right)^{m_l} \frac{L}{\Gamma(m_l)} \sum_{l=0}^{L-1}(-1)^l \binom{L-1}{l} \sum_{k=0}^{l(m_l-1)} c_k^{(l)} \left(\frac{m_l}{\bar{\gamma}_l}\right)^k \\ &\times \int_0^\infty Q\left(\sqrt{A_{i,j}\gamma}\right) \gamma^{k+m_l-1} \exp\left(-\frac{m_l(l+1)}{\bar{\gamma}_l}\gamma\right) d\gamma. \end{aligned} \tag{3.20}$$

Finally, the above expression can be simplified with the aid of the results from [15,37],

$$\begin{aligned} \bar{Q}_l\left(\sqrt{A_{i,j}\bar{\gamma}_l}\right) = &\frac{L}{\Gamma(m_l)} \sum_{l=0}^{L-1}(-1)^l \binom{L-1}{l} \sum_{k=0}^{l(m_l-1)} c_k^{(l)} \frac{\Gamma(k+m_l)}{(l+1)^{m_l+k}} \\ &\times \frac{1}{2}\left[1 - \mu\sum_{h=0}^{m_l+k-1}\binom{2h}{h}\left(\frac{1-\mu^2}{4}\right)^h\right], \end{aligned} \tag{3.21}$$

where[3] the coefficients $c_k^{(l)}$ can be recursively computed according to the formulas in (16) of [37], yielding

$$\begin{aligned} c_0^{(l)} = 1,\ c_1^{(l)} = l,\ c_{l(m_l-1)}^{(l)} &= \frac{1}{[(m_l-1)!]^l} \\ c_k^{(l)} &= \frac{1}{k}\sum_{j=1}^{\min(k,m_l-1)} \frac{j(l+1)-k}{j!} c_{k-j}^{(l)}. \end{aligned} \tag{3.22}$$

Furthermore, in (3.21), we have for $M \geq 4$

$$\mu = \sqrt{\frac{A_{i,j}^2 g \bar{\gamma}_l}{2m_l(l+1)/\bar{\gamma}_l + A_{i,j}^2 g \bar{\gamma}_l}},\ \text{with}\ g = \frac{1.5}{M-1}, \tag{3.23}$$

and, for BPSK ($M = 2$), we have $A_{i,j} = 2$, $g = 0.5$ and, correspondingly, $\mu = \sqrt{\frac{\bar{\gamma}_l}{m_l(l+1)/\gamma_h + \bar{\gamma}_l}}$ and $P_{Le}^{(l)} = \bar{Q}_l\left(\sqrt{2\bar{\gamma}_l}\right)$.

Finally, we note that the lower-bound single-hop BER $P_{Le}^{(l)}$ of the L-hop MHL supported by the proposed MHD principles can be evaluated by substituting (3.17) and the associated formulas into (3.13).

Having obtained the lower-bound single-hop BER $P_{Le}^{(l)}$ of (3.13), the lower-bound end-to-end BER P_{LE} can now be derived by exploiting that the decode-and-forward scheme of Fig. 3.1, where a packet is passed through the entire ad hoc chain from one node to another. Regardless of the number of hops, we are interested in the end-to-end constellation-constellation transition matrix.[4] Once we determined this transition matrix, the BER performance can be analyzed similarly to the single hop case. This equivalent end-to-end constellation-constellation transition matrix is $\prod_{l=1}^{L} \boldsymbol{P}_l^T$, which is created as the product of the transition matrix in each hop of the link. Hence, when considering all the $\sqrt{M}$ possible transmitted symbols, which have the a-priori probabilities of $\boldsymbol{p}$, as shown in (3.10), the lower-bound end-to-end average BER of the L-hop MHL can be expressed as (3.12), yielding

$$P_{LE} = \frac{2}{m}\mathbf{1}^T \left[\boldsymbol{E}^T \odot \left[\prod_{l=1}^{L} \boldsymbol{P}_l^T\right]\right] \boldsymbol{p}. \tag{3.24}$$

Note that, an end-to-end average BER expression for MHLs has been derived in [117](42), which has a similar form as (3.24). However, the expression [117](42) is only for BPSK/QPSK, but not for MQAM, when $M \geq 16$. Specifically, for BPSK

[3] Another expression of (3.19) is in the Appendix.

[4] The constellation-constellation transition matrix represents the transition probabilities from constellation points from transmitter to constellations points at the receiver.

we can readily obtain the lower-bound end-to-end BER expression, which is

$$P_{LE} = \frac{1}{2} - \frac{1}{2}\prod_{l=1}^{L}\left(1 - 2P_{Le}^{(l)}\right). \tag{3.25}$$

Let us now elaborate on (3.24) in a little more detail based on an example. This

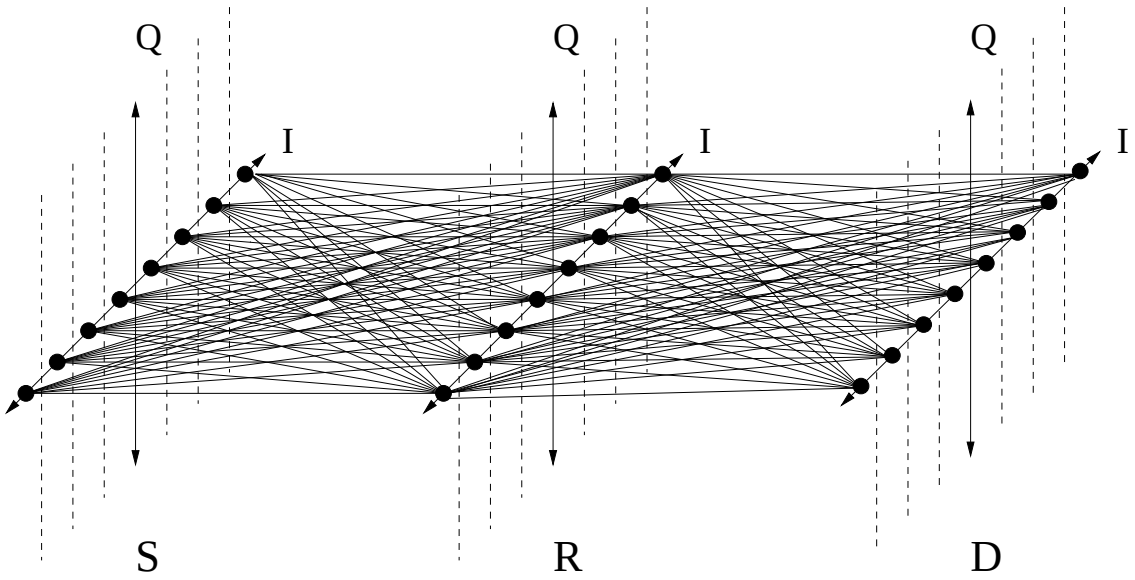

Figure 3.3: IQ-axis mapping of the 64QAM constellation in two hop link.

formula can be interpreted with the aid of Fig. 3.3, which shows the IQ-axis based mapping of the 64QAM constellation in a two-hop scenario. Assuming that the modulation scheme is 64QAM and the number of hops is two, both the I and Q components are 8-level signals. The constellation points at the Source (S), Relay (R) and Destination (D) are shown in this figure. Originally, the information symbols have an equal probability to be transmitted, which is represented by the probability $\boldsymbol{p}$ in (3.10). Every symbol transmitted from a constellation has a specific transition probability with respect to another received constellation point. In this figure, this transition is represented by the lines between the constellation points. A single-hop symbol-to-symbol transition can be described by a Markov state transition matrix, which is $\boldsymbol{P_l}^T$ in (3.22). Fig. 3.3 represents a two-hop link, hence the symbol-to-symbol transition matrix associated with the source to destination matrix is $\boldsymbol{P_1}^T\boldsymbol{P_2}^T$.

The lower-bound end-to-end BER of the MHLs has been derived above, which assumed that each RN has an infinite buffer size and the RNs always have packets to transmit. The exact end-to-end BER of the MHLs is considered below, where we assumed that every RN has a buffer of finite size. In this case, the hops obeying either of the following conditions should be excluded from the transmission list: a) the hops, whose transmit nodes do not have packets to transmit and b) the hops,

whose receive nodes are unable to accept packets, since their buffers are full. When taking the above two situations into account, the exact end-to-end BER of MHLs can be analyzed as follows.

When deriving the near exact BER of the MHD scheme, we have to consider the constraint that the L-hop link is forced to choose the best one from the set of $\hat{l}$ hops in order to send its information, when $(L-\hat{l})$ out of the L hops are unable to transmit information. This happens either when some of the transmit nodes' buffers are empty or when some of the receive nodes' buffers are full. Before finding the exact end-to-end BER P_e with finite size of buffer, the concept of state is proposed. Based on this concept, the packets transmitted over an L-hop link under the MHD scheme can be described as a Markov process.

Let us assume that the buffer size of every RN is B packets. When MQAM modulation is employed, then $\log_2 M$ packets are transmitted simultaneously. Hence, we can express the equivalent buffer size of a RN as $\hat{B} = B/\log_2 M$ packets. Let the numbers of packets stored in the $(L-1)$ RNs, $R_1, R_2, \ldots, R_{L-1}$, be $b_1, b_2, \ldots, b_{L-1}$, where $b_l = 0, 1, \ldots, B$. Then, upon considering MQAM, the corresponding equivalent numbers of packets are $\hat{b}_1, \hat{b}_2, \ldots, \hat{b}_{L-1}$, where $\hat{b}_i = b_i/\log_2 M$. Given the above definitions, the states of the L-hop link can be defined in terms of the number of packets stored in the $(L-1)$ RNs as

$$S_i = \left[\hat{b}_1^{(i)}, \hat{b}_2^{(i)}, \ldots, \hat{b}_{L-1}^{(i)}\right]^T, i = 0, 1, \ldots, N-1, \tag{3.26}$$

where $\hat{b}_l^{(i)}$ denotes the equivalent number of packets stored in the lth RN, when the L-hop link is in state i, while $N = (\hat{B}+1)^{L-1}$ is the total number of states of the Markov process, which constitute a set $\mathcal{S} = \{S_0, S_1, \ldots, S_{N-1}\}$. Based on the transitions among the N states, a state transition matrix denoted by $\boldsymbol{T}$ can be characterized by the state transition probabilities $\{P_{ij} = P(s(t+1) = S_j | s(t) = S_i),\ i, j = 0, 1, \ldots, N-1\}$.

For example, when considering a three-hop link having the parameters of $L = 3$ and $\hat{B} = 2$, there is a total of $N = 3^2 = 9$ states, which form a set

$$\begin{aligned}\mathcal{S} = \big\{&S_0 = [0,0]^T, S_1 = [0,1]^T, S_2 = [0,2]^T, S_3 = [1,0]^T, S_4 = [1,1]^T,\\ &S_5 = [1,2]^T, S_6 = [2,0]^T, S_7 = [2,1]^T, S_8 = [2,2]^T\big\}.\end{aligned}$$

Correspondingly, the state transition matrix becomes:

$$\boldsymbol{T} = \begin{bmatrix} 0 & 0 & 0 & 1 & 0 & 0 & 0 & 0 & 0 \\ 1/2 & 0 & 0 & 0 & 1/2 & 0 & 0 & 0 & 0 \\ 0 & 1/2 & 0 & 0 & 0 & 1/2 & 0 & 0 & 0 \\ 0 & 1/2 & 0 & 0 & 0 & 0 & 1/2 & 0 & 0 \\ 0 & 0 & 1/3 & 1/3 & 0 & 0 & 0 & 1/3 & 0 \\ 0 & 0 & 0 & 0 & 1/2 & 0 & 0 & 0 & 1/2 \\ 0 & 0 & 0 & 0 & 1 & 0 & 0 & 0 & 0 \\ 0 & 0 & 0 & 0 & 0 & 1/2 & 1/2 & 0 & 0 \\ 0 & 0 & 0 & 0 & 0 & 0 & 0 & 1 & 0 \end{bmatrix}. \tag{3.27}$$

Although the transition matrix $\boldsymbol{T}$ may be large, it can be readily constructed. An algorithm conceived for forming the matrix $\boldsymbol{T}$ may be described as follows:

1. The $(\hat{B}+1)^{L-1} \times (\hat{B}+1)^{L-1}$ matrix $\boldsymbol{T}$ is first initialized with zero elements.
2. For row i, $i = 0, 1, \ldots, (\hat{B}+1)^{L-1} - 1$, which corresponds to the ith state $S_i = \left[\hat{b}_1^{(i)}, \hat{b}_2^{(i)}, \ldots, \hat{b}_{L-1}^{(i)}\right]^T$, the following operations are carried out:
   - If $\hat{b}_1^{(i)} + 1 \leq \hat{B}$, the column corresponding to the output state $\left[\hat{b}_1^{(i)} + 1, \hat{b}_2^{(i)}, \ldots, \hat{b}_{L-1}^{(i)}\right]^T$ is set to one;
   - For $l = 1, 2, \ldots, L-2$, if $b_l^{(i)} - 1 \geq 0$ and $\hat{b}_{l+1}^{(i)} + 1 \leq \hat{B}$, the column corresponding to the output state $\left[\hat{b}_1^{(i)}, \ldots, \hat{b}_l^{(i)} - 1, \hat{b}_{l+1}^{i} + 1, \ldots, \hat{b}_{L-1}^{(i)}\right]^T$ is set to one;
   - If $\hat{b}_{L-1}^{(i)} - 1 \geq 0$, the column corresponding to the output state $\left[\hat{b}_1^{(i)}, \hat{b}_2^{(i)}, \ldots, \hat{b}_{L-1}^{(i)} - 1\right]^T$ is set to one.
3. Each of the rows is divided by the number of ones in the same row, to guarantee that the total transition probability from state S_i is one.

It can be shown that the state transition matrix $\boldsymbol{T}$ has the following properties:

- Matrix $\boldsymbol{T}$ is a sparse matrix. Every row has at most L number of non-zero elements, while the remaining at least $(\hat{B}+1)^{L-1} - L$ number of elements are zero elements.
- The sum of the probabilities in each row is one;
- The number of non-zero elements in a row represents the number of hops that may be chosen for transmission.

Having obtained the state transition matrix $\boldsymbol{T}$, the steady-state probabilities can be computed by the formula [181]

$$P_{\boldsymbol{\pi}} = \boldsymbol{T}^T P_{\boldsymbol{\pi}}, \tag{3.28}$$

where $P_{\boldsymbol{\pi}} = \left[P_{\pi_0}, P_{\pi_1}, \ldots, P_{\pi_{(\hat{B}+1)^{L-1}-1}}\right]^T$, in which P_{π_i} (or $P_{\pi_{S_i}}$) is the steady-state probability that the L-hop link is in state S_i. Note that $P_{\boldsymbol{\pi}}$ in (3.28) is the right eigenvector of the matrix $\boldsymbol{T}^T$ associated with an eigenvalue of one. Therefore, $P_{\boldsymbol{\pi}}$ can be obtained by solving the corresponding eigenvector problem [182]. However, the matrix $\boldsymbol{T}$ may be extreme by large. An approximate method of generating $P_{\boldsymbol{\pi}}$ will be provided in Subsection 3.3.2.

The next step is to find the exact end-to-end BER P_e based on $P_{\boldsymbol{\pi}}$. Firstly, a $(L \times L)$ element matrix $\boldsymbol{P}_{sel}^{\hat{B}}$ is computed, in which $\boldsymbol{P}_{sel}^{\hat{B}}(l, \hat{l})$ denotes the probability that the lth hop is selected from $\hat{l}$ available hops, when the equivalent buffer size per RN is $\hat{B}$. We assume that the total number of available hops corresponding to state S_i is N_{S_i}. Then, $\boldsymbol{P}_{sel}^{\hat{B}}$ can be determined by the following algorithm.

---

1. Initialization: $\boldsymbol{P}_{sel}^{\hat{B}} = \boldsymbol{0}$;
2. **for** $i = 1 : (\hat{B}+1)^{L-1}$ // all the $(\hat{B}+1)^{L-1}$ possible states;
   for $j = 1 : N_{S_i}$ // all the available hops in state S_i;
   compute:

$$\boldsymbol{P}_{sel}^{\hat{B}}(j_{S_i}, N_{S_i}) = \boldsymbol{P}_{sel}^{\hat{B}}(j_{S_i}, N_{S_i}) + \frac{P_{\pi_i}}{N_{S_i}}; \tag{3.29}$$

   End
   End

In (3.29), $j_{S_i} \in \{1, 2, \ldots, L\}$ denotes the hop index of the jth available hop in state S_i. After obtaining $\boldsymbol{P}_{sel}^{\hat{B}}$ of (3.29), the average BER $\boldsymbol{p}_l^{\hat{B}}$ of the lth hop can be computed with the aid of the whole probability formula, yielding

$$\boldsymbol{p}_l^{\hat{B}} = L \sum_{\hat{l}=1}^{L} \boldsymbol{P}_{sel}^{\hat{B}}(l, \hat{l}) P_{Le}^{(\hat{l})}, \tag{3.30}$$

where $P_{Le}^{(\hat{l})}$ is given by (3.13). Finally, the exact end-to-end BER of the MHL of the RNs can be obtained for a finite buffer by substituting (3.30) into (3.24).

3.3.2 Approximate Solution of (3.28)

The near exact value of $P_{\boldsymbol{\pi}}$ can be obtained by solving (3.28), when $\boldsymbol{T}$ is small. By contrast, if $\boldsymbol{T}$ is large, the achievable performance approaches the theoretical bound, which will be detailed in Section 3.4. If the size of $\boldsymbol{T}$ is mediocre, an approximate method is provided here for circumventing this problem. Note that all our discussions are based on assuming steady-state operation.

Actually, the number of packets in the RN buffers cannot be considered independent. Nevertheless, for the sake of simplicity to obtain the approximate expressions, they are treated as independent. Assuming that $p_{i,\hat{b}}$ represents the probability of having $\hat{b}$ packets in the ith relay, we can approximate $P_{\pi_{S_j=[\hat{b}_1^{(j)},\hat{b}_2^{(j)},\ldots,\hat{b}_{L-1}^{(j)}]^T}} \approx \prod_{i=1}^{L-1} p_{i,\hat{b}_i^{(j)}}$. Based on this formula, we can see that, in order to compute $P_{\pi_{S_j=[\hat{b}_1^{(j)},\hat{b}_2^{(j)},\ldots,\hat{b}_{L-1}^{(j)}]^T}}$ for all the $(\hat{B}+1)^{L-1}$ states, the total number of unknown probabilities is $(L-1)(\hat{B}+1)$, which are $p_{i,\hat{b}}$ for $i = 1, 2, \ldots, L-1$ and $b = 0, 1, \ldots, \hat{B}$. Hence, our objective is to compute these probabilities by finding at least $(L-1)(\hat{B}+1)$ equations, which are derived below by making use of the different properties.

3.3.2.1 Symmetric Proposition

Let the probability of a state $S_i = \left[\hat{b}_1^{(i)}, \hat{b}_2^{(i)}, \ldots, \hat{b}_{L-1}^{(i)}\right]^T, i = 0, 1, \ldots, N-1$ be P_{π_i}. Let the probability of another state $S_{\bar{i}} = \left[\hat{B} - \hat{b}_{L-1}^{(i)}, \hat{B} - \hat{b}_{L-2}^{(i)}, \ldots, \hat{B} - \hat{b}_1^{(i)}\right]^T$ be $P_{\pi_{\bar{i}}}$, where $\hat{b}_l^{(i)}$ for $l = 1, \ldots, L-1$ are given by the corresponding $\hat{b}_l^{(i)}$ in S_i. Then we have $P_{\pi_{\bar{i}}} = P_{\pi_i}$.

Proof: The unavailable channels are those ones that are linked to the specific RNs having either an empty or a full buffer. The channels available for state S_i are the same as for state $S_{\bar{i}}$. Since every node that has zero packets to send in S_i is treated as a node having $\hat{B}$ packets, this represents a full buffer. Hence it will be unable to receive any packets. By contrast, the nodes that have $\hat{B}$ packets to send in S_i are treated as nodes having zero packets. Since this is a node with an empty buffer, it will be unable to transmit any packet. Therefore, the number of available channels remains unchanged. The following is the mathematical proof. If the state S_i is substituted by $S_{\bar{i}}$ in (3.28), the equation remains unchanged. Therefore, we have $P_{\pi_{\bar{i}}} = P_{\pi_i}$.

Let us consider the same example as before. Again, the relevant parameters are $L = 3$ and $\hat{B} = 2$. Then, from (3.28) we have:

$$
\begin{aligned}
P_{\pi_{S_0=[0,0]^T}} &= P_{\pi_{S_1=[0,1]^T}} \times \frac{1}{2} \\
P_{\pi_{S_1=[0,1]^T}} &= P_{\pi_{S_2=[0,2]^T}} \times \frac{1}{2} + P_{\pi_{S_3=[1,0]^T}} \times \frac{1}{2} \\
P_{\pi_{S_2=[0,2]^T}} &= P_{\pi_{S_4=[1,1]^T}} \times \frac{1}{3} \\
P_{\pi_{S_3=[1,0]^T}} &= P_{\pi_{S_0=[0,0]^T}} \times 1 + P_{\pi_{S_4=[1,1]^T}} \times \frac{1}{3} \\
P_{\pi_{S_4=[1,1]^T}} &= P_{\pi_{S_1=[0,1]^T}} \times \frac{1}{2} + P_{\pi_{S_5=[1,2]^T}} \times \frac{1}{2} + P_{\pi_{S_6=[2,0]^T}} \times 1 \\
P_{\pi_{S_5=[1,2]^T}} &= P_{\pi_{S_2=[0,2]^T}} \times \frac{1}{2} + P_{\pi_{S_7=[2,1]^T}} \times \frac{1}{2} \\
P_{\pi_{S_6=[2,0]^T}} &= P_{\pi_{S_3=[1,0]^T}} \times \frac{1}{2} + P_{\pi_{S_7=[2,1]^T}} \times \frac{1}{2} \\
P_{\pi_{S_7=[2,1]^T}} &= P_{\pi_{S_4=[1,1]^T}} \times \frac{1}{3} + P_{\pi_{S_8=[2,2]^T}} \times 1 \\
P_{\pi_{S_8=[2,2]^T}} &= P_{\pi_{S_5=[1,2]^T}} \times \frac{1}{2}.
\end{aligned}
\tag{3.31}
$$

If all S_i values are substituted by $S_{\bar{i}}$, the above formula becomes:

$$
\begin{aligned}
P_{\pi_{S_8=[2,2]^T}} &= P_{\pi_{S_5=[1,2]^T}} \times \frac{1}{2} \\
P_{\pi_{S_5=[1,2]^T}} &= P_{\pi_{S_2=[0,2]^T}} \times \frac{1}{2} + P_{\pi_{S_7=[2,1]^T}} \times \frac{1}{2} \\
P_{\pi_{S_2=[0,2]^T}} &= P_{\pi_{S_4=[1,1]^T}} \times \frac{1}{3} \\
P_{\pi_{S_7=[2,1]^T}} &= P_{\pi_{S_8=[2,2]^T}} \times 1 + P_{\pi_{S_4=[1,1]^T}} \times \frac{1}{3} \\
P_{\pi_{S_4=[1,1]^T}} &= P_{\pi_{S_5=[1,2]^T}} \times \frac{1}{2} + P_{\pi_{S_1=[0,1]^T}} \times \frac{1}{2} + \pi_{S_6=[2,0]^T} \times 1 \\
P_{\pi_{S_1=[0,1]^T}} &= P_{\pi_{S_2=[0,2]^T}} \times \frac{1}{2} + P_{\pi_{S_3=[1,0]^T}} \times \frac{1}{2} \\
P_{\pi_{S_6=[2,0]^T}} &= P_{\pi_{S_7=[2,1]^T}} \times \frac{1}{2} + P_{\pi_{S_3=[1,0]^T}} \times \frac{1}{2} \\
P_{\pi_{S_3=[2,1]^T}} &= P_{\pi_{S_4=[1,1]^T}} \times \frac{1}{3} + P_{\pi_{S_0=[0,0]^T}} \times 1 \\
P_{\pi_{S_0=[2,2]^T}} &= P_{\pi_{S_1=[0,1]^T}} \times \frac{1}{2},
\end{aligned}
\tag{3.32}
$$

which is identical to (3.31). The only difference is in the terminology. Hence, the solution of (3.32) is also the same as that of (3.31), which means that we have $P_{\pi_{S_0}} = P_{\pi_{S_8}}$, $\P_{pi_{S_1}} = P_{pi_{S_5}}$, $P_{\pi_{S_3}} = P_{\pi_{S_7}}$, and so on.

Let us now elaborate further by considering transmission 'Process 1' of Fig. 3.4. The steady-state probability of the states in 'Process 1' is denoted as $P_{\boldsymbol{\pi}_{Pros1}}$. After

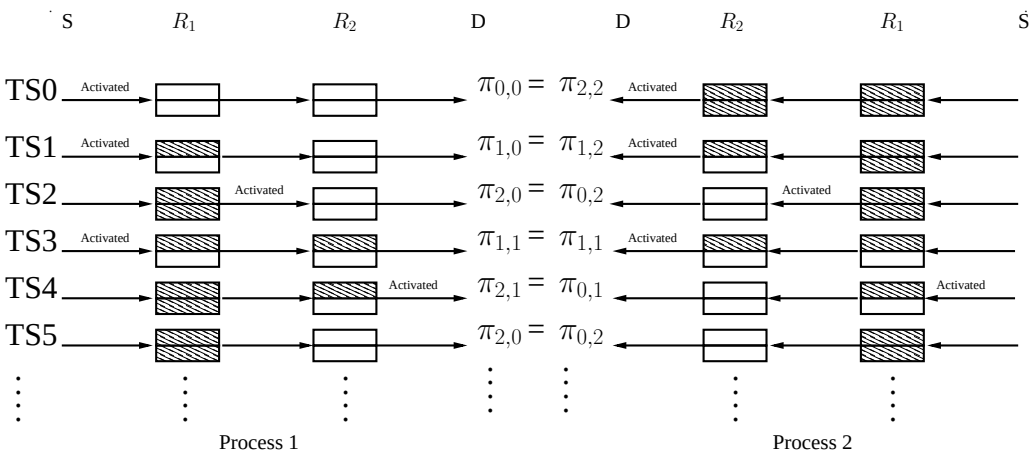

Figure 3.4: Example of a three-hop link, where each relay node stores upto two packets. This figures shows two identical processes based on substituting $S_i = \left[\hat{b}_1^{(i)}, \hat{b}_2^{(i)}, \ldots, \hat{b}_{L-1}^{(i)}\right]^T, i = 0, 1, \ldots, N-1$ for $S_{\bar{i}} = \left[\hat{B} - \hat{b}_{L-1}^{(i)}, \hat{B} - \hat{b}_{L-2}^{(i)}, \ldots, \hat{B} - \hat{b}_1^{(i)}\right]^T$. substituting $S_i = \left[\hat{b}_1^{(i)}, \hat{b}_2^{(i)}, \ldots, \hat{b}_{L-1}^{(i)}\right]^T, i = 0, 1, \ldots, N-1$ for $S_{\bar{i}} = \left[\hat{B} - \hat{b}_{L-1}^{(i)}, \hat{B} - \hat{b}_{L-2}^{(i)}, \ldots, \hat{B} - \hat{b}_1^{(i)}\right]^T$ 'Process 1' is mapped to 'Process 2'. The steady-state probability of the states in 'Process 2' is denoted as $P_{\boldsymbol{\pi}_{Pros2}}$. Owing to the bijective mapping[5], Processes 1 and 2 are identical. Hence the Markov Transmission Matrix $\boldsymbol{T}$ of both 'Process 1' and 'Process 2' is also the same, hence the solution of both $P_{\boldsymbol{\pi}_{Pros1}} = \boldsymbol{T}^T P_{\boldsymbol{\pi}_{Pros1}}$ and $P_{\boldsymbol{\pi}_{Pros2}} = \boldsymbol{T}^T P_{\boldsymbol{\pi}_{Pros2}}$ should be the same. Therefore, the state probability $P_{\pi_{S_i}}$ is constituted by the corresponding state probability $P_{\pi_{S_{\bar{i}}}}$. For example, as shown in Fig. 3.4, we have $P_{\pi_{0,0}} = P_{\pi_{2,2}}$.

Based on the proposition above, we arrive at

$$\begin{aligned} p_{i,\hat{b}} &= \sum_{j_1=0}^{\hat{B}} \sum_{j_2=0}^{\hat{B}} \cdots \sum_{j_{i-1}=0}^{\hat{B}} \sum_{j_{i+1}=0}^{\hat{B}} \cdots \sum_{i_{L-1}=0}^{\hat{B}} P_{\pi_{S=[j_1, j_2 \ldots, j_{i-1}, \hat{b}, j_{i+1} \ldots, j_{L-1}]^T}} \\ &= \sum_{j_1=0}^{\hat{B}} \sum_{j_2=0}^{\hat{B}} \cdots \sum_{j_{i-1}=0}^{\hat{B}} \sum_{j_{i+1}=0}^{\hat{B}} \cdots \sum_{i_{L-1}=0}^{\hat{B}} P_{\pi_{S=[\hat{B}-j_{L-1} \ldots, \hat{B}-j_{i+1}, \hat{B}-\hat{b}, \hat{B}-j_{i-1}, \ldots, \hat{B}-j_2, \hat{B}-j_1]^T}} \\ &= p_{L-i,\hat{B}-\hat{b}}, \; i = 1, 2, \ldots, L-1; \; b = 0, 1, \ldots, \lfloor (\hat{B}+1)/2 \rfloor. \end{aligned} \tag{3.33}$$

where $\lfloor x \rfloor$ returns the maximal integer less than x. From (3.33), we can see that the proposition can provide $\lfloor (L-1)(\hat{B}+1)/2 \rfloor$ equations.

3.3.2.2 The Probability of Using Every Channel is Identical

When our MHD scheme is employed and when the MHL is operated in steady state, every hop has approximately the same probability to be activated. According to the operational principles of the MHD, as described in Section 3.2, if the ith hop is

[5]Bijective mapping: a function between two sets. Every element in one set is paired with a element in the other set.

selected, the $(i-1)$st node's buffer must not be empty, which has a probability of $(1-p_{i-1,0})$, and the ith node's buffer should not be full, which has a probability of $(1-p_{i,\hat{B}})$. In addition to the above mentioned buffer condition, let us assume that every hop has a $\frac{1}{L}$ probability of experiencing the "best" channel. Naturally, this is not always exactly satisfied, hence it remains an approximation. For the SN and DN, we set $p_{0,0}=0$ and $p_{L,\hat{B}}=0$, since we assumed that the SN always has packets to transmit and the DN is always ready to receive a packet. Hence, when considering all the L hops, we have the following relationship

$$(1-p_{0,\hat{B}}) \approx (1-p_{i-1,0})(1-p_{i,\hat{B}}) \approx (1-p_{j-1,0})(1-p_{j,\hat{B}}) \approx (1-p_{L,0}),$$
$$i=1,\ldots,L-1;\ j=i+1,i+2,\ldots,L. \tag{3.34}$$

From (3.34), we can construct a total of $L(L-1)/2$ equations. However, some of them can be derived from some others, i.e. they are not independent. After a close consideration and applying the above "Symmetry Proposition", we arrive at $\lfloor (L-1)/2 \rfloor$ independent equations.

3.3.2.3 The System is in Its Steady State

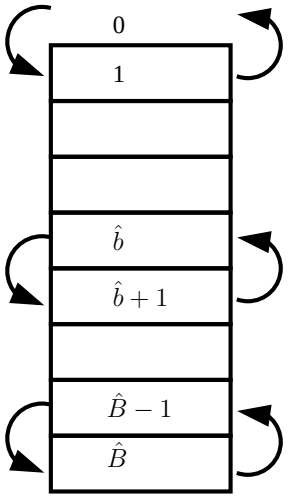

Figure 3.5: Considering node i, the probability of preceding from $\hat{b}$ to $\hat{b}+1$ is the same as that from $\hat{b}+1$ to $\hat{b}$, when system is steady. If the buffer of node i is empty, the $(i+1)$th hop is unavailable, while if that of node i is full, the ith hop is unavailable.

When this is in the case, for a single RN, the average number of transitions from $\hat{b}$ to $\hat{b}+1$ is the same as that from $\hat{b}+1$ to $\hat{b}$. By referring to Fig. 3.5, we may readily infer that for $\hat{b}=1,2,\ldots,\hat{B}-2$, we have

$$p_{i,\hat{b}}(1-p_{i-1,0})/L \approx p_{i,\hat{b}+1}(1-p_{i+1,\hat{B}})/L,\ i=1,2,\ldots,L-1, \tag{3.35}$$

where $(1-p_{i-1,0})/L$ at the left-hand side denotes the probability that node i receives a packet from node $(i-1)$, while $(1-p_{i+1,\hat{B}})/L$ is the probability that node i sends a packet to node $(i+1)$.

When $\hat{b}=0$, the $(i+1)$th hop is unavailable, as the ith node's buffer is empty. Hence, the transitions satisfy

$$p_{i,0}(1-p_{i-1,0})/(L-1) \approx p_{i,1}(1-p_{i+1,\hat{B}})/L,\ i=1,2,\ldots,L-1 \tag{3.36}$$

Similarly, when $\hat{b}=\hat{B}-1$, we have

$$p_{i,\hat{B}-1}(1-p_{i-1,0})/L \approx p_{i,\hat{B}}(1-p_{i+1,\hat{B}})/(L-1),\ i=1,2,\ldots,L-1. \tag{3.37}$$

where the factor $1/(L-1)$ at the righthand side is because there are only $(L-1)$ hops avaliable for selection, when node i is at state $\hat{B}$ (full), resulting in that the i hop is unavailable.

Consequently, when considering (3.35) - (3.37) and "Symmetry Proposition", we can obtain $\hat{B}(L-1)/2$ approximate equations.

3.3.2.4 The Total Probability is Unity Value

Finally, the sum of the probabilities of $p_{i,\hat{b}}$ at RN i should satisfy:

$$\sum_{\hat{b}=0}^{\hat{B}} p_{i,\hat{b}}=1,\ i=1,2,\ldots,L-1. \tag{3.38}$$

When considering the "Symmetry Proposition", we arrive at $\lfloor (L-1)/2 \rfloor$ equations.

By exploiting the properties of the MHL operated under our proposed MHD scheme, we can demonstrate that the number of equations is no less than the number of unknowns. If L is odd and $\hat{B}>1$, the number of equations is given by

$$\begin{aligned}
&\lfloor (L-1)(\hat{B}+1)/2 \rfloor + \underbrace{\lfloor L/2 \rfloor + \lfloor (L-1)/2 \rfloor}_{\text{L-1}} + \hat{B}(L-1)/2 \\
=&\frac{L-1}{2}(\hat{B}+1)+(L-1)+\hat{B}\frac{L-1}{2} \\
=&(L-1)(\hat{B}+\frac{3}{2}),
\end{aligned} \tag{3.39}$$

which is larger than the number of unknowns $(L-1)(\hat{B}+1)$. By contrast, if L is even and $\hat{B}>1$, the number of equations obeys:

$$\begin{aligned}&\lfloor (L-1)(\hat{B}+1)/2 \rfloor + \underbrace{\lfloor L/2 \rfloor + \lfloor (L-1)/2 \rfloor}_{\text{L-1}} + \hat{B}(L-1)/2 \\ =&\frac{L-1}{2}(\hat{B}+1) - \frac{1}{2} + (L-1) + (L-1)(\hat{B}/2) \\ =&(L-1)(\hat{B}+\frac{3}{2}) - \frac{1}{2}, \end{aligned} \tag{3.40}$$

which is larger than the number of unknowns $(L-1)(\hat{B}+1)$. All the above discussion is based on the assumption of $\hat{B}>1$. This is because the size of $\boldsymbol{T}$ is $2^{L-1}\times 2^{L-1}$ when $\hat{B}=1$, which is not large.

Hence, we can express the $(L-1)(\hat{B}+1)$ probabilities $p_{i,\hat{b}_i}$ for $i=1,2,\ldots,L-1$ and $\hat{b}_i=0,1,\ldots,\hat{B}$ by solving $(L-1)(\hat{B}+1)$ number of the equations. Consequently, the $(\hat{B}+1)^{L-1}$ steady state probabilities $\{P_{\pi_{S_j}}\}$ can be approximately determined using the relationship of $P_{\pi_{S_j=[\hat{b}_1^{(j)},\hat{b}_2^{(j)},\ldots,\hat{b}_{L-1}^{(j)}]^T}} \approx \prod_{i=1}^{L-1} p_{i,\hat{b}_i^{(j)}}$.

Specifically, a four step algorithm may be formulated as follows.

Step one: Consider all $p_{i,0}$ as unknowns.

Step two: Based on (3.33), all $p_{i,\hat{B}}$ can be determined.

Step three: Based on (3.35), (3.36) and (3.37), all other $p_{i,\hat{b}}$ can be found.

Step four: The variables $p_{i,0}$ for $i=1,2,\ldots,L-1$ may be found based on (3.38), since there are $(L-1)$ equations for $(L-1)$ unknowns.

Let us now expound a little further by determining the distribution of the buffer occupancy or buffer fullness characterized by its Probability Mass Function (PMF).

Explicitly, Fig. 3.6 shows the distribution of the buffer occupancy for $\hat{B}=32$, where the X-axis represents the equivalent buffer occupancy, while the Y-axis is the probability of a specific buffer-fullness. The continuous line portrays the theoretical distribution of the buffer occupancy of relay one, while the dotted line is the theoretical distribution of the buffer occupancy of relay two. The markers in Fig. 3.6 represent the simulation results, respectively. In other words, $P_{\boldsymbol{\pi}}$ in (3.28) is the joint probability density of the buffer occupancy, while Fig. 3.6 shows the marginal distribution of the buffer occupancy of a single relay. The results demonstrate that the accuracy of the approximation is confirmed by our simulation results.

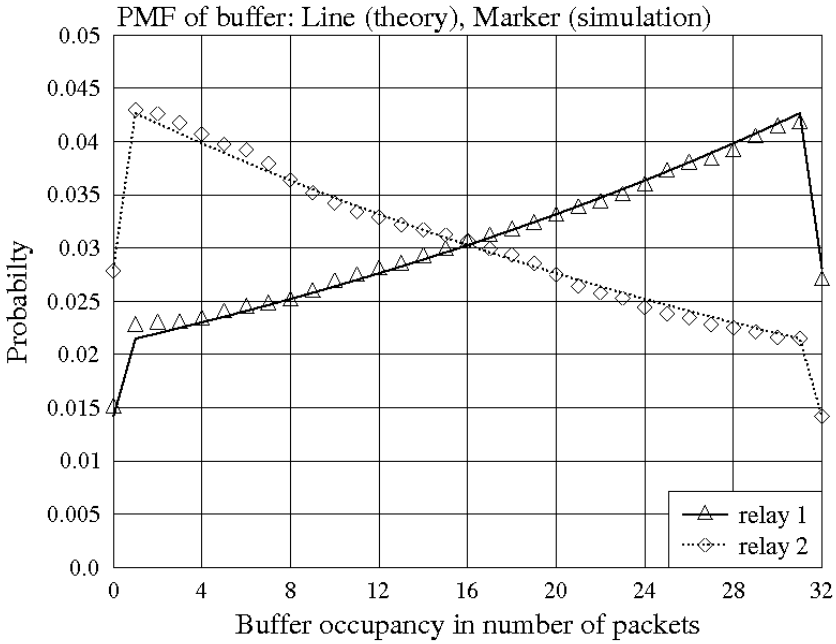

Figure 3.6: The distribution of the buffer occupancy for $\hat{B} = 32$. The X-axis represents the equivalent buffer size $\hat{B}$ while the Y-axis is the probability of a specific buffer-fullness. The solid curve is the theoretical distribution of the buffer occupancy of relay one, while the dotted curve is the theoretical distribution of the buffer occupancy of relay two. The markers are the simulation results respectively.

Below we consider the special case of two hops. In this case, all the approximate formulas provided above become near exact, yielding:

$$\begin{aligned} P_{\pi_0} &= P_{\pi_{\hat{B}}} = \frac{1}{2\hat{B}} \\ P_{\pi_i} &= \frac{1}{\hat{B}}, \ i = 1, 2, \ldots, \hat{B} - 1, \end{aligned} \tag{3.41}$$

which can be obtained either from the equations provided in this subsection or directly from (3.28). Note that, in (3.28), each line has no more then two unknowns. We assume $P_{\pi_0} = \kappa$ and $P_{\pi_i} = 2\kappa, i = 1, 2, \ldots, \hat{B} - 1$, as well as $P_{\pi_{\hat{B}}} = \kappa$. Finally, by exploiting (3.38) we arrive at $\kappa = \frac{1}{2\hat{B}}$.

Let us now analyze the outage probability (OP).

3.3.3 Outage Probability

The OP characterizes the specific event that the instantaneous SNR of the selected hop is lower than a pre-set threshold. When an outage occurs, no data will be transmitted over the MHL, in order to avoid violating the required target BER, since otherwise the BER would become higher than the target. Therefore, given the

set of thresholds γ_{T_l} for the L hops, the lower-bound OP is

$$P_{LO} = \frac{1}{L}\sum_{l=1}^{L}\left[\int_0^{\gamma_{T_l}} f_l^{SC}(\gamma)d\gamma\right], \tag{3.42}$$

when assuming that all the L hops have the same probability of $1/L$ being activated. Upon substituting $f_l^{SC}(\gamma)$ from (3.6) into the above equation, we readily arrive at:

$$P_{LO} = \frac{1}{L}\sum_{l=1}^{L}\left[\frac{\gamma(m_l, \frac{m_l\gamma_{T_l}}{\bar{\gamma}_l})}{\Gamma(m_l)}\right]^L. \tag{3.43}$$

Furthermore, given $P_{\boldsymbol{\pi}}$ and $\boldsymbol{P}_{sel}^{\hat{B}}$, the exact OP of the MHLs whose RNs have a finite buffer can be expressed as

$$P_O = \sum_{l=1}^{L}\sum_{\hat{l}=1}^{L}\boldsymbol{P}_{sel}^{\hat{B}}(l,\hat{l})\left[\frac{\gamma(m_l, \frac{m_l\gamma_{T_l}}{\bar{\gamma}_l})}{\Gamma(m_l)}\right]^{\hat{l}}. \tag{3.44}$$

3.3.4 Diversity Order

In a single hop, each $\bar{Q}_l\left(\sqrt{A_{i,j}\bar{\gamma}_l}\right)$ has the same $\bar{\gamma}_l$ and m_l, hence, $\bar{Q}_l\left(\sqrt{A_{i,j}\bar{\gamma}_l}\right)$ has the same diversity gain as $P_{Le}^{(l)}$. The diversity order DO_l can be derived for the lth hop from (3.18), yielding

$$\begin{aligned}\bar{Q}_l\left(\sqrt{A_{i,j}\bar{\gamma}_l}\right) = &\left(\frac{m_l}{\bar{\gamma}_l}\right)^{m_l}\frac{L}{\Gamma(m_l)} \\ &\times\int_0^{\infty} Q\left(\sqrt{A_{i,j}\gamma}\right)\gamma^{m_l-1}\left[\frac{\gamma\left(m_l, \frac{m_l\gamma}{\bar{\gamma}_l}\right)}{\Gamma(m_l)}\right]^{L-1}\exp\left(-\frac{m_l\gamma}{\bar{\gamma}_l}\right)d\gamma.\end{aligned} \tag{3.45}$$

When $\bar{\gamma}_l$ is large, the incomplete gamma function can be approximated as [188] (06.06.26.0002.01)

$$\begin{aligned}\gamma(m_l, \frac{m_l\gamma}{\bar{\gamma}_l})/\Gamma(m_l) =& \frac{(\frac{m_l\gamma}{\bar{\gamma}_l})^{m_l}}{\Gamma(m_l)m_l}\sum_{n=0}^{\infty}\frac{m_l}{m_l+n}\frac{(\frac{-m_l\gamma}{\bar{\gamma}_l})^n}{n!} \\ \approx& \frac{1}{\Gamma(m_l)m_l}\left(\frac{m_l\gamma}{\bar{\gamma}_l}\right)^{m_l}.\end{aligned} \tag{3.46}$$

Then, substituting (3.46) into (3.45), we arrive at:

$$\begin{aligned}\bar{Q}_l\left(\sqrt{A_{i,j}\bar{\gamma}_l}\right) \approx & \frac{m_l^{m_lL-L+1}}{\bar{\gamma}_l^{m_lL}}\frac{L}{\Gamma(m_l)^L}\int_0^\infty Q\left(\sqrt{A_{i,j}\gamma}\right)\gamma^{m_lL-1}\exp\left(-\frac{m_l\gamma}{\bar{\gamma}_l}\right)d\gamma \\ \approx & \frac{m_l^{m_lL-L+1}}{\bar{\gamma}_l^{m_lL}}\frac{L}{\Gamma(m_l)^L}\frac{1}{2\sqrt{\pi}m_lL}\left(\frac{2}{A}\right)^{m_lL}\Gamma(m_lL+\frac{1}{2}) \\ = & C\left(\frac{1}{\bar{\gamma}_l^{m_l}}\right)^L. \end{aligned} \tag{3.47}$$

where C is not related to $\bar{\gamma}_l$. From (3.47) we can explicitly see that the achievable diversity order of the lth hop is $DO_l = L$, when there are L available hops for activation. Furthermore, according to the operational principles of the MHD, the end-to-end performance of the MHL also benefits from attaining the diversity order of $DO_l = L$.

Note that the delay analysis of the MHLs employing the proposed MHD scheme is identical to that in [168]. More explicitly, the corresponding probability mass function (PMF) of the delay and the average delay of the system are the same as those in [168], but we have to replac B in [168] by the equivalent buffer size of $\hat{B} = B/\log_2 M$. Again, similarly to [168], the maximum and minimum packet delay are given by $\hat{B}L^2 - \hat{B}L - L + 2$ and L TSs. Finally the distribution of the delay is given by (36) of [168]. Given the distribution of the delay, the average delay may be readily calculated. The average delay increases with the number of hops and/or the size $\hat{B}$ of the buffer. The corresponding examples can be found in Fig. 10 and Fig.11 of [168].

3.4 Performance Results

In this section, we provide a range of performance results, in order to characterize both the BER and outage performance of the MHLs employing our MHD scheme, when communicating over Nakagami-m fading channels. We illustrate the effects of various MQAM schemes, buffer sizes, distances of the different hops and of different Nakagami-m fading parameters on the achievable performance. In our evaluations, we assume that the pathloss follows the negative exponential law of $d_l^{-\alpha}$, where α represents the pathloss exponent having a typical value between 2 to 6. In order to illustrate the impact of the number of hops per MHL on the achievable performance, we assume that the total energy assigned for transmitting one bit from the SN to the DN is constant, regardless of the number of hops per MHL. Specifically, we let the received energy at the DN is E_b unit when transmitting one bit directly from SN to DN, which is termed as the 'Average SNR per bit' in the figures. Then, when given

a pathloss exponent α and a distance d between SN and DN, the transmit energy required is then given by $E_{total} = \log_2 M \times d^{\alpha} E_b$. Then, if the MHL has L hops, the total energy E_{total} is assigned to the L transmit nodes, according to one of the following two scenarios. In the first scenario, appropriate energy allocation (EA) is implemented for assuming that all the hops have the same average SNR. In this case, the ith hop's transmit energy is $E_i = \frac{d_i^{\alpha} E_{total}}{\sum_{l=1}^{L} d_l^{\alpha}}$. Hence, all the L hops have the same received (signal) energy, which is $E' = \frac{E_{total}}{\sum_{l=1}^{L} d_l^{\alpha}}$. In the first scenario, we assume that different hops experience different fading CDFs, in order to illustrate the impact of diverse m-factors. In the second scenario, we assume that each of the L hops uses E_{total}/L unit of energy to transmit, while all the hops experience the same fading CDF. This allows us to investigate the effect of the distances between nodes on the achievable performance.

Note that in this section the theoretical results shown in the figures were evaluated from the formulas derived in Section 3.3, while the values represented by the markers were obtained via simulations. The curves corresponding to $B = 512$ were evaluated based on the approximation algorithm. Furthermore, the corresponding results for the conventional (Conv.) multihop transmission scheme are depicted as the benchmarkers.

Fig. 3.7 to Fig. 3.11 characterize the end-to-end BER performance. The impacts of the m-factor, of the buffer size of RN nodes, pathloss exponents, number of hops and of the modulation schemes on the end-to-end BER are investigated. Except for Fig. 3.9, where the different hops have different received average SNRs, in Fig. 3.7, 3.8, 3.10 and 3.11 all the hops have the same received average SNR, which is achieved with the aid of our hop-length-dependent EA. The parameters used in our investigations can be found in the corresponding figures. Note that, the distances shown in the figures are normalized distances obtained by assuming that the distance between SN and DN is unity.

Fig. 3.7 illustrates the impact of the buffer size on the end-to-end BER performance of three-hop links. Explicitly, the BER performance improves, as the buffer size of the RNs is increased, implying that MHD is indeed beneficial. When the buffer size is relatively large, such as $B = 512$ packets, corresponding to the equivalent buffer size of $\hat{B} = 128$, the attainable BER performance is close to the lower-bound BER achievable by using an infinite buffer size. As shown in the figure, in comparison to the conventional multihop diversity scheme, at a BER of 10^{-3}, the multihop diversity gain is over $14dB$, when a buffer of $B = 512$ packets is used by every RN.

Fig. 3.8 shows the impact of the propagation pathloss on the end-to-end BER

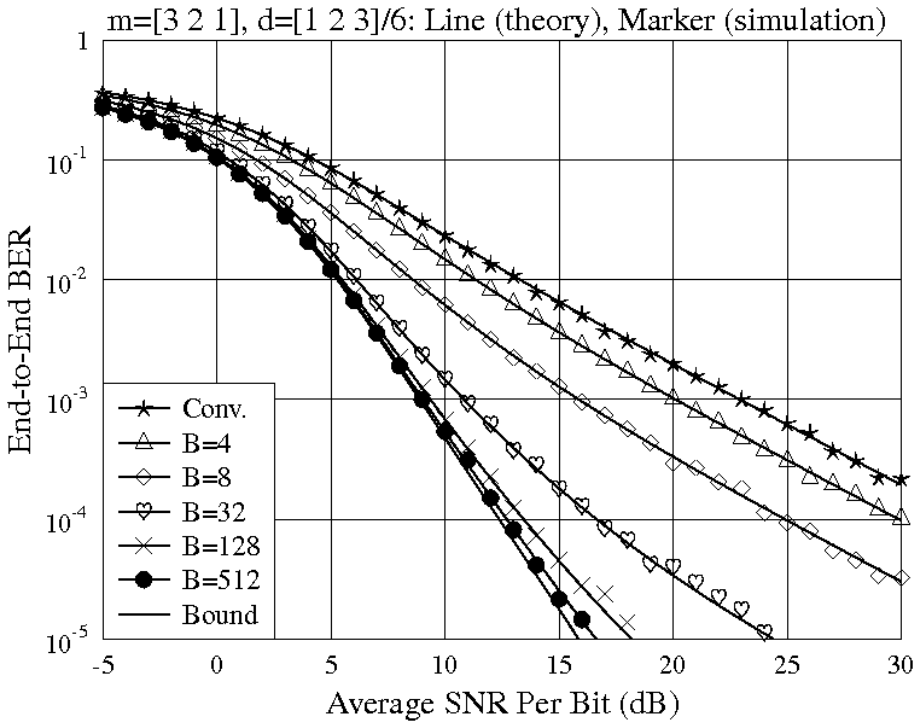

Figure 3.7: BER versus average SNR per bit performance of the three-hops having lengths of $d = [\frac{1}{6}\ \frac{2}{6}\ \frac{3}{6}]$ and experiencing different Nakagami-m fading associated with $m = [3\ 2\ 1]$, when the buffer size of every RN is $B = 4, \ldots, 512$ packets, the modulation scheme is 16QAM, and the EA is applied to ensure that all hops achieve the same received average SNR. The results were evaluated from (3.24) and (3.30).

performance of three-hop links experiencing different fading CDFs associated with $m = [3\ 2\ 1]$ for the first, second and third hops, respectively. The results show that the end-to-end BER performance improves, as the pathloss exponent becomes higher, implying a higher propagation pathloss. Hence, for high pathlosses, it is beneficial to use multihop transmission relaying on MHD. The reason behind it is that when the propagation pathloss increases, the total transmission energy required for single-hop transmission from SN to DN significantly increases. When this total energy is shared by multihop transmission, significant performance improvements can be obtained. Observe in Fig. 3.8 that our MHD scheme significantly outperforms the conventional multihop transmission scheme.

Fig. 3.9 shows the end-to-end BER of three-hop links experiencing the same Nakagami fading CDF of $m = 2$. In our simulations, equal energy allocation was applied. Hence, the different hops have different received average SNRs due to the different distances assumed. In this case, the system's BER performance will be dominated by that of the longest hop. As seen in Fig. 3.9, a significant MHD gain can be obtained in comparison to the conventional multihop transmission scheme. Specifically, at the BER of 10^{-3}, the MHD gain is in excess of than $7dB$, which is

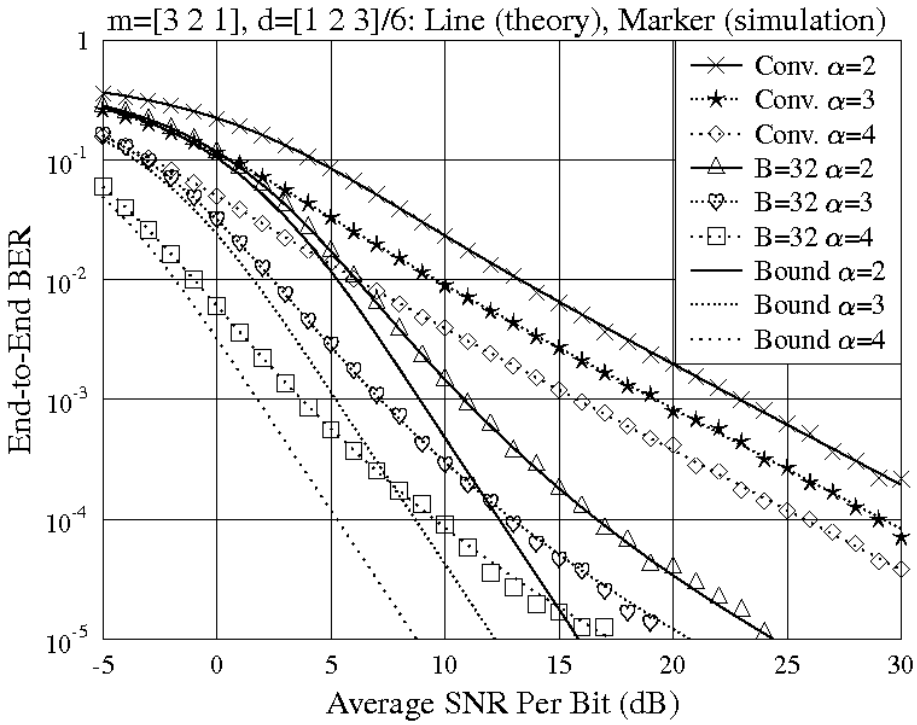

Figure 3.8: BER versus average SNR per bit performance of three-hop links of the three hops having the distances $d = [\frac{1}{6}\ \frac{2}{6}\ \frac{3}{6}]$ and experiencing different Nakagami-m fading associated with $m = [3\ 2\ 1]$ and different pathloss reflected by $\alpha = 2, 3, 4$, when the buffer size of every RN is $B = 32$ packets, the modulation scheme is 16QAM, and the EA is applied to make all hops achieve the same received average SNR. The results were evaluated from (3.24) and (3.30).

achieved by arranging every RN a buffer of $B = 128$ packets.

Fig. 3.10 demonstrates the impact of the number of hops on the end-to-end BER performance. In the simulations, we assumed that the modulation scheme was 16QAM and the buffer size was $B = 8$. Different hops were assumed to experience i.i.d Nakagami-m fading and all hops had the same distance. Explicitly, given the distance between SN and DN, the BER performance is improved, when the number of hops is increased, resulting in more diversity gain.

Fig. 3.11 shows the end-to-end BER performance for different modulation schemes employed by a 2-hop link with a RN of buffer size $B = 32$, when operated in Rayleigh fading ($m = 1$) channels. Compared to the conventional multihop diversity scheme, the MHD achieved a $9dB$ gain for QPSK and a $4dB$ gain for 256QAM at the BER of 10^{-3}. The reason for having a lower diversity gain for high order modulation schemes is that the equivalent buffer size is $\hat{B} = 32/\log_2 4 = 16$ for 4QAM and $\hat{B} = 32/\log_2 256 = 4$ for 256QAM.

Figs. 3.12, 3.13 and 3.14 characterize the outage probability of our multihop links, when various MQAM schemes, various buffer sizes and various number of hops are

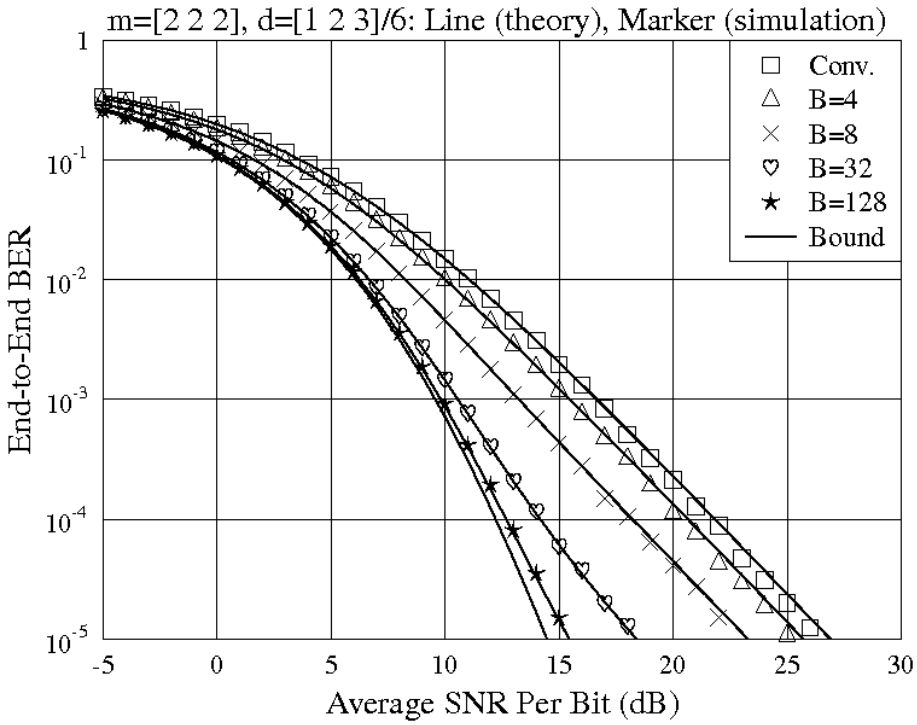

Figure 3.9: BER versus average SNR per bit performance of three-hop links of the three hops having the distances $d = [\frac{1}{6}\ \frac{2}{6}\ \frac{3}{6}]$ and experiencing the same type of Nakagami-m fading associated with $m = 2$, when the buffer size of every RN is $B = 4, \ldots, 128$ packets, the modulation scheme is 16QAM, and 1/3 of the total transmission energy is assigned to every hop, hence the hops have different received average SNR. The results were evaluated from (3.24) and (3.30).

considered. These figures stipulate the same assumptions, as Figs. 3.7, 3.10 and 3.11, respectively. Note that in our numerical computations and simulations, the threshold set of $\gamma_{T_1} = \ldots = \gamma_{T_L} = \gamma_T$ was adjusted for maintaining a BER of 0.03 for a single-hop link, when the received energy for a bit transmitted from the SN to DN was 1 [70]. The outage probability of the corresponding conventional multihop scheme is also provided for the sake of comparison in Fig. 3.12 and Fig. 3.14. From these figures, we may derive similar observations to those emerging from Figs. 3.7, 3.10 and 3.11. In summary, in Fig. 3.12, a significant multihop diversity gain is observed for the RNs employing buffers of a sufficiently high size. The line with solid circles, which represents the case of a large buffer size ($B = 512$ packets giving an equivalent buffer size of $\hat{B} = 128$), approaches the theoretical bound. Fig. 3.13 shows that the outage probability reduces, as the number of hops increases. Fig. 3.14 characterize the outage probability of two hop links relying on different modulation scheme, as evaluated from (3.30) and (3.44), which exhibits a lower improvement for higher-order modulation schemes, because the equivalent buffer size of higher-order modulation schemes is lower than for lower-order modulation schemes.

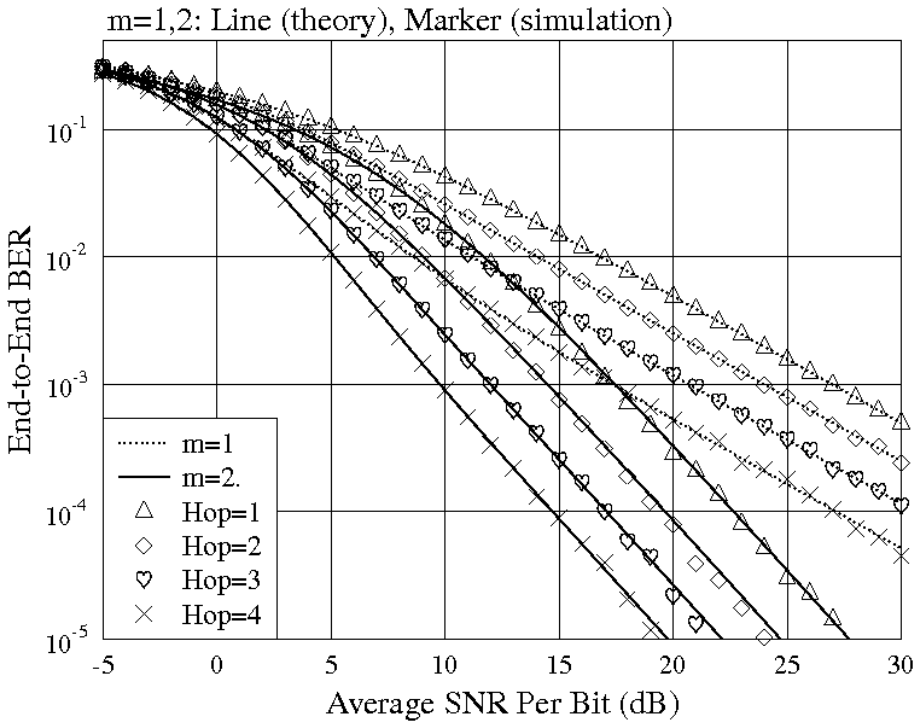

Figure 3.10: BER versus average SNR per bit performance with respect to different number of hops, when the buffer size of every RN is $B = 8$ packets and the modulation scheme is 16QAM. The distance between SN and DN is the same regardless of the number of hops and, for any case, all hops have the same distance. The results were evaluated from (3.24) and (3.30).

Finally, Fig. 3.15 shows the outage probability versus SNR. This figure also allows us to infer the achievable diversity order of the system for our three-hop link having the node-distances of $d = [\frac{1}{3}\ \frac{1}{3}\ \frac{1}{3}]$ and experiencing different Nakagami-m fading associated with $m = [3\ 2\ 1]$. The buffer size of every RN is $B = 4, \ldots, 128$ packets, the modulation scheme is 16QAM, and the EA of Section 3.2 is applied to allow all hops to achieve the same average received SNR. It can be observed that the diversity order is one for high average SNRs, which is dominated by the worst hop.[6]

3.5 Chapter Conclusions

In Section mqam:introduction, a generalized channel activation scheme was proposed for transmitting information over MHLs. Within a given TS, our MHD scheme activates a specific hop from the set of available hops based on the values given by their CDFs. Our analysis in Section 3.2 showed that this CDF-aware MHD scheme represents a generalized MHD scheme, which is suitable for arbitrary MHLs, where

[6] Although the diversity order is one for a finite buffer size, the curve approachs the theoretical bound more closely for a larger buffer size.

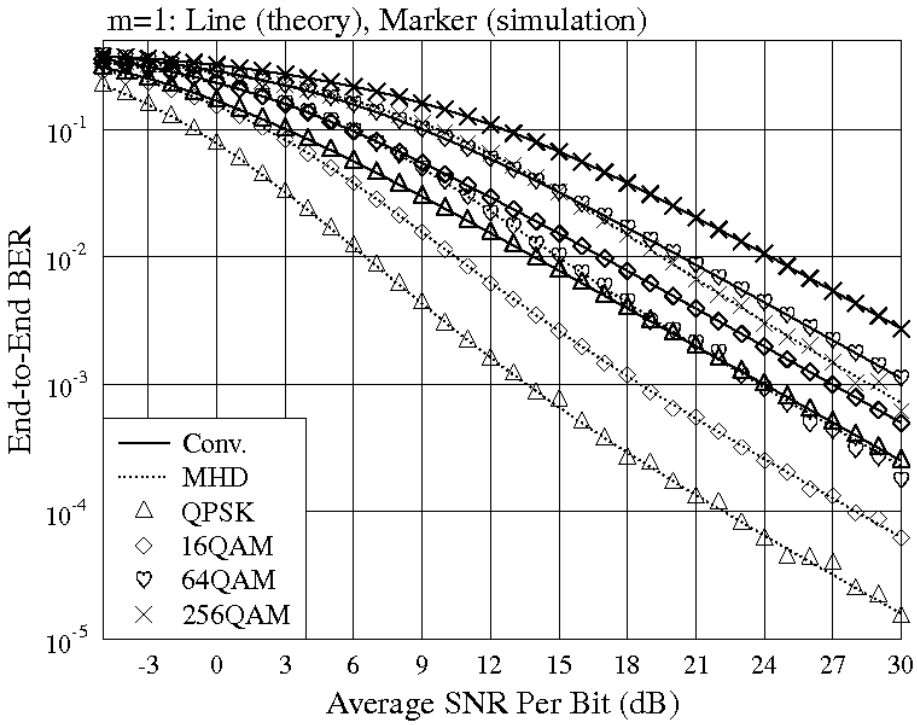

Figure 3.11: BER versus average SNR per bit performance of two-hop links with different modulation schemes, when communicating over Rayleigh ($m = 1$) fading channels. The buffer size of every RN is $B = 32$ packets, the modulation scheme is 16QAM and both hops have the same distance. The results were evaluated from (3.24) and (3.30).

different hops may have different average SNRs and experience different types of fading CDFs. Furthermore, as seen in (3.47), our MHD scheme is capable of achieving the maximum attainable diversity gain provided by the independent fading experienced by the different hops. Moreover, the performance of MHLs employing our MHD scheme was investigated in Section 3.3, when communicating over Nakagami-m fading channels. Both near exact and approximate expressions were derived in Sections 3.3.1 to 3.3.3 for both the end-to-end BER as well as for the outage probability of BPSK/MQAM signals. Our performance results of Fig. 3.7 to Fig. 3.9 showed that exploiting the independent fading of different hops results in a significant diversity gain. As seen in Fig. 3.10 and Fig. 3.13, the achievable multihop diversity gain increases, as the relay's buffer size increases, as well as when the affordable packet delay increases. The achievable multihop diversity gain improved as the number of hops increased. Therefore, the MHD-assisted multihop transmission regime is significantly more energy-efficient than the conventional multihop transmission, although both of them have higher energy-efficiency than single-hop transmissions.

As a natural evolution from Chapter 2, in this chapter we extended our analysis

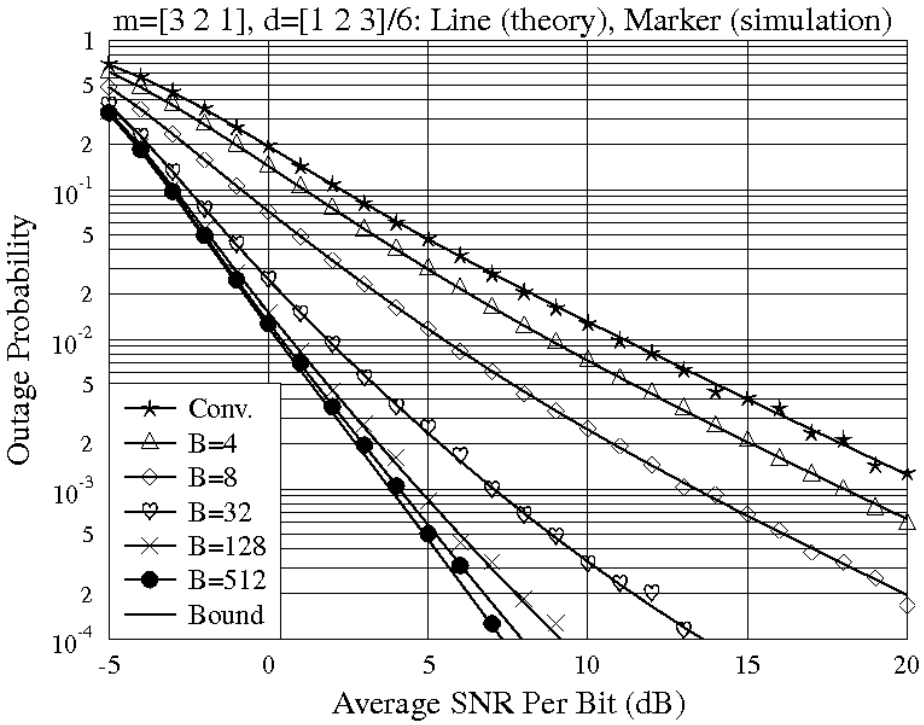

Figure 3.12: Outage performance of three-hop links of the three hops having the distances $d = [\frac{1}{6}\ \frac{2}{6}\ \frac{3}{6}]$ and experiencing different Nakagami-m fading associated with $m = [3\ 2\ 1]$, when the buffer size of every RN is $B = 4, \ldots, 512$ packets, the modulation scheme is 16QAM, and the EA is applied to make all hops achieve the same received average SNR. The results were evaluated from (3.44) and (3.30).

from BPSK transmissions over and Rayleigh channels to BPSK/MQAM communications over Nakagami-m channels. However, the time-invariant modulation schemes employed may be further generalized to near-instantaneously adaptive modulation based on the near-instantaneous channel conditions. Hence in the next chapter we will consider multihop transmission relying on adaptive modulation techniques.

3.6 Appendix

3.6.1 Alternative Derivation of (3.6)

The probability of the lth channel is selected at channel energy γ can be expressed by conditional probability: the probability of the lth hop which has the largest CDF is selected with energy γ (Event A) to the probability of the lth hop is selected (Event B). The latter probability (Event B) is $\frac{1}{L}$ cause every channel has the same probability of being chosen. Let's discuss the former probability (Event A).

Assuming the the probability the lth channel with channel energy γ is $f_l(\gamma)$. The CDF of this channel energy is $F_{m_l}(\gamma)$. The CDF of all other channels regardless the fading type should be lower than $F_{m_l}(\gamma)$ to keep the CDF of the lth channel is

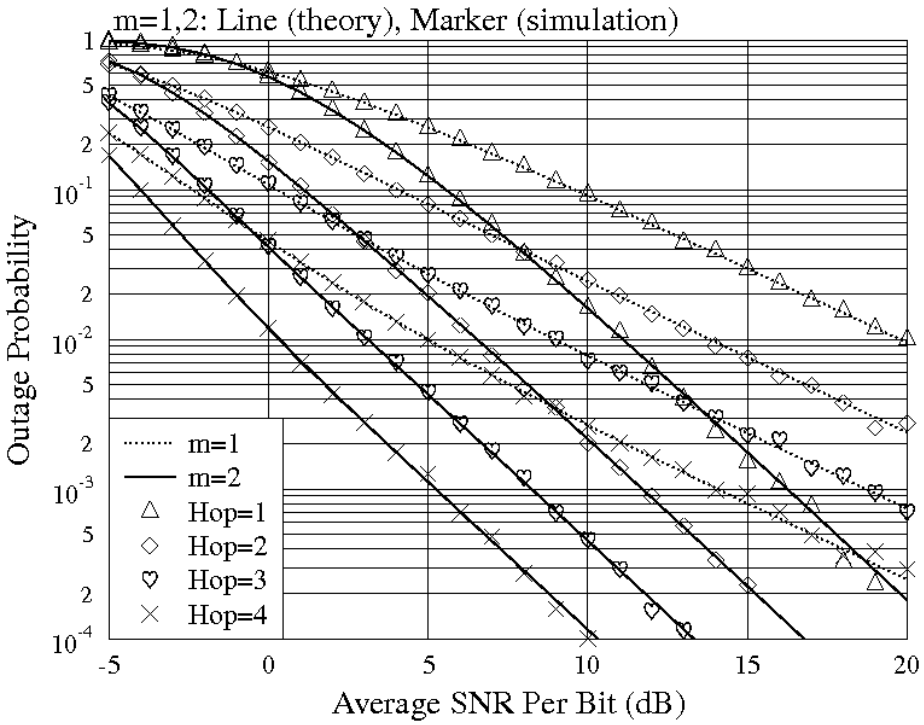

Figure 3.13: Outage performance with respect to different number of hops, when the buffer size of every RN is $B = 8$ packets and the modulation scheme is 16QAM. The distance between SN and DN is the same regardless of the number of hops and, for any case, all hops have the same distance. The results were evaluated from (3.44) and (3.30).

the largest one. Hence, the probability of Event A is $f_l(\gamma)[F_{m_l(\gamma)}]^{L-1}$. Finally, the probability of the lth channel is selected at channel energy γ as in (3.6) can be found, yielding

$$f_l^{SC}(\gamma) = \frac{f_l(\gamma)[F_{m_l(\gamma)}]^{L-1}}{\frac{1}{L}} = L_l(\gamma)[F_{m_l(\gamma)}]^{L-1} \tag{3.48}$$

3.6.2 Alternative Expression of (3.19)

The original expression of $\int_0^\infty e^{-at}t^{b-1}Q(\sqrt{ct})dt$ is in [15]. Another tighter expression is shown here. The Gaussian-Q function can be expressed as [188](06.27.26.0001.01)

$$Q(\sqrt{ct}) = \frac{1}{2} - \frac{\sqrt{ct/2}}{\sqrt{\pi}}{}_1F_1\left(\frac{1}{2}; \frac{3}{2}; \frac{-ct}{2}\right). \tag{3.49}$$

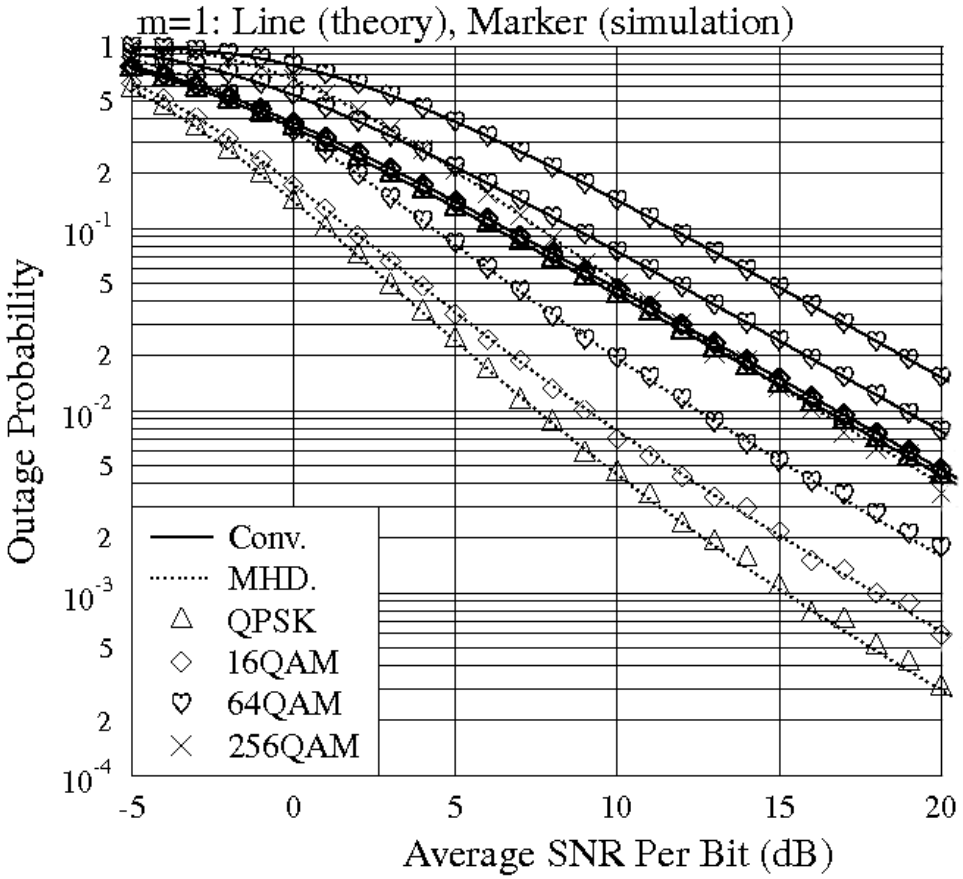

Figure 3.14: Outage performance of two-hop links with different modulation schemes, when communicating over Rayleigh ($m = 1$) fading channels. The buffer size of every RN is $B = 32$ packets, the modulation scheme is 16QAM and both hops have the same distance. The results were evaluated from (3.44) and (3.30).

The integral in (3.19) can be derived as

$$\begin{aligned}
&\int_0^\infty e^{-at}t^{b-1}Q(\sqrt{ct})dt \\
=&\int_0^\infty \left(\frac{1}{2}-\frac{\sqrt{ct/2}}{\sqrt{\pi}}{}_1F_1(\frac{1}{2};\frac{3}{2};\frac{-ct}{2})\right)e^{-at}t^{b-1}dt \\
=&\frac{\Gamma(b)}{2a^b}-\frac{c}{2\pi}\sum_{k=0}^{\infty}\frac{(\frac{1}{2})_k}{(\frac{3}{2})_k}(-\frac{c}{2})^k\int_0^\infty t^{k+b-\frac{1}{2}}e^{-at}dt \\
=&\frac{\Gamma(b)}{2a^b}-\frac{c}{2\pi}\frac{\Gamma(b+\frac{1}{2})}{a^{b+\frac{1}{2}}}{}_2F_1(\frac{1}{2},b;\frac{3}{2};-\frac{c}{2a})
\end{aligned} \tag{3.50}$$

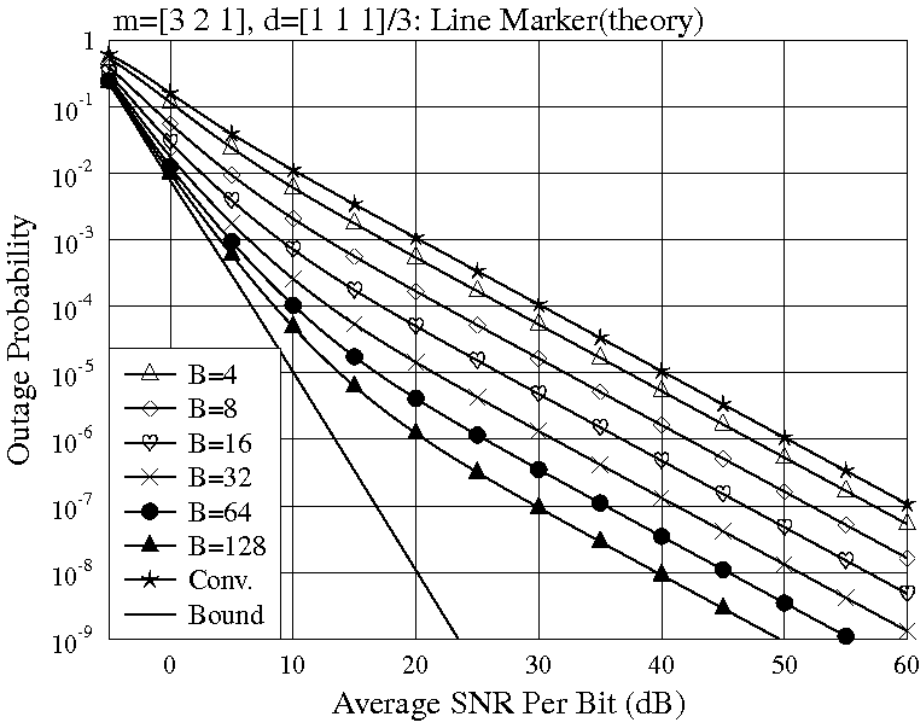

Figure 3.15: Outage performance of three-hop links of the three hops having the distances $d = [\frac{1}{3}\ \frac{1}{3}\ \frac{1}{3}]$ and experiencing different Nakagami-m fading associated with $m = [3\ 2\ 1]$, when the buffer size of every RN is $B = 4, \ldots, 128$ packets, the modulation scheme is 16QAM, and the EA is applied to make all hops achieve the same received average SNR. This figure shows the diversity order. It can be seen that the diversity order is one for very high average SNR which is dominated by the worst hop. The results were evaluated from (3.43).

Hence, the whole (3.19) can be expressed as

$$\begin{aligned}
&\bar{Q}_l\left(\sqrt{A_{i,j}\bar{\gamma}_l}\right) \\
&= \left(\frac{m_l}{\bar{\gamma}_l}\right)^{m_l} \frac{L}{\Gamma(m_l)} \sum_{l=0}^{L-1} (-1)^l \binom{L-1}{l} \sum_{k=0}^{l(m_l-1)} c_k^{(l)} \left(\frac{m_l}{\bar{\gamma}_l}\right)^k \left(\frac{\Gamma(k+m_l)(\bar{\gamma}_l)^{k+m_l}}{2(m_l(l+1))^{k+m_l}}\right. \\
&\quad \left. - \sqrt{\frac{A_{i,j}}{2\pi}} \frac{\Gamma(k+m_l+\frac{1}{2})}{(m(l+1)/\bar{\gamma}_l)^{k+m_l+\frac{1}{2}}} {}_2F_1\left(\frac{1}{2}, k+m_l+\frac{1}{2}; \frac{3}{2}; \frac{-A_{i,j}\bar{\gamma}_l}{2m_l(l+1)}\right)\right). \qquad (3.51)
\end{aligned}$$

Chapter 4

Multi-Hop Diversity Aided Multi-Hop AQAM Links for Nakagami-m Channels

In Chapter 2 buffer-aided multihop transmission was proposed for achieving multihop diversity where the specific hop having the highest channel SNR was activated. BPSK transmission over Rayleigh channels was considered. By contrast in Chapter 3, we investigated QAM transmissions over Nakagami$m$ channels. In order to guarantee that the number of input packets is the same as the number of output packets at each RN, when each hop experienced independent but non-identical distributed (i.n.i.d) flat Nakagami-m fading, a cumulative distribution function (CDF) based channel activation scheme was proposed. Although these transmission schemes were capable of achieving multihop diversity, the activated channel allows only transmitted the same number of packets in each time slot. Hence, for the sake of enhancing the achievable throughput, near-instantaneously adaptive modulation is invoked in this chapter.

4.1 Introduction

In Chapter 3, we have studied MHL, where a constant-rate time-invariant modulation scheme was assumed for transmission over a selected hop, regardless of the channel-quality. However, in order to achieve an increased throughput, adaptive modulation (AQAM) may be considered.

Adaptive modulation and coding (AMC) [186] is a term routinely used in wireless communications for indicating that system parameters are near-instantaneously adapted to the CQ, which will enhance the system's performance. The authors

of [189] characterized adaptive modulation relying on Space-Time Block Code (STBC) aided transmission using Maximum Ratio Combining (MRC) for single-hop transmissions over Nakagami-m channel. Maximum throughput optimization was studied in [70] by finding the AMC mode-switching thresholds of different modulation schemes. As a further advance, the authors of [147] discussed the performance of adaptive modulation in Amplify-and-Forward (AF) relaying networks relying on a limited feedback. However, data transmission typically relies on packet-by-packet regimes, where each packet has a specific AMC mode. The authors of [71] analyzed the Packet Error Ratio (PER) vs SNR relationship using AMC for the HIPERLAN/2 standard. Then Kwon and Cho [73] extended the application of AMC to a short-packet-based scenario relying on truncated Automatic Repeat Request (ARQ). Later, the effects of queuing were also taken into account at data link layer in [72]. Furthermore, Kwon and Cho [74] discussed the associated resource allocation issues. Then Ramis and Femenias [75] extended the results of [71] by providing a range of practical parameters. Yang *et al* [78] combined adaptive modulation with Generalized Selective Combining (GSC) under the terminology of *joint adaptive modulation and diversity combining*. This work was then carried on in [79,80]. Aniba and Aissa [189] discussed adaptive modulation in conjunction with packet combining and truncated ARQ for transmission over MIMO Nakagami fading channels. Against this background, we combine the advantages of MHD and adaptive modulation for improving the achievable performance.

The new contributions of this chapter are

1. We proposed the Maximum Throughput Adaptive Rate Transmission (MTART) regime.

2. The end-to-end BER, OP, capacity, throughput as well as the distribution of the delay are analyzed.

3. The MAC protocol for MTART is proposed.

The rest of this chapter is organized as follows. Section 4.2 presents our system model, while Section 4.3 proposes a MAC layer protocol for this transmission scheme. Then Section 4.4 and Section 4.5 analyze the achievable performance for transmission in both general and specific Nakagami-m-fading channel scenarios. In Section 4.6, our numerical and simulation results are compared, while our conclusions are offered in Section 4.7.

4.2 System Model

The MHL considered in this contribution is the same as the one studied in [178], which is shown in Fig. 4.1. The MHL consists of $(L+1)$ nodes, namely a SN S

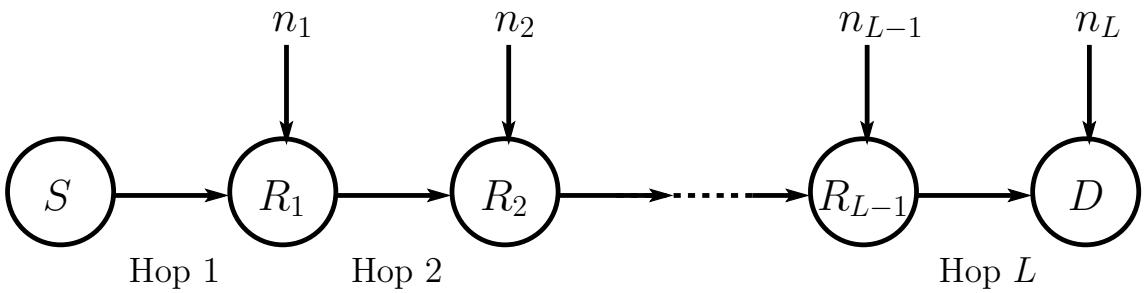

Figure 4.1: System model for a multihop wireless link, where the SN S sends messages to the DN D via $(L-1)$ intermediate RNs.

(node 0), $(L-1)$ RNs, $R_1, R_2, \cdots, R_{L-1}$, and a DN D (node L). The length of the hops is given by $d_1, d_2, \cdots, d_L$. The SN S sends messages to the DN D via L hops with the aid of the $(L-1)$ RNs. At the RNs, the classic decode-and-forward (DF) protocol [150] is employed for relaying the signals. We denote the symbol transmitted by node 0 as x_0 and its estimate at the DN D of node L by $x_L = \hat{x}_0$, while the symbol estimated at the lth RN by $x_l,\ l = 1, \ldots, L-1$. At the packet level, they are correspondingly represented by $\boldsymbol{x}_0$, $\boldsymbol{x}_l,\ l = 1, \ldots, L-1$, and $\boldsymbol{x}_L = \hat{\boldsymbol{x}}_0$. We assume that the signals are transmitted on the basis of TSs having a duration of T seconds. In addition to the propagation pathloss, the channels of the L hops are assumed to experience independent block-based flat fading, where the complex-valued fading envelope of a hop remains constant within a TS, but is independently faded for different TSs. In practice, the channel exhibits may have the correlation in the time-domain. However, in order to reduce the complexity of the problem, we may assume uncorrelated fading by adopting the coherence time as the length of a TS. In Rappaport's book [190], this time is calculated as $0.423/f_d$, where the f_d is the maximum Doppler frequency. The pathloss is assumed to obey the inverse-power law of $d_i^{-\alpha}$, where α is the pathloss exponent, having a value between 2 and 6. We assume that the total energy per symbol transmitted from the SN S to the DN D is $E_s = 1$ unit, regardless of the number of hops per MHL. This one unit of energy is shared among the L transmit nodes. Let us also assume that the MTART scheme supports five possible data rates associated with 0, 1, 2, 4, and 6 packets per TS, corresponding to using 'no transmission', BPSK, QPSK, 16QAM and 64QAM. In this case, the CQ of a hop is classified into one of the five CQ regions with the aid of the four thresholds, obeying $T_{h1} < T_{h2} < T_{h3} < T_{h4}$. The system is assumed to have a target end-to-end packet BER BER_{tar}^{e2e} and the four thresholds should be predetermined for ensuring that the packet-BER remains below the end-to-end target BER. In practice, the following two cases may occur.

Case One: we assume that appropriate energy allocation (EA) is used for ensuring that all the receivers have the same average SNR. In this case, the ith hop's transmit energy is $E_i = \frac{d_i^\alpha E_s}{\sum_{l=1}^{L} d_l^\alpha}$. Hence, all the L hops have the same received energy of $E' = \frac{E_s}{\sum_{l=1}^{L} d_l^\alpha}$. In this case, every hop is identical and has the same thresholds, which is the necessary condition for our MTART. The target BER may approximately equally assign to each hop. The target BER for each hop becomes $BER'_{tar} = BER^{e2e}_{tar}/L$. Therefore the thresholds can be determined. For example, as the lower bound of BPSK, the threshold T_{h1} obeys $Q(\sqrt{2E'T_{h1}}) = BER'_{tar}$.

Case Two: However, the same average hop SNR may not be ensured by EA. Our basic idea is to allocate the end-to-end target BER to each hop in order to allow every hop to have the same modulation thresholds. The specific hop having a higher average receive SNR may be allocated lower hop target BER, while the hop with a lower average receiver SNR may be allocated higher hop target BER. Let us also assume that the target BER for the ith hop is BER^i_{tar}. Approximately, we have $\sum BER^i_{tar} = BER^{e2e}_{tar}$. With the aid of a simple greedy algorithm, where the hop with lower thresholds is assigned a higher target BER, BER^i_{tar} may be readily found. The switching thresholds determined for each hop may have slight differences, hence we have $T^{hop1}_{h1} \approx T^{hop2}_{h1}$. Finally, we set the unified threshold to the largest value amongst the corresponding switching thresholds, according to $T_{h1} = \max(T^{hop1}_{h1}, T^{hop2}_{h1})$. We then also carry out the same operation for T_{h2}, T_{h3} and T_{h4}, respectively. The detailed discussions about the switching thresholds can be found in the extended version of this paper in [170].

In summary of **Case One** and **Case Two**, in this chapter, we assume that the switching thresholds for each hop are the same. When the $(l-1)$st node transmits a packet $\boldsymbol{x}_{l-1}$, the observations received by node l may be expressed as

$$\boldsymbol{y}_l = \sqrt{E_l} h_l \boldsymbol{x}_{l-1} + \boldsymbol{n}_l, \ l = 1, 2, \ldots, L, \tag{4.1}$$

where E_l is the transmission power and h_l represents the fast-fading channel's gain for the lth hop between node $(l-1)$ and node l, while $\boldsymbol{n}_l$ is the Gaussian noise added at node l. The fast fading channel gain h_l is assumed to be complex Gaussian with a zero mean and a variance of $E[|h_l|^2] = 1$. The noise samples in $\boldsymbol{n}_l$, $l = 1, \ldots, L$, obey the complex Gaussian distribution with zero mean and a common variance of $\sigma^2 = 1/2$ per dimension. Based on the above definitions and on (4.1), the instantaneous SNR of the lth hop is then given by $\gamma_l = E'|h_l|^2$.

Naturally, due to the store-and-wait characteristics of the RNs, the potential performance improvement is obtained at the cost of an increased delay. In this

contribution, we study both the *block delay* and the *packet delay*. In [168], the block delay is defined as the time required for a block of packets generated by the SN to reach the DN. By contrast, the packet delay is the time required for delivering a specific packet from the SN to the DN, when assuming that there is an infinite number of packets to transmit.

In this chapter, we investigate both the BER as well as the OP of MHLs employing our MHD scheme [175, 178] associated with adaptive M-ary Quadrature (MQAM) [70, 186]. Furthermore, the delay distribution of the MHLs is also studied, while stipulating the following assumptions:

- The SN always has packets for transmission in its buffer, when considering its steady state operation;
- Both the SN S and DN D can store an infinite number of packets. By contrast, each of the $(L-1)$ RNs can only store at most B packets;
- The fading processes of the L hops of a MHL are independent. The fading of a given hop remains constant within a packet's duration, but it is independently faded from one packet to another;
- According to the CQ, such as the SNR of a hop, the most appropriate MQAM scheme is chosen from the available set of MQAM modes for the sake of guaranteeing the required quality-of service (QoS), such as a specific BER;
- A MHD protocol is employed, which will be detailed in Section 4.3. Based on the CQ knowledge of the L hops within a given TS, the MHD protocol decides, which of the L hops is selected for transmission. For simplicity, all the operations of the MHD protocol are assumed to be carried out without delay and errors.

In the next section, we first propose a MAC protocol for controlling the operations of the MHLs employing adaptive MQAM.

4.3 MAC Protocol for Multihop Links Using Adaptive MQAM

In this section we design a MAC protocol for controlling the operations of a MHL employing adaptive MQAM, where the specific hop having the highest CQ and hence the highest throughput is chosen for transmission.

Our protocol is based on the following assumptions. Consider the L-hop link shown in Fig. 4.1, where the nodes are indexed from the SN to DN as node 0, node $1, \ldots$, node L. Each of the L nodes is aware of its own index, which determines its relative position along the link. We assume that the transmission range of a node

is at most one hop, implying that a node can only communicate with the pair of its adjacent nodes. The interference range of a node is assumed to be at most two hops, implying that any transmitted signal may affect upto five consecutive nodes of the link, including the one transmitting the designed signal. For a given node, we assume that the channel of a hop within its transmission range is divided into S CQ levels, denoted as $C_0, C_1, \ldots, C_{S-1}$ with C_{S-1} being the best-quality level and C_0 being the lowest-quality level. By contrast, a two-hop channel within its interference range is divided into two states, namely, 'interfered with (1)' or 'uninterfered with (0)'. Furthermore, the link-quality of the channel between node i and node j is denoted by $C_{i,j},\ i, j = 0, 1, \ldots, L$.

In addition to the above assumptions, we also assume that node $(k-1)$ can always receive the Request For Transmission (RFT) [168] signal from node k, provided that we have $C_{k-1,k} \geq C_1$. Furthermore, for the signalling of the RFT and Clear For Transmission (CFT) [168] signal generated in response to a received RFT signal, the error-resilient binary signalling is assumed.

In order to activate the most appropriate hop from the set of L hops for transmission, our proposed protocol consists of the following two stages of operations.

a) The first stage uses five Symbol Durations (SDs) for the $(L + 1)$ nodes to broadcast their CQ information, in order to assist both their immediately adjacent neighbour (one hop) nodes and the interfering (two hops away) nodes for estimating the qualities of the corresponding channels;

b) During the second stage, the most appropriate hops are selected for transmission. We will show that this stage may require a variable number of SDs. To elaborate a little further, the operations associated with the above-mentioned two stages are described as follows.

Stage 1 (Channel State Identification): Again, this stage requires five SDs. Within the ith, $i = 0, 1, 2, 3, 4$, symbol duration, the nodes having the position indices obeying $(i + 5j)$, $j = 0, 1, \ldots$, and $i + 5j \leq L$, broadcast their pilot signals. After receiving the pilot signal, the two adjacent nodes of a transmitting node estimate the corresponding CQ and classify each of them into one of the S levels. Specifically, for node k, the quality of the channel between node $(k - 1)$ and node k is expressed as $C_{k-1,k}$, while that of the channel spanning from node k to node $(k+1)$ is expressed as $C_{k,k+1}$, both of which belong to $\{C_0, C_1, \ldots, C_{S-1}\}$. For any of the two nodes within the interference range of a transmitting node, if any of them receives the pilot signal, it sets the interference flag to logical one. Otherwise, the interference flag is set to zero.

Table 4.1: MAC State List

State	Meaning	Action
R1	*Candidate for receiving*	Broadcast RFT1
R2	*Receiving*	Broadcast RFT2
T	*Transmission*	Broadcast CFT
W1	*Possible of waiting*	Keep silent and listen to the channel
W2	*Waiting*	Keep silent
X	*Unknown*	Keep silent and listen to the channel

Stage 2 (Selection of Desired Hops): In general, the specific hop having the highest Potential Rate (PR) has the priority to transmit, as motivated by achieving the highest possible throughput for the MHL. Here, the PR of a hop from node i to node $(i+1)$ is determined by the minimum number of packets associated with the following situations. a) The number of packets stored in the buffer of node i. b) The number of available storage packets in the buffer of node $(i+1)$. c) The maximum transmission rate expressed in packets per TS that is derived based on the CQ between node i and node $(i+1)$, i.e. based on $C_{i,i+1}$. Explicitly, determining the PR requires the knowledge of the buffer fullness for transmission from both node i and node from $(i+1)$.

For the sake of using decentralized algorithms, we also introduce the concept of the Potential Rate at the Transmitter (PRT), which is defined as the minimum of the number of packets associated with the situations a) and c), and the Potential Rate at the Receiver (PRR), which is defined as the minimum of the numbers of packets associated with the situations b) and c). For the ith hop, the values of PR, PRT and PRR are associated with a subscript i. Note that if there are two or more hops having the same PR, then the hop related to a transmit node having the highest position index has the priority to be selected over the other hops. This is justified, since they have a higher probability of being successfully delivered to the DN, hence yielding a lower delay.

Again, it can be shown that the number of SDs required by the second stage is a variable, but it is at most $[L \times (S-1)]$ SDs. Furthermore, since both the transmit and receive nodes of a hop rely on the CQ information of a hop, the hop may be activated either by its transmit node or by its receive node. In our MAC protocol to be described below, we assume that a hop selected for transmission is activated by the corresponding receive node. For convenience, we define the node states as well as the corresponding actions in Table 4.1. Here, a possible signalling scheme for the RFT and the CFT signals may be RFT1=RFT2=1 and CFT=-1. Based on the

above definitions of the MAC states, the transition between the different types of MAC states may be discussed as follows, where only two sequences of actions occur in the MAC layer, as shown in Fig. 4.2 and Fig. 4.3.

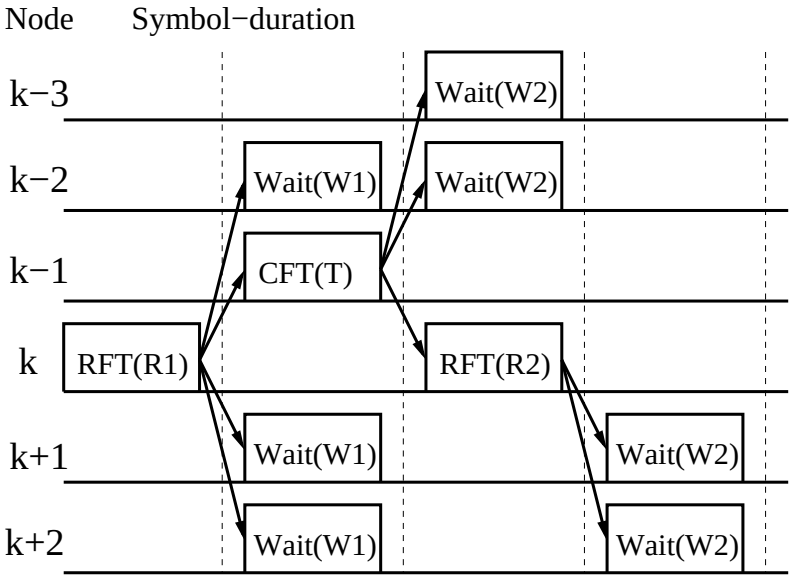

Figure 4.2: Node k broadcasts a RFT in the first SD. Node $(k-1)$ responses with a CFT in the second SD. The other nodes such as node $(k+1)$, $(k+2)$ and $(k-2)$ which have received the RFT in the first SD will set their states to $W1$. In the third SD, after receiving the CFT transmitted by node $(k-1)$, node k rebroadcasts a RFT. In the same SD, the nodes such as $(k-3)$ and $(k-2)$ that have received the CFT will set their states to $W2$. In the fourth SD, the nodes such as $(k+1)$ and $(k+2)$ which are in the waiting state $W1$ and have received the second RFT will set their states to $W2$. The detailed conditions to be satisfied before the above actions are triggered will be discussed later in the context of Fig. 4.4.

Firstly, as shown in Fig. 4.2, relying on the states seen in Table 4.1, node k first broadcasts a RFT signal in the first SD. Then, node $(k-1)$ responds with a CFT signal in the second SD after it receives the RFT signal. The other nodes, such as node $(k+1)$, $(k+2)$ and $(k-2)$, which received the RFT signal in the first SD set their states to $W1$, which represents 'possible waiting'. In the third SD, after receiving the CFT signal, node k rebroadcasts a RFT signal. In the same SD, the nodes such as node $(k-3)$ and $(k-2)$ that have received the CFT signal transmitted by node $(k-1)$ in the second SD will set their states to $W2$ of 'waiting'. In the fourth SD, the nodes in state W1, such as node $(k+1)$ and $(k+2)$ that have received the second RFT will set their states to $W2$. In the above-mentioned state transition signalling, there are certain trigger conditions to be satisfied for the actions to be initiated, which will be analyzed later in the context of Fig. 4.4.

Secondly, as the example of Fig. 4.3 shows, node k first broadcasts a RFT signal in the first SD. However, node $(k-1)$ does not respond with a CFT signal in the

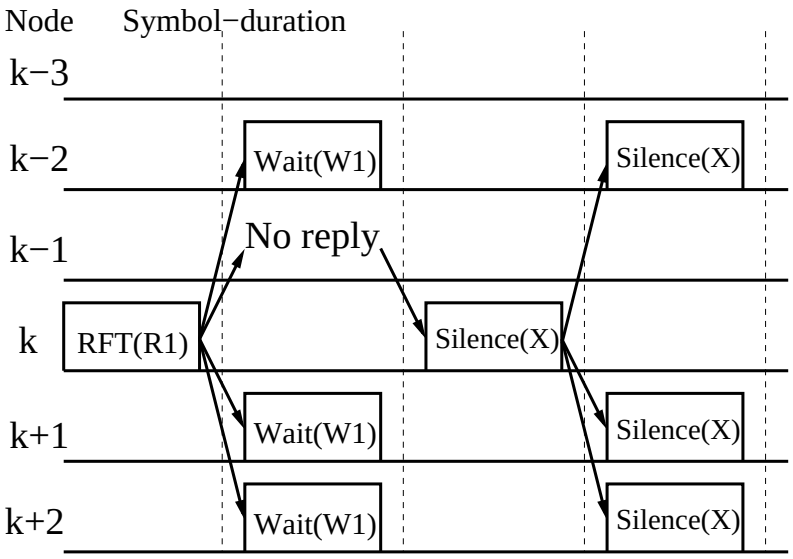

Figure 4.3: Node k broadcasts a RFT in the first SD. Node $(k-1)$ does not respond in the second SD. The other nodes, such as node $(k+1)$, $(k+2)$ and $(k-2)$ that have received the RFT in the first SD will set their states to $W1$. In the third SD, node k changes its state to X and remains silent, since it did not received the CFT from node $(k-1)$. In the fourth SD, the nodes that have not received the second RFT signal from node k and are in the waiting state $W1$ such as $(k-2)$, $(k+1)$ and $(k+2)$ will reset their states to X and remain silent. The detailed conditions to be satisfied before the above actions are triggered will be discussed later in the context of Fig. 4.4.

second SD. This may occur because the state of node $(k-1)$ may not be the unknown state 'X' of Table 4.1. Instead, it may be waiting in the state "W" of Table 4.1, which corresponds to the 'Hidden Terminal' problem. The other nodes, such as node $(k+1)$, $(k+2)$ and $(k-2)$ have received the RFT signal in the first SD, hence they set their states to $W1$ of Table 4.1. In the third SD, node k changes its state back to X and will remain silent, since it did not receive a CFT signal in the second SD. In the fourth SD, since the nodes $(k-2)$, $(k+1)$ and $(k+2)$ did not receive the second RFT in the third SD, these nodes change their states back to X of Table 4.1 and remain silent.

Based on the above two series of actions portrayed in Fig. 4.2 and Fig. 4.3, the algorithm used for determining the action of a node within a SD is summarized in Fig. 4.4. Every node of the MHL invokes this algorithm and carries out a single action during a SD. Let us use the index of $S_D = 0, 1, \ldots, (LS-1)$ for the SDs of the MAC protocol and the index of $l = 1, 2, \ldots, L$ for the L nodes. For a given SD, the node considered has the following local knowledge: the index S_D of the SD, its node index l representing its relative position along the link, its current state according to Table 4.1 (X, R1, R2, W1, W2 or T), the CQs of its two adjacent neighbours and the interference flags related to its pair of double-hops neighbours. The process

commences from $S_D = 0$ and continues until all the nodes change their states to one of the states W2, T and R2 or, otherwise, when the maximum delay time $S_D = L(S-1)$ is reached. However, when the maximum time $L(S-1)$ is reached, while the state of a node is still X, it then changes its state to W2 of Table 4.1.

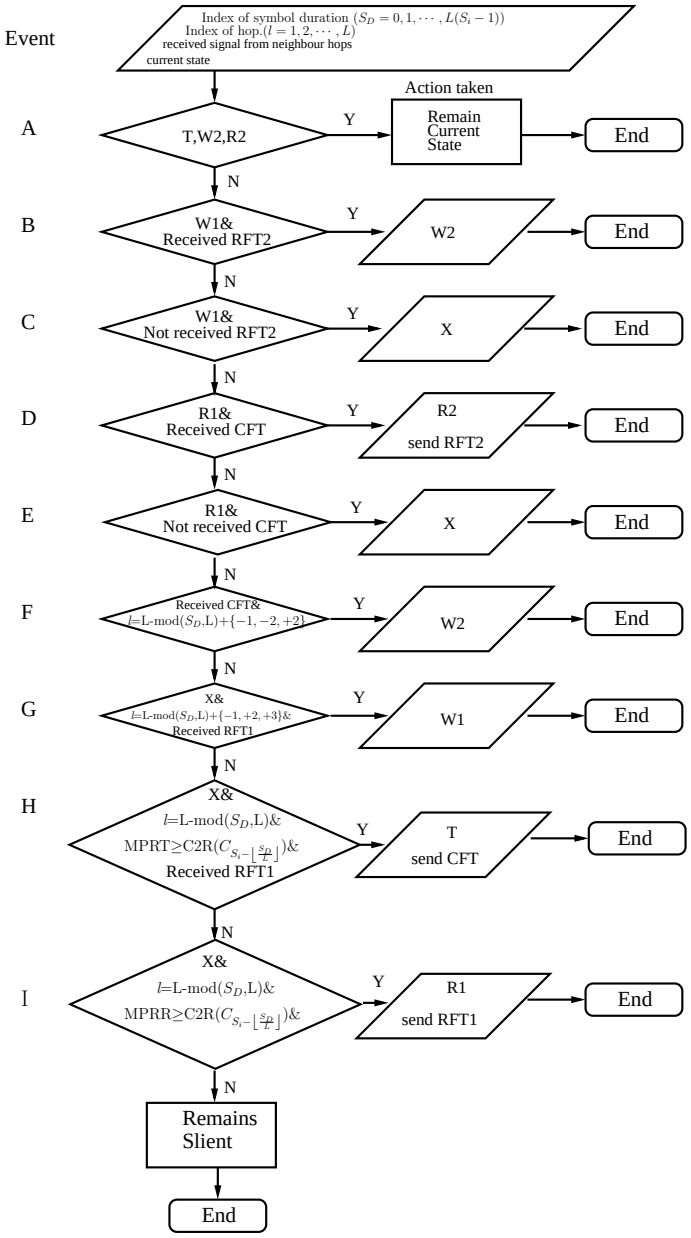

Figure 4.4: Algorithm determining the action of a node for a specific SD during the time of selecting the hop for transmission.

At the beginning, the states of all the nodes are initialized to 'X' of Table 4.1. At the S_Dth SD, the state of a node changes to another state based on its current state, the index of its SD, the index of the hop and on the signal received. For example, as shown in Fig. 4.4, corresponding to the Event A, if the current state of a node is T, R2 or W2, then the node remains in its state, regardless of the specific signal

received. However, if this is not the case, and if the node's current state is W1 and, simultaneously, a RFT2 signal is received, then the state of the node is changed to W2. Similarly, the other cases of Fig. 4.4 may be readily analyzed. Note that for a given SD $S_D = 0, 1, \ldots, L(S-1)$, only a single action may be taken. In other words, every action may only belong to one of the events, A, B,..., I of Fig. 4.4, within a pecific SD. Note furthermore that except for the Event I in Fig. 4.4, the action corresponding to all the other actions are 'passive' actions. By contrast, only Event I is 'active', which is encountered when the specific node considered is in the state 'X' and its node index is '$l = L - mod(S_D, L)$' and additionally, if it is capable of supporting a data rate of 'PRR$\geq$ C-to-R($C_{S-\lfloor \frac{S_D}{L} \rfloor}$)'. To elaborate further, $\lfloor x \rfloor$ represents the integer part of x and C-to-R is a function mapping a specific CQ to a given data rate. For example, $C - to - R(C_i) = b$ means that a node is capable of transmitting at most b packets per time slot at a CQ of C_i. Furthermore, the notation of $C_{S-\lfloor \frac{S_D}{L} \rfloor}$ indicates that the CQ is decreased one level by every L SD from the highest level of C_S to the lowest level C_1. According to this procedure, the specific hop associated with a higher PRR has the priority to be chosen for transmission within a TS.

It summary, our protocol has the following characteristics:

- Even though the maximum time required for the second stage to identify the desired hops is $L(S-1)$ SDs, the selection process is completed, once all the nodes, including $SN, R_1, R_2, \ldots$, and DN, have changed their states from X to one of the states W2, T or R2 of Table 4.1.
- Due to the propagation pathloss and fading of wireless channels, an interferring signal only has a limited interference range, which was assumed to be two hops in this chapter. Based on our proposed MAC protocol, after the selection process, several hops of a MHL might be activated for transmitting their data simultaneously. This may happen more often, especially when a relatively long MHL is considered. Our MAC protocol guarantees the selection of the best hop. However, the second best hop might not necessarily be activated, as it might fall within the interference range of the best one. Nevertheless, the adaptive modulation scheme invoked is capable of guaranteeing the required QoS.
- Based on the above-mentioned arguments, the proposed the MAC protocol equips us with a degree of freedom for striking a trade-off between the achievable throughput and the BER performance.

Note that the above protocol is suitable for general MHLs relying on at least three hops. For the specific case of a two-hop link, the MHL has a single RN, which

may collect the CQ information of both hops and make the required decision to active a hop. Specifically, the best hop may be selected as follows. Within the first SD, the SN broadcasts its pilot signal for the RN to estimate the CQ of the first hop. In the second SD, the DN broadcasts its pilot for the RN to estimate the CQ of the second hop. At this point, the RN has the CQ information of both the SN-RN and the RN-DN channels. Hence, it can make a selection. In the third SD, the RN transmits a RFT signal, if it chooses the first hop, while sends a CFT signal, if it selects the second hop. Data transmission may now commence from the fourth symbol duration. Therefore, the full selection process requires three symbol durations. In the next section, we consider the adaptive-rate transmission regime of MHLs.

4.4 Adaptive Rate Transmission over Multihop Links: General Cases

As mentioned in Section 4.3, during a TS the hop having the highest possible PR is chosen to send a number of packets. In this section, the principles of our MTART regime are first introduced. Then, in Section 4.5, the performance of the MHLs employing MTART is investigated, when communicating over i.i.d Nakagami-m channels. Let us commence by introducing a simple two-hop scenario, which is then extended to the general L-hop case. Furthermore, the probability density function (PDF) and cumulative distribution function (CDF) of the SNR of selected hops, as well as the BER, the capacity and the OP formulas of the MHL are derived. Let us now continue by considering the two-hop scenario to highlight the basic principles of the MTART.

4.4.1 Maximum Throughput Adaptive Rate Transmission: Two-Hop Case

Let us introduce the MTART scheme according to the MAC protocol of Section 4.3. The criterion used for activating a specific hop to transmit during a TS is that of transmitting the highest number of packets. When there are more than one hops offering to transmit the same number of packets, the particular hop having the highest CQ is activated. Hence, our MTART scheme achieves the highest throughput based on the predetermined thresholds and on the assumption that only one hop is activated at a, while maintaining the target BER. Below we use a simple two-hop example associated with Fig. 4.5 and Fig. 4.6 for further augmenting the principles of the MTART.

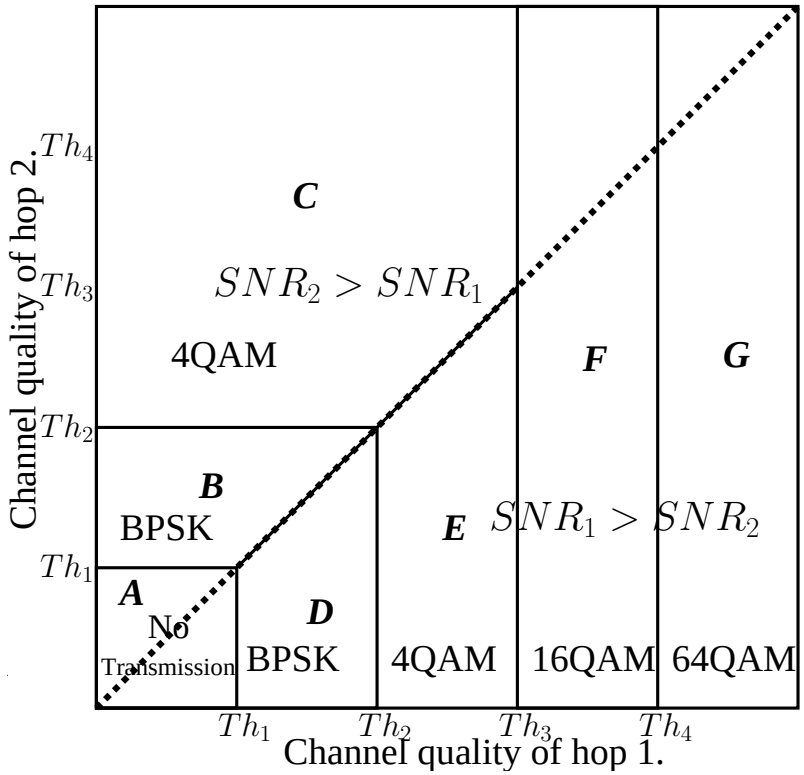

Figure 4.5: Schematic diagram for explaining the maximum throughput adaptive rate transmission scheme for a two-hop link, when assuming that the RN holds two packets, while the SN has an infinite number of packets.

Let us assume that the MRART scheme supports five possible data rates, associated with, 0, 1, 2, 4, and 6 packets per TS, corresponding to using 'no transmission', BPSK, QPSK, 16QAM and 64QAM. In this case, the CQ of a hop is classified into one of the five regions with the aid of four thresholds, $T_{h1} < T_{h2} < T_{h3} < T_{h4}$, as shown in Fig. 4.5. For the example considered in Fig. 4.5, we assume that the RN currently has only two packets stored in its buffer. However, the number of packets stored in the buffer can be arbitrary, this number does not affect the system's operation or its analysis. Hence, the highest rate of the second hop is two packets per TS, regardless of the CQ of the second hop is. By contrast, on the first hop, any one of the five rates can be transmitted, which is dependent on the near-instantaneous CQ of the first hop. Consequently, as shown in Fig. 4.5, the space according to the CQ (SNR values) of the first and second hops can be divided into seven regions by the solid lines, which are the regions A, B, C, D, E, F and G. Observe in Fig. 4.5 that the dashed line divides the CQ space into two regions. In the region above the dashed line, the CQ of the first hop is worse than that of the second hop, while in the region below the dashed line, the CQ of the first hop is better than that of the second hop. Finally, the CQs of both hops are the same along the dashed line.

As shown in Fig. 4.6, when the CQs of the first and second hops fall within the

region A, no data transmission is activated over either of the hops, since the channels of both hops are too poor for maintaining the required BER. Within region B, the second hop is better than the first hop and 1 packet per TS may be transmitted reliably. In region D, the first hop's CQ is better than the second hop's and it can support the transmission of 1 packet per TS. As shown in Fig. 4.6, when the CQs fall in the region C, 2 packets per TS are transmitted by the second hop, regardless of how good the CQ is, because the RN has only two packets stored in its buffer. When the CQs fall in the region E, 2 packets per TS are transmitted by the first hop. Finally, when the CQs are within the region F or G, the first hop is always activated for transmission, even when the second hop is more reliable than the first hop, because the first hop can now transmit 4 or 6 packets per TS. Let us now derive the PDF and CDF of the SNR for the activated hop.

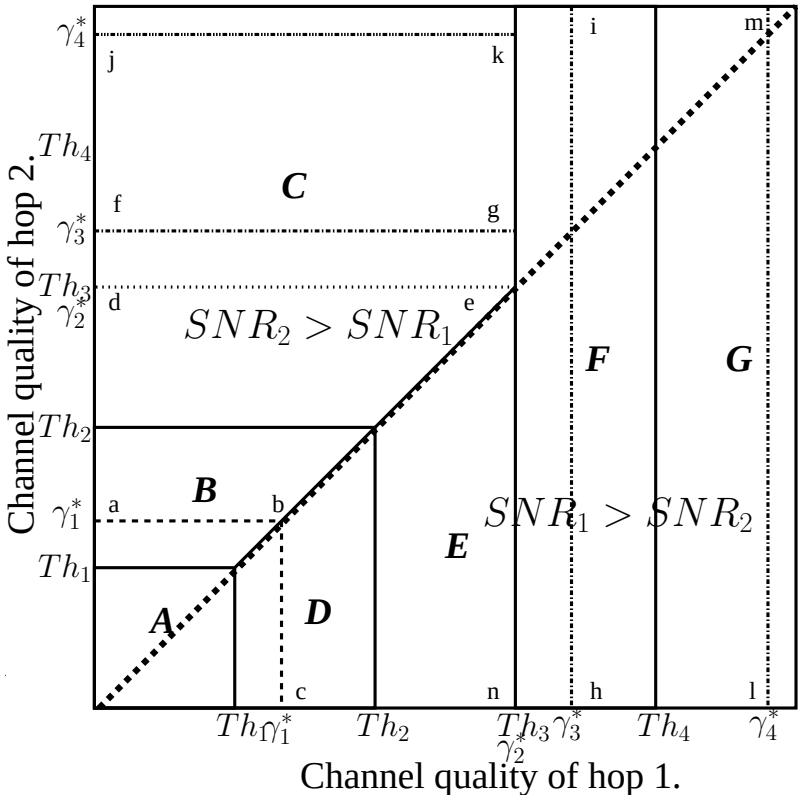

Figure 4.6: Schematic diagram for explaining the maximum throughput adaptive rate transmission on a two-hop link, when assuming that the RN holds two packets, while the SN has an infinite number of packets.

4.4.2 PDF and CDF of the SNR for the Hop Selected Based on MTART: Two-Hop Links

Let us assume that the instantaneous SNR of the first hop is γ_1 and that of the second hop is γ_2. The same PDFs of γ_1 and γ_2 are $f_{\gamma_1}(\gamma)$ and $f_{\gamma_2}(\gamma)$. Let the PDF of the SNR for the hop activated from the two hops be expressed as $p_{\gamma|\widehat{r_1},\widehat{r_2}}(\gamma)$,

where $\widehat{r}_i$ is the potential rate (PR) of the ith hop, $i = 1, 2$. Moreover, let $|\bullet|$ represent the number of logical '1' values in $|\bullet|$. For example, $|1 > 0|$=1, $|0 > 1|$=0, $\underbrace{|1 > 0, 2 > 0|}_{\text{two logic ture}}$=2, $\underbrace{|\{1, 2\} > 0|}_{\text{two logic ture}}$=2. Furthermore, for convenience of description, a number of terminologies are used for describing the relationship between the SNR γ_i, rate r_i and the thresholds, T_{hi}. First, the lower boundary of the PR region of the ith hop is expressed as $T_{h\widehat{r}_i}$. For example, the PR of the second hop in Fig. 4.5 is $\widehat{r}_2$=2 packets per TS, which is achieved in region C. Hence, the lower boundary of the second hop is $T_{h\widehat{r}_2}$=T_{h2}. Similarly, the PR of the first hop in Fig. 4.5 is $\widehat{r}_2$=6 BPS packets, which is achieved in region G. Correspondingly, the lower boundary of the first hop is $T_{h\widehat{r}_1}$=T_{h4}. Secondly, in our description, a symbol $\oplus$ used in the subscript represents a specifically defined operation "plus in subscript" as exemplified by $T_{h3\oplus 1} = T_{h4}$, $T_{h\widehat{r}_2\oplus 1} = (T_{h\widehat{r}_2})_{\oplus 1} = T_{h2\oplus 1} = T_{h3}$. Furthermore, when the CQ of the lth hop is γ_i, the region constrained by the two thresholds and the corresponding rate, which expressed as $T^l_{h\gamma_i}$, $T^l_{h\gamma_i\oplus 1}$ and $r^l_{\gamma_i}$, respectively becomes known. For example, as shown in Fig. 4.6, γ^*_3 of the first hop is between T_{h3} and T_{h4}. Hence, we have $T^1_{h\gamma^*_3} = T_{h3}$ and $T^1_{h\gamma^*_3\oplus 1} = T_{h4}$, and correspondingly, $r^1_{\gamma^*_3} = 4$, since 16QAM is transmitted, when γ_1 is in this region.

Having defined the above terminologies, let us now derive the PDF $p_{\gamma|\widehat{r}_1,\widehat{r}_2}(\gamma)$ of the SNR step by step. Firstly, $p_{\gamma|\widehat{r}_1,\widehat{r}_2}(0)$ is the probability that none of the two hops is activated, since we have $\gamma_1 < T_{h1}$ and $\gamma_2 < T_{h1}$, hence an outage occurs. This probability corresponds to region A in Fig. 4.6, which can be expressed as

$$p_{\gamma|\widehat{r}_1,\widehat{r}_2}(0) = \left[\int_0^{T_{h1}} f_{\gamma_1}(\gamma)d\gamma\right]^{|\widehat{r}_1>0|} \left[\int_0^{T_{h1}} f_{\gamma_2}(\gamma)d\gamma\right]^{|\widehat{r}_2>0|}. \tag{4.2}$$

Owing to the assumption that both channels obey the same distribution $f(\gamma)$, we have

$$p_{\gamma|\widehat{r}_1,\widehat{r}_2}(0) = \left[\int_0^{T_{h1}} f(\gamma)d\gamma\right]^{|\{\widehat{r}_1,\widehat{r}_2\}>0|}, \tag{4.3}$$

where, according to our previous definitions, we have $|\{\widehat{r}_1, \widehat{r}_1\} > 0|$=2.

According to our MTART regime, once a hop has been activated, the minimum channel SNR of the activated hop is T_{h1}. Hence, the activated hop's SNR is either larger than T_{h1} or 0. Consequently, we have

$$p_{\gamma|\widehat{r}_1,\widehat{r}_2}(\gamma) = 0, \text{ when } \gamma \in (0, T_{h1}). \tag{4.4}$$

As shown in Fig. 4.6, if the activated hop's SNR falls between (T_{h1}, T_{h3}), such as γ_1^* of Fig. 4.6, then the specific hop having the higher SNR is activated. Hence, $p_{\gamma|\widehat{r_1},\widehat{r_2}}(\gamma)$ can be expressed as

$$p_{\gamma|\widehat{r_1},\widehat{r_2}}(\gamma) = f_{\gamma_2}(\gamma)\int_0^{\gamma} f_{\gamma_1}(\gamma)d\gamma + f_{\gamma_1}(\gamma)\int_0^{\gamma} f_{\gamma_2}(\gamma)d\gamma,$$
$$\text{when } \gamma \in [T_{h1}, T_{h\min(\widehat{r_1},\widehat{r_2})\oplus 1}), \tag{4.5}$$

where $T_{h\min(\widehat{r_1},\widehat{r_2})\oplus 1}$=$T_{h3}$ is the upper boundary of the region. Note that here we have $\min(\widehat{r_1}, \widehat{r_2}) = 2$. Hence, $T_{h\min(\widehat{r_1},\widehat{r_2})\oplus 1} = 3$.

Finally, when the channel SNR of the activated hop is higher than T_{h3}, $p_{\gamma|\widehat{r_1},\widehat{r_2}}(\gamma)$ may be characterized as follows. As shown in Fig. 4.6, if the first hop having an SNR of γ_3^* is activated, the second hop's SNR can be any arbitrary value, since the second hop can only transmit a maximum of 2 packets, while the first hop transmits 4 packets at γ_3^*. By contrast, if the second hop having an SNR of γ_3* is activated, the first hop's SNR is at most T_{h3}. If the first hop's SNR is higher than T_{h3}, the first hop would be activated. Consequently, for $\gamma > T_{h3}$, $p_{\gamma|\widehat{r_1},\widehat{r_2}}(\gamma)$ can be formulated as

$$\begin{aligned} p_{\gamma|\widehat{r_1},\widehat{r_2}}(\gamma) =& \underbrace{f_{\gamma_1}(\gamma)\int_0^{\infty} f_{\gamma_2}(\gamma)d\gamma}_{\text{first hop activated}} + \underbrace{f_{\gamma_2}(\gamma)\int_0^{T_{h\min(\widehat{r_1},\widehat{r_2})\oplus 1}} f_{\gamma_1}(\gamma)d\gamma}_{\text{second hop activated}} \\ =& f_{\gamma_1}(\gamma) + f_{\gamma_2}(\gamma)\int_0^{T_{h\min(\widehat{r_1},\widehat{r_2})\oplus 1}} f_{\gamma_1}(\gamma)d\gamma, \\ & \text{when } \gamma \in (T_{h\min(\widehat{r_1},\widehat{r_2})\oplus 1}, \infty). \end{aligned} \tag{4.6}$$

Fig. 4.7 shows the PDF $p_{\gamma|\widehat{r_1},\widehat{r_2}}(\gamma)$ of a two-hop link, where each hop experiences flat Rayleigh fading having an SNR obeying the PDF of $f(\gamma) = \frac{1}{\bar{\gamma}}e^{-\frac{\gamma}{\bar{\gamma}}}$ associated with $\bar{\gamma} = 1$. The curves were evaluated from (4.2), (4.4), (4.5) and (4.6), respectively. In our evaluations, we assumed that the average received SNR of each hop was $10dB$. Correspondingly, the MQAM switching thresholds were set to [0.17 0.35 1.53 5.6]. In the figure, four sets of PRs were considered, which were [6 0], [6 1], [6 2] and [6 6] packets. As shown in Fig. 4.7, when $\widehat{r_1}, \widehat{r_2}$ = [6 0] is considered, only the first hop may be activated. Hence, the PDF of the SNR is the same as that of a single Rayleigh fading channel, when $\gamma \in (T_{h1}, \infty)$. The OP evaluated from (4.2) is 16% in this scenario, which is represented by a triangle marker at SNR=0. For all the other cases, the outage probability is 2.6%, which is also shown in the figure by the overlapping circle, star and square markers at channel $SNR = 0$. In the case of $\widehat{r_1}, \widehat{r_2}$ = [6 2] packets, we observe a sharp PDF peak indicated by a square, which

occurs at T_{h3}. We infer from Fig. 4.7 that the average CQ of the activated hop associated with $\widehat{r_1}, \widehat{r_2} = [6\ 1]$ packets and $\widehat{r_1}, \widehat{r_2} = [6\ 2]$ packets is better than that of $\widehat{r_1}, \widehat{r_2} = [6\ 0]$ packets, but worse than that of $\widehat{r_1}, \widehat{r_2} = [6\ 6]$ packets.

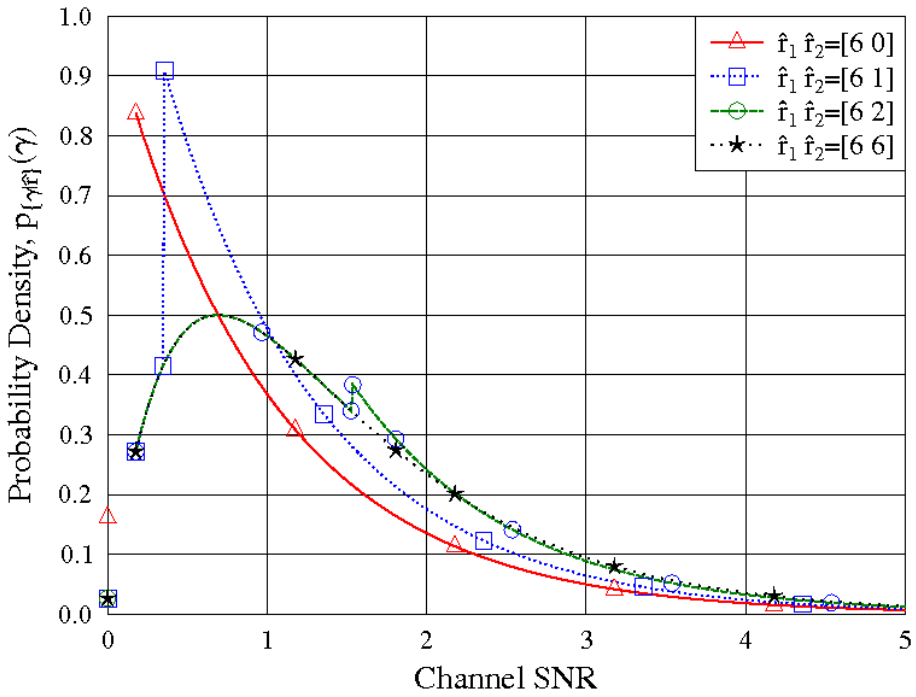

Figure 4.7: The PDF of $p_{\{\gamma|\widehat{\boldsymbol{r}}\}}(\gamma)$ versus non-logarithmic SNR, where each hop obeys flat Rayleigh fading associated with the channel SNR's PDF of $f(\gamma) = \frac{1}{\bar{\gamma}} e^{-\frac{\gamma}{\bar{\gamma}}}$ and $\bar{\gamma} = 1$. The thresholds $T_{hi}, i = 1, 2, 3, 4$ were set to [0.17 0.35 1.53 5.6], which were configured for maintaining BER<0.03 as used in [70]. The SNR-PDFs were evaluated from (4.2), (4.4), (4.5) and (4.6).

4.4.3 PDF of the SNR for the Hop Activated Based on MTART: L-Hop Links

Having derived the PDFs $p_{\gamma|\widehat{r_1},\widehat{r_2}}(\gamma)$ for the two-hop links, let us now generalize them for L-hop links. Let us express the PDF of the SNR for the activated hop as $p_{\{\gamma|\widehat{\boldsymbol{r}}\}}(\gamma)$, where we have $\{\gamma|\widehat{\boldsymbol{r}}\} = \{\widehat{r_1}, \widehat{r_2}, \cdots, \widehat{r_L}\}$, with $\widehat{r_l}$ being the PR of the lth hop. Let $p^l_{\{\gamma|\widehat{\boldsymbol{r}}\}}(\gamma)$ represents the probability that the lth hop is activated, which has an SNR of γ. Explicitly, we have

$$p_{\{\gamma|\widehat{\boldsymbol{r}}\}}(\gamma) = \sum_{l=1}^{L} p^l_{\{\gamma|\widehat{\boldsymbol{r}}\}}(\gamma). \tag{4.7}$$

Let us consider the OP $p_{\{\gamma|\widehat{\boldsymbol{r}}\}}(0)$, which is the probability that none of the L hops is activated, since we have $\gamma_i < T_{h1}$, for $i = 1, 2, \cdots, L$, yielding:

$$p_{\{\gamma|\widehat{\boldsymbol{r}}\}}(0) = \prod_{l=1}^{L} \left[\int_0^{T_{h1}} f_{\gamma_l}(\gamma) d\gamma \right]^{|\widehat{r}_l > 0|}. \tag{4.8}$$

Owing to the assumption that the channels of all the L hops obey the same distribution $f(\gamma)$, we have

$$p_{\{\gamma|\widehat{\boldsymbol{r}}\}}(0) = \left[\int_0^{T_{h1}} f(\gamma) d\gamma \right]^{|\widehat{\boldsymbol{r}}_{\boldsymbol{l}} > 0|}. \tag{4.9}$$

Furthermore, according to the principles of the MTART as well as to our analysis for the two-hop links, once a hop has been activated, the SNR of the activated hop will be either higher then T_{h1} or 0. Consequently, we have

$$p_{\{\gamma|\widehat{\boldsymbol{r}}\}}(\gamma) = 0, \text{ when } \gamma \in (0, T_{h1}). \tag{4.10}$$

As mentioned above, the activated hop may be any of the L hops, hence we have $p_{\{\gamma|\widehat{\boldsymbol{r}}\}}(\gamma) = \sum_{l=1}^{L} p^l_{\{\gamma|\widehat{\boldsymbol{r}}\}}(\gamma)$, when $\gamma \in [T_{h1}, \infty)$. Therefore, $p_{\{\gamma|\widehat{\boldsymbol{r}}\}}(\gamma)$ may be derived hop-by-hop. Let us specifically assume that the lth hop is activated and that the SNR of the lth hop is γ_l, which supports a data rate of r_l. Based on these assumptions, all the other $(L-1)$ hops may be divided into three groups. The first group consist of the hops that have a PR lower than r_l. The second group is constituted by the hops having the same PR as the lth hop's PR. Finally, the third group accommodates the hops, whose PR are higher than r_l. It can be shown that the hops in the first group cannot compete with the lth hop, regardless of how high their channel SNR is. This is because the data rate of any hop belonging to the first group cannot reach r_l. By contrast, the hops belonging to the second group compete with the lth hop, since they may provide the same data rate as the lth hop. Finally, for the hops belonging to the third group, the associated impact should be further analyzed for two specific cases with respect to the value of γ_l. Firstly, when $\gamma_l \geq T_{h\widehat{r}_l \oplus 1}$, the channel SNR of the hops in the third group cannot exceed $T_{h\widehat{r}_l \oplus 1}$. Otherwise the lth hop would not be activated. In this case, upon following a similar procedure to the derivations of

Section 4.4.2 valid for the two-hop links, we have

$$p^{l}_{\{\gamma|\widehat{\boldsymbol{r}}\}}(\gamma) = f_{\gamma_l}(\gamma) \underbrace{\left[\int_0^{T_{h\widehat{r}_l\oplus 1}} f_{\gamma_j}(\gamma)d\gamma\right]^{|\{\widehat{\boldsymbol{r}}\}>\widehat{r}_l|}}_{\text{third group}} \underbrace{\left[\int_0^{\gamma} f_{\gamma_i}(\gamma)d\gamma\right]^{|\{\widehat{\boldsymbol{r}}\}=\widehat{r}_l|-1}}_{\text{second group}}, \quad \text{when } \gamma \geq T_{h\widehat{r}_l\oplus 1}, \tag{4.11}$$

where γ_i and γ_j denote the channel SNRs of the hops in the second and third groups, respectively, while $|\{\widehat{\boldsymbol{r}}\} = \widehat{r}_l| - 1$ and $|\{\widehat{\boldsymbol{r}}\} > \widehat{r}_l|$ are the number of hops in the second and third groups. Note that, for the hops belonging to the first group, we have $\int_0^{\infty} f(\gamma)d\gamma = 1$, which is not shown in (4.11). Secondly, when $\gamma_l < T_{h\widehat{r}_l\oplus 1}$, the channel SNR of the hops in the third group cannot exceed γ_l, therefore we have the same channel SNRs as for the hops in the second group. Hence, we arrive at,

$$p^{l}_{\{\gamma|\widehat{\boldsymbol{r}}\}}(\gamma) = f_{\gamma_l}(\gamma) \underbrace{\left[\int_0^{\gamma} f_{\gamma_j}(\gamma)d\gamma\right]^{|T_{h\{\widehat{\boldsymbol{r}}\}\oplus 1}\geq T_{h\gamma\oplus 1}|-1}}_{\text{second and third group}}, \quad \text{when } \gamma \in [T_{h1}, T_{h\widehat{r}_l\oplus 1}), \tag{4.12}$$

where γ_j is the channel SNR of a hop either in the second or in the third group.

Having derived the PDFs, the CDFs may now be derived by their integration. However, since they are not going to be used in the rest of this treatise, we do not provide their expressions, in order to save space.

4.4.4 Performance of MHLs Relying on MTART

In this section, we study the performance of MHLs employing our proposed MTART. Firstly, we derive the single-hop BER of the MHLs using the proposed MTART. Then, the single-hop bandwidth-efficiency of a activated hop is studied. Finally, the diversity order of the MHLs is discussed.

4.4.4.1 Single-Hop BER

The single-hop BER $p_{H,ber\{\gamma|\widehat{\boldsymbol{r}}\}}$ of the MHLs employing the MTART scheme can be evaluated by the following formula [191] (8.100)

$$p_{H,ber\{\widehat{\boldsymbol{r}}\}} = \frac{1}{1 - p_{\{\gamma|\widehat{\boldsymbol{r}}\}}(0)} \int_{T_{h1}}^{\infty} p_{M_r}(\gamma) p_{\{\gamma|\widehat{\boldsymbol{r}}\}}(\gamma)d\gamma, \tag{4.13}$$

where $p_{\{\gamma|\widehat{\boldsymbol{r}}\}}(0)$ is the outage probability given in (4.9), while p_{M_r} is the single-hop BER formula of MQAM/BPSK transmitted over an AWGN channel, which is the same as p_m of (47) in [70]. In our chapter, we use $p_{2_r}(\gamma) = Q(\sqrt{2\gamma})$ (BPSK); $p_{4_r}(\gamma) = Q(\sqrt{\gamma})$ (QPSK); $p_{16_r}(\gamma) = \frac{3}{4}Q(\sqrt{\frac{\gamma}{5}}) + \frac{2}{4}Q(3\sqrt{\frac{\gamma}{5}}) - \frac{1}{4}Q(5\sqrt{\frac{\gamma}{5}})$ (16QAM) and $p_{64_r}(\gamma) = \frac{7}{12}Q(\sqrt{\frac{\gamma}{21}}) + \frac{6}{12}Q(3\sqrt{\frac{\gamma}{21}}) - \frac{1}{12}Q(5\sqrt{\frac{\gamma}{21}}) + \frac{1}{12}Q(9\sqrt{\frac{\gamma}{21}}) - \frac{1}{12}Q(13\sqrt{\frac{\gamma}{21}})$ (64QAM). Naturally, the modulation schemes may be different for the hops, when their SNRs are different. Furthermore, as shown in Fig. 4.6, the modulation schemes might be different, even if the activated hop's SNRs are the same. Specifically, 16QAM may be used, when the first hop having a channel SNR γ_3^* is activated, while QPSK may be employed, when the second hop is activated with the same channel SNR γ_3^*, because the PR of the second hop is 2packets. Consequently, when considering the different modulation schemes as well as the PDFs derived in Section 4.4.3 and substituting (4.9), (4.10), (4.11) and (4.12) into (4.13), it may be readily shown that, for $\gamma \in [T_{h1}, T_{h\widehat{r}_l\oplus 1})$, we have

$$p_{H,ber\{\widehat{\boldsymbol{r}}\}}^{(1)} = \sum_{l=1}^{L} \int_{T_{h1}}^{T_{h\widehat{r}_l\oplus 1}} f_{\gamma_l}(\gamma) \times \left[\int_0^{\gamma_l} f_{\gamma_j}(\gamma)d\gamma\right]^{|T_{h\{\widehat{\boldsymbol{r}}\}\oplus 1} \geq T_{h\gamma\oplus 1}|-1} p_{M_{r_{\gamma_l}}}(\gamma)d\gamma. \tag{4.14}$$

By contrast, for $\gamma \geq T_{h\widehat{r}_l\oplus 1}$, we obtain

$$p_{H,ber\{\widehat{\boldsymbol{r}}\}}^{(2)} = \sum_{l=1}^{L} \int_0^{T_{h\widehat{r}_l\oplus 1}} f_{\gamma_l}(\gamma) \left[\int_0^{T_{h\widehat{r}_l\oplus 1}} f_{\gamma_j}(\gamma)d\gamma\right]^{|\{\widehat{\boldsymbol{r}}\}>\widehat{r}_l|} \times \left[\int_0^{\gamma_l} f_{\gamma_i}(\gamma)d\gamma\right]^{|\{\widehat{\boldsymbol{r}}\}=\widehat{r}_l|-1} p_{M_{\widehat{r}_l}}(\gamma)d\gamma. \tag{4.15}$$

Finally, we arrive at the single-hop BER of the activated hop, in the form of

$$p_{H,ber\{\widehat{\boldsymbol{r}}\}} = \frac{1}{1 - p_{\{\gamma|\widehat{\boldsymbol{r}}\}}(0)} \left(p_{H,ber\{\widehat{\boldsymbol{r}}\}}^{(1)} + p_{H,ber\{\widehat{\boldsymbol{r}}\}}^{(2)}\right). \tag{4.16}$$

4.4.4.2 Single-Hop Bandwidth-Efficiency

The single-hop bandwidth-efficiency of the activated hop is

$$C_{\{\gamma|\widehat{\boldsymbol{r}}\}} = \int_0^{\infty} \log_2(1+\gamma) p_{\{\gamma|\widehat{\boldsymbol{r}}\}}(\gamma)d\gamma, \tag{4.17}$$

which can be obtained by substituting (4.9), (4.10), (4.11) and (4.12) into (4.17).[1]

[1]The detailed discussions considering a specific fading channel are provided in the next section.

4.4.4.3 The Diversity Order

It is plausible that if the average received SNR is high, the activated hop can always transmit its data using 64QAM. In this case, activating the best one from the L hops results in a diversity order of L. Therefore, the diversity order of L-hop links is L, which has also been demonstrated in (28-30) of [168] and in [192].

4.5 Adaptive Rate Transmission over Multihop Links Experiencing i.i.d Nakagami-m Fading

In Section 4.4 we have discussed the general case of using our MTART regime over MHLs. In this section, the general results are applied to the specific scenario of a i.i.d Nakagami-m fading channel. Specifically, the expressions of the BER, OP, bandwidth-efficiency as well as transmission delay are analyzed.

4.5.1 Channel Models

When communicating over i.i.d Nakagami-m fading channels, statistically speaking the fading magnitude of each hop may be assumed to obey the same Nakagami-m fading. In this case, it may be shown that the channel SNR γ of a hop obeys the PDF [185]

$$f(\gamma) = \frac{1}{\Gamma(m)}(\frac{m}{\bar{\gamma}})^m \gamma^{m-1} \exp(-\frac{m}{\bar{\gamma}}\gamma), \tag{4.18}$$

where $m \geqslant \frac{1}{2}$ is the fading parameter controlling the fading severity[2], while the average SNR of a hop is $\bar{\gamma}$. Furthermore, in (4.18) $\Gamma(\bullet)$ is the Gamma function (8.310.1) of [10].

4.5.2 Single-Hop Bit Error Probability of a Given $\{\widehat{\boldsymbol{r}}\}$

In this subsection, the single-hop BER $p_{H,ber\{\widehat{\boldsymbol{r}}\}}$ of a given $\{\widehat{\boldsymbol{r}}\}$ is derived. For the sake of simplicity, we consider only a BPSK scheme as an example. However, our analysis may be readily extended to MQAM schemes with the aid of [70](46-47).

[2]In this chapter, we assume that every hop has the same fading parameter (i.i.d) and that the EA defined in Section 4.2 is applied, which results in every hop having the same probability of being chosen. By contrast, if the fading parameters are different, the MQAM/BPSK mode-switching thresholds of each hop will be different. In that case, arranging for each hop to have the same single-hop throughput is challenging. However, it may still be reasonable to assume that every hop has a similar length, so that the hops may be assumed to have the same fading parameter, as assumed in [87, 193, 194].

Upon substituting (4.18) into (4.14), (4.15) and then into (4.16), we arrive at

$$
\begin{aligned}
& p_{H,ber\{\widehat{\boldsymbol{r}}\}} \\
=& \frac{1}{(1-p_{out\{\widehat{\boldsymbol{r}}\}})}\left[\sum_{l=1}^{L}\int_{T_{h1}}^{T_{h\widehat{r}_l\oplus 1}} Q(\sqrt{2\gamma})\frac{1}{\Gamma(m)}(\frac{m}{\bar{\gamma}})^m\gamma^{m-1}\right. \\
& \times \exp(-\frac{m}{\bar{\gamma}}\gamma)\left(\frac{\gamma(m,\gamma\frac{m}{\bar{\gamma}})}{\gamma(m)}\right)^{|T_{h\{\widehat{\boldsymbol{r}}\}\oplus 1}\geq T_{h\gamma\oplus 1}|-1} d\gamma \\
& + \sum_{l=1}^{L}\int_{T_{h\widehat{r}_l\oplus 1}}^{\infty} Q(\sqrt{2\gamma})\frac{1}{\Gamma(m)}(\frac{m}{\bar{\gamma}})^m\gamma^{m-1}\exp(-\frac{m}{\bar{\gamma}}\gamma) \\
& \times \left.\left(\frac{\gamma(m,\gamma\frac{m}{\bar{\gamma}})}{\gamma(m)}\right)^{|\{\widehat{\boldsymbol{r}}\}=\widehat{r}_l|-1}\left(\frac{\gamma(m,T_{h\widehat{r}_l\oplus 1}\frac{m}{\bar{\gamma}})}{\gamma(m)}\right)^{|\{\widehat{\boldsymbol{r}}\}>\widehat{r}_l|} d\gamma\right].
\end{aligned}
\tag{4.19}
$$

When m is an integer, (4.19) can be simplified by representing the incomplete Gamma function as [10](8.352.6):

$$
\frac{\gamma(m,x)}{\Gamma(m)} = \left(1-e^{-x}\sum_{n=0}^{m-1}\frac{x^n}{n!}\right). \tag{4.20}
$$

Upon substituting (4.20) into (4.19) and then completing the integration as well as carrying out a number of further manipulations, we arrive at:

$$
\begin{aligned}
& p_{H,ber\{\widehat{\boldsymbol{r}}\}} \\
=& \sum_{l=1}^{L}\frac{|T_{h\{\widehat{\boldsymbol{r}}\}\oplus 1}\geq T_{h\gamma\oplus 1}|}{(1-p_{out\{\widehat{\boldsymbol{r}}\}})\Gamma(m)}(\frac{m}{\bar{\gamma}})^m \sum_{j=0}^{|T_{h\{\widehat{\boldsymbol{r}}\}\oplus 1}\geq T_{h\gamma\oplus 1}|-1}(-1)^j \\
& \times \binom{|T_{h\{\widehat{\boldsymbol{r}}\}\oplus 1}\geq T_{h\gamma\oplus 1}|-1}{j}\sum_{k=0}^{j(m-1)} b_k^j(\frac{m}{\bar{\gamma}})^k \\
& \times N(2,k+m-1,(j+1)m,T_{h1},T_{h\widehat{r}_l\oplus 1}) \\
& + \sum_{l=1}^{L}\left(\frac{\gamma(m,T_{h\widehat{r}_l\oplus 1}\frac{m}{\bar{\gamma}})}{\gamma(m)}\right)^{|\{\widehat{\boldsymbol{r}}\}>\widehat{r}_l|}\frac{|\{\widehat{\boldsymbol{r}}\}=\widehat{r}_l|}{(1-p_{out\{\widehat{\boldsymbol{r}}\}})\Gamma(m)}(\frac{m}{\bar{\gamma}})^m \\
& \times \sum_{j=0}^{|\{\widehat{\boldsymbol{r}}\}=\widehat{r}_l|-1}(-1)^j\binom{|\{\widehat{\boldsymbol{r}}\}=\widehat{r}_l|-1}{j}\sum_{k=0}^{j(m-1)} b_k^j(\frac{m}{\bar{\gamma}})^k \\
& \times N(2,k+m-1,(j+1)m,T_{h\widehat{r}_l\oplus 1},\infty).
\end{aligned}
\tag{4.21}
$$

where the coefficients b_k^j may be recursively computed as shown in [37](16). Explicitly, they may be formulated as

$$\begin{aligned} b_0^j = 1, b_1^j = j, b_{j(m-1)}^j &= \frac{1}{((m-1)!)^j} \\ b_k^j = \frac{1}{k} \sum_{i=1}^{\min(k,m-1)} &\frac{i(j+1)-k}{i!} b_{k-i}^j, \ 2 \le k \le j(m-1)-1. \end{aligned} \tag{4.22}$$

In (4.22), $N(a,p,q,T_1,T_2)$ is defined as $N(a,p,q,T_1,T_2) = \int_{T_1}^{T_2} Q(\sqrt{a\gamma})\gamma^p \exp(-\frac{q\gamma}{\bar{\gamma}})d\gamma$, where a,p,q are integers, as detailed in the Appendix.

4.5.3 Outage Probability Based on an Existing $\{\widehat{\boldsymbol{r}}\}$

The OP may be readily derived for a given $\{\widehat{\boldsymbol{r}}\}$ by substituting (4.18) into (4.9), which yields

$$p_{out\{\widehat{\boldsymbol{r}}\}} = \left[\frac{\gamma(m, m\frac{T_{h1}}{\bar{\gamma}})}{\Gamma(m)}\right]^{|\widehat{\boldsymbol{r}}>0|}. \tag{4.23}$$

Below we will study the BER, OP and bandwidth-efficiency of the MHLs using our MTART. In order to achieve this, we first have to define the states of the system and then derive the transition probability amongst the states. Hence, in the next subsection, we will derive the state-transition matrix, which contains the probability of transition from one state to another in the system.

4.5.4 State Transition Matrix

Recall that the buffer size of every RN is B packets. Then, the states of the L-hop link may be defined in terms of the number of packets stored in the buffers of the $(L-1)$ RNs as

$$S_i = \left[b_1^{(i)}, b_2^{(i)}, \cdots, b_{L-1}^{(i)}\right]^T, i = 0, 1, \ldots, N-1, \tag{4.24}$$

where $b_l^{(i)}$ denotes the number of packets stored by the lth RN, and the L-hop link is in state i, while $N = (B+1)^{L-1}$ is the total number of states, which constitute the set $\mathcal{S} = \{S_0, S_1, \ldots, S_{N-1}\}$. For example, let us consider a three-hop link having the parameters of $L = 3$ and $B = 2$. Then, there are in total $N = 3^2 = 9$ states, which

form the set

$$\mathcal{S} = \{S_0 = [0,0]^T, S_1 = [0,1]^T, S_2 = [0,2]^T, \\ S_3 = [1,0]^T, S_4 = [1,1]^T, S_5 = [1,2]^T, \\ S_6 = [2,0]^T, S_7 = [2,1]^T, S_8 = [2,2]^T\}.$$

Given N states, the state transition matrix $\boldsymbol{T}$ host the state transition probabilities of $\{P_{ij} = P(s(t+1) = S_j | s(t) = S_i),\ i,j = 0,1,\ldots,N-1\}$. In the following, we will derive the transition matrix $\boldsymbol{T}$ of the MHLs using our MTART.

In $\boldsymbol{T}$, $\boldsymbol{T}_{i,j}$ denotes the state transition probability from state i to state j after a single TS. If state j cannot be reached from state i in a single TS, $\boldsymbol{T}_{i,j}$ is zero. Specifically, $\boldsymbol{T}_{i,i}$ means that no packets are transmitted by the system, hence an outage occurs. Therefore, $\boldsymbol{T}_{i,i}$ represents the OP. When state i is changed to state j, a unique hop should be correspondingly activated and the number of packets to be transmitted is also known. Let us assume that the lth hop should be activated and that $r_{i->j}$ packets should be transmitted, when the system evolves from state i to j. In this case, the state-transition probability $\boldsymbol{T}_{i,j}$ can be evaluated as

$$\boldsymbol{T}_{i,j} = \int_{T_{hr_{i->j}}}^{T_{hr_{i->j}\oplus 1}} p^l_{\{\gamma|\widehat{\boldsymbol{r}}\}}(\gamma) d\gamma, \tag{4.25}$$

where $p^l_{\{\gamma|\widehat{\boldsymbol{r}}\}}(\gamma)$ is given by (4.11) and (4.12). For the example of $L = 2$, $B = 8$, $SNR = 10dB$ and assuming that all hops experience Nakagami-m fading associated with $m = 1$, with the aid of (4.25), we arrive at:

$$\boldsymbol{T} = \begin{bmatrix} 0.162 & 0.136 & 0.486 & 0 & 0.212 & 0 & 0.004 & 0 & 0 \\ 0.241 & 0.026 & 0.031 & 0.486 & 0 & 0.212 & 0 & 0.004 & 0 \\ 0.433 & 0.031 & 0.026 & 0.031 & 0.263 & 0 & 0.212 & 0 & 0.004 \\ 0 & 0.433 & 0.031 & 0.026 & 0.31 & 0.263 & 0 & 0.216 & 0 \\ 0.193 & 0 & 0.263 & 0.031 & 0.026 & 0.31 & 0.263 & 0 & 0.193 \\ 0 & 0.216 & 0 & 0.263 & 0.31 & 0.26 & 0.31 & 0.433 & 0 \\ 0.004 & 0 & 0.212 & 0 & 0.263 & 0.031 & 0.026 & 0.031 & 0.432 \\ 0 & 0.004 & 0 & 0.212 & 0 & 0.486 & 0.031 & 0.026 & 0.241 \\ 0 & 0 & 0.004 & 0 & 0.212 & 0 & 0.486 & 0.136 & 0.162 \end{bmatrix}. \tag{4.26}$$

Note that the third row of (4.26) represents that there are two packets in the buffer of the RN, which is the case considered in Fig. 4.6, where $\boldsymbol{T}_{3,3}$ is the OP associated with region A of Fig. 4.6 based on (4.23). Furthermore, $\boldsymbol{T}_{3,1}$ is the probability that two

packets are transmitted from the RN to the DN, which corresponds to region C of Fig. 4.6. Note additionally that the probabilities in (4.26) depend on the SNR. This is different from the MHLs employing a single fixed modulation scheme, as shown in [168](18).

Having obtained the state transition matrix $\boldsymbol{T}$, the steady-state probabilities can be computed according to [181] as

$$P_{\boldsymbol{\pi}} = \boldsymbol{T}^T P_{\boldsymbol{\pi}}, \tag{4.27}$$

where we have $P_{\boldsymbol{\pi}} = \left[P_{\pi_0}, P_{\pi_1}, \ldots, P_{\pi_{(B+1)^{L-1}-1}}\right]^T$ and P_{π_i} is the steady-state probability that the L-hop link is in state S_i [110]. The steady-state probability of a state is applied as the expected value of the probability of this specific state in system. The knowledge of the steady-state probability of every state allows us to determine the Probability Mass Function (PMF) of a buffer. Equation (4.27) shows that $P_{\boldsymbol{\pi}}$ is the right eigenvector of the matrix $\boldsymbol{T}^T$ corresponding to an eigenvalue of one. Therefore, $P_{\boldsymbol{\pi}}$ can be derived with the aid of classic methods conceived for solving the corresponding eigenvalue problem [182].

4.5.5 Achievable Throughput

Given the state transition matrix $\boldsymbol{T}$ and the steady-state probabilities $P_{\boldsymbol{\pi}}$, the throughput Φ_T of a MHL can be evaluated. Given that the probability of the system evolving from state i to state j is $P_{\pi_{i-1}}\boldsymbol{T}_{i,j}$ and that $r_{i->j}$ packets are transmitted over a hop, the achievable throughput may be expressed by considering all possible state transitions, yielding

$$\Phi_T = \sum_{i=1}^{(B+1)^{(L-1)}} \sum_{j=1}^{(B+1)^{(L-1)}} P_{\pi_{i-1}}\boldsymbol{T}_{i,j} r_{i->j}. \tag{4.28}$$

4.5.6 Bit Error Ratio

In this subsection, we consider the exact single-hop BER and exact end-to-end BER of the MHLs. The exact single-hop BER can be evaluated by taking into account all the states S_i [168](17) and their corresponding BERs of $p_{H,ber\{\widehat{\boldsymbol{r}}\}}$, which was given in (4.21). Let us assume that the maximum transmission rate of the modulation schemes used is r_{max} packets per TS. In the example considered in 4.4.1, the highest-order modulation scheme is 64QAM, hence we have $r_{max} = \log_2 64 = 6$ packets.

Given S_i, $\{\widehat{\boldsymbol{r}}\}$ may be calculated as

$$\begin{aligned}\{\widehat{\boldsymbol{r}}\}_{S_i} =& \min([r_{max}\ S_i^T], [B - S_i^T\ r_{max}]) \\ =& [\min(r_{max}, B - b_1^{(i)}), \min(b_1^{(i)}, B - b_2^{(i)}), \\ & \cdots, \min(b_{L-1}^{(i)}, r_{max})],\end{aligned} \tag{4.29}$$

where $b_1^{(i)}, b_2^{(i)}, \cdots, b_{L-1}^{(i)}$ are defined in (4.24). Specifically, for the two-hop link considered in our specific example shown in (4.26), there are two packets at the RN, hence we have $\{\widehat{\boldsymbol{r}}\}_{S_2}$=min([6 2], [8 − 2 6])={min(6, 6), min(2, 6)}={6, 2} packets. Based on the above discussions, the exact single-hop BER can be expressed as

$$p_{H,ber} = \sum_{i=1}^{(B+1)^{(L-1)}} P_{\pi_{i-1}} p_{H,ber\{\widehat{\boldsymbol{r}}\}_{S_i}}. \tag{4.30}$$

The end-to-end exact BER can be derived with the aid of the exact single-hop BER of Section 4.5.2 ,from [168](13) or [184](17) for BPSK or MQAM, respectively.

4.5.7 Outage Probability and Its Bound

Similarly to Subsection 4.5.5, given the state transition matrix $\boldsymbol{T}$ and the steady-state probabilities $P_{\boldsymbol{\pi}}$, the OP of an L-hop MHL may be readily expressed as

$$P_O = \sum_{i=1}^{(B+1)^{(L-1)}} P_{\pi_{i-1}} \boldsymbol{T}_{i,i}. \tag{4.31}$$

Note that the lower-bound of the OP is given by (4.23) associated with the setting of $|\widehat{r} > 0| = L$.

4.5.8 Bandwidth-Efficiency

In this subsection, the single-hop bandwidth-efficiency is derived for a given $\{\widehat{\boldsymbol{r}}\}$, when communicating over Nakagami-m fading channels. Upon substituting (4.7), (4.9), (4.10), (4.11), and (4.12) into (4.17), and carrying out some futher manipulations,

we arrive at:

$$
\begin{aligned}
& C_{\{\widehat{\boldsymbol{r}}\}} \\
=& \sum_{l=1}^{L} \frac{|T_{h\{\widehat{\boldsymbol{r}}\}\oplus 1} \geq T_{h\gamma\oplus 1}|}{\ln 2\Gamma(m)} \left(\frac{m}{\gamma_h}\right)^m \sum_{j=0}^{|T_{h\{\widehat{\boldsymbol{r}}\}\oplus 1} \geq T_{h\gamma\oplus 1}|-1} (-1)^j \\
& \times \binom{|T_{h\{\widehat{\boldsymbol{r}}\}\oplus 1} \geq T_{h\gamma\oplus 1}| - 1}{j} \sum_{k=0}^{j(m-1)} b_k^j \left(\frac{m}{\gamma_h}\right)^k \\
& \times NC(2, k+m-1, (j+1)m, T_{h1}, T_{h\widehat{r}_l\oplus 1}) \\
& + \sum_{l=1}^{L} \left(\frac{\gamma(m, T_{h\widehat{r}_l\oplus 1}\frac{m}{\gamma_h})}{\gamma(m)}\right)^{|\{\widehat{\boldsymbol{r}}\}>\widehat{r}_l|} \frac{|\{\widehat{\boldsymbol{r}}\} = \widehat{r}_l|}{\ln 2\Gamma(m)} \left(\frac{m}{\gamma_h}\right)^m \\
& \times \sum_{j=0}^{|\{\widehat{\boldsymbol{r}}\}=\widehat{r}_l|-1} (-1)^j \binom{|\{\widehat{\boldsymbol{r}}\} = \widehat{r}_l| - 1}{j} \sum_{k=0}^{j(m-1)} b_k^j \left(\frac{m}{\bar{\gamma}}\right)^k \\
& \times NC(2, k+m-1, (j+1)m, T_{h\widehat{r}_l\oplus 1}, \infty),
\end{aligned} \tag{4.32}
$$

where b_k^j was given in (4.22), and $NC(a, p, q, T_1, T_2)$ is defined as $NC(a, p, q, T_1, T_2) = \int_{T_1}^{T_2} \ln(1 + a\gamma)\gamma^p \exp(-\frac{q\gamma}{\bar{\gamma}})d\gamma$, where a, p and q are integers, as detailed in the Appendix.

Given $C_{\{\widehat{\boldsymbol{r}}\}}$ of (4.32), the exact end-to-end bandwidth-efficiency C of a MHL may be calculated by considering all the possible states, yielding

$$
C = \frac{1}{L} \sum_{i=1}^{(B+1)^{(L-1)}} P_{\pi_{i-1}} C_{\{\widehat{\boldsymbol{r}}\}_{S_i}}, \tag{4.33}
$$

where the factor $\frac{1}{L}$ is due to having L TSs owing to the orthogonal time division operation assumed in [163].

4.5.9 Probability Mass Function of Delay

In this subsection, we study the delay of the MHL system. Firstly, an algorithm is proposed for calculating the PMF of the delay. Then the average delay of packets transmitted over our MHLs is considered.

The procedure conceived for deriving the PMF of delay is summarized in Fig. 4.8 and Fig. 4.9. The basic idea behind it relies on using the concept of a test packet hypothetically transmitted by the SN in $TS = 0$. Then we derive the probability that this hypothetical test packet arrives at the DN when TS=t_s. Let the probabilities corresponding to the different values of t_s be collected in a vector $\boldsymbol{P_d}(t_s)$. Upon encountering an outage event, the length of the vector $\boldsymbol{P_d}(t_s)$ may become infinite.

In practice, any t_s value having a probability less than 10^{-8} is ignored. Therefore, the length of the vector $\boldsymbol{P_d}(ts)$ is finite in practice. Let us now detail our procedure conceived for deriving the PMF of the delay step-by-step.

The inputs of the procedure include the average received SNR values of all the hops, $\boldsymbol{T}, P_{\boldsymbol{\pi}}$ given in (4.27) and $TS = 0$. Note that the PMF of the packet delay is different for different average received SNR values. Let us define a matrix $\boldsymbol{M}(TS)$ of size $(L-1)(B+1) \times (B+1)^{L-1}$, whose elements are initialized to zero. In $\boldsymbol{M}$, $\boldsymbol{M}_{i,j}$ denotes the probability that $(i-1)$ packets are stored at the RNs before hypothetically transmitted test packet enters the system, provided that the state of the system is S_j. Following this initialization, the algorithm is divided into two parts. The first part corresponds to hypothetically transmitting the test packet from SN to RN_1, while the second part controls to passage of the hypothetically transmitted test packet from RN_1 to DN.

4.5.9.1 Test Packet Transmission from SN to RN_1

This step is shown in Fig. 4.8. The delay-distribution of the test packet depends on three factors, namely on the system's state at the beginning of $TS = 0$; on the transition probabilities of the first hop; and on the data rate at $TS = 0$. Before we elaborate on the details, let us consider an example first.

Assuming that two packets are stored at the RN of a two-hop link, as assumed in the previous example of Section IV, the probability of this state is P_{π_2}, which may be found upon solving $P_{\boldsymbol{\pi}} = \boldsymbol{T}^T P_{\boldsymbol{\pi}}$. The transition matrix of this example was shown in (4.26). Let us assume that the CQ of the first hop at $TS = 0$ facilitates the transmission of two packets/TS. Therefore, the test packet has the probability $P_{\pi_2}\boldsymbol{T}_{3,5}$ of entering the system by being transmitted from the SN to the RN. The test packet will have the same probabilities of being at the third and fourth position of the RN's buffer, which implies that two or three packets are transmitted, before the test packet enters the system. Hence, we have $\boldsymbol{M}_{3,4} = \boldsymbol{M}_{4,4} = P_{\pi_2}\boldsymbol{T}_{3,5}/2$. After considering all the possible P_{π_i} values and their corresponding transition probabilities $\boldsymbol{T}_{i,j}$, $\boldsymbol{M}$ can be computed. In order to facilitate for the test packet to enter the system, $\boldsymbol{M}$ should be normalized at the end of $TS = 0$. Below, we provided a detailed general description of this part with reference to Fig. 4.8.

We labelled the stages as "a)" to "e)" in Fig. 4.8. Let us now elaborate on them one by one. a) shows the inputs of the procedure including: $\boldsymbol{T}$, $P_{\boldsymbol{\pi}}$, $\boldsymbol{M}(0)$, $TS = 0$ and SNR. b) Let us now find the transition probabilities by considering all the states P_{π_i} and all corresponding possible rate. A specific example was shown in the previous paragraph. Based on the data rate r, either action "c)" or action "d)" of Fig. 4.8 will

be executed. c) Assuming that there are k packets in the buffer of RN_1 and the data rate is 1 packet per TS, the test packet will be considered as the last packet in RN_1 after transmission and the corresponding probability of where is the hypothetically transmitted test packet will be evaluated and entered into $\boldsymbol{M}(0)$. d) Assuming that there are k packets in the buffer of RN_1 and that the data rate is more than 1 packet per TS, the test packet will be assumed to have a $\frac{1}{r}$ probability to be stored at the each of the last r packet positions of in RN_1 and the corresponding probability of where is the hypothetically transmitted test packet will be evaluated and entered into $\boldsymbol{M}(0)$. e) Finally, each of the L hops has the same probability to be activated, hence a factor L is used in Fig. 4.8 for ensuring that the sum of the probabilities in $\boldsymbol{M}$ is 1[3].

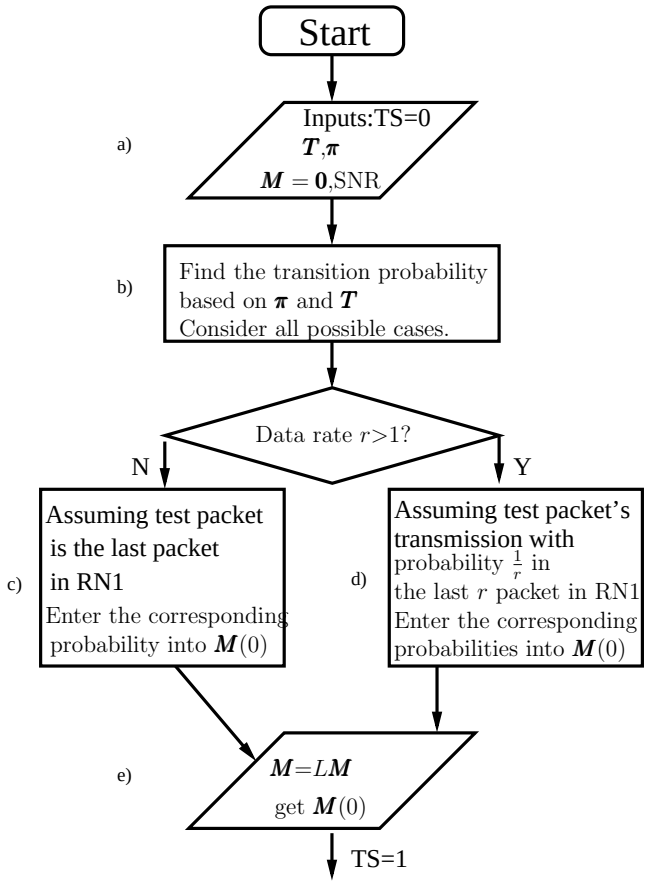

Figure 4.8: The first part of the procedure conceived for deriving the PMF of the packet delay.

4.5.9.2 Propagate the Test Packet from RN_1 to DN

This step is detailed in Fig. 4.9 which can be divided into three constituent steps: a) Testing, whether to terminate the process; b) calculating $\boldsymbol{M}(ts)$ based on $\boldsymbol{M}(ts-1)$

[3]The summation of all elements in $\boldsymbol{M}(0)$ has to be one, which corresponds to the probability that the test packet entered the system.

and c) removing the probability of the first row in $\boldsymbol{M}(ts)$, where ts is the number of TS after the hypothetically transmitted test packet entered the system. Let us discuss these three steps further below in the order of b), c) and a) order.

b) Given a fixed $\boldsymbol{M}_{i,j}(ts-1)$ and the system's state transition probability of $\boldsymbol{T}_{j,k}$ from j to k, the corresponding data rate and the probability of where is the test packet of a specific position in the buffer can be calculated. Then the appropriate value can be entered into $\boldsymbol{M}(ts)$ by considering all possible i, j, k in $\boldsymbol{M}(ts-1)$ and $\boldsymbol{T}$. c) Having determined $\boldsymbol{M}(ts)$, the summation of the values in the first row of this matrix, namely of $\boldsymbol{M}_{i,j}, j = 1, 2, \ldots, (B+1)^{L-1}$, determines the probability of the test packet arriving at the DN at $TS = ts$, which should be stored in $\boldsymbol{P_d}(ts)$. Then we will set all values in the first row in $\boldsymbol{M}(ts)$ to zero. a) Let us now increase the TS-counter according to $ts = ts + 1$ and repeat this process, until we satisfy the condition of $\boldsymbol{M} < 10^{-8}$.

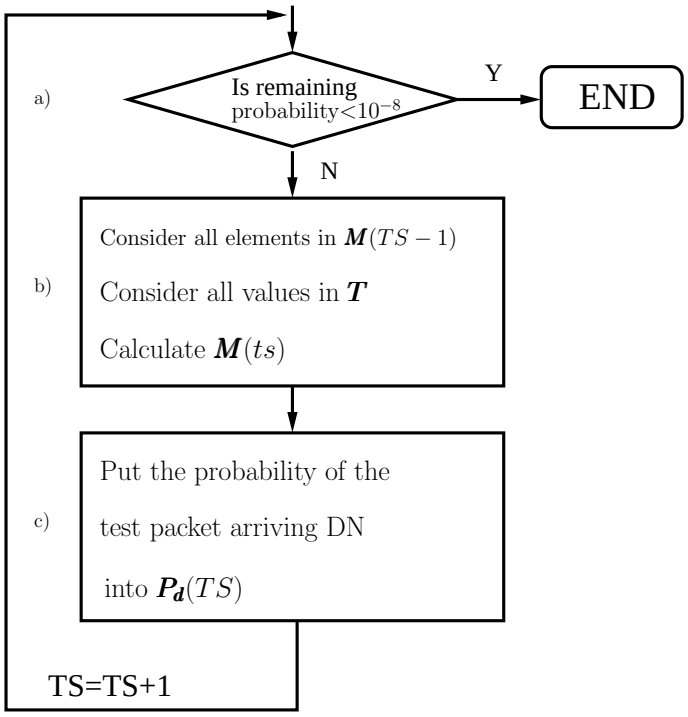

Figure 4.9: The second part of the procedure conceived for deriving the PMF of the packet delay.

Having determined the distribution $\boldsymbol{P_d}(t_s)$ of the delay, the average packet delay $\bar{\tau}$ can now be expressed as

$$\bar{\tau} = \sum_{t_s=L}^{\infty} P_d(t_s) \cdot t_s. \tag{4.34}$$

4.6 Performance Results

In this section, a range of numerical and/or simulation results are provided in Fig. 4.10 to Fig. 4.12 for calculating the BER and the OP of the MHLs, in order to illustrate the effect of the buffer size B of the RNs. Following these investigations, in Fig. 4.13 and Fig. 4.14, the delay of the MHLs using our MTART regime is characterized. Finally, the attainable throughput is quantified in Fig. 4.15 of the MHLs. The MQAM mode-switching thresholds are the same as those used for Fig. 4.7.

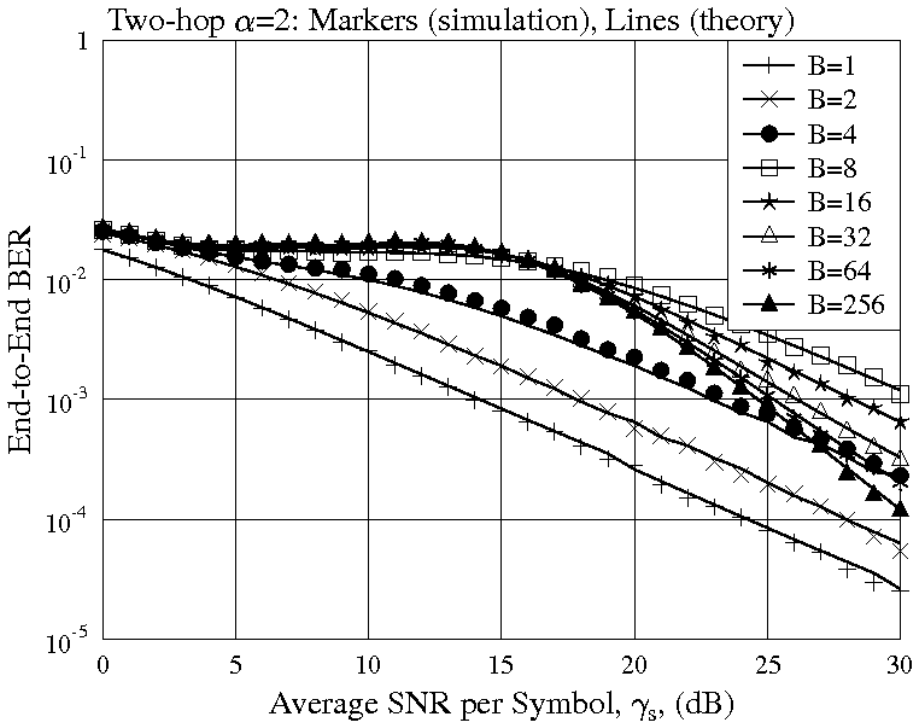

Figure 4.10: BER performance of two-hop links employing MTART over Rayleigh fading channels. The MQAM switching - thresholds were configured for BER=0.03 according to [70]. The related formulas used for computing the results are (4.13), (4.14), (4.15) and (4.16).

Fig. 4.10 shows the impact of the RN's buffer size B on the end-to-end BER performance of two-hop links operated in Rayleigh fading channels. The results are plotted versus the average SNR γ_s per symbol, which is the equivalent average SNR per symbol for a single-hop link. The related formulas used for computing the results are (4.13), (4.14), (4.15) and (4.16). As shown in Fig. 4.10, when the RN's buffer size B is lower than the maximum packet per TS throughput of the modulation scheme, which is $r_{max} = 6$, the achievable BER decreases smoothly, since the system is operated using lower throughput modulation schemes, owing to the lack of data for transmission, when the CQ is high. On the other hand, when the buffer size is higher than r_{max}, observed in Fig. 4.10 that the BER curves remain near horizonal

in the low-SNR range. Observe furthermore in Fig. 4.10 that once the average SNR per symbol exceeded about $18dB$, the 64QAM mode was used at a high probability, since the throughput cannot be increased further. Hence the BER became lower than the target of 3%.

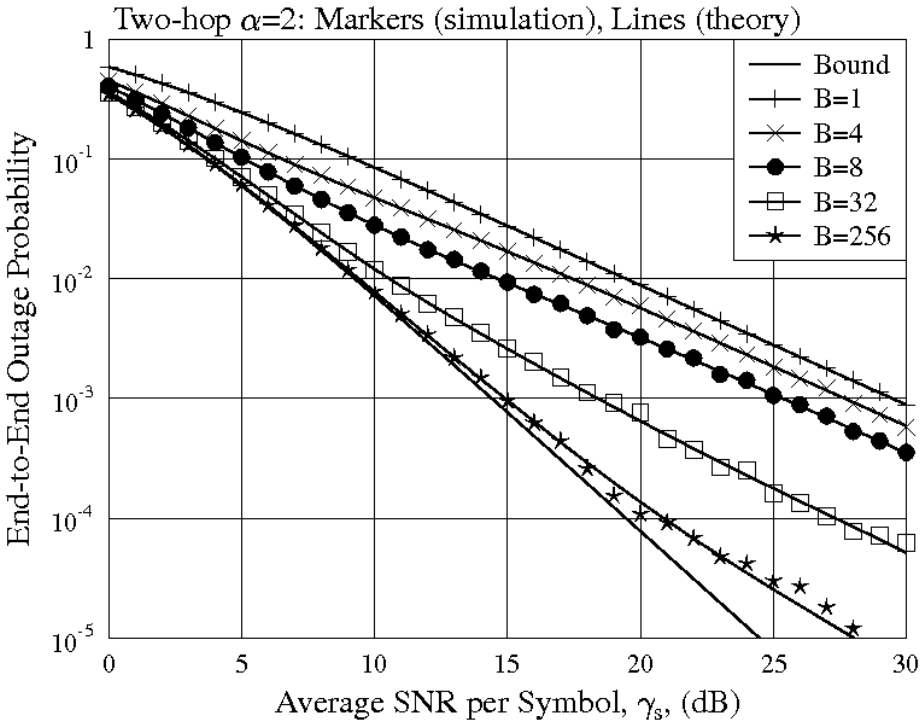

Figure 4.11: The OP performance using our MTART in a two-hop link over Rayleigh channel. The MQAM switching - thresholds were configured for BER=0.03 according to [70]. The related formula used for computing the results is (4.31).

Fig. 4.11 and Fig. 4.12 characterize the OP of two-hop links communicating over Rayleigh (Fig. 4.11) or Nakagami-m (Fig. 4.12) fading channels. Note that in our numerical computations and simulations, the outage threshold (T_{h1}) of each hop was adjusted for maintaining a BER of 0.03 for a single-hop link. The theoretical results were obtained by evaluating (4.31). The OP of conventional adaptive modulation is also provided for the sake of comparison in these figures, which corresponds to $B = 1$, i.e. to the absence of buffer. From these figures, we may derive similar observations to those emerging from [168]. In summary, a significant improvement is observed for the RNs employing buffers of a sufficiently high size. For example, the SNR gain at OP=10^{-3} is $15dB$ in Fig. 4.11, because in conventional adaptive modulation an outage occurs, when the CQ of a *single* hop is lower than the outage threshold. By contrast, in our proposed MTART regime an outage occurs only when the CQs of *all* hops are lower than the outage threshold of the RNs employing buffers.

Fig. 4.13 and Fig. 4.14 show the distributions of the packet delay in two- or three-hop links employing our MTART regime. The curves seen in these figures were

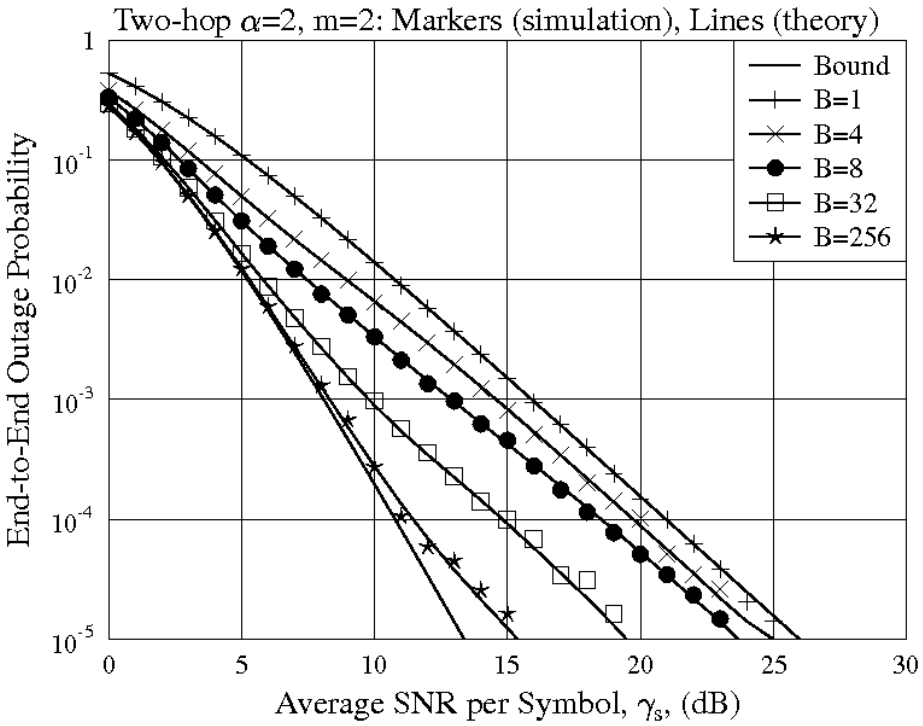

Figure 4.12: The OP performance using our MTART in a two-hop link over Nakagami-m channel when $m = 2$. The MQAM switching - thresholds were configured for BER=0.03 according to [70]. The related formula used for computing the results is (4.31).

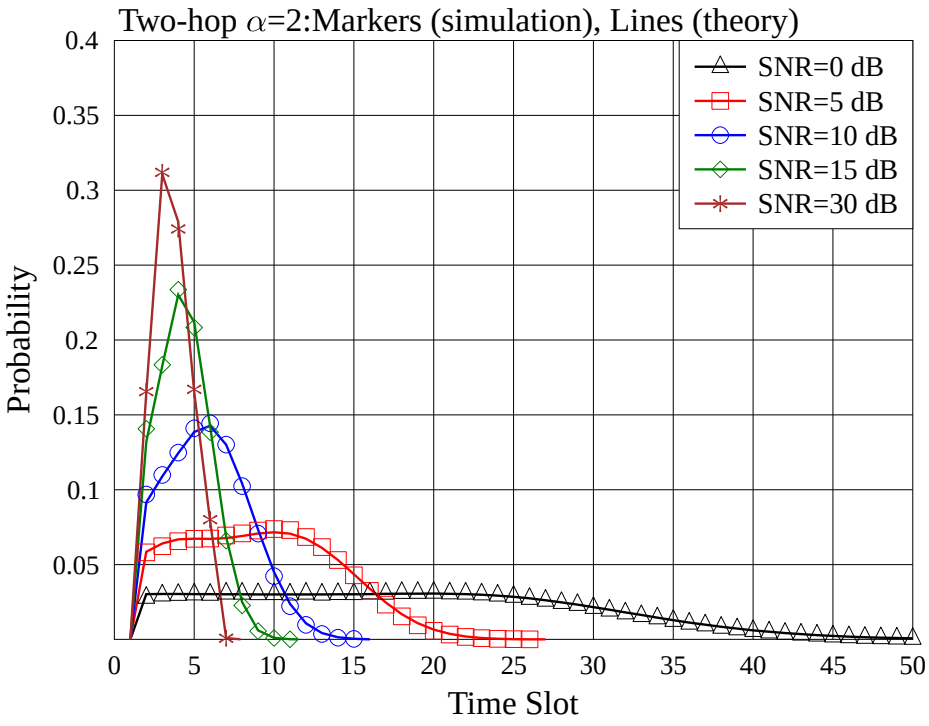

Figure 4.13: The distribution of delay for a two-hop link, when $B = 16$ for transmission over Rayleigh channels.

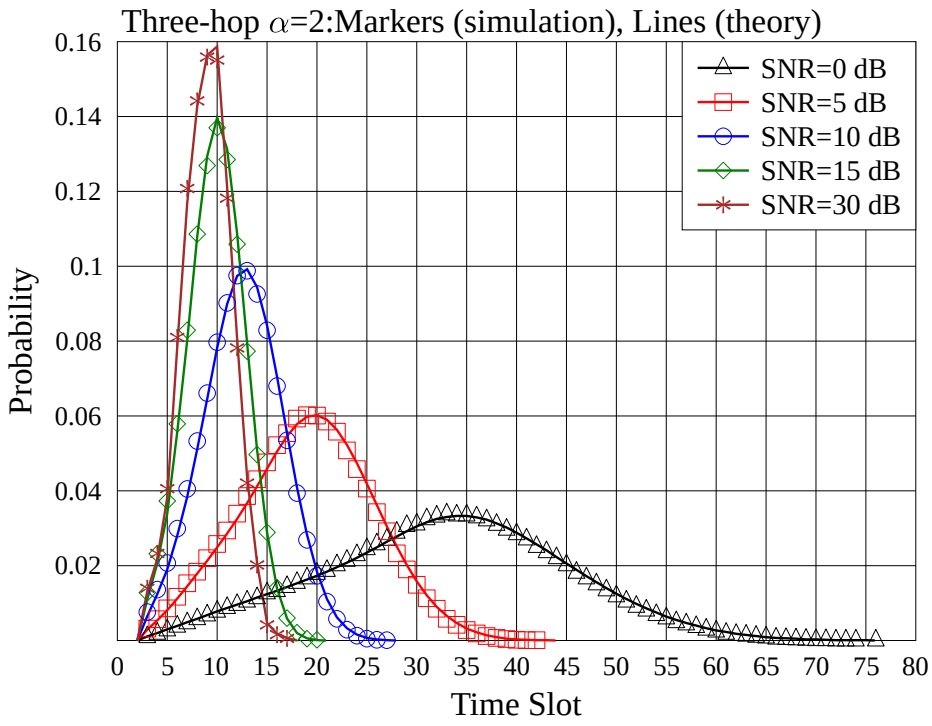

Figure 4.14: The distribution of delay for a three-hop link, when $B = 16$ for transmission over Rayleigh channels.

evaluated using the procedure described in Section 4.5, while the markers represent our simulations. From these figures, we may infer that both the average and the maximum delay decreases upon increasing the SNR. Note that we defined both the *packet delay* and the *block delay* in [168]. Although, the average delay of a packet is longer for buffer-aided transmission than that of the conventional scheme, the block delay of MTART is lower than that of the conventional adaptive transmission scheme due to the higher end-to-end throughput.

Finally, Fig. 4.15 shows the throughput/bandwidth-efficiency of two-hop links communicating over Rayleigh channels. The theoretical throughput results were evaluated using (4.28), while the bandwidth-efficiency results were obtained from (4.32) and (4.33). Furthermore, the curves with markers represent the end-to-end throughput for a specific buffer size. The solid line at the top represents the bandwidth-efficiency, when the RNs employ an infinite buffer size. By contrast, the second line from the top, which is a dashed-curve, represents the bandwidth-efficiency of the conventional adaptive scheme. The dotted line, which is roughly overlapping with the buffer scenario of $B = 8$ line represents the throughput $\Phi_{Conv.}$ for the conventional

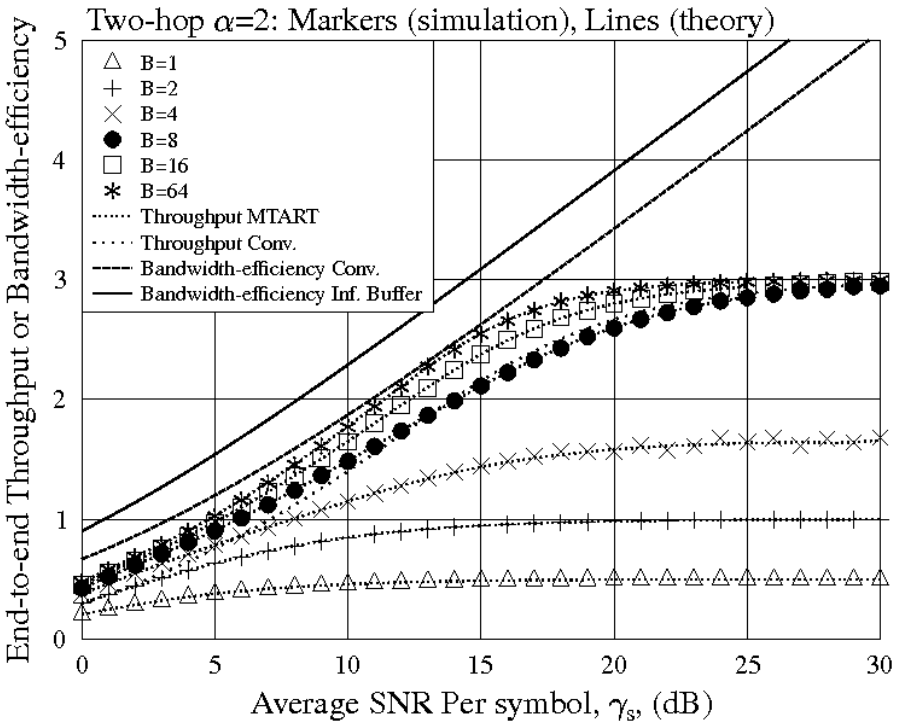

Figure 4.15: The throughput and capacity for two-hop link over Rayleigh channel.

two-hop link, which was evaluated in [195](8)[4]:

$$\Phi_{Conv.} = \frac{1}{L}\left[2\frac{\gamma(m,(\frac{T_{h4}}{\bar{\gamma}}))}{\Gamma(m)} + 2\frac{\gamma(m,(\frac{T_{h3}}{\bar{\gamma}}))}{\Gamma(m)} + \frac{\gamma(m,(\frac{T_{h2}}{\bar{\gamma}}))}{\Gamma(m)} + \frac{\gamma(m,(\frac{T_{h1}}{\bar{\gamma}}))}{\Gamma(m)}\right]. \quad (4.35)$$

As shown in Fig. 4.15, compared to the throughput of the conventional adaptive modulation scheme, that of the MTART regime has an approximately $2.5dB$ gain across a wide range of SNRs. Similarly, in terms of its bandwidth-efficiency, our MTART regime has an approximately $3dB$ gain across a wide range of SNRs.

4.7 Chapter Conclusions

In this chapter, the MTART scheme of Section 4.3 was proposed for supporting adaptive rate transmission of data over multihop links. The corresponding MAC protocol was conceived in the same section. In figure 4.4, a decentralized MAC layer algorithm was designed for identifying the most beneficial hop to be activated.

[4]Strictly speaking, the conventional adaptive modulation scheme cannot be applied based on our current assumptions due to the potentially unequal rate of the each hops. For example, in a two-hop link, if the RN already has two packets stored and the RN-DN channel only allows us to transmit one packet, the two packets stored in the RN cannot be transmitted within one TS. However, we may relax the associated assumptions for the sake of finding the throughput of the conventional scheme. Let us assume that the transmission duration is adjustable, therefore, the RN can transmit the two packets to the DN in 2TSs. Then the corresponding throughput based on the CQ and the threshold can be evaluated from (4.35).

The principle of the proposed MTART was detailed in Section 4.4. Our discussion commenced from a simple two-hop link in Section 4.4.2, followed by an L-hop link in Section 4.4.3 and transmissions over Nakagami-m fading channels were considered in Section 4.5. The BER, OP, the PDF of the packet-delay, throughput as well as bandwidth-efficiency were analyzed in Sections 4.5.2 to 4.5.9. A range of related formulas were obtained. When assuming that the adaptive modulation was used for transmitting over all hops experiencing i.i.d fading, our performance results of Fig. 4.11 show that we have a significant OP improvement, when we adopt MTART. The PDF of the packet-delay was characterized in Fig. 4.13. Finally, as shown in Fig. 4.15, in comparison to conventional adaptive modulation, we achieve an approximately $3dB$ gain, when we employ our MTART scheme.

Although, the MTART regime was proposed for achieving an increased throughput, the system model we considered was the simple one-dimensional link of Fig. 4.1. In order to extend the buffer-aided transmission regime to a more general scenarios, we will consider a three-node network in Chapter 5.

4.8 Appendix

4.8.1 The Closed-Form Expression of $N(a,p,q,T_1,T_2)$

In (4.21), the specific function $N(a,p,q,T_1,T_2)$ represents the integral of

$$N(a,p,q,T_1,T_2)=\int_{T_1}^{T_2} Q(\sqrt{a\gamma})\gamma^p \exp(-\frac{q\gamma}{\bar{\gamma}})d\gamma, \tag{4.36}$$

where a,p,q are integers. The derivation process is similar to that in the Appendix of [147], which eventually leads to

$$\begin{aligned}
&N(a,p,q,T_1,T_2)\\
=&(\frac{\bar{\gamma}}{q})^{p+1}\Gamma(p+1)\left[\left(Q(\sqrt{aT_1})\exp(-\frac{qT_1}{\bar{\gamma}})-Q(\sqrt{aT_2})\exp(-\frac{qT_2}{\bar{\gamma}})\right)\right.\\
&\left.+\sqrt{\frac{a\bar{\gamma}}{a\bar{\gamma}+2q}}\left(Q\left(\sqrt{T_2(a+\frac{2q}{\bar{\gamma}})}\right)-Q\left(\sqrt{T_1(a+\frac{2q}{\bar{\gamma}})}\right)\right)\right]\\
&+\sum_{\hat{p}=1}^{p}(\frac{\bar{\gamma}}{q})^{\hat{p}}\frac{\Gamma(p+1)}{\Gamma(p-\hat{p}+1)}\exp(-\frac{q\gamma}{\bar{\gamma}})Q(\sqrt{a\gamma})\gamma^{\hat{p}}|_{T_1}^{T_2}\\
&-\sum_{\hat{p}=1}^{p}(\frac{\bar{\gamma}}{q})^{\hat{p}}\sqrt{\frac{a}{2\pi}}\frac{1}{2}(\frac{q}{\bar{\gamma}}+\frac{a}{2})^{-\hat{p}-\frac{1}{2}}\left(\gamma\left(\hat{p}+\frac{1}{2},T_2(\frac{q}{\bar{\gamma}}+\frac{a}{2})\right)-\gamma\left(\hat{p}+\frac{1}{2},T_1(\frac{q}{\bar{\gamma}}+\frac{a}{2})\right)\right).
\end{aligned} \tag{4.37}$$

Based on (4.37), the closed-form expression of (4.21) can be obtained.

4.8.2 The Closed-Form Expression of $NC(a,p,q,T_1,T_2)$

In (4.32), the specific function $NC(a,p,q,T_1,T_2)$ represents the integral

$$NC(a,p,q,T_1,T_2)=\int_{T_1}^{T_2}\ln(1+a\gamma)\gamma^p\exp(-\frac{q\gamma}{\bar{\gamma}})d\gamma, \tag{4.38}$$

where a,p,q are integers. Base on the same approaches as used for the derivation of (4.37), we arrive at

$$\begin{aligned}NC(a,p,q,T_1,T_2)\frac{1}{\bar{\gamma}}+\exp(-\frac{q\gamma}{\bar{\gamma}})\ln(1+a\gamma)\gamma^p|_{T_1}^{T_2}+\frac{q-1}{\bar{\gamma}}NC(a,p,q,T_1,T_2)-\\ \int_{T_1}^{T_2}\gamma^p\exp(-\frac{q\gamma}{\bar{\gamma}})\frac{a}{1+a\gamma}d\gamma=pNC(a,p-1,q,T_1,T_2).\end{aligned} \tag{4.39}$$

The integral in above formula can be evaluated, leading to the following closed-form expression:

$$\begin{aligned}ND(a,p,q,T_1,T_2)=&\int_{T_1}^{T_2}\gamma^p\exp(-\frac{q\gamma}{\bar{\gamma}})\frac{a}{1+a\gamma}d\gamma\\ \overset{t=1+a\gamma}{=}&\int_{\frac{T_1-1}{a}}^{\frac{T_2-1}{a}}(\frac{t-1}{a})^p\exp(-\frac{q}{\bar{\gamma}}(\frac{t-1}{a}))\frac{1}{t}dt\\ =&\frac{\exp(\frac{q}{a\bar{\gamma}})}{a^p}\sum_{\acute{p}=0}^{p}\binom{p}{\acute{p}}(-1)^{\acute{p}}\int_{\frac{T_1-1}{a}}^{\frac{T_2-1}{a}}t^{p-\acute{p}-1}\exp(-\frac{qt}{\bar{\gamma}a})dt\\ =&\frac{\exp(\frac{q}{a\bar{\gamma}})}{a^p}\sum_{\acute{p}=0}^{p-1}\binom{p}{\acute{p}}(-1)^{\acute{p}}\\ &\times\left(\left(\frac{q}{a\bar{\gamma}}\right)^{\acute{p}-p}\left(\gamma\left(p-\acute{p},\frac{q}{a\bar{\gamma}}\frac{T_2-1}{a}\right)-\gamma\left(p-\acute{p},\frac{q}{a\bar{\gamma}}\frac{T_1-1}{a}\right)\right)\right)\\ &+\exp(\frac{q}{a\bar{\gamma}})\left(Ei\left(-\frac{q}{a\bar{\gamma}}T_1\right)-Ei\left(-\frac{q}{a\bar{\gamma}}T_2\right)\right),\end{aligned} \tag{4.40}$$

where $p>0$ is an integer and Ei is given by [10](8.211.1). Upon substituting (4.40) into (4.39), we obtain

$$\begin{aligned}NC(a,p,q,T_1,T_2)=&NC(a,p-1,q,T_1,T_2)\frac{\bar{\gamma}p}{q}-\frac{\bar{\gamma}}{q}\exp(-\frac{q\gamma}{\bar{\gamma}})\ln(1+a\gamma)\gamma^p|_{T_1}^{T_2}+\\ &\frac{\bar{\gamma}}{q}ND(a,p,q,T_1,T_2).\end{aligned} \tag{4.41}$$

We can then readily express $NC(a, 0, q, T_1, T_2)$ as

$$NC(a,0,q,T_1,T_2) = -\frac{\bar{\gamma}}{q}\left(\exp(-\frac{q\gamma}{\bar{\gamma}})\ln(1+a\gamma)|_{T_1}^{T_2}\right) + \frac{\bar{\gamma}}{q}ND(a,0,q,T_1,T_2). \quad (4.42)$$

Furthermore, we can express $ND(a, 0, q, T_1, T_2)$ as

$$ND(a,0,q,T_1,T_2) = \exp(\frac{q}{a\bar{\gamma}})\left(Ei\left(-\frac{q}{a\bar{\gamma}}T_1\right) - Ei\left(-\frac{q}{a\bar{\gamma}}T_2\right)\right). \quad (4.43)$$

Finally, when substituting (4.42) and (4.43) into (4.41), we arrive at

$$NC(a,p,q,T_1,T_2) = \sum_{\acute{p}=0}^{p}(\frac{\bar{\gamma}}{q})^{p+1-\acute{p}}\frac{\gamma(p+1)}{\gamma(\acute{p}+1)} \times \left(ND(a,\acute{p},q,T_1,T_2) - \gamma^{\acute{p}}\ln(1+a\gamma)\exp(-\frac{q\gamma}{\bar{\gamma}})|_{T_1}^{T_2}\right). \quad (4.44)$$

Based on this formula, the closed-form formula of (4.32) can be obtained.

Chapter 5

Minimum Average End-to-end Packet Energy Consumption of a Buffer-Aided Three-Node Network Relying on Opportunistic Routing

In Chapter 2 and 3, the buffer-aided multihop links of Figure 2.1 and 3.1 have been studied, which benefitted from multihop diversity. The scope of buffer-aided transmission was then further extended to adaptive modulation techniques in Chapter 4. Our buffer-aided adaptive modulation regime was characterized in terms of the throughput versus SNR in Fig. 4.15. Although this transmission scheme was capable of achieving an increased throughput, it considered the idealized simplifying assumption of having nodes along the one-dimensional link of Figure 2.1 and 3.1. By contrast, in this chapter we consider the buffer-aided transmissions in a three-node network. Our discussions are also extended to the issuses of energy consumption.

5.1 Introduction

Minimizing the energy consumption of a relay-aided wireless communication system is still an open problem at the time of writing. Employing a relay between the Source Node (SN) and the Destination Node (DN) is one of the most basic methods that can be used for minimizing energy consumption. In this three-node relaying system, it is traditionally assumed that a packet is transmitted from the SN to the DN via the Relay Node (RN) sequentially. For convenience of description, we refer to this as "*the conventional three-nodes transmission scheme*" in our forthcoming discourse.

This transmission scheme results in a range of advantages over conventional single-hop communications. These advantages may include an extended coverage area, an improved link performance and high-flexibility network planning, etc. [78,88,110,121, 140, 145, 173]. However, this transmission scheme has a limited diversity order and a limited throughput. Let us discuss these drawbacks in order to conceive possible solutions.

The first drawback of conventional transmission is that the Bit Error Ratio (BER)/outage performance cannot benefit from the maximum achievable diversity order, because no link prioritization scheme invoked, given that the channel activated at a specific time instant is predefined, regardless of its instantaneous Channel Quality (CQ). In order to improve the achievable performance of relaying systems, novel signalling schemes have been proposed [110,173,177], which require the nodes to have a store-and-wait capability. Additionally, in our previous contributions [168,183,184], we proposed a buffer-aided transmission scheme, namely the Multihop Diversity (MHD) transmission philosophically, which relies on temporarily storing the received packets and on activating the specific channel having the highest instantaneous SNR. Both our simulation results and theoretical analysis demonstrated that MHD transmissions are capable of achieving a substantial selection diversity gain. Very recently, a relay-relation scheme was proposed in [196], while full-duplex relaying was discussed in [197]. As a further advance, adaptive link selection was proposed in [198].

The second drawback of conventional relaying is its limited throughput, since the effective transmission duration of a specific hop in a two-hop link is halved compared to classic direct transmission [163]. More specifically, if the direct transmission has a throughput of 1bit/s/Hz, the single-hop throughput of the two-hop system should be at least 2bits/s/Hz for achieving the same throughput, which is a challenge in most practical cases [163]. However, Opportunistic Routing (OR) [172, 199–201] was shown to be capable of significantly enhancing the system's throughput in relay-aided wireless transmission. For example, Liu *et al.* [199] illustrated that OR substantially increases both the transmission reliability and the throughput by exploiting the broadcast nature of the wireless medium, where all transmissions can be overheard by multiple neighbours. Biswas and Morris [172] proposed an Extremely Opportunistic Routing (ExOR) scheme, which relied on the expected end-to-end transmission delay as the metric used for deciding on the priority order of selecting a RN from the potential forwarder set. The proposed routing regime intrinsically amalgamated the routing protocol and the Medium Access Control (MAC) protocol for the sake of increasing the attainable throughput of multi-hop wireless networks. Their solution [172] also exploited the less reliable long-distance SD-DN links, which

would have been ignored by traditional routing protocols. Zeng *et al.* [200] proposed multi-rate OR by incorporating rate-adaptation into their candidate-selection algorithm, which was shown to achieve a higher throughput and lower delay than the corresponding traditional single-rate routing and its opportunistic single-rate routing counterpart. Moreover, in our previous chapter [201], we proposed an energy-efficient cross-layer aided opportunistic routing for ad hoc networks, which formulated both the normalized energy consumption as well as the end-to-end throughput and theoretically analyzed their performances. The simulation results demonstrated that the proposed OR algorithm has a lower normalized energy consumption and higher end-to-end throughput than the traditional multi-hop routing algorithm.

The motivation behind this chapter is to combine the advantages of buffer-aided transmission with the added benefits of opportunistic routing. In the three-node network, we assumed that the RN is capable of storing a maximum of B packets and the SN can transmit its packets to the DN either directly or indirectly via a RN. Without loss of generality, let us consider the scenario, where the SN-RN distance is lower than the RN-DN distance. Even though the SN-RN distance may be different from the RN-DN distance, the probability of either of those two hops being selected should be the same, otherwise the system becomes unstable, which results in a buffer-overflow at the RN. In order to solve this problem, a new channel selection scheme relying on both buffer-aided transmissions and on opportunistic routing is proposed. There are three channels constituted by the SN-RN, SN-DN and RN-DN links, which form a 3D Transmission Activation Probability Space (TAPS), where the TAPS is divided into four regions representing the above-mentioned three channels and the outage region. In a specific time slot, the instantaneous CQ values may be directly mapped to a specific point in this 3D channel space. The Buffer-aided Opportunistic Routing (BOR) scheme uses this point for selecting the most appropriate channel for its next transmission. After investigating this new channel selection scheme, the end-to-end energy consumption, OP, the position of the RN as well as the packet delay are studied. We will demonstrate that a significant energy consumption-reduction can be achieved in comparison to the benchmark scheme. Furthermore, a meritorious MAC layer protocol is proposed for disseminating the global CQ knowledge and the Buffer-Fullness (BF) of the RN.

The new contributions of this chapter are summarized as follows:

1. The concept of non-linear channel space partitioning is proposed.

2. Both the end-to-end normalized energy consumption and the system's OP are studied in the context of specific buffer sizes.

The remainder of this chapter is organized as follows. Section 5.2 and 5.3 present our system model and highlight the implementation of the system. Then Section 5.4 to Section 5.7 detail the concept of channel space and elaborate on the choice of channel selection schemes. Section 5.8 analyses the distribution of packet delay. In Section 5.9, we provide our numerical and simulation results. Finally, our conclusions are offered in Section 5.10.

5.2 System Model

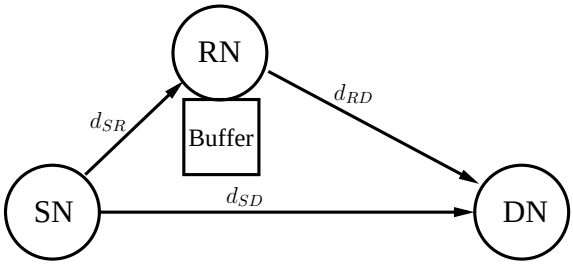

Figure 5.1: System model for a buffer-aided three-node network, where SN sends messages to DN via RN, directly or indirectly.

Our system model is portrayed in the next three sections related to buffering, the physical layer and the transmission scheme.

5.2.1 Buffering at the RN

Our three-node network considered in this chapter is shown in Fig. 5.1, which consists of a SN, a buffer-aided RN and a DN. The distances between corresponding pairs of nodes are d_{SR}, d_{SD} and d_{RD}. We assume that the RN is capable of storing a maximum of B packets and that the classic Decode-and-Forward (DF) protocol [150] is employed for relaying the signals. Finally, each node is capable of adjusting its transmit power between zero and the maximum transmit power P_{max}.

5.2.2 Physical Layer

In this chapter, we rely on the assumption of using perfect capacity-achieving channel coding operating exactly at the Discrete-input Continuous-output Memoryless Channel's (DCMC) capacity. This assumption specifies the Packet Error Ratio (PER) vs SNR relationship. However, this relationship may be replaced by any other PER-SNR relationship relevant for a specific coding scheme [201]. Based on this assumption and on the knowledge of the instantaneous CQ, the transmitter adjusts its transmit power for ensuring that the required SNR of γ_{T_h} is achieved at the receiver. Hence, the transmit power required is inversely proportional to the instantaneous CQ.

We assume that the signals are transmitted on the basis of TSs having a duration of T seconds. In addition to the propagation pathloss, the channels are assumed to experience independent block-based flat Rayleigh fading, where the complex-valued fading envelope of a hop remains constant within a TS, but it is independently faded for different TSs. The pathloss is assumed to obey the negative exponential law of $d^{-\alpha}$, where α is the pathloss exponent having a value between 2 to 6. It is also assumed that the instantaneous CQ of TS t between each node pairs is denoted by γ_{SR}, γ_{SD} and γ_{RD}. The instantaneous transmit power $\mathcal{E}_{SD}$, $\mathcal{E}_{RD}$ or $\mathcal{E}_{RD}$ of each node can then be calculated with the aid of $\kappa = 9.895 \times 10^{-05}$ and the noise power for $N = 10^{-13}W$ which corresponds to a receiver sensitivity of $-110dBm$. An example of calculating $\mathcal{E}_{SD}$ is given by

$$\mathcal{E}_{SD} = \frac{\gamma_{T_h}}{\gamma_{SD}} \frac{d_{SD}^{\alpha} N}{\kappa}, \ \mathcal{E}_{SD} \leq P_{max}. \tag{5.1}$$

5.2.3 Transmission Scheme

The Buffer-aided Three-node Network's (B3NN) MAC layer protocol will be detailed in Section 5.3, which activates a single channel during any TS. A packet will be transmitted from the SN to DN either directly or indirectly. Note that, if no packets are stored in RN, the RN-DN channel must not be activated. By contrast, if the buffer at RN is full, the SN-RN channel must not be activated. Our studies are based on the following assumptions:

- The SN always has packets to send, which hence facilitates for the B3NN to operate in its steady state.
- Both the SN and DN are capable of storing an infinite number of packets. By contrast, the RN can only store a maximum of B packets.
- The fading processes of the three channels are independent. The fading envelope of a given hop remains constant within a packet's duration, but it is independently faded from one packet to another.
- Each node accurately adjusts its transmission power to achieve the required received SNR of γ_{T_h}.
- In each TS, only a single packet is transmitted, when the corresponding link is activated.
- Our B3NN protocol provides every node with the global CQ and Buffer Fullness (BF) knowledge of the RNs within a given TS. All the operations of the B3NN protocol are assumed to have been carried out without a delay and without errors.

Let us now conceive a MAC protocol for controlling the operations of our B3NN.

5.3 MAC Protocol of the Buffer-Aided Three-node Network

Again, we assume that every node has the global CQ knowledge and the BF knowledge of the RNs. This facilitates the decisions as to which of the nodes is allowed to transmit. In practice, however, it is a challenge to realize this idealized assumption. Therefore, we have to design protocols for efficiently exchanging the related information, so that the specific hop requiring the least 'resources' is activated.

In a new TS, we assume that none of the nodes has any CQ knowledge or non-local BF knowledge. The operations have three stages. 1) The CQ of the adjacent nodes is measured first. 2) Then the RN obtain the CQ of the SN-DN channel. 3) Finally, the RN broadcasts its decision. To elaborate a little further, the operations associated with the above-mentioned three stages are described as follows.

Stage 1 - Channel State Identification: This stage requires three symbol durations in which the SN, RN and DN broadcast their pilot signals. Upon receiving the pilot signal, the receiver node estimates the corresponding CQ.

Stage 2 - Disseminate the Remaining Channel Quality Information: Following ***Stage 1***, every node becomes aware of the CQs of the pair of links connected to itself. For example, the SN is informed of the SN-RN and SN-DN link qualities. However, the RN also needs the CQ of the SN-DN link for deciding upon which of the channels will be activated. In order to satisfy this requirement, this stage needs another symbol duration. Accordingly, in the 4th symbol duration, the SN broadcasts $\frac{\gamma_{SD}}{h_{SR}}$. Hence, the RN receives $\frac{\gamma_{SD}}{h_{SR}} h_{SR} = \gamma_{SD}$.

Stage 3 - The decision carried out by the RN: Following ***Stage 1*** and ***Stage 2***, the RN becomes aware of all the CQ and BF knowledge. Based on this knowledge, the RN decides which particular channel will be activated and broadcasts this decision to the SN and DN. This step requires two more symbol durations.

Following these three stages, the communications may be established. We now formulate a procedure to be applied at the RN and discussed it in the context of our idealized simplifying assumptions.

5.4 The Energy Consumption Expressions

In this section, we stipulate our idealized simplifying assumptions and propose a novel node-activation scheme.

5.4.1 Idealized Simplifying Assumptions

Our main assumption is that the average number of packets conveyed from SN to RN should be the same as those transmitted from RN to DN, which implies that the SN-RN channel and RN-DN channel should have the same probability of being activated. This assumption is automatically satisfied, when we have $d_{SR} = d_{RD}$ and when both the SN-RN and the RN-DN channel experience the same type of fading, since we have identical channel conditions in both hops. For the sake of simplicity, our node-selection scheme is highlighted in the next subsection by ignoring this assumption.

5.4.2 Node-Activation When $d_{SR} = d_{RD}$

Our goal is to activate that particular transmitter, which minimizes the expected end-to-end Packet-Energy-Consumption (PEC) based on the knowledge of the instantaneous SNR. Since we have only three channels in the system, their PEC is discussed one by one below.

1) When the SN-DN channel is activated, the end-to-end PEC ($\mathcal{E}_{SD}$) is given by (5.1).

2) When the SN-RN channel is activated, the total PEC of the SN-RN-DN route becomes the sum of the PEC in each hop. However, the PEC of the SN-RN hop ($\mathcal{E}_{SR}$) and that of the RN-DN hop ($\mathcal{E}_{RD}$) take place in two different Time Slots (TSs). Although $\mathcal{E}_{SR}$ may be known based on the current channel condition, $\mathcal{E}_{RD}$ of the RN-DN hop remains unknown in the current TS. Therefore, we use the expected PEC $\bar{\mathcal{E}}_{RD}$ for estimating $\mathcal{E}_{RD}$. Hence, when the SN-RN channel is activate in TS t, the expected end-to-end PEC becomes:

$$\mathcal{E}_{SR-\overline{RD}} = \frac{\gamma_{T_h}}{\gamma_{SR}} \frac{d_{SR}^{\alpha} N}{\kappa} + \bar{\mathcal{E}}_{RD}. \tag{5.2}$$

3) When the RN-DN channel is activated in TS t, the expected end-to-end PEC is:

$$\mathcal{E}_{\overline{SR}-RD} = \bar{\mathcal{E}}_{SR} + \frac{\gamma_{T_h}}{\gamma_{RD}} \frac{d_{RD}^{\alpha} N}{\kappa}. \tag{5.3}$$

Finally, in each TS, the system activates that particular channel, which minimises the expected end-to-end PEC, as formulated in:

$$\mathcal{E} = \min\{\mathcal{E}_{SD}, \mathcal{E}_{SR-\bar{RD}}, \mathcal{E}_{\bar{SR}-RD}\}. \tag{5.4}$$

5.4.3 Node-Activation When $d_{SR} \neq d_{RD}$

The previous subsection discussed both the node-activation and the PEC associated with $d_{SR} = d_{RD}$, albeit in practice the RN is rarely expected in the middle. In the realistic scenario of $d_{SR} \neq d_{RD}$ the node-activation regime has to be modified, which implies that the PEC is increased. Our objective is to **minimize the expected end-to-end PEC**. As a first step, we formulate the concept of Transmission Activation Probability Space (TAPS) in the next section.

5.5 Principles of Channel Activation Probability Space

In this section, the concept of TAPS is proposed[1]. As seen from Fig. 5.2, the TAPS is divided into 8 subspaces based on the reception thresholds of the three channels. The following discussion will consider each of them.

Again, a three-node network is considered, where a packet can be transmitted from SN to DN both directly or indirectly via the RN. Based on Fig. 5.1 and on the operational principles described in Section 5.2.3, we can now infer that if the RN has a buffer of size of B packets, the following events may occur. 1) Firstly, the buffer of a RN may be empty at some instants. In this case, this RN cannot be the transmit node, since it has no data to transmit. 2) Secondly, the buffer of a RN may be full at some instants. Then, this RN cannot be the receive node, since it cannot accept further packets. In these cases, the system has to choose a hop for transmission from a reduced set of hops, which results in an increased energy consumption and outage probability. Therefore, our performance bounds are derived by relaxing the above-mentioned constraints, namely by assuming that the RN has an unlimited buffer size and that a node always has packets to transmit, which are discussed in Sections 5.5 - 5.7. However, even with unlimited buffer size, the system should be operated in its steady state. The average number of input and output packets should be the same at the RN, which implies that that the SN-RN channel and the RN-DN channel should have the same probability of being activated, when the system is in its steady state. If we have $d_{SR} = d_{RD}$, this constraint is automatically satisfied. However, we consider a more realistic TAPS division for dealing with the scenario of $d_{SR} \neq d_{RD}$.

Assuming that there is a three-dimensional space $\mathbb{S}$, a specific point associated with the coordinates $(\gamma_{SD}\ \gamma_{SR}\ \gamma_{RD})$ in $\mathbb{S}$ represents the corresponding instantaneous channel conditions of the system, hence $\mathbb{S}$ represents the TAPS of the system. The outage SNR-threshold associated with each coordinate γ_{SD}^{out}, γ_{SR}^{out} and γ_{RD}^{out} dissects

[1]In order to elaborate further, the appendix in this chapter states the basic principle of TAPS in details.

each coordinate into two segments, hence $\mathbb{S}$ is decomposed into $2^3 = 8$ subspaces. Fig. 5.2 shows the resultant TAPS. A system outage occurs, when we have instan-

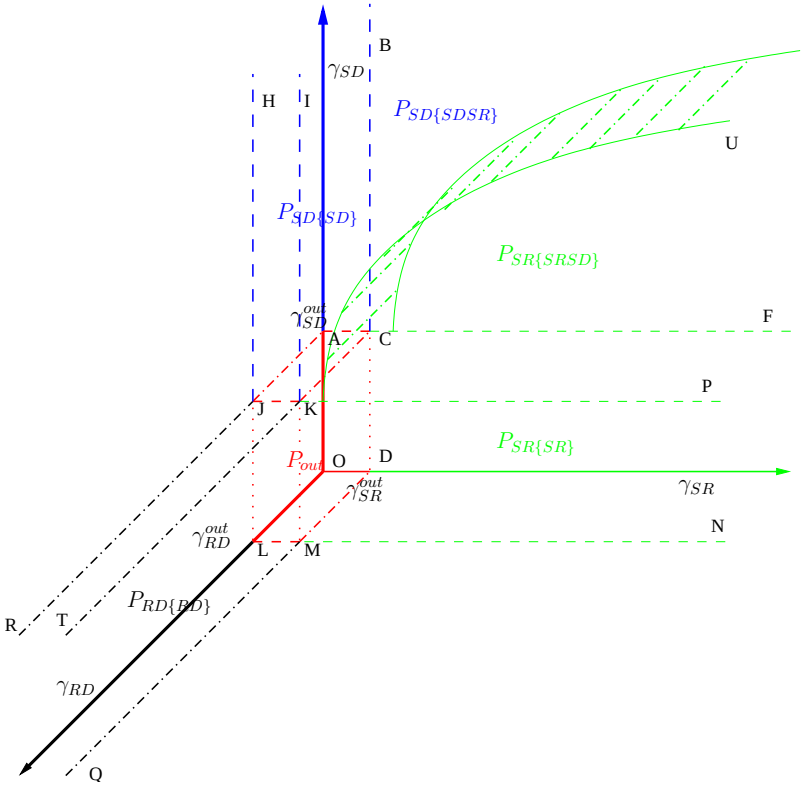

Figure 5.2: The Transmission Activation Probability Space (TAPS) is divided by the outage SNR-thresholds into 8 regions. P_{out} is the outage probability of the system, while $P_{SR\{SR\}}$, $P_{RD\{RD\}}$ and $P_{SD\{SD\}}$ represent the probability that only the SN-RN, the RN-DN or the SN-DN channel is available, respectively.

taneous $\gamma_{SR} < \gamma_{SR}^{out}$, $\gamma_{RD} < \gamma_{RD}^{out}$ and $\gamma_{SD} < \gamma_{SD}^{out}$. The outage probability is denoted by P_{out} (which is represented by the cube defined by the points ACDOLMKJ in Fig. 5.2), yielding

$$P_{out} = (1 - e^{-\gamma_{SR}^{out}})(1 - e^{-\gamma_{RD}^{out}})(1 - e^{-\gamma_{SD}^{out}}). \tag{5.5}$$

Let P_{SR}, P_{RD} and P_{SD} represent the probability that the corresponding channel is selected. Naturally, we expect $P_{SR} + P_{RD} + P_{SD} + P_{out} = 1$. Let us introduce a subscript $\{\bullet\}$ in curly blackets, which represents that the instantaneous SNR of the set of channels is higher than the corresponding outage threshold. For example, $P_{SR\{SR\ RD\}}$ represents the probability of the SR channel being activated, when we have $\gamma_{SR} \geq \gamma_{SR}^{out}$, $\gamma_{RD} \geq \gamma_{RD}^{out}$ and $\gamma_{SD} < \gamma_{SD}^{out}$. Naturally, we have $P_{SR} = P_{SR\{SR\}} + P_{SR\{SR\ RD\}} + P_{SR\{SR\ SD\}} + P_{SR\{SR\ RD\ SD\}}$ and the same properties are valid for P_{RD} and P_{SD}[2]. If there is only a single instantaneous CQ above the corresponding outage

[2]Later, the same properties are valid for E_{SD}, E_{SR} and E_{RD}.

threshold, the system will activate that particular channel. For example, $P_{SR\{SR\}}$ is the probability represented by the prism defined by the points KCDMNXFP in Fig. 5.2. The corresponding probabilities are

$$\begin{aligned} P_{SR\{SR\}} =& P(\gamma_{SR} \geq \gamma_{SR}^{out}) P(\gamma_{RD} < \gamma_{RD}^{out}) P(\gamma_{SD} < \gamma_{SD}^{out}) \\ =& e^{-\gamma_{SR}^{out}} (1 - e^{-\gamma_{RD}^{out}})(1 - e^{-\gamma_{SD}^{out}}), \end{aligned} \tag{5.6}$$

Similarly, we have

$$P_{RD\{RD\}} = (1 - e^{-\gamma_{SR}^{out}}) e^{-\gamma_{RD}^{out}} (1 - e^{-\gamma_{SD}^{out}}), \tag{5.7}$$

$$P_{SD\{SD\}} = (1 - e^{-\gamma_{SR}^{out}})(1 - e^{-\gamma_{RD}^{out}}) e^{-\gamma_{SD}^{out}}. \tag{5.8}$$

Having introduced the concept of TAPS and the calculation of the probabilities of P_{out}, $P_{SR\{SR\}}$, $P_{RD\{RD\}}$ and $P_{SD\{SD\}}$, more complicated scenarios, such as $P_{SR\{SR\ SD\}}$ are discussed in the next section.

5.6 Partitioning the Transmission Activation Probability Space

In this section, we commence by introducing the energy efficiency factor E_{ffe} and then the probabilities $P_{SR\{SR\ SD\}}$ as well as $P_{SD\{SR\ SD\}}$ represented by the prism defined by the points BCFPKI in Fig. 5.2 are explored. The associated activation process can be applied under diverse channel selection scenarios represented by this system model.

5.6.1 The Energy Efficiency Factor E_{ffe}

The channel selection associated with the region BCFPKI of Fig. 5.2 is further restricted by the specific conditions of $\gamma_{SR} \geq \gamma_{SR}^{out}$, $\gamma_{RD} < \gamma_{RD}^{out}$ and $\gamma_{SD} \geq \gamma_{SD}^{out}$. Explicitly, since we have $\gamma_{RD} < \gamma_{RD}^{out}$, let us find the activation boundary between the region of activating the SR or SD links in the region BCFPKI. As shown in Fig. 5.2, let us only discuss the projection to the surface XOY, which is shown as Fig. 5.3. The line OCE' of this surface in Fig. 5.3 represents the scenario, where the SR and SD channels have the same received SNR.

In order to deal with the problem of $P_{SR} > P_{RD}$, some of the regions that used to correspond to the activation of the SR hop have to be reassigned, either to the RD hop or to the SD hop. However, this adjustment imposes extra energy consumption.

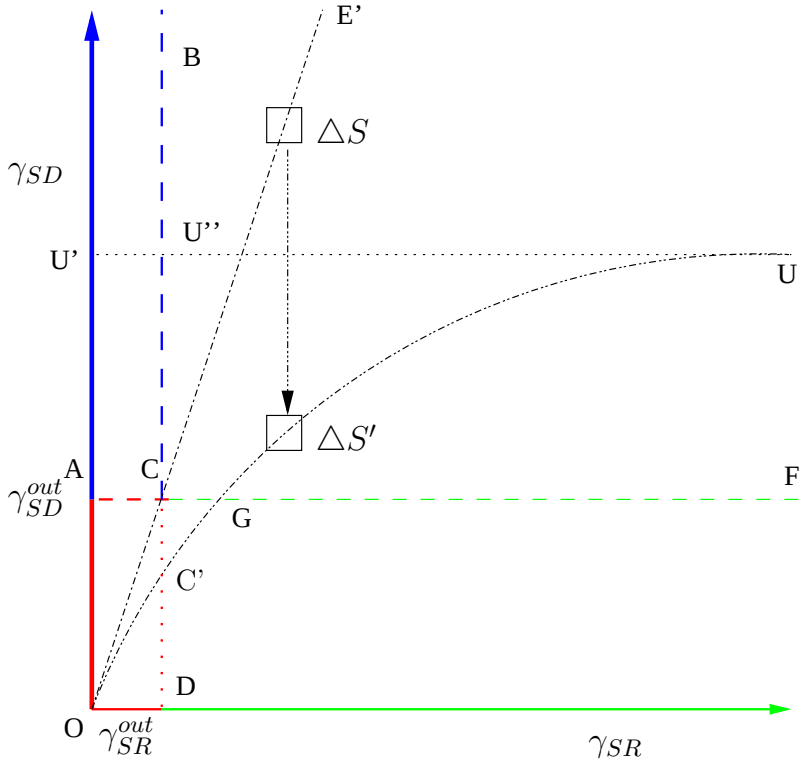

Figure 5.3: A plane in TAPS which shows that the channel selection is only between SN-RN hop and SN-DN hop.

Hence, the activation regions are carefully reassigned based on the associated energy efficiency factor E_{ffe}, which is defined as the extra energy consumption divided by the reassignment probability. This process is detailed below.

Let us denote the probability of encountering a small region ΔS on the surface OCE of Fig. 5.3 by $p_{\Delta S}$. The coordinates of ΔS are $(\gamma_{\Delta S_{SR}}, \gamma_{\Delta S_{SD}})$. When the region ΔS belongs to the SR hop and the SR hop is activated, then the expected end-to-end energy dissipated upon encountering the region ΔS is calculated from (5.2), yielding

$$\mathcal{E}_{\Delta S \in SR} = p_{\Delta S}\left(\frac{\gamma_{T_h} d_{SR}^{\alpha} N}{\gamma_{\Delta S_{SR}} \kappa} + \bar{\mathcal{E}}_{\mathcal{RD}}\right). \tag{5.9}$$

By contrast, when the region ΔS belongs to the SD hop and the SD hop is activated, the expected end-to-end energy dissipated upon encountering the region ΔS is calculated from (5.1), yielding

$$\mathcal{E}_{\Delta S \in SD} = p_{\Delta S}\left(\frac{\gamma_{T_h} d_{SD}^{\alpha} N}{\gamma_{\Delta S_{SD}} \kappa}\right). \tag{5.10}$$

If the region ΔS is reassigned from the SR hop to the SD hop, the extra energy consumption becomes

$$\Delta\mathcal{E}_{\Delta S} = p_{\Delta S}\left(\frac{\gamma_{T_h} d_{SD}^{\alpha} N}{\gamma_{\Delta S_{SD}}\kappa} - \frac{\gamma_{T_h} d_{SR}^{\alpha} N}{\gamma_{\Delta S_{SR}}\kappa} - \bar{\mathcal{E}}_{\mathcal{RD}}\right). \tag{5.11}$$

Hence, if we know the probability $p_{\Delta S}$ of encountering the region ΔS of Fig. 5.3, E_{ffe} is defined as

$$E_{ffe} = \frac{\gamma_{T_h} d_{SD}^{\alpha} N}{\gamma_{\Delta S_{SD}}\kappa} - \frac{\gamma_{T_h} d_{SR}^{\alpha} N}{\gamma_{\Delta S_{SR}}\kappa} - \bar{\mathcal{E}}_{\mathcal{RD}}. \tag{5.12}$$

The specific value of E_{ffe} may then be determined from the equations, whilst a practical algorithm will be provided for solving these equations in Section 5.7. In the remainder of this section, E_{ffe} is considered to be a known parameter.

5.6.2 Definition of $P_{SR\{SR\ SD\}}$ and $P_{SD\{SR\ SD\}}$

Having introduced E_{ffe}, this subsection explores the boundary of two activation regions, which was formulated in (5.12). Explicitly, the boundary is expressed with the aid of $\gamma_{SR\{SR\ SD\}}$ and $\gamma_{SD\{SR\ SD\}}$ instead of $\gamma_{\Delta S_{SR}}$ and $\gamma_{\Delta S_{SD}}$. Given E_{ffe} in (5.12), the relationship between $\gamma_{SR\{SR\ SD\}}$ and $\gamma_{SD\{SR\ SD\}}$ is shown below

$$\gamma_{SD\{SR\ SD\}} = f_{\{SR->SD\}}(\gamma_{SR\{SR\ SD\}}) \tag{5.13}$$

$$= \frac{\gamma_{T_h} d_{SD}^{\alpha}\kappa}{E_{ffe}\kappa + \bar{\mathcal{E}}_{RD}\kappa + \frac{\gamma_{T_h} d_{SR}^{\alpha} N}{\gamma_{SR\{SR\ SD\}}}}, \tag{5.14}$$

where the domain of definition for $\gamma_{SD\{SR\ SD\}}$ is $(\gamma_{SD}^{out}, \infty)$[3] (CB in Fig. 5.3), and hence that for $\gamma_{SR\{SR\ SD\}}$ is $(\gamma_{SR\{SR\ SD\}}^{min}, \gamma_{SR\{SR\ SD\}}^{max})$ (GF in Fig. 5.3), yielding

$$\gamma_{SR\{SR\ SD\}}^{min} = \max\{\gamma_{SR}^{out}, f_{\{SR->SD\}}^{-1}(\gamma_{SD}^{out})\} \tag{5.15}$$

$$\gamma_{SR\{SR\ SD\}}^{max} = f_{\{SR->SD\}}^{-1}(\infty). \tag{5.16}$$

If $f_{\{SR->SD\}}^{-1}(\infty)$ has no positive solution[4], we have $\gamma_{SD\{SR\ SD\}}^{max} = \infty$. A specific example of $E_{ffe} > 0$ is shown in Fig. 5.3, where γ_{SR}^{out} is at point C and $f_{\{SR->SD\}}^{-1}(\gamma_{SD}^{out})$ is at point G. Hence $\gamma_{SR\{SR\ SD\}}^{min}$ is at point G, while $f_{\{SR->SD\}}^{-1}(\infty)$ has no solution, therefore, we have $\gamma_{SD\{SR\ SD\}}^{max} = \infty$. Finally, the boundary for this example between activating the two hops is the curve GU.

[3]When we have $\gamma_{SD} > \gamma_{SD}^{out}$, the SD channel has a certain probability to be selected and we want to find this probability. On the other hand, if a channel has an infinite SNR, this channel will be definitely selected. It is plausible that the domain of definition of this input value is $(\gamma_{SD}^{out}, \infty)$.

[4]This principle is suitable for all functions $f_{\{\bullet\}}^{-1}(\infty)$, regardless of the sign of E_{ffe}.

Assuming that we have $\mathcal{F}_1(\gamma_{SR\{\bullet\}}) = 1$, $\mathcal{F}_2(\gamma_{SR\{\bullet\}}) = \frac{\gamma_{T_h} N}{\kappa} \frac{d_{SR}^{\alpha}}{\gamma_{SR\{\bullet\}}}$ and $\mathcal{F}_3(\gamma_{SR\{\bullet\}}) = \log_2(1 + \gamma_{SR}\gamma_{h_{SR}})$, the resultant activation probability $P_{SR\{SR\ SD\}}$, the energy consumption $\bar{\mathcal{E}}_{SR\{SR\ SD\}}$ and the capacity $C_{SR\{SR\ SD\}}$ of the SR link (region FGU in Fig. 5.3) with the domain BCFPKI of Fig. 5.2 may be formulated as:

$$P_{SR\{SR\ SD\}} = (1 - e^{-\gamma_{RD}^{out}}) \int_{\gamma_{SR\{SR\ SD\}}^{min}}^{\gamma_{SR\{SR\ SD\}}^{max}} \mathcal{F}_1(\gamma_{SR\{SR\ SD\}}) e^{-\gamma_{SR\{SR\ SD\}}} \times \int_{\gamma_{SD}^{out}}^{f_{\{SR->SD\}}(\gamma_{SR\{SR\ SD\}})} e^{-\gamma_{SD\{SR\ SD\}}} d\gamma_{SD\{SR\ SD\}} d\gamma_{SR\{SR\ SD\}}, \quad (5.17)$$

$$\bar{\mathcal{E}}_{SR\{SR\ SD\}} = (1 - e^{-\gamma_{RD}^{out}}) \int_{\gamma_{SR\{SR\ SD\}}^{min}}^{\gamma_{SR\{SR\ SD\}}^{max}} \mathcal{F}_2(\gamma_{SR\{SR\ SD\}}) e^{-\gamma_{SR\{SR\ SD\}}} \times \int_{\gamma_{SD}^{out}}^{f_{\{SR->SD\}}(\gamma_{SR\{SR\ SD\}})} e^{-\gamma_{SD\{SR\ SD\}}} d\gamma_{SD\{SR\ SD\}} d\gamma_{SR\{SR\ SD\}}, \quad (5.18)$$

$$C_{SR\{SR\ SD\}} = (1 - e^{-\gamma_{RD}^{out}}) \int_{\gamma_{SR\{SR\ SD\}}^{min}}^{\gamma_{SR\{SR\ SD\}}^{max}} \mathcal{F}_3(\gamma_{SR\{SR\ SD\}}) e^{-\gamma_{SR\{SR\ SD\}}} \times \int_{\gamma_{SD}^{out}}^{f_{\{SR->SD\}}(\gamma_{SR\{SR\ SD\}})} e^{-\gamma_{SD\{SR\ SD\}}} d\gamma_{SD\{SR\ SD\}} d\gamma_{SR\{SR\ SD\}}. \quad (5.19)$$

In the remainder of this treatise only the activation probability of the links is formulated explicitly, which may be readily extended to the energy consumption and capacity formulas[5].

To elaborate a little further, the relationship between $\gamma_{SR\{SR\ SD\}}$ and $\gamma_{SD\{SR\ SD\}}$ is also based on (5.12), which may be written as

$$\gamma_{SR\{SR\ SD\}} = f_{\{SD->SR\}}(\gamma_{SD\{SR\ SD\}}) \quad (5.20)$$

$$= \frac{\gamma_{T_h} d_{SR}^{\alpha} \kappa}{-E_{ffe}\kappa - \bar{\mathcal{E}}_{RD}\kappa + \frac{\gamma_{T_h} d_{SD}^{\alpha} N}{\gamma_{SD\{SR\ SD\}}}}. \quad (5.21)$$

[5]Note that, some integrals derived in this chapter cannot be expressed in closed-form. However, all formulas can be simplified to a single integral. The infinite value of the channel SNR may be considered as a large finite value, such as say 10. Therefore, a finite single integral can be efficiently evaluated by commercial software, such as MATLAB®, Maple® and Mathematica®.

The domain of definition for $\gamma_{SD\{SR\ SD\}}$ is $(\gamma^{min}_{SD\{SR\ SD\}}, \gamma^{max}_{SD\{SR\ SD\}})$[6], yielding

$$\gamma^{min}_{SD\{SR\ SD\}} = \max\{\gamma^{out}_{SD}, f^{-1}_{\{SD->SR\}}(\gamma^{out}_{SR})\} \tag{5.22}$$

$$\gamma^{max}_{SD\{SR\ SD\}} = f^{-1}_{\{SD->SR\}}(\infty) = \frac{\gamma_{T_h} d^{\alpha}_{SD} N}{E_{ffe}\kappa + \bar{\mathcal{E}}_{RD}\kappa}, \tag{5.23}$$

where $\gamma^{max}_{SD\{SR\ SD\}}$ is less than infinity. For example, in Fig. 5.3, $\gamma^{max}_{SD\{SR\ SD\}}$ is represented by the U' point. The region above the U' point (i.e. that region $UU''B$) belongs to the SD hop. The activation probability $P_{SD\{SR\ SD\}}$ of the SD link associated with $\gamma_{SD\{SR\ SD\}}$. $P_{SD\{SR\ SD\}}$ is expressed as:

$$\begin{aligned} P_{SD\{SR\ SD\}} =& (1 - e^{-\gamma^{out}_{RD}}) \int_{\gamma^{min}_{SD\{SR\ SD\}}}^{\gamma^{max}_{SD\{SR\ SD\}}} \mathcal{F}_1(\gamma_{SD\{SR\ SD\}}) e^{-\gamma_{SD\{SR\ SD\}}} \\ & \times \int_{\gamma^{out}_{SR}}^{f_{\{SD->SR\}}(\gamma_{SD\{SR\ SD\}})} e^{-\gamma_{SR\{SR\ SD\}}} d\gamma_{SR\{SR\ SD\}} d\gamma_{SD\{SR\ SD\}} \\ & + (1 - e^{-\gamma^{out}_{RD}}) e^{-\gamma^{out}_{SR}} \int_{\gamma^{max}_{SD\{SR\ SD\}}}^{\infty} \mathcal{F}_1(\gamma_{SD\{SR\ SD\}}) e^{-\gamma_{SD\{SR\ SD\}}} d\gamma_{SD\{SR\ SD\}}. \end{aligned} \tag{5.24}$$

5.6.3 Determining $P_{SD\{SD\ RD\}}$ and $P_{RD\{SD\ RD\}}$

By repeating the process described in the previous subsection, we may readily derive $P_{SD\{SD\ RD\}}$ and $P_{RD\{SD\ RD\}}$. The related formulas of $P_{SD\{SD\ RD\}}$ and $P_{RD\{SD\ RD\}}$ are similar to those of $P_{SD\{SD\ SR\}}$ and $P_{SR\{SD\ SR\}}$, which are derived by replacing RD by SR, yielding:

$$\gamma_{SD\{RD\ SD\}} = f_{\{RD->SD\}}(\gamma_{RD\{RD\ SD\}}) \tag{5.25}$$

$$= \frac{\gamma_{T_h} d^{\alpha}_{SD} \kappa}{-E_{ffe}\kappa + \bar{\mathcal{E}}_{SR}\kappa + \frac{\gamma_{T_h} d^{\alpha}_{RD} N}{\gamma_{RD\{RD\ SD\}}}}. \tag{5.26}$$

The domain of definition for $\gamma_{RD\{RD\ SD\}}$ is $(\gamma^{min}_{RD\{RD\ SD\}}, \gamma^{max}_{RD\{RD\ SD\}})$, yielding

$$\gamma^{min}_{RD\{RD\ SD\}} = \max\{\gamma^{out}_{RD}, f^{-1}_{\{RD->SD\}}(\gamma^{out}_{SD})\} \tag{5.27}$$

[6]The domain of γ_{SD} is $(\gamma^{out}_{SD}, \infty)$ which is CB in Fig. 5.2. However, it should be discussed into two cases. When channel SR competes with channel SD, the range of channel SD is $(\gamma^{min}_{SD\{SR\ SD\}}, \gamma^{max}_{SD\{SR\ SD\}})$, which is CU" in Fig. 5.2. While, the range of channel SD is $(\gamma^{max}_{SD\{SR\ SD\}}, \infty)$ when no channel competes with channel SD, which is represented by U"B in Fig. 5.2.

$$\gamma^{max}_{RD\{RD\ SD\}} = \begin{cases} \frac{\gamma_{T_h} d^{\alpha}_{RD} N}{E_{ffe}\kappa - \bar{\mathcal{E}}_{SR}\kappa}, & E_{ffe} > \bar{\mathcal{E}}_{SR} \\ \infty, & \text{otherwise.} \end{cases} \tag{5.28}$$

The activation probability $P_{RD\{RD\ SD\}}$ of the RD link associated with $\gamma_{RD\{RD\ SD\}}$. $P_{RD\{RD\ SD\}}$ is expressed as

$$\begin{aligned} P_{RD\{RD\ SD\}} =& (1 - e^{-\gamma^{out}_{SR}}) \int_{\gamma^{min}_{RD\{RD\ SD\}}}^{\gamma^{max}_{RD\{RD\ SD\}}} \mathcal{F}_1(\gamma_{RD\{RD\ SD\}}) e^{-\gamma_{RD\{RD\ SD\}}} \\ & \times \int_{\gamma^{out}_{SD}}^{f_{\{RD->SD\}}(\gamma_{RD\{RD\ SD\}})} e^{-\gamma_{SD\{RD\ SD\}}} d\gamma_{SD\{RD\ SD\}} d\gamma_{RD\{RD\ SD\}} \\ & + (1 - e^{-\gamma^{out}_{SR}}) e^{-\gamma^{out}_{SD}} \int_{\gamma^{max}_{RD\{RD\ SD\}}}^{\infty} \mathcal{F}_1(\gamma_{RD\{RD\ SD\}}) e^{-\gamma_{RD\{RD\ SD\}}} d\gamma_{RD\{RD\ SD\}}, \end{aligned} \tag{5.29}$$

where we have:

$$\gamma_{RD\{RD\ SD\}} = f_{\{SD->RD\}}(\gamma_{SD\{RD\ SD\}}) \tag{5.30}$$

$$= \frac{\gamma_{T_h} d^{\alpha}_{RD} \kappa}{E_{ffe}\kappa - \bar{\mathcal{E}}_{SR}\kappa + \frac{\gamma_{T_h} d^{\alpha}_{SD} N}{\gamma_{SD\{RD\ SD\}}}}. \tag{5.31}$$

The domain of definition for $\gamma_{SD\{RD\ SD\}}$ is $(\gamma^{min}_{SD\{RD\ SD\}}, \gamma^{max}_{SD\{RD\ SD\}})$, yielding

$$\gamma^{min}_{SD\{RD\ SD\}} = \max\{\gamma^{out}_{SD}, f^{-1}_{\{SD->RD\}}(\gamma^{out}_{RD})\} \tag{5.32}$$

$$\gamma^{max}_{SD\{RD\ SD\}} = \begin{cases} \frac{\gamma_{T_h} d^{\alpha}_{SD} N}{-E_{ffe}\kappa + \bar{\mathcal{E}}_{SR}\kappa}, & E_{ffe} < \bar{\mathcal{E}}_{SR} \\ \infty, & \text{otherwise.} \end{cases} \tag{5.33}$$

The activation probability $P_{SD\{RD\ SD\}}$ of the SD link associated with $\gamma_{SD\{RD\ SD\}}$, is formulated as:

$$\begin{aligned} P_{SD\{RD\ SD\}} =& (1 - e^{-\gamma^{out}_{SR}}) \int_{\gamma^{min}_{SD\{RD\ SD\}}}^{\gamma^{max}_{SD\{RD\ SD\}}} \mathcal{F}_1(\gamma_{SD\{RD\ SD\}}) e^{-\gamma_{SD\{RD\ SD\}}} \\ & \times \int_{\gamma^{out}_{RD}}^{f_{\{SD->RD\}}(\gamma_{SD\{RD\ SD\}})} e^{-\gamma_{RD\{RD\ SD\}}} d\gamma_{RD\{RD\ SD\}} d\gamma_{SD\{RD\ SD\}} \\ & + (1 - e^{-\gamma^{out}_{SR}}) e^{-\gamma^{out}_{RD}} \int_{\gamma^{max}_{SD\{RD\ SD\}}}^{\infty} \mathcal{F}_1(\gamma_{SD\{RD\ SD\}}) e^{-\gamma_{SD\{RD\ SD\}}} d\gamma_{SD\{RD\ SD\}}. \end{aligned} \tag{5.34}$$

5.6.4 Deriving $P_{SR\{SR\ RD\}}$ and $P_{RD\{SR\ RD\}}$

Again, the process is the same as before. Note that value of the E_{ffe} is doubled, when changing the region from SR to RD, provided that we have $P_{SR\{SR\ RD\}} > P_{RD\{SR\ RD\}}$, because the assumption without loss of generality in that we have $d_{SR} < d_{RD}$. This yields:

$$\gamma_{SR\{RD\ SR\}} = f_{\{RD->SR\}}(\gamma_{RD\{RD\ SR\}}) \tag{5.35}$$

$$= \frac{\gamma_{T_h} d_{SR}^{\alpha} \kappa}{-2E_{ffe}\kappa + (\bar{\mathcal{E}}_{SR} - \bar{\mathcal{E}}_{RD})\kappa + \frac{\gamma_{T_h} d_{RD}^{\alpha} N}{\gamma_{RD\{RD\ SR\}}}}. \tag{5.36}$$

The domain of definition for $\gamma_{RD\{RD\ SR\}}$ is $(\gamma_{RD\{RD\ SR\}}^{min}, \gamma_{RD\{RD\ SR\}}^{max})$, yielding

$$\gamma_{RD\{RD\ SR\}}^{min} = \max\{\gamma_{RD}^{out}, f_{\{RD->SR\}}^{-1}(\gamma_{SR}^{out})\} \tag{5.37}$$

$$\gamma_{RD\{RD\ SR\}}^{max} = \begin{cases} \frac{\gamma_{T_h} d_{RD}^{\alpha} N}{2E_{ffe}\kappa - (\bar{\mathcal{E}}_{SR} - \bar{\mathcal{E}}_{RD})\kappa}, & 2E_{ffe} > (\bar{\mathcal{E}}_{SR} - \bar{\mathcal{E}}_{RD}) \\ \infty, & \text{otherwise.} \end{cases} \tag{5.38}$$

The activation probability $P_{RD\{RD\ SR\}}$ of the RD link associated with $\gamma_{RD\{RD\ SR\}}$ is formulated as:

$$\begin{aligned} P_{RD\{RD\ SR\}} =& (1 - e^{-\gamma_{SD}^{out}}) \int_{\gamma_{RD\{RD\ SR\}}^{min}}^{\gamma_{RD\{RD\ SR\}}^{max}} \mathcal{F}_1(\gamma_{RD\{RD\ SR\}}) e^{-\gamma_{RD\{RD\ SR\}}} \\ & \times \int_{\gamma_{SR}^{out}}^{f_{\{RD->SR\}}(\gamma_{RD\{RD\ SR\}})} e^{-\gamma_{SR\{RD\ SR\}}} d\gamma_{SR\{RD\ SR\}} d\gamma_{RD\{RD\ SR\}} \\ & + (1 - e^{-\gamma_{SD}^{out}}) e^{-\gamma_{SR}^{out}} \int_{\gamma_{RD\{RD\ SR\}}^{max}}^{\infty} \mathcal{F}_1(\gamma_{RD\{RD\ SR\}}) e^{-\gamma_{RD\{RD\ SR\}}} d\gamma_{RD\{RD\ SR\}}, \end{aligned} \tag{5.39}$$

where

$$\gamma_{RD\{RD\ SR\}} = f_{\{SR->RD\}}(\gamma_{SR\{RD\ SR\}}) \tag{5.40}$$

$$= \frac{\gamma_{T_h} d_{RD}^{\alpha} \kappa}{2E_{ffe}\kappa + (\bar{\mathcal{E}}_{RD} - \bar{\mathcal{E}}_{SR})\kappa + \frac{\gamma_{T_h} d_{SD}^{\alpha} N}{\gamma_{SR\{RD\ SR\}}}}. \tag{5.41}$$

The domain of definition for $\gamma_{SR\{RD\ SR\}}$ is $(\gamma^{min}_{SR\{RD\ SR\}}, \gamma^{max}_{SR\{RD\ SR\}})$, yielding

$$\gamma^{min}_{SR\{RD\ SR\}} = \max\{\gamma^{out}_{SR}, f^{-1}_{\{SR->RD\}}(\gamma^{out}_{RD})\} \tag{5.42}$$

$$\gamma^{max}_{SR\{RD\ SR\}} = \begin{cases} \frac{\gamma_{T_h} d^{\alpha}_{RD} N}{-2E_{ffe}\kappa + (\bar{\mathcal{E}}_{SR} - \bar{\mathcal{E}}_{RD})\kappa}, & 2E_{ffe} < (\bar{\mathcal{E}}_{SR} - \bar{\mathcal{E}}_{RD}) \\ \infty, & \text{otherwise.} \end{cases} \tag{5.43}$$

The activation probability $P_{RD\{RD\ SR\}}$ of the RD link associated with $\gamma_{RD\{RD\ SR\}}$ is given by:

$$\begin{aligned} P_{RD\{RD\ SR\}} =& (1 - e^{-\gamma^{out}_{SD}}) \int_{\gamma^{min}_{SR\{RD\ SR\}}}^{\gamma^{max}_{SR\{RD\ SR\}}} \mathcal{F}_1(\gamma_{SR\{RD\ SR\}}) e^{-\gamma_{SR\{RD\ SR\}}} \\ & \times \int_{\gamma^{out}_{RD}}^{f_{\{SR->RD\}}(\gamma_{SR\{RD\ SR\}})} e^{-\gamma_{RD\{RD\ SR\}}} d\gamma_{RD\{RD\ SR\}} d\gamma_{SR\{RD\ SR\}} \\ & + (1 - e^{-\gamma^{out}_{SD}}) e^{-\gamma^{out}_{RD}} \int_{\gamma^{max}_{SR\{RD\ SR\}}}^{\infty} \mathcal{F}_1(\gamma_{SR\{RD\ SR\}}) e^{-\gamma_{SR\{RD\ SR\}}} d\gamma_{SR\{RD\ SR\}}. \end{aligned} \tag{5.44}$$

5.6.5 Deriving $P_{SD\{SD\ SR\ RD\}}$, $P_{SR\{SD\ SR\ RD\}}$ and $P_{RD\{SD\ SR\ RD\}}$

The activation decisions of three channels are more complex than those of two channels, where the latter is associated with the region PKTI of Fig. 5.2. The calculation of the three-channel system's activation probability relies on our previous results, such as the previous γ^{max} and γ^{min} results. Based on the specific parameters of $(E_{ffe}, \bar{\mathcal{E}}_{SR}, \bar{\mathcal{E}}_{RD})$, it can be decided whether $\gamma^{max}_{SR\{SR\ RD\}}$ or $\gamma^{max}_{SR\{SR\ SD\}}$ is higher. Let us assume that we have $\gamma^{max}_{SR\{SR\ RD\}} < \gamma^{max}_{SR\{SR\ SD\}}$. Hence the activation probability

of the SR hop is formulated as:

$$
\begin{aligned}
& P_{SR\{SR\ SD\ RD\}} \\
= & \int_{\max\{\gamma_{SR}^{out},\gamma_{SR\{SR\ RD\}}^{min},\gamma_{SR\{SR\ SD\}}^{min}\}}^{\max\{\gamma_{SR\{SR\ RD\}}^{max},\gamma_{SR\{SR\ RD\}}^{min},\gamma_{SR\{SR\ SD\}}^{min}\}} \mathcal{F}_1(\gamma_{SD\{SR\ SD\ RD\}}) e^{-\gamma_{SR\{SR\ SD\ RD\}}} \\
& \times \int_{\gamma_{RD}^{out}}^{f_{\{SR->RD\}}(\gamma_{SR\{SR\ SD\ RD\}})} e^{-\gamma_{RD\{SR\ SD\ RD\}}} \\
& \times \int_{\gamma_{SD}^{out}}^{f_{\{SR->SD\}}(\gamma_{SR\{SR\ SD\ RD\}})} e^{-\gamma_{SD\{SR\ SD\ RD\}}} \\
& \times d\gamma_{SD\{SR\ SD\ RD\}} d\gamma_{RD\{SR\ SD\ RD\}} d\gamma_{SR\{SR\ SD\ RD\}} \\
& + e^{-\gamma_{RD}^{out}} \int_{\max\{\gamma_{SR}^{out},\gamma_{SR\{SR\ SD\}}^{min},\gamma_{SR\{SR\ SD\}}^{min}\}}^{\max\{\gamma_{SR}^{out},\gamma_{SR\{SR\ RD\}}^{max}\}} \mathcal{F}_1(\gamma_{SD\{SR\ SD\ RD\}}) e^{-\gamma_{SR\{SR\ SD\ RD\}}} \\
& \times \int_{\gamma_{SD}^{out}}^{f_{\{SR->SD\}}(\gamma_{SR\{SR\ SD\ RD\}})} e^{-\gamma_{SD\{SR\ SD\ RD\}}} \\
& \times d\gamma_{SD\{SR\ SD\ RD\}} d\gamma_{SR\{SR\ SD\ RD\}} \\
& + e^{-\gamma_{RD}^{out}} e^{-\gamma_{SD}^{out}} \int_{\max\{\gamma_{SR}^{out},\gamma_{SR\{SR\ RD\}}^{max}\}}^{\infty} \mathcal{F}_1(\gamma_{SD\{SR\ SD\ RD\}}) e^{-\gamma_{SR\{SR\ SD\ RD\}}} \\
& d\gamma_{SR\{SR\ SD\ RD\}}. \qquad (5.45)
\end{aligned}
$$

The relevant formulas may also be readily derived for $\gamma_{SR\{SR\ RD\}}^{max} > \gamma_{SR\{SR\ SD\}}^{max}$. Based on the same process, we may formulate the equations of $P_{RD\{SR\ SD\ RD\}}$ and

$P_{SD\{SR\ SD\ RD\}}$, yielding:

$$
\begin{aligned}
&P_{RD\{SR\ SD\ RD\}} \\
&= \int_{\max\{\gamma_{RD}^{out},\gamma_{RD\{SR\ SD\}}^{max},\gamma_{RD\{RD\ SD\}}^{min}\}}^{\max\{\gamma_{RD}^{out},\gamma_{RD\{SR\ RD\}}^{min},\gamma_{RD\{RD\ SD\}}^{min}\}} \mathcal{F}_1(\gamma_{RD\{SR\ SD\ RD\}}) e^{-\gamma_{RD\{SR\ SD\ RD\}}} \\
&\quad \times \int_{\gamma_{SD}^{out}}^{f_{\{RD->SD\}}(\gamma_{RD\{SR\ SD\ RD\}})} e^{-\gamma_{SD\{SR\ SD\ RD\}}} \\
&\quad \times \int_{\gamma_{SR}^{out}}^{f_{\{RD->SR\}}(\gamma_{RD\{SR\ SD\ RD\}})} e^{-\gamma_{SR\{SR\ SD\ RD\}}} \\
&\quad \times d\gamma_{SR\{SR\ SD\ RD\}} d\gamma_{SD\{SR\ SD\ RD\}} d\gamma_{RD\{SR\ SD\ RD\}} \\
&\quad + e^{-\gamma_{SR}^{out}} \int_{\max\{\gamma_{RD}^{out},\gamma_{RD\{SR\ RD\}}^{max},\gamma_{RD\{SD\ RD\}}^{min}\}}^{\max\{\gamma_{RD}^{out},\gamma_{RD\{SR\ SD\}}^{max},\gamma_{RD\{RD\ SD\}}^{min}\}} \mathcal{F}_1(\gamma_{RD\{SR\ SD\ RD\}}) e^{-\gamma_{RD\{SR\ SD\ RD\}}} \\
&\quad \times \int_{\gamma_{SD}^{out}}^{f_{\{RD->SD\}}(\gamma_{RD\{SR\ SD\ RD\}})} e^{-\gamma_{SD\{SR\ SD\ RD\}}} \\
&\quad \times d\gamma_{SD\{SR\ SD\ RD\}} d\gamma_{RD\{SR\ SD\ RD\}} \\
&\quad + e^{-\gamma_{SD}^{out}} e^{-\gamma_{SR}^{out}} \int_{\max\{\gamma_{RD}^{out},\gamma_{RD\{SR\ RD\}}^{max},\gamma_{RD\{SD\ RD\}}^{max}\}}^{\infty} \mathcal{F}_1(\gamma_{RD\{SR\ SD\ RD\}}) e^{-\gamma_{RD\{SR\ SD\ RD\}}} \\
&\quad d\gamma_{RD\{SR\ SD\ RD\}}.
\end{aligned}
\tag{5.46}
$$

$$
\begin{aligned}
&P_{SD\{SR\ SD\ RD\}} \\
&= \int_{\max\{\gamma_{SD}^{out},\gamma_{SD\{SR\ SD\}}^{max},\gamma_{SD\{SD\ RD\}}^{min}\}}^{\max\{\gamma_{SD}^{out},\gamma_{SD\{SD\ RD\}}^{min},\gamma_{SD\{SD\ SR\}}^{min}\}} \mathcal{F}_1(\gamma_{SD\{SR\ SD\ RD\}}) e^{-\gamma_{SD\{SR\ SD\ RD\}}} \\
&\quad \times \int_{\gamma_{RD}^{out}}^{f_{\{SD->RD\}}(\gamma_{SD\{SR\ SD\ RD\}})} e^{-\gamma_{RD\{SR\ SD\ RD\}}} \\
&\quad \times \int_{\gamma_{SR}^{out}}^{f_{\{SD->SR\}}(\gamma_{SD\{SR\ SD\ RD\}})} e^{-\gamma_{SR\{SR\ SD\ RD\}}} \\
&\quad \times d\gamma_{SR\{SR\ SD\ RD\}} d\gamma_{RD\{SR\ SD\ RD\}} d\gamma_{SD\{SR\ SD\ RD\}} \\
&\quad + e^{-\gamma_{SR}^{out}} \int_{\max\{\gamma_{SD}^{out},\gamma_{SD\{SR\ SD\}}^{max},\gamma_{SD\{SD\ RD\}}^{min}\}}^{\max\{\gamma_{SD}^{out},\gamma_{SD\{SD\ RD\}}^{max}\}} \mathcal{F}_1(\gamma_{SD\{SR\ SD\ RD\}}) e^{-\gamma_{SD\{SR\ SD\ RD\}}} \\
&\quad \times \int_{\gamma_{RD}^{out}}^{f_{\{SD->RD\}}(\gamma_{SD\{SR\ SD\ RD\}})} e^{-\gamma_{RD\{SR\ SD\ RD\}}} \\
&\quad \times d\gamma_{RD\{SR\ SD\ RD\}} d\gamma_{SD\{SR\ SD\ RD\}} \\
&\quad + e^{-\gamma_{RD}^{out}} e^{-\gamma_{SR}^{out}} \int_{\max\{\gamma_{SD}^{out},\gamma_{SD\{SD\ RD\}}^{max}\}}^{\infty} \mathcal{F}_1(\gamma_{SD\{SR\ SD\ RD\}}) e^{-\gamma_{SD\{SR\ SD\ RD\}}} \\
&\quad d\gamma_{SD\{SR\ SD\ RD\}},
\end{aligned}
\tag{5.47}
$$

where we assumed that $\gamma^{max}_{SD\{SD\ SR\}} < \gamma^{max}_{SD\{SD\ RD\}}$.

5.7 Finding the Optimal E_{ffe}

In the previous sections, we had three unknowns: $\bar{\mathcal{E}}_{SR}$, $\bar{\mathcal{E}}_{SR}$ and E_{ffe}. Given all the instantaneous energy consumptions $\mathcal{E}_{\{\bullet\}}$ and all activation probabilities $P_{\bullet\{\bullet\}}$, the three unknowns can be obtained from the following three equations:

$$\begin{aligned}\bar{\mathcal{E}}_{SR} &= \frac{\mathcal{E}_{SR}}{P_{SR}} \\ &= \frac{\mathcal{E}_{SR\{SR\}} + \mathcal{E}_{SR\{SR\ SD\}} + \mathcal{E}_{SR\{SR\ RD\}} + \mathcal{E}_{SR\{SR\ SD\ RD\}}}{P_{SR\{SR\}} + P_{SR\{SR\ SD\}} + P_{SR\{SR\ RD\}} + P_{SR\{SR\ SD\ RD\}}} \end{aligned} \tag{5.48}$$

$$\begin{aligned}\bar{\mathcal{E}}_{RD} &= \frac{\mathcal{E}_{RD}}{P_{RD}} \\ &= \frac{\mathcal{E}_{RD\{RD\}} + \mathcal{E}_{RD\{SR\ SD\}} + \mathcal{E}_{RD\{RD\ SD\}} + \mathcal{E}_{RD\{SR\ SD\ RD\}}}{P_{RD\{RD\}} + P_{RD\{SR\ SD\}} + P_{RD\{RD\ SD\}} + P_{RD\{SR\ SD\ RD\}}} \end{aligned} \tag{5.49}$$

$$P_{SR} = P_{RD}. \tag{5.50}$$

However, it is not practical to directly solve these integral equations. Hence, we conceive a simple algorithm for finding the solution.

The basic principle is that of employing an exhaustive search for finding the optimal E_{ffe}. All energy consumptions and activation probabilities as well as (5.48) and (5.49) can be evaluated for a specific E_{ffe}. Therefore, we search for specific E_{ffe} values starting from zero and terminating when (5.50) is satisfied.

Algorithm 1 The algorithm of finding E_{ffe}.

$E_{ffe} = 0$;
Calculate all activation probabilities and energy consumptions;
Update $\bar{\mathcal{E}}_{SR}$ and $\bar{\mathcal{E}}_{RD}$ based on (5.48) and (5.49);
While $P_{SR} \neq P_{RD}$ Increase E_{effe};
Calculate all selection probabilities and energy consumptions;
Update $\bar{\mathcal{E}}_{SR}$ and $\bar{\mathcal{E}}_{RD}$ based on (5.48) and (5.49);

Finally, the theoretical end-to-end energy consumption is given by the ratio of the total energy consumption to the throughput, yielding

$$\bar{\mathcal{E}}_{SD} = \frac{\mathcal{E}_{SD} + \mathcal{E}_{SR} + \mathcal{E}_{RD}}{P_{SD} + P_{SR}}. \tag{5.51}$$

5.8 Probability Mass Function of Delay

The previous sections discussed our buffer-aided channel selection scheme, which reduces the end-to-end energy consumption. However, the cost of saving energy is that of having a higher end-to-end packet delay. In order to analyze the behaviour of the system, we have to study both the average packet delay and the distribution of packet delay. In this section, we first restate the concept of *State* defined in our previous papers [168, 184]. Then, a specific Markov State Transition Matrix (MSTM) is designed. Finally, an algorithm is provided for finding the Probability Mass Function (PMF) of the packet delay.

5.8.1 The Concept of State

The concept of State in buffer-aided systems was proposed in [168, 184]. Upon assuming that the buffer size of the RN is B packets, the state is defined as $S_b = b$, when b packets are stored in the RN. Therefore, the total number of states is $(B+1)$. Given $(B+1)$ states, a state transition matrix denoted by $\boldsymbol{T}$ can be populated by the state transition probabilities $\{\boldsymbol{T}_{i,j} = P(s(t+1) = S_j | s(t) = S_i),\ i, j = 0, 1, \ldots, B\}$. Let us now find the elements of the MSTM $\boldsymbol{T}$.

5.8.2 The Transition Matrix $\boldsymbol{T}$

Based on our discussions in Sections 5.6, the activation probability of each hop is known, when all three channels are available. However, the activation criterion is unknown, when the buffer is either empty or full at the RN. Since this activation criterion does not affect the energy consumption and outage prediction bound, the system will activate the specific channel having the highest instantaneous SNR amongst the available channels. For example, a state transition matrix associated with $B = 4$ is given below,

$$\boldsymbol{T} = \begin{bmatrix} 1 - P_{0,1} & P_{0,1} & 0 & 0 & 0 \\ P_{RD} & P_{SD} + P_{out} & P_{SR} & 0 & 0 \\ 0 & P_{RD} & P_{SD} + P_{out} & P_{SR} & 0 \\ 0 & 0 & P_{RD} & P_{SD} + P_{out} & P_{SR} \\ 0 & 0 & 0 & P_{B,B-1} & 1 - P_{B,B-1} \end{bmatrix}. \tag{5.52}$$

The probability $P_{0,1}$ is represented by the region XOCE in Fig. 5.3, yielding

$$P_{0,1} = \int_{\gamma_{SR}^{out}}^{\infty} e^{-\gamma_{SR}} \int_{0}^{\frac{\gamma_{SR} d_{SD}^{\alpha}}{d_{SR}^{\alpha}}} e^{-\gamma_{SD}} d\gamma_{SD} d\gamma_{SR} \tag{5.53}$$

and $P_{B,B-1}$ is given by

$$P_{B,B-1} = \int_{\gamma_{RD}^{out}}^{\infty} e^{-\gamma_{RD}} \int_{0}^{\frac{\gamma_{RD} d_{SD}^{\alpha}}{d_{RD}^{\alpha}}} e^{-\gamma_{SD}} d\gamma_{SD} d\gamma_{RD}. \tag{5.54}$$

If the SD hop is activated or a system outage occurs, the system's state remains unchanged. Having obtained the MSTM $\boldsymbol{T}$, the steady-state transition probabilities may be computed as follows [110]:

$$P_{\boldsymbol{\pi}} = \boldsymbol{T}^T P_{\boldsymbol{\pi}}, \tag{5.55}$$

where we have $P_{\boldsymbol{\pi}} = [P_{\pi_0}, P_{\pi_1}, \ldots, P_{\pi_B}]^T$ and P_{π_i} is the steady-state probability of the state S_i [110]. The steady-state probability of a state is the expected probability of this specific state of the system, where (5.55) shows that $P_{\boldsymbol{\pi}}$ is the right eigenvector of the matrix $\boldsymbol{T}^T$ corresponding to an eigenvalue of one. Therefore, $P_{\boldsymbol{\pi}}$ can be derived with the aid of classic methods conceived for solving the corresponding eigenvalue problem [182].

5.8.3 An Algorithm for Determining the PMF of Packet Delay

Having determined $P_{\boldsymbol{\pi}}$ and $\boldsymbol{T}$, let us now find the PMF of the delay. Let $P_d(t)$ represent the probability of a specific end-to-end packet delay of t TSs. The probability $P_d(1)$ of direct transmission from the SN to DN can be described mathematically, as discussed below.

If a packet is transmitted directly from the SN to DN, the delay of this packet is 1 TS. Then $P_d(1)$ is the ratio of the probability P_{1TS}^{suc} of the packet being successfully transmitted in 1 TS and of the probability of the packet being entered into the buffer-aided queuing system, yielding

$$\begin{aligned} P_{1TS}^{suc} =& P_{\pi_0}\left[1 - P_{0,1} - (1 - e^{-\gamma_{SR}})(1 - e^{-\gamma_{SD}})\right] + \sum_{i=1}^{B-1} P_{\pi_i} P_{SD} \\ &+ P_{\pi_B}\left[1 - P_{B,B-1} - (1 - e^{-\gamma_{RD}})(1 - e^{-\gamma_{SD}})\right], \end{aligned} \tag{5.56}$$

where $(1 - e^{-\gamma_{SR}})(1 - e^{-\gamma_{SD}})$ and $(1 - e^{-\gamma_{RD}})(1 - e^{-\gamma_{SD}})$ in the first and last terms represent the outage probability. Therefore, we have:

$$P_d(1) = \frac{P_{1TS}^{suc}}{P_{1TS}^{suc} + P_{\pi_0} P_{0,1} + \sum_{i=1}^{B-1} P_{\pi_i} P_{SR}}, \tag{5.57}$$

where $P_{\pi_0} P_{0,1} + \sum_{i=1}^{B-1} P_{\pi_i} P_{sr}$ is the probability of the packet entering the RN's buffer-aided queue.

Having determined $P_d(1)$, let us now find $P_d(i), i > 1$ by applying an algorithm similar to that proposed in [170]. We assumed that a so-called test packet is available at the SN when $t = 0$. Then we can find the probability $P_d(i), i = 2, 3, \ldots, \infty$ upon detecting that the test packet arrived at the DN, when we have $t = i\ TS$. For the details, please refer to [170].

With the aid of the PMF of the delay $P_d(t)$, which is the probability of the packet delay being t TSs, the average packet delay $\bar{\tau}$ may be then expressed as

$$\bar{\tau} = \sum_{d=1}^{\infty} P_d(t) \cdot t. \tag{5.58}$$

5.9 Performance Results

In this section, we provide a range of numerical and/or simulation results for characterizing the energy consumption, the OP and the delay of the B3NN considered, in order to illustrate the effects of both the position of the RN and of the buffer size B of the RN. In all experiments, the SN is at the position $(0, 0)$, while DN is at the position $(1000m, 0)$. Again, the parameters of N and κ are $N = 10^{-13}$ and $\kappa = 9.895 \times 10^{-05}$. The pathloss factor α and the maximum transmit power are $\alpha = 2$ and $P_{max} = 0.003$ Watt in Fig. 5.4 - Fig. 5.8. For convenience, "normalized energy consumption" refers to the "average normalized end-to-end energy consumption per packet", which is the optimization objective of this chapter.

The first set of results characterizes the impact of the RN's buffer size on the end-to-end normalized energy consumption and the OP. The results of Fig. 5.4 and Fig. 5.5 are plotted against the buffer size. In both figures, the RN is at the position $P1 : (400, 400)$ or $P2 : (500, 0)$, while the buffer size ranges from $B = 1$ to $B = 256$ packets. In Sections 5.4 - 5.7, we discussed the proposed nonlinear channel space division method, its parameters and the associated theoretical bound (dashed line). Given the principle encapsulated in (5.4), the analysis of our nonlinear channel space division method can be carried out. The simulation results and the corresponding theoretical results are represented by the solid line marked by a triangle or a cross. The theoretical results associated with a specific buffer size can be obtained by applying the principles detailed in [168] with $P_{\boldsymbol{\pi}}$ from (5.55). Observe in both Fig. 5.4 and Fig. 5.5 that the simulation based performance approaches the theoretical energy consumption bound, as the buffer size increases and that a significant improvement (89.6% for P1) can be achieved over conventional OR [172] (dashed dotted line).

Fig. 5.6 portrays the normalized energy consumption versus the position of the RN. This figure applied the same parameters and methodology as those used for

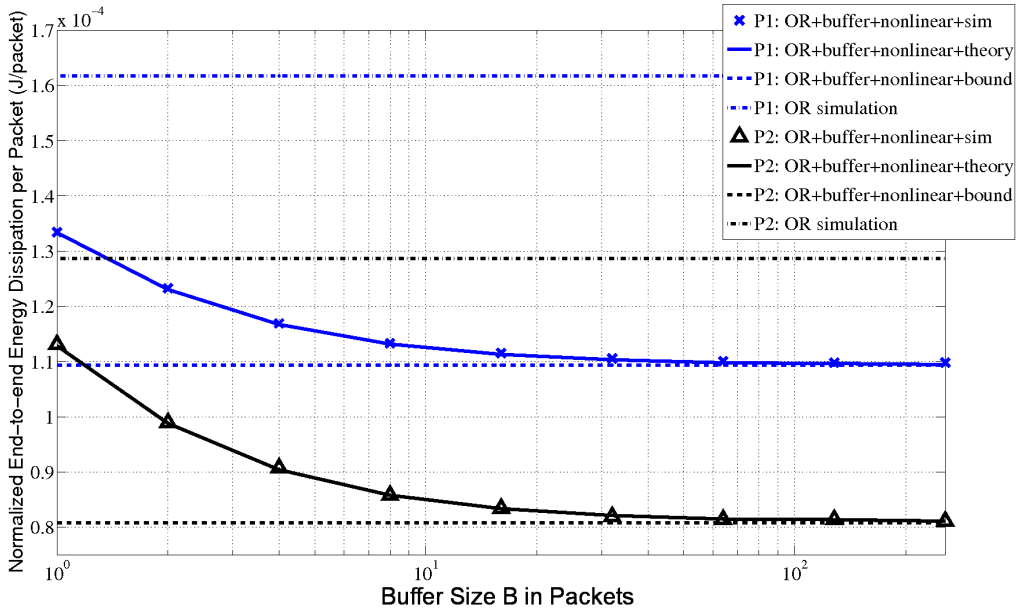

Figure 5.4: Average normalized end-to-end energy consumption per packet as defined in Section 5.4.2 when the RN is at the position of P1:$(400, 400)$, P2:$(500, 0)$ and the pathloss factor is $\alpha = 2$. The theoretical curve was evaluated from (5.51).

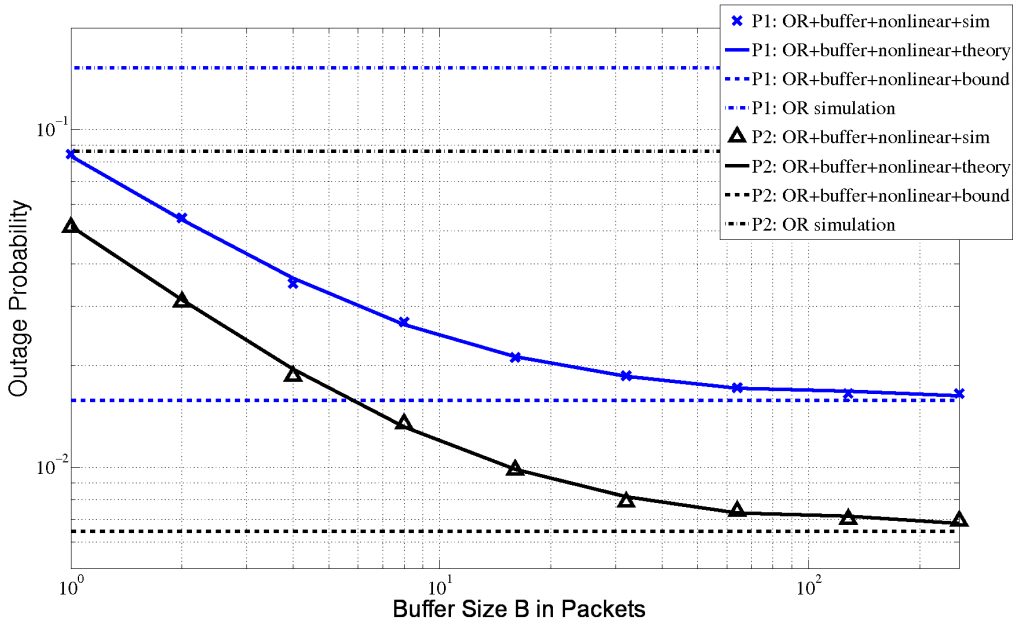

Figure 5.5: The simulated and theoretical outage probability evaluated from (5.5) when the RN is at the position of P1:$(400, 400)$, P2:$(500, 0)$.

Fig. 5.4, except for the position of the RN. The position of both the SN and DN are marked in this figure, while the RN may be located at any position. The normalized energy consumption can be theoretically calculated from (5.51), when the RN is in a specific position. Observe in Fig. 5.6 that the normalized energy consumption is characterized by a surface as a function of the RN position. Additionally, it is reasonable to expect that the normalized energy consumption is the lowest, when the RN is in the half-way position between the SN and DN (bottom of the surface), while it is higher, when the RN is far away from both the SN and DN, as indicated by the corners of the surface.

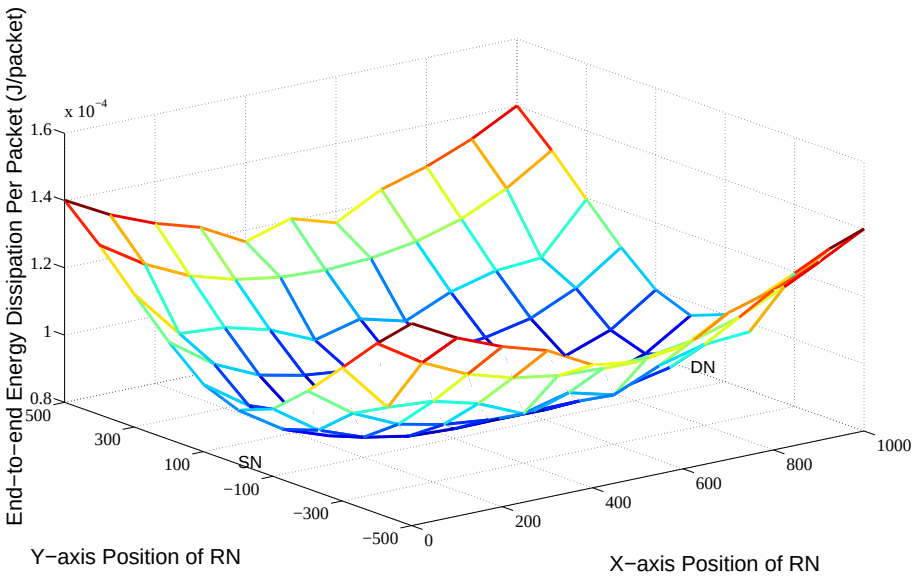

Figure 5.6: Average normalized end-to-end energy consumption vs the RN position.

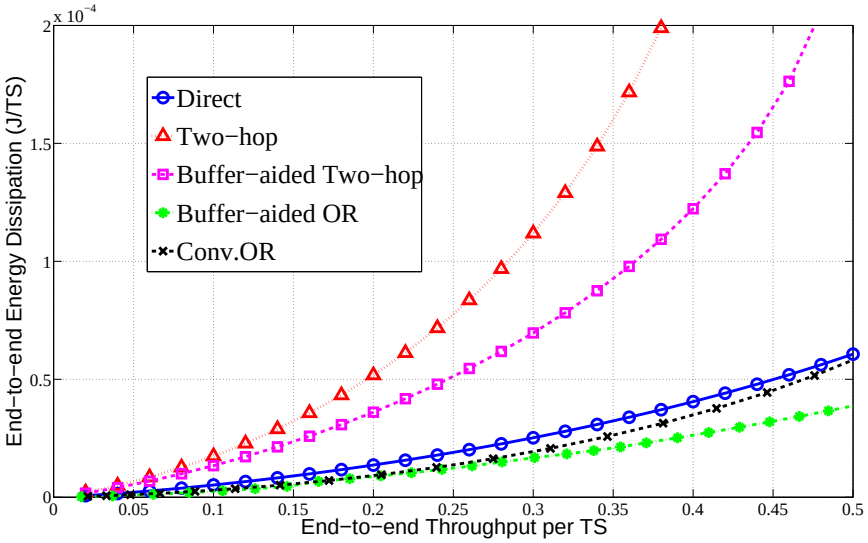

Figure 5.7: The end-to-end (system) energy consumption per TS for various transmission schemes operated at a given target end-to-end throughput where the RN is at the position of $(400, 400)$.

Fig. 5.7 compares the normalized energy consumption for various transmission schemes. The RN is at the normalized position of $(400, 400)$ and the pathloss factor is $\alpha = 2$. The label "Direct" implies that the packet is transmitted directly from the SN to DN without relaying, while the label "Two-hop" means that the packet is transmitted from the SN to DN via the RN sequentially in two hops without buffering. The "Buffer-aided two-hop" scenario implies that the RN has a buffer, therefore the system relies on channel-quality aided activation, however the SN is unable to directly transmit a packet to the DN. This scheme is identical to that proposed in [168,183,184]. The power allocation method mentioned in [169] is applied both in the "Two-hop" scenario and in the "Buffer-aided two-hop" transmission scheme, which makes the average receive SNR for each hop the same. The label "Conv. OR" represents the conventional opportunistic routing method [**?**,172], where each packet is transmitted either via the SN-DN or the SN-RN-DN route, one by one. The next packet does not enter the system unless the previous packet has been received by the DN. In other words, the RN is only capable of storing one packet. Finally, the "Buffer-aided OR" is our proposed scheme. The corresponding results are based on our theoretical analysis relying on an infinite buffer size. The X-coordinate represents the end-to-end target throughput, while the Y-coordinate represents the energy dissipation. Observe from Fig. 5.7 that the performance of both the "Two-hop" and of the "Buffer-aided two-hop" schemes is worse than that of the "Direct" scheme. The "Buffer-aided OR" scheme performs best. The performance of conventional opportunistic routing is worse than that of Buffer-aided OR, but better than that of direct transmission. The reason for this is because compared to direct transmission, conventional OR has more potential routes while in contrast to the buffer-aided OR scheme, conventional OR may only store a single packet in the RN. For example, observe in Fig 5.7 that when the system is operated at a normalized end-to-end throughput of $0.4 packet/TS$, the end-to-end PEC of "Buffer-aided OR" was reduced by 88.2%, 77.6%, 32.3% and by 24.8%, when compared to the "Two-hop", "Buffer-aided Two-hop", "Direct" and to the "Conv. OR" transmission schemes, respectively. Compared to classic direct transmission, again, the "Buffer-aided OR" scheme is capable of activating the best of the three channels, hence it attains the best performance. Furthermore, the reciprocal of the throughput is related to the average delay, which also shows the advantages of the "Buffer-aided OR" aided transmission scheme.

Fig. 5.8 shows the distribution of the packet delay, when stipulating the same assumptions, as those for Fig. 5.4. The theoretical results obtained from Section 5.8 are represented by the solid lines, while the simulation results are represented by

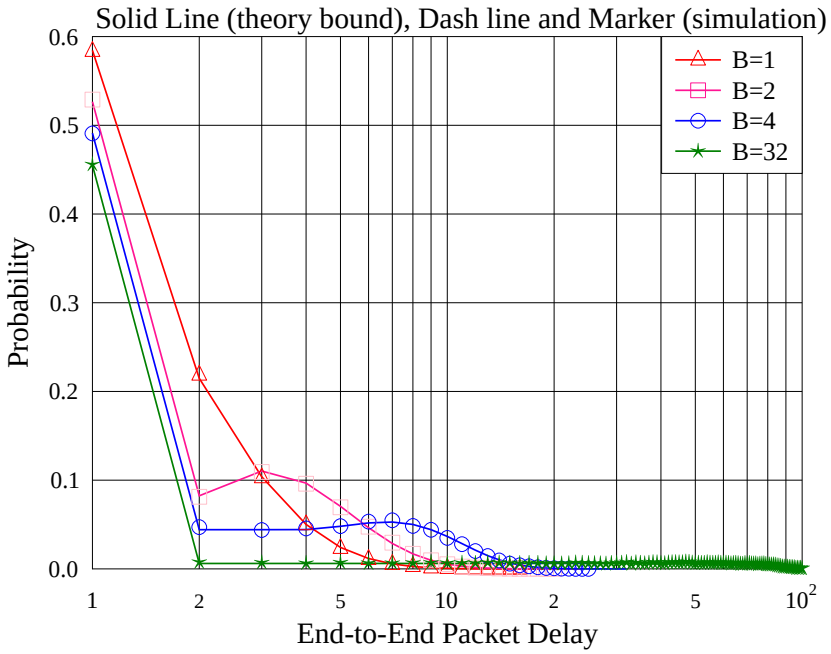

Figure 5.8: The distribution of the packet delay evaluated from Section 5.8, when the RN is at the position of $(400, 400)$. The buffer size ranges from 1 to 32.

the markers. It is clear from Fig. 5.8 that the probability of direct transmission associated with $B = 1$ is relatively high. As shown in Fig. 5.8, when the buffer size B increases, the probability of direct transmission decays below that of buffer-aided OR.

5.10 Chapter Conclusions

In this chapter, we have proposed and investigated a new routing scheme in Section 5.1, which we referred to as the BOR regime. The BOR routing regime was capable of combining the advantages of buffer-aided transmissions with the benefits of opportunistic routing. In Section 5.2, the system model was introduced, where all hops experienced Rayleigh fading. Then, a specific MAC layer protocol was designed in Section 5.3 for supporting the proposed BOR. In Section 5.4, the concept of energy consumption was defined. Moreover, the three-dimensional channel space concept was proposed in Section 5.5 while our new division method was discussed in Section 5.6, relying on a parameter which may be calculated by our algorithm proposed in Section 5.7. Finally, the normalized energy consumption, the outage probability and the distribution of the delay have been analyzed and verified by simulations in Fig. 5.4, 5.5 and 5.8, respectively, when assuming that the packets can be correctly received, provided that the received SNR was in excess of a certain threshold. Our analysis and performance results showed that exploiting the BOR scheme results in a significant reduction of the energy consumption. The results also show that the

theoretical energy consumption and the outage probability bound can be approached by employing a sufficiently large buffer at the RN.

5.11 Appendix: Basic Principle of TAPS and a Proof of Optimal in a Two-hop Link

The concept of TAPS is the "heart and soul" of this chapter. In order to augment the relevant concept as explicitly as possible, three examples of a two-hop link are shown below, which are simpler than a multi-node network. We commence from a two-hop link having an identical distance in both hops and conclude with the rationale of our non-linear channel space partitioning.

The first example is a simple one relying on the buffer-aided conventional selection combining (SC), philosophy where the channel having the highest SNR is activated. We consider a two-hop link, where the SN-RN channel quality is identical to the RN-DN channel quality, as shown in Fig. 5.9. Note that the SN cannot communicate directly with the DN. The RN has a buffer. In the two hops, the receive SNRs γ_{SR}^{rec} and γ_{RD}^{rec} are given by the product of the corresponding instantaneous channel fading values (γ_{SR}, γ_{RD}) and the related average receive SNRs ($\bar{\gamma}_{SR}$, $\bar{\gamma}_{RD}$), respectively. The two instantaneous channel fading values (γ_{SR} and γ_{RD}) form a so-called channel space, as shown in Fig. 5.10. The X-axis represents the channel fading value γ_{SR} of the SN-RN channel, while the Y-axis represents the channel fading value γ_{RD} of the RN-DN channel. In each time slot, the instantaneous channel fading values of both the SN-RN (γ_{SR}) and of the RN-DN (γ_{RD}) channels map to a specific point $(\gamma_{SR}, \gamma_{RD})$ in the 2D channel space. Obviously, if the mapped point is in the region below the OE line, because we have $\gamma_{RD} < \gamma_{SR}$, then the SN-RN link should be activated. By contrast, if the mapped point is in the region above the OE line, because $\gamma_{RD} > \gamma_{SR}$, then the RN-DN link should be activated. The boundary is the OE line and the slope of it is one. The activation probabilities of the two hops are identical because both channels obey the same distribution. Therefore, the system can be operated in its **steady** state.

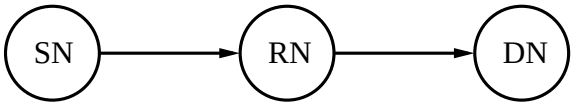

Figure 5.9: A two-hop link. The SN-RN channel and RN-DN channel are assumed to be identical.

The second example discusses a buffer-aided two-hop link associated with non-identical average receive SNRs, because the RN is not half-way between the SN and

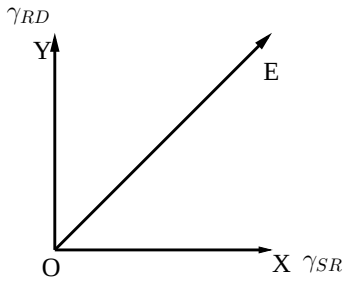

Figure 5.10: The transmission activation probability space (TAPS) of a two-hop link, where the average SN-RN channel SNR $\bar{\gamma}_{SR}$ and the average RN-DN channel SNR $\bar{\gamma}_{RD}$ are identical.

DN, as seen in Fig 5.11. Let us assume that the average receive SNR $\bar{\gamma}_{SR}$ of the SN-RN channel is higher than the average receive SNR $\bar{\gamma}_{RD}$ of the RN-DN channel. If the channel having the higher received channel SNR ($\bar{\gamma}_{SR}\gamma_{SR}$ or $\bar{\gamma}_{RD}\gamma_{RD}$) is activated, the boundary of the two activation regions should be the OE_0 line in Fig. 5.12. However, the area of the region encompassed by the points $\gamma_{SR}OE_0$ is higher than that of the other region determined by $EP\gamma_{RD}$. Therefore, the activation probability of the two hops is different and the system operates in an unstable mode, potentially leading to a buffer overflow.

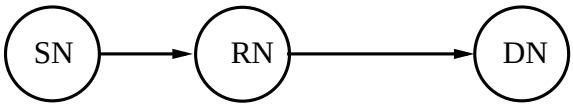

Figure 5.11: A two-hop link, where the average receive SNR of the SN-RN channel is higher than that of the RN-DN channel.

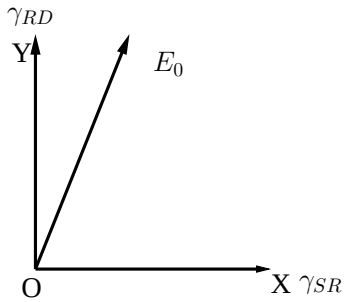

Figure 5.12: The transmission activation probability space (TAPS) of a two-hop link, where the average receive SNRs of the SN-RN and the RN-DN channel are non-identical.

In order to allow the system to operate in its steady state rather than in the unstable mode of Fig 5.11 and 5.12, there are two plausible methods to adjust the boundary OE_0:

a) If we force the boundary OE_0 to be linear, OE_0 should be moved back to OE. However, this method is not optimum;

b) If the OE_0 boundary is non-linear.

Please allow us to discuss the second method directly, which is more beneficial than the first method, because we may get an optimum boundary, as detailed below.

In order to elaborate on the process of transmission-probability adjustment, let us partition the transmission activation probability space (TAPS) into perfectly tiling squares, as shown in Fig. 5.13. The light-grey region represents the activation-region of the SN-RN channel, while the dark-grey region represents that of the RN-DN channel. Now, the activation probability of the SN-RN channel is higher. Let us now move some of the dark-grey tiles to the light-grey region, albeit we realize that this is achieved at a performance penalty, as detailed below.

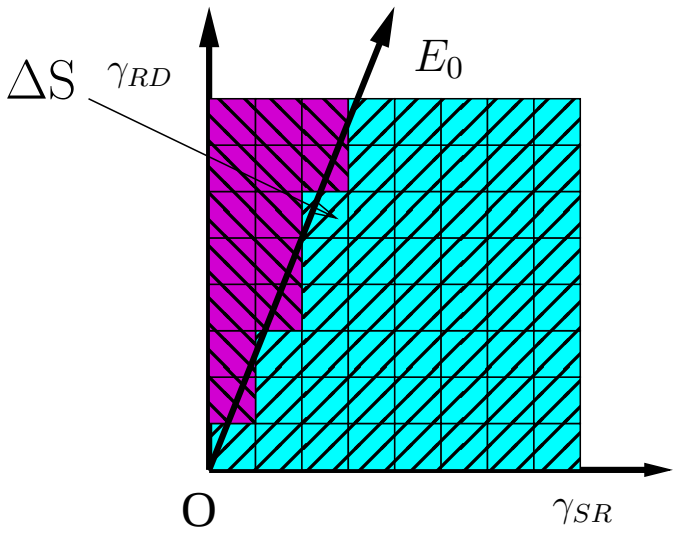

Figure 5.13: The transmission activation probability space (TAPS) of a two-hop link, where the average receive SNR of the SN-RN hop and of the RN-DN hop are non-identical. The transmission activation probability space is partitioned into tiles.

When considering a tile ΔS, the question arises: what is the energy dissipation ($\mathcal{E}_{\Delta S \in SR}$) caused by ΔS, when ΔS belongs to the activation region of the SN-RN hop? This is quantified as

$$\mathcal{E}_{\Delta S \in SR} = p_{\Delta S} \left(\frac{C_{SR}}{\gamma_{SR}} \right), \tag{5.59}$$

where, $p_{\Delta S}$ is the probability of the point $(\gamma_{SR}, \gamma_{RD})$ falling into the ΔS region of Fig. 5.13, C_{SR} is a constant value and $\frac{C_{SR}}{\gamma_{SR}}$ indicates that the energy dissipation imposed is inversely proportional to the channel quality experienced. By contrast, what is the energy dissipation ($\mathcal{E}_{\Delta S \in RD}$) caused by ΔS, when ΔS belongs to the activation region of the RN-DN hop? This is given by

$$\mathcal{E}_{\Delta S \in RD} = p_{\Delta S} \left(\frac{C_{RD}}{\gamma_{RD}} \right), \tag{5.60}$$

where, C_{RD} is a constant value and again, $\frac{C_{RD}}{\gamma_{RD}}$ indicates that the energy dissipation is inversely proportional to the RN-DN channel SNR encountered. If the region ΔS is reassigned from the SN-RN channel to the RN-DN channel, how much extra energy in dissipated? This is quantified by $\mathcal{E}_{\Delta S \in RD} - \mathcal{E}_{\Delta S \in SR}$, which should be as low as possible. Then the transmission probability is modified by $p_{\Delta S}$. Therefore, the power-dissipation cost of this probability adjustment is

$$E_{ffe} = \frac{\mathcal{E}_{\Delta S \in RD} - \mathcal{E}_{\Delta S \in SR}}{p_{\Delta S}} \tag{5.61}$$

$$= \frac{C_{RD}}{\gamma_{RD}} - \frac{C_{SR}}{\gamma_{SR}}. \tag{5.62}$$

By contrast, if we are willing to tolerate a higher energy-dissipation penalty for the sake of having the same transmit probability for the unequal-SNR links, the OE_0 boundary may be reshaped, as seen in Fig. 5.14.

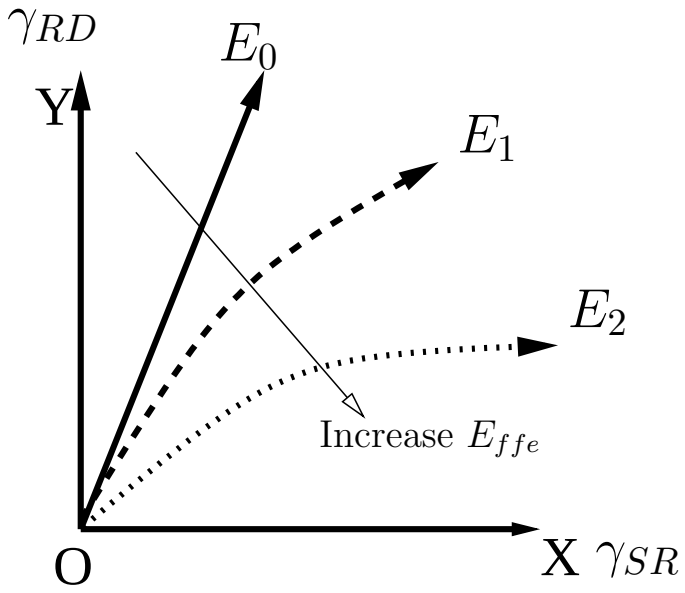

Figure 5.14: The transmission activation probability space (plane) of a two-hop link, where the SN-RN channel and the RN-DN channel are non-identical. The transmission-probability boundary is reshaped for various values of E_{ffe}.

In order to allow the two hop link to operate in its steady state, we may continue increasing E_{ffe}, until the probability represented by the region $\gamma_{SR}OE_2$ becomes the same as that represented by $E_2O\gamma_{RD}$. In this reassignment process, the tiles imposing a lower E_{ffe} are adjusted firstly, followed by those imposing a higher power-dissipation penalty E_{ffe}, until the above-mentioned condition is satisfied. Let us now show formally that this boundary is optimal.

In Fig. 5.15, the TAPS is now partitioned into unequal tiles by assuming that each tile represents the same probability. The fading envelope of the channel usually

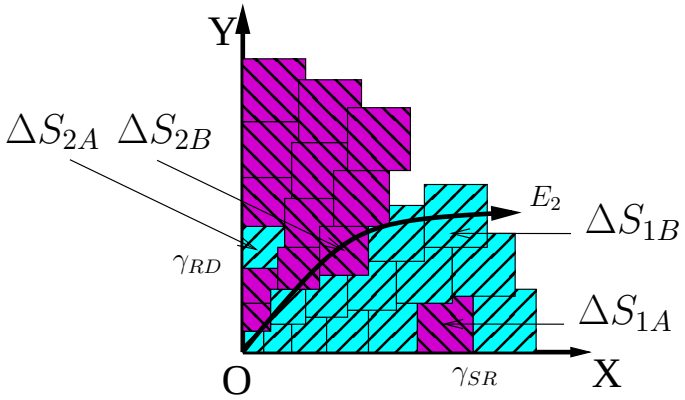

Figure 5.15: The transmission activation probability space (plane) of a two-hop link, where the SN-RN channel and the RN-DN channel are non-identical. The transmission activation probability space is partitioned into many small tiles, each of which has the same probability.

does not obey a uniform distribution. In order to allow each tile to represent the same probability, the area of each tile may be different. **Below we will show that the boundary OE_2 is optimum by involving the method of contradiction.**

Contradiction statement: Let us assume that there is an optimal TAPS partitioning, which is different from the partitioning OE_2 in seen Fig. 5.14 and 5.15. Due to the assumption, optimality the energy dissipation of this partitioning is lower than that of the partitioning OE_2 in Fig. 5.14.

Due to having the same probability of encountering the regions of $\gamma_{SD}OE_2$ and $E_2O\gamma_{RD}$, there are $N, (N > 0)$ tiles in region $E_2O\gamma_{RD}$ representing the activation the SN-RN hop, while there are also N tiles in the region $\gamma_{SD}OE_2$ corresponding to activating the RN-DN hop. Let us consider a specific pair of them (say ΔS_{1A} and ΔS_{2A}), as shown in Fig. 5.15. Correspondingly, there is a tile ΔS_{1B} on the boundary OE_2, which has the same X coordinate value as ΔS_{1A}. Similarly, there is also a tile ΔS_{2B} on the boundary OE_2, which has the same Y coordinate value, as ΔS_{2A}. Let us now consider three different actions:

1) exchange the affiliation of ΔS_{1A} and ΔS_{1B} by remapping them between the two parts of the TAPS;

2) exchange the affiliation of ΔS_{2A} and ΔS_{2B};

3) exchange the affiliation of ΔS_{1B} and ΔS_{2B}.

This has the same transmit probability effect, as exchanging the affiliation of ΔS_{1A} and ΔS_{2A}, but their energy-dissipation effects are rather different, when compared to 'no action'. To elaborate a little further, if we exchange the TAPS affiliation of ΔS_{1A} and ΔS_{1B}, as shown in Fig. 5.16, the activation probability of each hop remains the same. However, the energy dissipation is reduced due to the fact that the energy

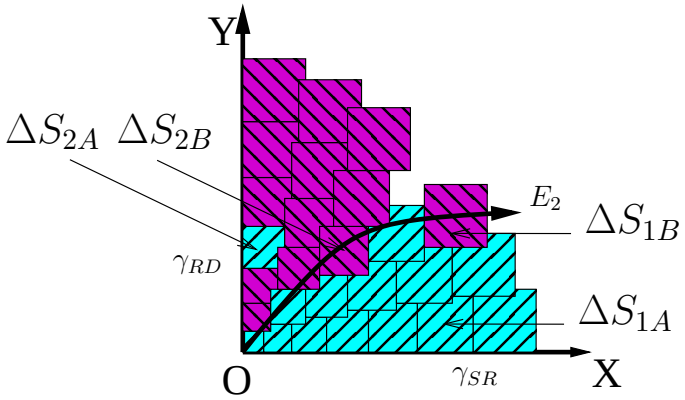

Figure 5.16: Compared to Fig. 5.15, the TAPS affiliation of ΔS_{1A} and ΔS_{1B} has been exchanged.

dissipated within the tile ΔS_{1B} of Fig. 5.16 is lower than that within ΔS_{1A} of Fig. 5.15, because γ_{RD} is higher for ΔS_{1B} than for ΔS_{1A}, while the energy dissipated by the SN-RN hop remained the same due to having the same γ_{SD} ordinate values for ΔS_{1A} and for ΔS_{1B}.

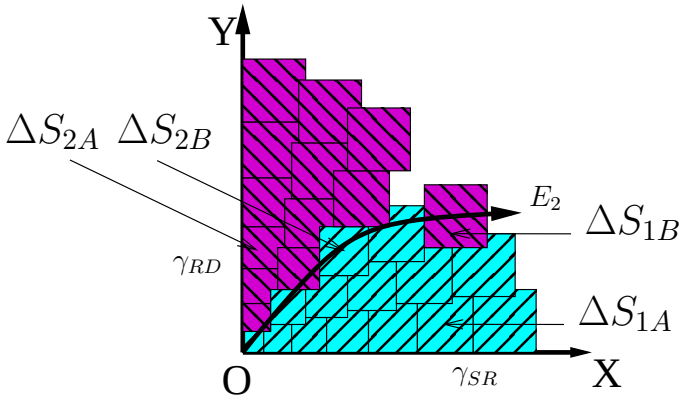

Figure 5.17: Compared to Fig. 5.16, the TAPS affiliation of ΔS_{2A} and ΔS_{2B} has been exchanged.

Similarly, if we exchange the TAPS affiliation of ΔS_{2A} and ΔS_{2B} as shown in Fig. 5.17, the activation probability of each hop remains the same. However, the energy dissipation is reduced due to the fact that the energy dissipated within the tile ΔS_{2B} of Fig. 5.17 is lower than that of ΔS_{2A} in Fig. 5.16, while the energy dissipated by the RN-DN hop remained the same during the above process since both ΔS_{2A} and ΔS_{2B} have the same γ_{RD} ordinate values.

Lastly, both the tiles ΔS_{1B} and ΔS_{2B} are on the boundary OE_2, as shown in Fig. 5.18. Hence, exchanging the TAPS affiliation of ΔS_{2A} and ΔS_{2B} does not affect the energy dissipation. Following the above three actions, the TAPS affiliation of the tiles ΔS_{1A} and ΔS_{2A} was exchanged and the energy dissipation imposed was decreased. The energy dissipation of the partitioning seen in Fig. 5.18 is lower than

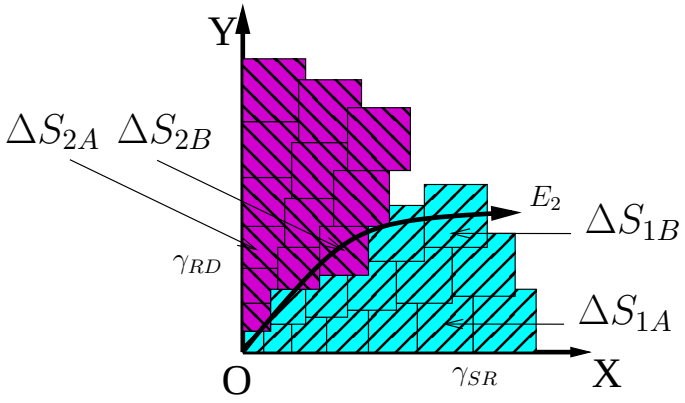

Figure 5.18: Both the tiles ΔS_{1B} and ΔS_{2B} are on the boundary OE_2. Hence exchanging the TAPS affiliation of ΔS_{2A} and ΔS_{2B} does not affect the energy dissipation.

that observed in Fig. 5.15 and the probabilities represented by light-grey and dark-grey tiles are the same in both figures. This however contradicts to the statement that there is a better boundary than OE_2, which demonstrates that the tile-based partitioning seen in Fig. 5.15 is not optimal. Therefore, no better tile-based TAPS partitioning can be found than OE_2.

Chapter 6

Conclusions and Future Work

In Section 6.1, we summarise the main findings of our investigations, while our design guidelines are presented in Section 6.2. Additionally, a range of ideas concerning our future research is presented in Section 6.3.

6.1 Conclusions

In this thesis, we have investigated buffer-aided transmissions in multihop scenarios for the sake of enhancing the achievable BER and/or outage probability and/or energy consumption. More specifically, we proposed the concept of multihop diversity and investigated the impact of both the number of hops and of the channel's fading distribution as well as the quantitative impact of the buffer size in the context of SNR-based, CDF-based and non-linear channel space division based channel activation. Table 6.1 summarizes the basic characteristics of all the buffer-aided transmission regimes proposed in this thesis, chapter by chapter, including the channel model employed, the system parameters and the preformance metrics. Basic performance comparisons between our proposed buffer-aided transmission and the corresponding conventional algorithms are provided as well.

- In Section 2.1, a multi-hop transmission scheme is proposed, where all the relay nodes (RNs) of a multi-hop link (MHL) are assumed to have buffers for temporarily storing their received packets. As a benefit of storing packets at the RNs, the best hop typically has the highest signal-to-noise ratio (SNR) during each time-slot (TS), which can be selected from the set of those hops that have packets awaiting transmission in the buffer. A packet is then transmitted over the highest-quality hop. The system model and an example of the hop-selection procedure are described in Section 2.2.

In Section 2.3, a decentralized MAC layer protocol was constructed for supporting this buffer-aided transmission regime. There are three stages in this protocol. In the first two stages, each node may assume the knowledge of the buffer-fullness in its immediately adjacent nodes as well as the channel condition knowledge of the nearby nodes within one or two hops. In the third stage, each node will broadcast different MAC layer control signals at specific time instants based on both the above-mentioned buffer and channel knowledge, as well as by exploiting the knowledge of both the hop index of this node and of the previously received MAC layer control signals. Given this knowledge, the 'best' hop to be activated can be selected within less than $(9 + L \times S_i)$ symbol durations, where L is the total number of hops and S_i is the channel quality identifier. Physically this delay corresponds to the maximum MAC layer delay. Note that the delay of the first transmission is significantly lower than the maximum MAC layer delay.

In Section 2.4, the theoretical analysis of both the hop-by-hop and of the end-to-end BER performance was provided, while assuming an infinite buffer. After introducing the concept of buffer state, both the hop-by-hop and end-to-end the BER performance was analyzed while relying on a finite buffer. Furthermore, the theoretical analysis of the outage performance was carried out, when assuming that each hop experiences both propagation pathloss and independent identically distributed (i.i.d) flat Rayleigh fading. Naturally, the associated performance improvement was achieved at the cost of an increased delay. Therefore, the discussion of the associated delay is important. In Section 2.4.4, the maximum delay, the minimum delay, the distribution of the delay and the average delay of MHD transmission over MHLs was discussed. It can be seen in Fig. 2.25 that the average delay increases with the number of hops and/or the size of the buffer.

In Section 2.5, a number of numerical and simulation results are provided for characterizing the BER, outage probability and delay performance. The results of Fig. 2.13 to Fig. 2.22 characterize the achievable performance of the buffer-aided scheme and show that relying on multiple hops has the potential of providing a significant diversity gain. In Section 2.4.4, an algorithm is proposed for calculating the PMF of the delay associated with all discrete buffer states of the system. The results of Fig. 2.13 to Fig. 2.22 show that the theoretical analysis and the simulation results matched each other well.

- In Chapter 3, we investigated the transmission schemes that are similar to those in Chapter 2. We assumed that each hop experiences both propagation pathloss and independent but not necessarily identical distributed (i.n.i.d) flat

Nakagami-m fading. In order to guarantee that the number of input packets is the same as the number of output packets at each RN, we conceived a cumulative distribution function based node-activation regime. Furthermore, the modulation scheme used in Chapter 3 ranged from BPSK to MQAM.

In Section 3.3, the concept of the constellation-point to constellation-point transition matrix was defined on a hop-by-hop basis. Given this transition matrix concept, the L-hop link may be interpreted as a single-hop system associated with a specific transition matrix. Therefore, the end-to-end BER performance associated with an infinite buffer was then obtained. Upon applying the concept of buffer-state, the probability of the system operating in various diversity-order modes can be determined. Thus, the end-to-end BER associated with a finite buffer size can be calculated. Specifically, in Section 3.3.2, the approximate buffer fullness expression were are provided for a mediocre-sized transition matrix. Finally, the achievable diversity order was analyzed theoretically.

In Section 3.4, a number of numerical and simulation results were provided for characterizing both the BER and the outage probability as well as the diversity order. This analysis and the associated performance results show that exploiting the independent fading of multiple hops results in a significant diversity gain.

- In Chapter 4, we also comceived transmission schemes that are similar to those studied in Chapters 2 and 3. We assumed that each hop experiences both propagation pathloss and independent identically distributed (i.i.d) flat Nakagami-m fading. Since adaptive modulation was employed, the number of bits in each time slot was affected both by the channel quality and the buffer fullness. During each time-slot (TS), the criterion used for activating a specific hop was that of transmitting the highest possible number of bits (packets). When more than one hops are capable of transmitting the same number of bits, the particular hop having the highest channel quality (reliability) was activated. Hence we referred to this regime as the Maximum Throughput Adaptive Rate Transmission (MTART) scheme.

  In Section 4.3, a decentralized MAC-layer protocol was constructed, which was similar to the protocol conceived in Section 2.3 for supporting this adaptive modulation assisted and buffer-aided transmission regime. There are three stages in this protocol. The first two stages are the same as the corresponding stages in Section 2.3, while in the third stage, two basic processes have been discussed, including both the cases of successful and unsuccessful access. Then a decentralized MAC layer algorithm was designed for finding the activated hop based on these two basic processes.

In Section 4.4, the principle of MTART was detailed. Then both the PDF and CDF of the activated channel's SNR was derived for a two-hop link, followed by the derivation of the PDF of the activated channel's SNR in an L hop link. These discussions did not consider any specific fading channel. Hence, as a further advance, Nakagami-m fading channels were considered in Section 4.5. The single-hop BER, the buffer state transition matrix, the achievable throughput, the exact end-to-end BER, the outage probability as well as the bandwidth-efficiency were discussed in Section 4.5.8 to Section 4.5.9, respectively.
Finally, the results of Fig. 4.11 in Section 4.6 characterize the outage probability. The PMF of the delay as well as the throughput and the bandwidth-efficiency was characterized from Fig. 4.13 to Fig. 4.15. Compared to the conventional adaptive modulation scheme, the MTART scheme has a $3dB$ gain across a large range of SNRs.

- In Chapter 5, a buffer-aided opportunistic routing scheme was proposed, which combines the benefits of both opportunistic routing and of multihop diversity aided transmissions. A Buffer-aided Three-node Network (B3NN) composed of a Source Node (SN), a buffer-aided Relay Node (RN) and a Destination Node (DN) was studied. When applying opportunistic routing, each packet is transmitted from the SN to the DN either directly or indirectly via the RN, depending on the instantaneous channel qualities. In MHD assisted transmission, the RN is capable of temporarily storing the received packets, which facilitates the flexible activation of the channels. In Section 5.3, a specific MAC layer protocol was proposed for this routing scheme applied in our B3NN. The corresponding channel activation criterion was detailed in Section 5.4. Then, in Section 5.5 and Section 5.6 the three channels were characterized with the aid of a three-dimensional (3D) Transmission Activation Probability Space (TAPS), which is divided into four regions, representing each of the three channels' quality, plus an outage region. In a specific time slot (TS), the instantaneous Channel Quality (CQ) values may be directly mapped to a particular point in this 3D channel space. The buffer-aided opportunistic routing scheme then relies on the specific position of this point for selecting the most appropriate channel for its transmission. The energy consumption and the outage probability of this scheme were also investigated and the PMF of the delay was derived in Section 5.8 for transmission in this network. The results of Section 5.9 demonstrate that both the energy consumption and the OP were significantly reduced.

Table 6.1: Summary of buffer-aided transmission design.

Chapter No.		**Chapter 2**	**Chapter 3**	**Chapter 4**	**Chapter 5**			
Metric		BER	BER	Throughput	Throughput			
Channel		Rayleigh +path loss	Nakagami-m +path loss	Nakagami-m +path loss	Rayleigh +path loss			
MAC		MHD-MAC	MHD-MAC	MHD-AMC-MAC	MHD-OR-MAC			
NET		No. of hops	No. of hops	No. of hops	3 nodes			
Selection metric		Highest SNR	Highest CDF	Highest SNR	Non-linear 3D space division			
Performance	Compared Scheme	Conv.	Conv.	Conv.	Direct	Conv.	OR	Buffer-aided
	SNR-gain at BER=10^{-3}	$\alpha = 2^f$ $13dB^a$	$\alpha = 2$ $13dB^b$	-	-	-	-	-
	SNR-gain at OP=10^{-3}	$\alpha = 2$ $15dB$	$\alpha = 2$ $18dB^a$	$15dB^a$	-	-	89.6% $\downarrow^c$	-
	Throughput	-	-	$3dB$	-	-	-	
	Energy	-	-	-	32.3% $\downarrow^d$	88.2% $\downarrow^d$	24.8% $\downarrow^c$	77.6% $\downarrow^d$

[a] Compared the conventional curve to the curve associated with infinite buffer size at 10^{-3} BER/outage probability in a two-hop link.

[b] Compared the conventional curve to the curve associated with infinite buffer size at 10^{-3} BER/outage probability in a three-hop link and exemplified parameters.

[c] The SN, RN and DN are at $(0m, 0m)$, $(400m, 400m)$, and $(0, 1000m)$.

[d] The throughput of the system is at $0.4packet/TS$.

[e] MAC: medium access control; MHD: multihop diversity; AMC: adaptive modulation coding; OR: opportunistic routing; BER: bit error ratio; OP: outage probability; 3D: three dimension

[f] α is the pathloss factor.

6.2 Design Guildlines

In general, three basic design steps may be identified, when designing a buffer-aided transmission system, which are:

1) Determining the design specifications, such as the required BER performance, outage probability, energy consumption, the tolerable delay etc. We may opt for maintaining a single-target specification or multiple-target specifications.

2) Determining the physical layer components.

3) Determining the algorithmic parameters based on theoretical analysis.

Let us now detail these design steps as follows:

- In a buffer-aided transmission system, the design targets specifications play a crucial role in the design process. The fundamental design targets of the system model mentioned in Chapters 2 and 3 are the BER performance and the outage probability. By contrast, the design targets of the system model considered in Chapter 4 are the outage probability and throughput specifications while simultaneously meeting a specific BER constraint. In contrast to the previous chapters, in Chapter 5 the design target is that of meeting the end-to-end expected energy consumption specification. However, the integrity of a link may only be improved at the cost of a reduced throughput or increased delay as well as complexity. For example, a tradeoff has to be struck between the energy consumption and outage probability.
- The number of relays is one of the most important design issues. Given a specific number of relays, all the properties of the system can be analytically calculated. The required number of relays may then be found based on these calculations.
- The pathloss factor α heavily affects the attainable performance. Practically, the typical values of α range from 2 to 6. When this value is even higher, the system may choose a specific hop spanning a shorter distance. By contrast, when α is lower, the system may opt for a hop spanning a longer distance. The probability of direct transmission in a buffer-aided opportunistic routing network may decrease upon encountering higher values of α. The comparison of these results as a function of α may be found in Sections 2.5 and 3.4.
- The distance of each hop may be similar or dissimilar. Even if the length of each hop is different, which results in different channel qualities, the number of input packets/bits has to be the same as the number of output packets/bits of a RN. In order to satisfy this constraint, there are two possible solutions, namely

the employment of power control and that of our non-linear channel space division concept. Accurate power control allows each hop to have the same average receiver SNR, which guarantees the fulfillment of the above-mentioned main constraint. By contrast, the non-linear channel space division concept of Secion 5.1 may also be applied. The channel space is divided into $(l+1)$ regions, where l is the channel index and the extra region is the outage region. For a specific time slot, the instantaneous channel quality value maps to a particular point in the channel space and the corresponding hop can be activated or an outage occurs. One of the main disadvantages of this predetermined channel space division is its high complexity. However, all the calculations may also be carried out off-line to find the required parameters. Specific solutions were proposed in Section 2.2, 5.5 and 5.6.

- Diverse fading types may be considered. The Rayleigh fading channel model is widely used in wireless research for non-line-of-sight scenarios. By contrast, the Nakagami-m model associated with a parameter m is capable of accurately modelling diverse fading channels. However, the m parameter of each hop may be different. Therefore, the above-mentioned main constraint may not be satisfied. In order to deal with this problem, a CDF-based link-activation solution was proposed in Section 3.1, where the link-activation regime relies on the highest CDF-SNR ordinate value amongst all the available hops.
- Furthermore, having considered the factors influencing the design of the physical layer, we have to proceed by characterizing the influence of the MAC layer in our buffer-aided transmission design, whilst relying on the instantaneous channel and buffer fullness knowledge. This MAC layer protocol can be a centralized protocol or a decentralized protocol. However, using a decentralized protocol is significantly more practical. The design of this decentralized protocol may have three stages. In the first two stages, each node broadcasts both its own pilot and its buffer-fullness knowledge within its transmission range. By the end of the second stage each node would have acquired both the channel knowledge and the buffer-fullness knowledge of its contactable neighbour nodes. In the third stage, each receiver node calculates the cost of activating the corresponding channel and the channel having the highest SNR/CDF or lowest end-to-end energy consumption has priority to be activated. In this process, an activated node may commerce its transmission and changes the state/knowledge of the nodes in its vicinity. Upon carrying out this process, all possible transmissions can be picked up one by one and interference free transmissions can be set up simultaneously. A beneficial MAC layer protocol was proposed in Section 2.3 for buffer-aided transmission.

- Additionally, adaptive modulation and coding (AMC) may be invoked both for increasing the throughput and for reducing the BER or PER. Both the physical layer and the upper-layer specifications have to be satisfied, therefore both the modulation scheme and the code rate should be carefully selected. Combining the concept of buffer-aided transmission and AMC was proposed in Section 4.1.
- Maintaining a low end-to-end packet delay is another important design target for near-real-time services, such as lip-synchronized video-telephony, where a high end-to-end delay may become intolerable. Hence the distribution of packet delay was also analyzed. In Chapters 2 and 3, this distribution was expressed by an analytic formula, while in Chapters 4 and 5 this distribution was estimated by an algorithm.

6.3 Future Research

A number of topics related to buffer-aided transmission require further study, relying on the research reported in this thesis and in its references. Further studies may be classified, as theoretical (group A) and application-oriented investigations (group B).

A1: Tradeoff Between the Delay and the BER/Outage Probability/Energy consumption

As mentioned in Chapters 2-5 and in [202], the BER/outage probability/energy consumption may be improved upon increasing the packet delay. Three aspects related to this trade-off should be made clear: the factors affecting the delay, the metric of quantifying the delay and the general principles of designing a buffer-aided system. It is plausible that the delay is increased, by a system invoking a higher number of hops as well as buffer-aided channel activation. Hence the associated design trade-offs have to be studied.

6.3.1 A1: Multi-user Transmissions

As mentioned in Chapters 2 and 4, the related MHD-MAC layer protocol requires both sophisticated interference management and power control. Naturally, multi-user transmission increases the system's total throughput at the cost of deteriorating its BER/outage probability performance. This is another tradeoff, which should be further studied.

6.3.2 A2: Outdated CSI

Our buffer-aided transmission scheme relies on local/global channel quality information. Although the corresponding MAC layer protocols are described in Chapter 2

and Chapter 4, the channel information becomes outdated during the channel selection/transmission procedure. Hence, the system's sensitivity to outdated CSI has to be mitigated with the aid of channel prediction techniques.

6.3.3 A3: Channel Coding

A buffer-aided system relying on a specific coding scheme was studied in [201]. It was observed that the packet error ratio may become vanishingly low, when the receiver's SNR is higher than a threshold for a specific type of channel coding. This performance enhancement was also exploited in Chapter 5. However, there are numerous channel coding families. Hence it is worth investigating the impact of the PER versus SNR relationship of different coding schemes.

6.3.4 A4: The Traffic Generation Model

The assumptions stipulated in this thesis entail that the source node has an infinite amount of data to transmit. However, the source data may obey some specific distribution, such as Possion distribution, which is commonly used in the research of wireless sensor networks, for example.

6.3.5 B1: Interference Cancellation

Let us now consider the potential applications of buffer-aided transmissions. In this section we focus our attention on the principle of interference cancellation based on using a buffer in a link. Here, we only introduce the transmission scheme and the MAC-layer protocol of a simple three-hop link.

Our protocol is based on the following assumptions. Consider the three-hop link shown in Fig. 6.1, where the nodes are indexed from the SN to DN as node 0, node $1 \cdots$ node 3. Each of the four nodes is aware of its own index, which indicates its relative position within the link. We assume that the transmission range of a node is at most one hop, i.e. a node can only communicate with its pair of adjacent nodes. By contrast, the interference range of a node is assumed to be at most four hops, implying that a transmitted signal may affect all nodes in the link.

Based on the above assumptions, let us now describe a beneficial transmission scheme and MAC-layer protocol. Let us commence with the introduction of the MAC layer protocol shown in Fig. 6.1. The nodes having an even index are activated in odd time slots, while the nodes with odd index are activated in even time slots, as long as at least one packet is ready for transmission in the buffer. According to this policy, we activate the specific nodes within the interference range of the others.

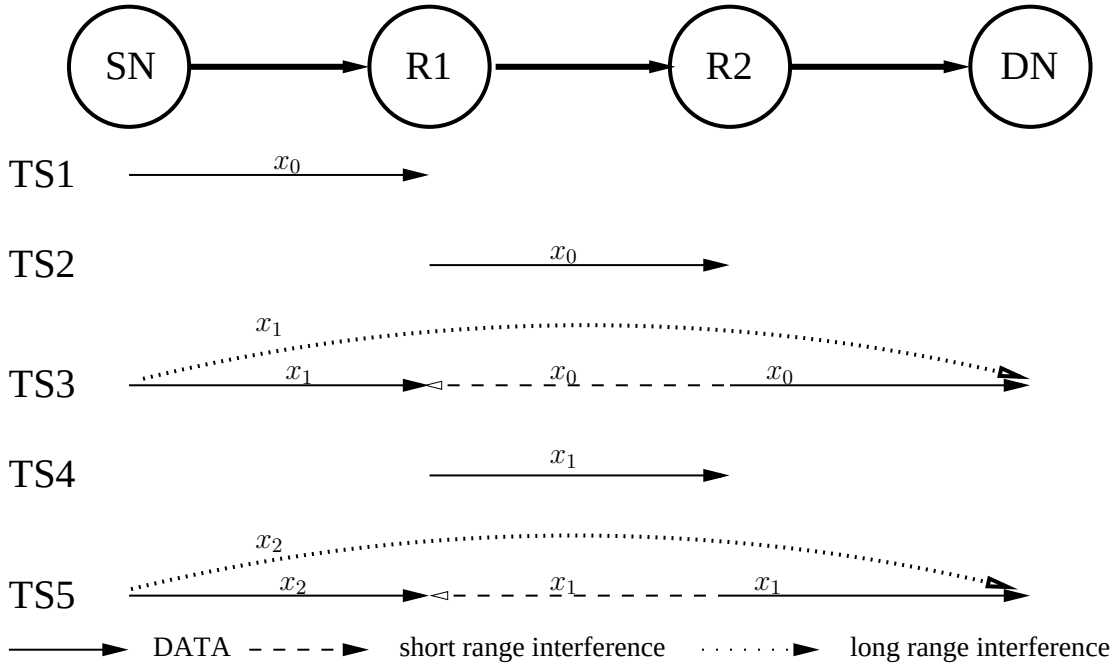

Figure 6.1: Transmission Scheme and the MAC Layer Protocol for Three-Hops.

However, in order to cancel the interference, the instantaneous channel quality of each link is required.

A possible solution that would satisfy this requirement is that: within the ith, $i = 0, 1, 2$, symbol duration of an odd time slot, the nodes having a position index obeying $(2i+6j)$, $j = 0, 1, \ldots$ and $2i+6j \leq L = 4$, broadcast their pilot signals. After receiving the pilot signal, all nodes having an odd index will be in possession of the CSI of all channels having an even index within the interference range. Conversely, within the ith, $i = 0, 1, 2$, symbol duration of an even time slot, the nodes having a position index obeying $(1 + 2i + 6j)$, $j = 0, 1, \ldots$ and $1 + 2i + 6j \leq L = 4$, broadcast their pilot signals. After receiving the pilot signal, all nodes associated with an even index have the CSI of all channels of the nodes with an odd index within the interference range.

Having acquired the CSI, the nodes store this, which may be used during interference cancellation within each time slot.

Following the description of the MAC layer protocol, we propose an appropriate transmission scheme operating on a time-slot by time-slot basis. In TS1, only the SN is activated to transmit the signal x_0 to R1. Then in TS2, R1 transmits x_0 to R2. In TS3, both SN and R2 are activated, which imposes interference. As shown in Fig. 6.1, R1 received the desired signal x_1 from SN and the interference x_0 from

R2, yielding,

$$y_1(TS3) = x_1 h_{01}(TS3) + x_0 h_{12}(TS3) + n, \tag{6.1}$$

where R1 already knows both x_0 and $h_{12}(TS2)$. Hence $x_0 h_{12}(TS2)$ can be cancelled. On the other hand, the signal received at DN is

$$y_3(TS3) = x_0 h_{23}(TS3) + x_1 h_{03}(TS3) + n, \tag{6.2}$$

where DN already knows $h_{23}(TS3)$. However, DN does not know x_1 during this time slot. The signal received by the DN is x_0, contaminated by the interference imposed by x_1, which can be written as $x_0 I x_1$, where "I" represents the interference. During this TS, DN then stores both $h_{03}(TS3)$ and $x_0 I x_1$.

During TS3, only R1 is activated and x_1 is transmitted to R2. In TS4, all the actions are the same as in TS2 and DN receives $x_1 I x_2$. Let us consider $x_1 I x_2$ as x_1 and substitute this x_1 into (6.2). Then the interference $x_1 h_{03}(TS3)$ can be cancelled and DN receives x_0 without any interference.

6.3.6 B3: Buffer-aided Transmission Relying on OR in a Large Network

In Chapter 5, the exact theoretical analysis of buffer-aided transmission relying on opportunistic routing in a three-node network was provided. However, in practice a larger network has to be considered.

Let us assume that all the assumptions are the same as in Chapter 5. Based on these assumptions, let us introduce the new concept of "energy-distance" ($\bar{\mathcal{E}}$) as detailed in [201]. Explicitly, the energy-distance of node i ($\bar{\mathcal{E}}_i$) is defined as the expected energy consumption, when node i transmits a packet to DN. Naturally, we have $\bar{\mathcal{E}}_{DN} = 0$. Then a large network may be described based on the following four stages.

1, In stage one, the order of energy distance is determined for each node. Note that this may not be the final order. We also assume that a packet can only be transmitted from a node associated with a higher energy-distance to a node having a lower energy-distance from the DN, implying that transmissions are always directed towards DN.

2, In stage two, all required parameters have to be obtained. Theoretically, the system activates the specific hop associated with the minimum expected end-to-end energy consumption. For a specific hop spanning from node i to node j, this energy

consumption study requires the determination of: a) the expected energy consumption of transmitting from the SN to node i, which is $\bar{\mathcal{E}}_{SN}$-$\bar{\mathcal{E}}_i$; b) the instantaneous energy consumption of this hop, which is inversely proportional to the instantaneous channel gain $\gamma_{i,j}$; c) the expected energy consumption of transmitting from the SN to node i which is $\bar{\mathcal{E}}_j$; d) a compensation factor $Effe_{i,j}$, which guarantees that the stability constraint is satisfied, namely that the number of input packets and output packets is the sameat each RN. It can be shown that the number of equations to be solved is the same as the number of unknowns, including $\bar{\mathcal{E}}$ and $Effe$. A practical iterative algorithm may also be conceived for finding all the required parameters.

In stage three, having determined the above-mentioned parameters, simulation results will be generated for confirming the theoretical analysis, including the outage probability and the PMF of the packet delay as a function of the buffer-size of each node.

Finally, a specific MAC layer protocol will be conceived, which may be similar to that of Section 4.3, containing three stages: broadcasting the pilots, broadcasting the buffer fullness as detailed in Section 4.3 and the 'clear-to-send' message based on the expected end-to-end energy consumption of each hop.

Glossary

3D	Three-dimensional.
AF	Amplify-and-Forward.
AMC	Adaptive Modulation and Coding.
AoD	Average Outage Duration.
AQAM	Adaptive Modulation.
ARDO	Asymptotical Relative Diversity Order.
ARQ	Automatic Repeat reQuest.
B3NN	Buffer-aided Three-node Network.
BER	Bit Error Ratio.
BF	Buffer Fullness.
BICM	Bit-Interleaved Coded Modulation.
BOR	Buffer-aided Opportunistic Routing.
BPSK	Binary Phase-Shift Keying.
BS	Base Station.
CCU	Central Control Unit.
CDF	Cumulative Distribution Function.
CFT	Clear for transmission.
CQ	Channel Quality.
CSI	Channel Side Information.
DARPA	Defense Advanced Research Project Agency.
DCMC	Discrete input Continuous output Memoryless Channel.
DF	Decode-and-Forward.
DN	Destination Node.
DO	Diversity Order.

DS-CDMA	Direct-sequence Code Division Multiple Access.
E2E	End-to-End.
EGC	Equal Gain Combining.
ExOR	Extremely Opportunistic Routing.
GG	Generalized Gamma.
GSC	Generalized Selection Combining.
HIPERLAN	High Performance Radio LAN.
HOS	Higher Order Statistics.
i.i.d	Independent and identically distributed.
i.n.i.d	Independent and non-identically distributed.
MAC	Media Access Control.
MC-CDMA	Multicarrier Code Division Multiple Access.
MGF	Moment-Generating Function.
MHD	Multihop Diversity.
MHL	Multihop Link.
MHLN	Multihop Lattice Networks.
MIMO	Multiple-Input Multiple-Output.
MPSK	M-ary Phase Shift Keying.
MQAM	M-ary Quadrature Amplitude Modulation.
MRC	Maximal Ratio Combining.
MSTM	Markov State Transition Matrix.
MTART	Maximum Throughput Adaptive Rate Transmission.
OP	Outage Probability.
OR	Opportunistic Routing.
OSTBC	Orthogonal Space-Time Block Code.
PA	Power Allocation.
PAM	Pulse Amplitude Modulation.
PDF	Probability Density Function.
PEC	Packet-Energy-Consumption.
PER	Packet Error Ratio.
PMF	Probability Mass Function.
PR	Potential Rate.

PRR	Potential Rate at the Receiver.
PRT	Potential Rate at the Transmitter.
QoS	Quality of Service.
QPSK	Quadrature Phase Shift Keying.
RFT	Request for transmission.
RNs	Relay Nodes.
SC	Single Selective.
SD	Symbol Duration.
SER	Symbol Error Ratio.
SF	Store-and-Forward.
SISO	Single Input Single Output.
SN	Source Node.
SNR	Signal to Noise Ratio.
SSC	Switch Single Selective.
STBC	Space-Time Block Code.
TAPS	Transmission Activation Probability Space.
TS	Time Slot.
UWB	Ultra-Wide-Band.

Bibliography

[1] H. Labiod, *Wireless Ad Hoc and Sensor Networks.* ISTE, 2008.

[2] C. K. Toh, *Ad Hoc mobile wireless networks.* John Wiley & Sons, Inc., 2002.

[3] O. Tonguz and G. Ferrari, *Ad Hoc Wireless Networks.* Wiley-Blackwell, Mar 2006.

[4] J. W. Craig, "A new, simple and exact result for calculating the probability of error for two-dimensional signal constellations," in *IEEE Military Communications Conference (MILCOM'91)*, pp. 571 –575 vol.2, Nov 1991.

[5] M.-S. Alouini and A. J. Goldsmith, "A unified approach for calculating error rates of linearly modulated signals over generalized fading channels," *IEEE Transactions on Communications*, vol. 47, pp. 1324 –1334, Sept. 1999.

[6] A. J. Goldsmith, *Wireless Communications.* Cambridge University Press, Apr. 2005.

[7] M. K. Simon and D. Divsalar, "Some new twists to problems involving the Gaussian probability integral," *IEEE Transactions on Communications*, vol. 46, no. 2, pp. 200–210, 1998.

[8] M. K. Simon, "Single integral representations of certain integer powers of the Gaussian Q-function and their application," *IEEE Communications Letters*, vol. 6, no. 12, pp. 532–534, 2002.

[9] N. C. Beaulieu, "Generalization of Craig's second formula," *IEEE Communications Letters*, vol. 17, no. 3, pp. 433–434, 2013.

[10] I. Gradshteyn and I. Ryzhik, *Table of Integrals, Series, and Products, Seventh Edition.* Elsevier Pte Ltd., 2007.

[11] C. Fox, "The G and H functions as symmetrical Fourier kernels," *Transactions of the American Mathematical Society*, vol. 98, no. 3, pp. pp. 395–429, 1961.

[12] H. M. Srivastava and R. Panda, "Some bilateral generating functions for a class of generalized hypergeometric plynomials," *J.Reine Argew. Math.*, pp. 265–274, 1976.

[13] H. Q. Ngo, T. Q. S. Quek, and H. Shin, "Amplify-and-forward two-way relay channels: Error exponents," in *IEEE International Symposium on Information Theory (ISIT'09), Coex, Seoul, Koera*, pp. 2028 –2032, Jul 2009.

[14] I. S. Ansari, S. Al-Ahmadi, F. Yilmaz, M.-S. Alouini, and H. Yanikomeroglu, "A new formula for the BER of binary modulations with dual-branch selection over generalized-K channels," *IEEE Transactions on Communications*, vol. 59, no. 10, pp. 2654–2658, 2011.

[15] T. Eng and L. B. Milstein, "Coherent DS-CDMA performance in Nakagami multipath fading," *IEEE Transactions on Communications*, vol. 43, pp. 1134 –1143, Feb. 1995.

[16] P. Mary, M. Dohler, J.-M. Gorce, G. Villemaud, and M. Arndt, "BPSK bit error outage over Nakagami-m fading channels in lognormal shadowing environments," *IEEE Communications Letters*, vol. 11, pp. 565 –567, July 2007.

[17] M. Horvat, Z. Bai, G. H. Bruck, and P. Jung, "Lower bounds and bit error outage of the linear sfbc combiner in an lte system with imperfect channel state information," in *3rd International Symposium on Applied Sciences in Biomedical and Communication Technologies (ISABEL'10), Rome, Italy*, pp. 1–5, Nov 2010.

[18] G. Huo and M.-S. Alouini, "Another look at the BER performance of FFH/BFSK with product combining over partial-band jammed Rayleigh-fading channels," *IEEE Transactions on Vehicular Technology*, vol. 50, no. 5, pp. 1203–1215, 2001.

[19] V. A. Aalo, T. Piboongungon, and C.-D. Iskander, "Bit-error rate of binary digital modulation schemes in Generalized Gamma fading channels," *IEEE Communications Letters*, vol. 9, no. 2, pp. 139–141, 2005.

[20] K. Yao, M. K. Simon, and E. Biglieri, "Statistical modeling of fading channel statistics based on SIRP and h-functions," in *International Conference on Communications, Circuits and Systems (ICCCAS'04)*, vol. 1, pp. 265–268 Vol.1, 2004.

[21] K. Yao, M. K. Simon, and E. Biglieri, "Unified theory on wireless communication fading statistics based on SIRP," in *IEEE 5th Workshop on Signal Processing Advances in Wireless Communications, Lisbon, Portugal*, pp. 135–139, Jul 2004.

[22] P. S. Bithas, N. C. Sagias, P. T. Mathiopoulos, G. K. Karagiannidis, and A. A. Rontogiannis, "On the performance analysis of digital communications over generalized-K fading channels," *IEEE Communications Letters*, vol. 10, pp. 353 – 355, may 2006.

[23] P. M. Shankar, "Error rates in generalized shadowed fading channels," *Wireless Personal Communications*, vol. 28, no. 3, pp. 233–238, 2004.

[24] M. D. Yacoub, "The $\kappa - \mu$ distribution and the $\eta - \mu$ distribution," *IEEE Antennas and Propagation Magazine*, vol. 49, pp. 68 –81, Feb. 2007.

[25] M. Di Renzo, F. Graziosi, and F. Santucci, "A comprehensive framework for performance analysis of dual-hop cooperative wireless systems with fixed-gain relays

over generalized fading channels," *IEEE Transactions on Wireless Communications*, vol. 8, pp. 5060 –5074, Oct. 2009.

[26] M. Di Renzo, F. Graziosi, and F. Santucci, "Channel capacity over generalized fading channels: A novel MGF-based approach for performance analysis and design of wireless communication systems," *IEEE Transactions on Vehicular Technology*, vol. 59, no. 1, pp. 127–149, 2010.

[27] F. Yilmaz and M.-S. Alouini, "A unified MGF-based capacity analysis of diversity combiners over generalized fading channels," *IEEE Transactions on Communications*, vol. 60, pp. 862 –875, Mar. 2012.

[28] G. K. Karagiannidis and A. Lioumpas, "An improved approximation for the Gaussian Q-function," *IEEE Communications Letters*, vol. 11, pp. 644 –646, Aug. 2007.

[29] J. S. Dyer and S. A. Dyer, "Corrections to, and comments on, 'An improved approximation for the Gaussian Q-function'," *IEEE Communications Letters*, vol. 12, p. 231, Apr. 2008.

[30] Q. Shi and Y. Karasawa, "An intuitive methodology for efficient evaluation of the nuttall Q-function and performance analysis of energy detection in fading channels," *IEEE Wireless Communications Letters*, vol. 1, pp. 109 –112, Apr. 2012.

[31] N. C. Beaulieu, G. Farhadi, and Y. Chen, "A precise approximation for performance evaluation of amplify-and-forward multihop relaying systems," *IEEE Transactions on Wireless Communications*, vol. 10, no. 12, pp. 3985–3989, 2011.

[32] M. Di Renzo, A. Guidotti, and G. E. Corazza, "Average rate of downlink heterogeneous cellular networks over generalized fading channels: A stochastic geometry approach," *IEEE Transactions on Communications*, vol. 61, no. 7, pp. 3050–3071, 2013.

[33] M. K. Simon and M.-S. Alouini, *Digital Communication over Fading Channels:A unified Approach to Performance Analysis*. Wiley-IEEE Press, Apr. 2000.

[34] L.-L. Yang and L. Hanzo, "'errors-and-erasures' decoding performance of rs coded ds-cdma using m-ary orthogonal signalling," in *IEEE 54th Vehicular Technology Conference (VTC2010-Fall), Atlantic City, New Jersey USA*, vol. 3, pp. 1467–1471 vol.3, 2001.

[35] T. Eng, N. Kong, and L. B. Milstein, "Comparison of diversity combining techniques for Rayleigh fading channels," *IEEE Transactions on Communications*, vol. 44, pp. 1117 –1129, Sept. 1996.

[36] M.-S. Alouini and A. J. Goldsmith, "Capacity of Rayleigh fading channels under different adaptive transmission and diversity-combining techniques," *IEEE Transactions on Vehicular Technology*, vol. 48, pp. 1165 –1181, July 1999.

[37] M.-S. Alouini and M. K. Simon, "Performance of coherent receivers with hybrid SC/MRC over Nakagami-m fading channels," *IEEE Transactions on Vehicular Technology*, vol. 48, pp. 1155 –1164, July 1999.

[38] P. M. Hahn, "Theoretical diversity improvement in multiple frequency shift keying," *IRE Transactions on Communications Systems*, vol. 10, pp. 177 –184, June 1962.

[39] G. Fedele, "N-branch diversity reception of mary DPSK signals in slow and nonselective Nakagami fading," *European Transactions on Telecommunications*, vol. 7, no. 2, pp. 119–123, 1996.

[40] N. C. Sagias and P. T. Mathiopoulos, "Switched diversity receivers over Generalized Gamma fading channels," *IEEE Communications Letters*, vol. 9, pp. 871 – 873, Oct. 2005.

[41] P. S. Bithas, P. T. Mathiopoulos, and S. A. Kotsopoulos, "Diversity reception over generalized-K fading channels," *IEEE Transactions on Wireless Communications*, vol. 6, pp. 4238 –4243, Dec. 2007.

[42] H. Nam, Y.-C. Ko, and M.-S. Alouini, "Performance analysis of joint switched diversity and adaptive modulation," *IEEE Transactions on Wireless Communications*, vol. 7, pp. 3780 –3790, Oct. 2008.

[43] N. D. Chatzidiamantis and G. K. Karagiannidis, "On the distribution of the sum of gamma-gamma variates and applications in RF and optical wireless communications," *IEEE Transactions on Communications*, vol. 59, pp. 1298 –1308, May 2011.

[44] R. Subadar and P. R. Sahu, "Performance of a L-MRC receiver over equally correlated $\eta - \mu$ fading channels," *IEEE Transactions on Wireless Communications*, vol. 10, pp. 1351 –1355, May 2011.

[45] D. Chen and J. N. Laneman, "Modulation and demodulation for cooperative diversity in wireless systems," *IEEE Transactions on Wireless Communications*, vol. 5, pp. 1785 –1794, July 2006.

[46] A. Jain, G. V. Sharma, U. B. Desai, and S. N. Merchant, "Exact analysis of the piecewise linear combiner for decode and forward cooperation with three relays," *IEEE Transactions on Wireless Communications*, vol. 10, pp. 2461 –2467, Aug. 2011.

[47] Y. Ma and C. C. Chai, "Unified error probability analysis for generalized selection combining in Nakagami fading channels," *IEEE Journal on Selected Areas in Communications*, vol. 18, pp. 2198 –2210, Nov. 2000.

[48] R. K. Mallik and M. Z. Win, "Analysis of hybrid selection/maximal-ratio combining in correlated Nakagami fading," *IEEE Transactions on Communications*, vol. 50, pp. 1372 – 1383, Aug. 2002.

[49] G. K. Karagiannidis, D. A. Zogas, and S. A. Kotsopoulos, "An efficient approach to multivariate Nakagami-m distribution using Green's matrix approximation," *IEEE Transactions on Wireless Communications*, vol. 2, pp. 883 – 889, Sept. 2003.

[50] H.-C. Yang, "New results on ordered statistics and analysis of minimum-selection Generalized Selection Combining (GSC)," *IEEE Transactions on Wireless Communications*, vol. 5, pp. 1876 –1885, July 2006.

[51] P. S. Bithas, N. C. Sagias, and P. T. Mathiopoulos, "GSC diversity receivers over Generalized Gamma fading channels," *IEEE Communications Letters*, vol. 11, pp. 964 –966, Dec. 2007.

[52] K. A. Qaraqe, Z. Bouida, and M.-S. Alouini, "Performance analysis of joint diversity combining, adaptive modulation, and power control schemes," *IEEE Transactions on Communications*, vol. 59, pp. 106 –115, Jan. 2011.

[53] G. C. Alexandropoulos, N. C. Sagias, F. I. Lazarakis, and K. Berberidis, "New results for the multivariate Nakagami-m fading model with arbitrary correlation matrix and applications," *IEEE Transactions on Wireless Communications*, vol. 8, pp. 245 –255, Jan. 2009.

[54] P. S. Bithas, N. C. Sagias, and P. T. Mathiopoulos, "The bivariate generalized-k distribution and its application to diversity receivers," *IEEE Transactions on Communications*, vol. 57, pp. 2655 –2662, Sept. 2009.

[55] F. Xu, F. C. Lau, D.-W. Yue, and S. F. Hau, "Error rate and diversity order of multinode cooperative communications in dissimilar Nakagami fading channels," *IET Communications*, vol. 3, pp. 1843 –1850, Dec. 2009.

[56] S. S. Nam, M.-S. Alouini, and H.-C. Yang, "An MGF-based unified framework to determine the joint statistics of partial sums of ordered random variables," *IEEE Transactions on Information Theory*, vol. 56, pp. 5655 –5672, Nov. 2010.

[57] S. S. Nam, M. O. Hasna, and M.-S. Alouini, "Joint statistics of partial sums of ordered exponential variates and performance of GSC RAKE receivers over Rayleigh fading channel," *IEEE Transactions on Communications*, vol. 59, pp. 2241 –2253, Aug. 2011.

[58] N. C. Beaulieu and K. T. Hemachandra, "Novel simple representations for Gaussian class multivariate distributions with generalized correlation," *IEEE Transactions on Information Theory*, vol. 57, pp. 8072 –8083, Dec. 2011.

[59] P. S. Bithas, G. P. Efthymoglou, and N. C. Sagias, "Spectral efficiency of adaptive transmission and selection diversity on generalised fading channels," *IET Communications*, vol. 4, no. 17, pp. 2058 –2064, 2010.

[60] T. L. Marzetta and B. M. Hochwald, "Capacity of a mobile multiple-antenna communication link in Rayleigh flat fading," *IEEE Transactions on Information Theory*, vol. 45, pp. 139 –157, Jan. 1999.

[61] J. F. Hayes, "Adaptive feedback communications," *IEEE Transactions on Communication Technology*, vol. 16, no. 1, pp. 29–34, 1968.

[62] W. T. Webb and R. Steele, "Variable rate qam for mobile radio," *IEEE Transactions on Communications*, vol. 43, no. 7, pp. 2223–2230, 1995.

[63] A. J. Goldsmith and S.-G. Chua, "Variable-rate variable-power mqam for fading channels," *IEEE Transactions on Communications*, vol. 45, no. 10, pp. 1218–1230, 1997.

[64] X. Qiu and K. K. Chawla, "On the performance of adaptive modulation in cellular systems," *IEEE Transactions on Communications*, vol. 47, no. 6, pp. 884–895, 1999.

[65] X. Dong, N. C. Beaulieu, and P. H. Wittke, "Signaling constellations for fading channels," *IEEE Transactions on Communications*, vol. 47, pp. 703 –714, May 1999.

[66] W. T. Webb, L. Hanzo, and R. Steele, "Bandwidth efficient qam schemes for rayleigh fading channels," *IEE Proceedings I Communications, Speech and Vision*, vol. 138, no. 3, pp. 169–175, 1991.

[67] W. Jeong, J. Lee, and D. Yoon, "New BER expression of MPSK," *IEEE Transactions on Vehicular Technology*, vol. 60, pp. 1916 –1924, May 2011.

[68] J. Lee, D. Yoon, and I. C. Im, "General expression for the error probability of arbitrary two-dimensional signaling with I/Q amplitude and phase unbalances," in *The 8th International Conference on Advanced Communication Technology (ICACT'06), Phoenix Park, Gangwon-Do, Republic of Korea.*, vol. 3, pp. 1781 –1784, Feb 2006.

[69] M.-S. Alouini and A. J. Goldsmith, "Adaptive modulation over Nakagami fading channels," *Wireless Personal Communications*, vol. 13, pp. 119 – 143, 2000.

[70] B. J. Choi and L. Hanzo, "Optimum mode-switching-assisted constant-power single- and multicarrier adaptive modulation," *IEEE Transactions on Vehicular Technology*, vol. 52, pp. 536 – 560, May 2003.

[71] Q. Liu, S. Zhou, and G. B. Giannakis, "Cross-layer combining of adaptive modulation and coding with truncated ARQ over wireless links," *IEEE Transactions on Wireless Communications*, vol. 3, pp. 1746 – 1755, Sept. 2004.

[72] Q. Liu, S. Zhou, and G. B. Giannakis, "Queuing with adaptive modulation and coding over wireless links: cross-layer analysis and design," *IEEE Transactions on Wireless Communications*, vol. 4, pp. 1142 – 1153, May 2005.

[73] T. Kwon and D.-H. Cho, "AMC-based transmission of resource allocation messages for short-sized packet services," *IEEE Communications Letters*, vol. 11, pp. 577 –579, July 2007.

[74] T. Kwon and D.-H. Cho, "Adaptive-modulation-and-coding-based transmission of control messages for resource allocation in mobile communication systems," *IEEE Transactions on Vehicular Technology*, vol. 58, pp. 2769 –2782, July 2009.

[75] J. Ramis and G. Femenias, "Cross-layer design of adaptive multirate wireless networks using truncated HARQ," *IEEE Transactions on Vehicular Technology*, vol. 60, pp. 944 –954, Mar. 2011.

[76] A. Doufexi, S. M. D. Armour, M. Butler, A. R. Nix, D. Bull, J. P. McGeehan, and P. Karlsson, "A comparison of the hiperlan/2 and ieee 802.11a wireless lan standards," *IEEE Communications Magazine*, vol. 40, no. 5, pp. 172–180, 2002.

[77] S. Aissa and G. Aniba, "BER analysis of M-QAM with packet combining over space-time block coded MIMO fading channels," *IEEE Transactions on Wireless Communications*, vol. 7, no. 3, pp. 799–805, 2008.

[78] H.-C. Yang, N. Belhaj, and M.-S. Alouini, "Performance analysis of joint adaptive modulation and diversity combining over fading channels," *IEEE Transactions on Communications*, vol. 55, pp. 520 –528, Mar. 2007.

[79] Y.-C. Ko, H.-C. Yang, S.-S. Eom, and M.-S. Alouini, "Adaptive modulation with diversity combining based on output-threshold MRC," *IEEE Transactions on Wireless Communications*, vol. 6, pp. 3728 –3737, Oct. 2007.

[80] A. Gjendemsjo, H.-C. Yang, G. E. Oien, and M.-S. Alouini, "Joint adaptive modulation and diversity combining with downlink power control," *IEEE Transactions on Vehicular Technology*, vol. 57, pp. 2145 –2152, July 2008.

[81] S. Hara and R. Prasad, "Design and performance of multicarrier cdma system in frequency-selective rayleigh fading channels," *IEEE Transactions on Vehicular Technology*, vol. 48, no. 5, pp. 1584–1595, 1999.

[82] J. Cheng and N. C. Beaulieu, "Accurate ds-cdma bit-error probability calculation in rayleigh fading," *IEEE Transactions on Wireless Communications*, vol. 1, no. 1, pp. 3–15, 2002.

[83] L.-L. Yang and L. Hanzo, "Performance of generalized multicarrier ds-cdma over nakagami-m fading channels," *IEEE Transactions on Communications*, vol. 50, no. 6, pp. 956–966, 2002.

[84] X. Liu and L. Hanzo, "A unified exact ber performance analysis of asynchronous ds-cdma systems using bpsk modulation over fading channels," *IEEE Transactions on Wireless Communications*, vol. 6, no. 10, pp. 3504–3509, 2007.

[85] B. Smida, L. Hanzo, and S. E. E. Affes, "Exact ber performance of asynchronous mc-ds-cdma over fading channels [transactions letters]," *IEEE Transactions on Wireless Communications*, vol. 9, no. 4, pp. 1249–1254, 2010.

[86] M. O. Hasna and M.-S. Alouini, "Outage probability of multihop transmission over Nakagami fading channels," *IEEE Communications Letters*, vol. 7, pp. 216 – 218, May 2003.

[87] M. O. Hasna and M.-S. Alouini, "End-to-end performance of transmission systems with relays over Rayleigh-fading channels," *IEEE Transactions on Wireless Communications*, vol. 2, pp. 1126 – 1131, Nov. 2003.

[88] M. O. Hasna and M.-S. Alouini, "Harmonic mean and end-to-end performance of transmission systems with relays," *IEEE Transactions on Communications*, vol. 52, pp. 130 – 135, Jan. 2004.

[89] M. O. Hasna and M.-S. Alouini, "A performance study of dual-hop transmissions with fixed gain relays," *IEEE Transactions on Wireless Communications*, vol. 3, pp. 1963 – 1968, Nov. 2004.

[90] M. O. Hasna and M.-S. Alouini, "Optimal power allocation for relayed transmissions over Rayleigh-fading channels," *IEEE Transactions on Wireless Communications*, vol. 3, pp. 1999 – 2004, Nov. 2004.

[91] G. K. Karagiannidis, "Performance bounds of multihop wireless communications with blind relays over generalized fading channels," *IEEE Transactions on Wireless Communications*, vol. 5, pp. 498 – 503, Mar. 2006.

[92] O. Waqar, D. C. McLernon, and M. Ghogho, "Exact evaluation of ergodic capacity for multihop variable-gain relay networks: A unified framework for generalized fading channels," *IEEE Transactions on Vehicular Technology*, vol. 59, pp. 4181 –4187, Oct. 2010.

[93] I. Trigui, S. E. E. Affes, and A. Stephenne, "A useful integral for wireless communication theory and its application in amplify-and-forward multihop relaying," in *IEEE Global Telecommunications Conference, Miami (Globecom'10), Florida, USA*, pp. 1 –5, Dec 2010.

[94] F. Yilmaz, H. Tabassum, and M.-S. Alouini, "On the computation of the higher order statistics of the channel capacity for amplify-and-forward multihop transmission," *IEEE Transactions on Vehicular Technology*, vol. 63, no. 1, pp. 489–494, 2014.

[95] I.-H. Lee and D. Kim, "Outage probability of multi-hop MIMO relaying with transmit antenna selection and ideal relay gain over Rayleigh fading channels," *IEEE Transactions on Communications*, vol. 57, pp. 357 –360, Feb. 2009.

[96] X. Zhang and Y. Gong, "Adaptive power allocation for regenerative relaying with multiple antennas at the destination," *IEEE Transactions on Wireless Communications*, vol. 8, pp. 2789 –2794, June 2009.

[97] A. I. Sulyman, G. Takahara, H. S. Hassanein, and M. Kousa, "Multi-hop capacity of MIMO-multiplexing relaying systems," *IEEE Transactions on Wireless Communications*, vol. 8, pp. 3095 –3103, June 2009.

[98] Y. Ma, D. Zhang, A. Leith, and Z. Wang, "Error performance of transmit beamforming with delayed and limited feedback," *IEEE Transactions on Wireless Communications*, vol. 8, pp. 1164 –1170, Mar. 2009.

[99] D. B. da Costa and S. Aissa, "Cooperative dual-hop relaying systems with beamforming over Nakagami-m fading channels," *IEEE Transactions on Wireless Communications*, vol. 8, pp. 3950 –3954, Aug. 2009.

[100] J.-B. Kim and D. Kim, "Performance of dual-hop amplify-and-forward beamforming and its equivalent systems in Rayleigh fading channels," *IEEE Transactions on Communications*, vol. 58, pp. 729 –732, Mar. 2010.

[101] G. Farhadi and N. C. Beaulieu, "Capacity of amplify-and-forward multi-hop relaying systems under adaptive transmission," *IEEE Transactions on Communications*, vol. 58, pp. 758 –763, Mar. 2010.

[102] K. Maichalernnukul, F. Zheng, and T. Kaiser, "Design and performance of dual-hop MIMO UWB transmissions," *IEEE Transactions on Vehicular Technology*, vol. 59, pp. 2906 –2920, July 2010.

[103] S. Xu and Y. Hua, "Optimal design of spatial source-and-relay matrices for a non-regenerative two-way MIMO relay system," *IEEE Transactions on Wireless Communications*, vol. 10, pp. 1645 –1655, May 2011.

[104] R. Vaze and R. W. J. Heath, "On the capacity and diversity-multiplexing tradeoff of the two-way relay channel," *IEEE Transactions on Information Theory*, vol. 57, pp. 4219 –4234, July 2011.

[105] N. S. Ferdinand and N. Rajatheva, "Unified performance analysis of two-hop amplify-and-forward relay systems with antenna correlation," *IEEE Transactions on Wireless Communications*, vol. 10, pp. 3002 –3011, Sept. 2011.

[106] K. P. Peppas, C. K. Datsikas, N. C. Sagias, and G. S. Tombras, "Dual-hop multi-input multi-output relay systems over spatially correlated Nakagami-m fading channels," *IET Communications*, vol. 5, no. 15, pp. 2106 –2115, 2011.

[107] I.-H. Lee and D. Kim, "End-to-End BER analysis for dual-hop OSTBC transmissions over Rayleigh fading channels," *IEEE Transactions on Communications*, vol. 56, pp. 347 –351, Mar. 2008.

[108] Q. Yang, K.-S. Kwak, and F. Fu, "Closed-form symbol error rate expression of decode-and-forward relaying using orthogonal space-time block coding," *IET Communications*, vol. 4, no. 3, pp. 368 –375, 2010.

[109] H.-C. Yang and S. Sasankan, "Analysis of channel-adaptive packet transmission over fading channels with transmit buffer management," *IEEE Transactions on Vehicular Technology*, vol. 57, pp. 404 –413, Jan. 2008.

[110] A. Muller and H.-C. Yang, "Dual-hop adaptive packet transmission systems with regenerative relaying," *IEEE Transactions on Wireless Communications*, vol. 9, pp. 234 –244, Jan. 2010.

[111] K. Zheng, Y. Wang, L. Lei, and W. Wang, "Cross-layer queuing analysis on multi-hop relaying networks with adaptive modulation and coding," *IET Communications*, vol. 4, pp. 295 –302, Dec. 2010.

[112] H. Ding, J. Ge, D. B. da Costa, and Z. Jiang, "Outage performance of fixed-gain bidirectional opportunistic relaying in Nakagami-m fading," *Electronics Letters*, vol. 46, pp. 1297 –1299, Sept. 2010.

[113] Q. You, Z. Chen, and Y. Li, "A multihop transmission scheme with detect-and-forward protocol and network coding in two-way relay fading channels," *IEEE Transactions on Vehicular Technology*, vol. 61, no. 1, pp. 433–438, 2012.

[114] N. B. Mehta, V. Sharma, and G. Bansal, "Performance analysis of a cooperative system with rateless codes and buffered relays," *IEEE Transactions on Wireless Communications*, vol. 10, pp. 1069 –1081, Apr. 2011.

[115] N. Rahnavard, B. Vellambi, and F. Fekri, "Rateless codes with unequal error protection property," *IEEE Transactions on Information Theory*, vol. 53, pp. 1521–1532, April 2007.

[116] H. A. Suraweera and G. K. Karagiannidis, "Closed-form error analysis of the non-identical Nakagami-m relay fading channel," *IEEE Communications Letters*, vol. 12, pp. 259 –261, Apr. 2008.

[117] E. Morgado, I. Mora-Jimenez, J. J. Vinagre, J. J. Ramos, and A. J. Caamano, "End-to-end average BER in multihop wireless networks over fading channels," *IEEE Transactions on Wireless Communications*, vol. 9, pp. 2478 –2487, Aug. 2010.

[118] R. Babaee and N. C. Beaulieu, "Cross-layer design for multihop wireless relaying networks," *IEEE Transactions on Wireless Communications*, vol. 9, pp. 3522 –3531, Nov. 2010.

[119] A. Bletsas, H. Shin, and M. Z. Win, "Cooperative communications with outage-optimal opportunistic relaying," *IEEE Transactions on Wireless Communications*, vol. 6, pp. 3450 –3460, Sept. 2007.

[120] B. Gui, L. Dai, and L. J. J. Cimini, "Routing strategies in multihop cooperative networks," *IEEE Transactions on Wireless Communications*, vol. 8, no. 2, pp. 843 –855, 2009.

[121] D. Wubben, "High quality end-to-end-link performance," *IEEE Vehicular Technology Magazine*, vol. 4, pp. 26 –32, Sept. 2009.

[122] G. Pan, E. Ekici, and Q. Feng, "Performance analysis of multi-branch multi-hop wireless relay systems over log-normal channels," *IEEE Transactions on Wireless Communications*, vol. 13, no. 1, pp. 1–11, 2014.

[123] S. Borade, L. Zheng, and R. G. Gallager, "Amplify-and-forward in wireless relay networks: Rate, diversity, and network size," *IEEE Transactions on Information Theory*, vol. 53, pp. 3302 –3318, Oct. 2007.

[124] Y. Li, Q. Yin, W. Xu, and H.-M. Wang, "On the design of relay selection strategies in regenerative cooperative networks with outdated CSI," *IEEE Transactions on Wireless Communications*, vol. 10, pp. 3086 –3097, Sept. 2011.

[125] P. Liu and I.-M. Kim, "Optimum/sub-optimum detectors for multi-branch dual-hop amplify-and-forward cooperative diversity networks with limited CSI," *IEEE Transactions on Wireless Communications*, vol. 9, pp. 78 –85, Jan. 2010.

[126] K.-S. Hwang, Y.-C. Ko, and M.-S. Alouini, "Performance analysis of two-way amplify and forward relaying with adaptive modulation over multiple relay network," *IEEE Transactions on Communications*, vol. 59, pp. 402 –406, Feb. 2011.

[127] J.-B. Kim, I.-H. Lee, D. Kim, and J. Lim, "Asymptotic performances of near-optimal selective distributed beamforming for two-way relaying with partial channel state information," *IEEE Communications Letters*, vol. 15, pp. 512 –514, May 2011.

[128] H. Chen, J. Liu, Z. Dong, Y. Zhou, and W. Guo, "Exact capacity analysis of partial relay selection under outdated CSI over Rayleigh fading channels," *IEEE Transactions on Vehicular Technology*, vol. 60, pp. 4014 –4018, Oct. 2011.

[129] L.-L. Xie and P. R. Kumar, "Multisource, multidestination, multirelay wireless networks," *IEEE Transactions on Information Theory*, vol. 53, pp. 3586 –3595, Oct. 2007.

[130] S. Sengupta, S. Rayanchu, and S. K. Banerjee, "Network coding-aware routing in wireless networks," *IEEE/ACM Transactions on Networking*, vol. 18, pp. 1158 –1170, Aug. 2010.

[131] O. Oyman, "Opportunistic scheduling and spectrum reuse in relay-based cellular networks," *IEEE Transactions on Wireless Communications*, vol. 9, pp. 1074 –1085, Mar. 2010.

[132] X. Zhang, W. Wang, and X. Ji, "Multiuser diversity in multiuser two-hop cooperative relay wireless networks: System model and performance analysis," *IEEE Transactions on Vehicular Technology*, vol. 58, pp. 1031 –1036, Feb. 2009.

[133] H. Ding, J. Ge, D. B. da Costa, and Z. Jiang, "A new efficient low-complexity scheme for multi-source multi-relay cooperative networks," *IEEE Transactions on Vehicular Technology*, vol. 60, pp. 716 –722, Feb. 2011.

[134] Z. Zhang, T. Lv, and X. Su, "Combining cooperative diversity and multiuser diversity: A fair scheduling scheme for multi-source multi-relay networks," *IEEE Communications Letters*, vol. 15, pp. 1353 –1355, Dec. 2011.

[135] L. Sun, T. Zhang, L. Lu, and H. Niu, "On the combination of cooperative diversity and multiuser diversity in multi-source multi-relay wireless networks," *IEEE Signal Processing Letters*, vol. 17, pp. 535 –538, June 2010.

[136] T. C.-Y. Ng and W. Yu, "Joint optimization of relay strategies and resource allocations in cooperative cellular networks," *IEEE Journal on Selected Areas in Communications*, vol. 25, pp. 328 –339, Feb. 2007.

[137] M. M. Fareed and M. Uysal, "BER-optimized power allocation for fading relay channels," *IEEE Transactions on Wireless Communications*, vol. 7, pp. 2350 –2359, June 2008.

[138] A. Abdaoui, S. S. Ikki, M. H. Ahmed, and E. Chatelet, "On the performance analysis of a MIMO-relaying scheme with space time block codes," *IEEE Transactions on Vehicular Technology*, vol. 59, pp. 3604 –3609, Sept. 2010.

[139] L. Yang and Q. Zhang, "Performance analysis of MIMO relay wireless networks with orthogonal STBC," *IEEE Transactions on Vehicular Technology*, vol. 59, pp. 3668 –3674, Sept. 2010.

[140] F. A. Onat, A. Adinoyi, Y. Fan, H. Yanikomeroglu, J. S. Thompson, and I. D. Marsland, "Threshold selection for SNR-based selective digital relaying in cooperative wireless networks," *IEEE Transactions on Wireless Communications*, vol. 7, pp. 4226 –4237, Nov. 2008.

[141] S. Lee, W. Su, S. N. Batalama, and J. D. Matyjas, "Cooperative decode-and-forward ARQ relaying: Performance analysis and power optimization," *IEEE Transactions on Wireless Communications*, vol. 9, pp. 2632 –2642, Aug. 2010.

[142] G. A. Ropokis, A. A. Rontogiannis, and K. Berberidis, "BER performance analysis of cooperative DaF relay networks and a new optimal DaF strategy," *IEEE Transactions on Wireless Communications*, vol. 10, pp. 1044 –1049, Apr. 2011.

[143] A. Bin Sediq and H. Yanikomeroglu, "Performance analysis of selection combining of signals with different modulation levels in cooperative communications," *IEEE Transactions on Vehicular Technology*, vol. 60, pp. 1880 –1887, May 2011.

[144] M. Benjillali, L. L. Szczeciski, and M.-S. Alouini, "A spectrally efficient detect-and-forward scheme with two-tier adaptive cooperation," *IEEE Transactions on Communications*, vol. 59, pp. 2367 –2372, Sept. 2011.

[145] B. Xia, Y. Fan, J. S. Thompson, and H. V. Poor, "Buffering in a three-node relay network," *IEEE Transactions on Wireless Communications*, vol. 7, pp. 4492 –4496, Nov. 2008.

[146] F. A. Onat, Y. Fan, H. Yanikomeroglu, and J. S. Thompson, "Asymptotic BER analysis of threshold digital relaying schemes in cooperative wireless systems," *IEEE Transactions on Wireless Communications*, vol. 7, pp. 4938 –4947, Dec. 2008.

[147] T. Nechiporenko, P. Kalansuriya, and C. Tellambura, "Performance of optimum switching adaptive M -QAM for amplify-and-forward relays," *IEEE Transactions on Vehicular Technology*, vol. 58, pp. 2258 –2268, June 2009.

[148] Y. Zhao, R. S. Adve, and T. J. Lim, "Improving amplify-and-forward relay networks: optimal power allocation versus selection," *IEEE Transactions on Wireless Communications*, vol. 6, pp. 3114 –3123, Aug. 2007.

[149] Y. Zhao, R. S. Adve, and T. J. Lim, "Symbol error rate of selection amplify-and-forward relay systems," *IEEE Communications Letters*, vol. 10, pp. 757 –759, Nov. 2006.

[150] N. C. Beaulieu and J. Hu, "A closed-form expression for the outage probability of decode-and-forward relaying in dissimilar Rayleigh fading channels," *IEEE Communications Letters*, vol. 10, pp. 813 –815, Dec. 2006.

[151] I.-H. Lee and D. Kim, "BER analysis for decode-and-forward relaying in dissimilar Rayleigh fading channels," *IEEE Communications Letters*, vol. 11, pp. 52 –54, Jan. 2007.

[152] A. Adinoyi and H. Yanikomeroglu, "Cooperative relaying in multi-antenna fixed relay networks," *IEEE Transactions on Wireless Communications*, vol. 6, pp. 533 –544, Feb. 2007.

[153] S. S. Ikki and M. H. Ahmed, "Performance analysis of cooperative diversity wireless networks over Nakagami-m fading channel," *IEEE Communications Letters*, vol. 11, pp. 334 –336, Apr. 2007.

[154] N. C. Sagias, F. I. Lazarakis, G. S. Tombras, and C. K. Datsikas, "Outage analysis of decode-and-forward relaying over Nakagami-m fading channels," *IEEE Signal Processing Letters*, vol. 15, pp. 41 –44, 2008.

[155] D. H. Nguyen and H. H. Nguyen, "Power allocation in wireless multiuser multi-relay networks with distributed beamforming," *IET Communications*, vol. 5, no. 14, pp. 2040 –2051, 2011.

[156] R. Pabst, B. H. Walke, D. C. Schultz, P. Herhold, H. Yanikomeroglu, S. Mukherjee, H. Viswanathan, M. Lott, W. Zirwas, M. Dohler, A. H. Aghvami, D. D. Falconer, and G. P. Fettweis, "Relay-based deployment concepts for wireless and mobile broadband radio," *IEEE Communications Magazine*, vol. 42, pp. 80 – 89, Sept. 2004.

[157] W. Ge, J. Zhang, and X. Shen, "A cross-layer design approach to multicast in wireless networks," *IEEE Transactions on Wireless Communications*, vol. 6, no. 3, pp. 1063–1071, 2007.

[158] P. Gupta and P. R. Kumar, "The capacity of wireless networks," *IEEE Transactions on Information Theory*, vol. 46, pp. 388 –404, Mar. 2000.

[159] M. Grossglauser and D. N. Tse, "Mobility increases the capacity of Ad Hoc wireless networks," *IEEE/ACM Transactions on Networking*, vol. 10, pp. 477 – 486, Aug. 2002.

[160] P. Gupta and P. R. Kumar, "Towards an information theory of large networks: an achievable rate region," *IEEE Transactions on Information Theory*, vol. 49, pp. 1877 – 1894, Aug. 2003.

[161] A. Sendonaris, E. Erkip, and B. Aazhang, "User cooperation diversity. Part I. system description," *IEEE Transactions on Communications*, vol. 51, pp. 1927 – 1938, Nov. 2003.

[162] A. Sendonaris, E. Erkip, and B. Aazhang, "User cooperation diversity. Part II. implementation aspects and performance analysis," *IEEE Transactions on Communications*, vol. 51, pp. 1939 – 1948, Nov. 2003.

[163] J. N. Laneman, D. N. Tse, and G. W. Wornell, "Cooperative diversity in wireless networks: Efficient protocols and outage behavior," *IEEE Transactions on Information Theory*, vol. 50, no. 12, pp. 3062 – 3080, 2004.

[164] A. S. Ibrahim, A. K. Sadek, W. Su, and K. Liu, "Cooperative communications with relay-selection: when to cooperate and whom to cooperate with?," *IEEE Transactions on Wireless Communications*, vol. 7, pp. 2814 –2827, July 2008.

[165] G. Farhadi and N. C. Beaulieu, "Fixed relaying versus selective relaying in multi-hop diversity transmission systems," *IEEE Transactions on Communications*, vol. 58, pp. 956 – 965, Mar. 2010.

[166] J. Boyer, D. D. Falconer, and H. Yanikomeroglu, "Multihop diversity in wireless relaying channels," *IEEE Transactions on Communications*, vol. 52, pp. 1820 – 1830, Oct. 2004.

[167] I. Maric, A. J. Goldsmith, and M. Medard, "Multihop analog network coding via amplify-and-forward: The high SNR regime," *IEEE Transactions on Information Theory*, vol. 58, pp. 793 –803, Feb. 2012.

[168] C. Dong, L.-L. Yang, and L. Hanzo, "Performance analysis of multi-hop diversity aided multi-hop links," *IEEE Transactions on Vehicular Technology*, vol. 61, no. 6, pp. 2504 –2516, 2012.

[169] C. Dong, L.-L. Yang, and L. Hanzo, "Multi-hop diversity aided multi-hop communications: A cumulative distribution function aware approach," *IEEE Transactions on Communications*, vol. 61, no. 11, pp. 4486–4499, 2013.

[170] C. Dong, L.-L. Yang, and L. Hanzo, "Adaptive modulation for multihop communications exploiting multihop diversity," *Submitted to IEEE Transactions on Wireless Communications*.

[171] C. Dong, L.-L. Yang, J. Zuo, S. X. Ng, and L. Hanzo, "Minimum average end-to-end packet energy dissipation of a buffer-aided three-node network relying on opportunistic routing," *Submitted to IEEE Transactions on Communications*.

[172] S. Biswas and R. Morris, "ExOR: Opportunistic multi-hop routing for wireless networks," in *ACM Special Interest Group on Data Communication (SIGCOMM), Philadelphia, PA*, pp. 133–144, Aug. 2005.

[173] M. Mardani, J. S. Harsini, F. Lahouti, and B. Eliasi, "Joint adaptive modulation-coding and cooperative ARQ for wireless relay networks," in *IEEE International Symposium on Wireless Communication Systems (ISWCS'08), Reykjavik, Iceland*, pp. 319 –323, Oct 2008.

[174] V. Asghari, A. Maaref, and S. Aissa, "Symbol error probability analysis for multihop relaying over Nakagami fading channels," in *IEEE Wireless Communications and Networking Conference (WCNC'10), Sydney, Australia*, pp. 1 –6, Apr 2010.

[175] J. Cao, L.-L. Yang, and Z. Zhong, "Performance of multihop wireless links over generalized-K fading channels," in *IEEE 72nd Vehicular Technology Conference Fall (VTC2010-Fall), Ottawa, Canada*, pp. 1 –5, Sept 2010.

[176] G. K. Karagiannidis, T. A. Tsiftsis, and R. K. Mallik, "Bounds for multihop relayed communications in Nakagami-m fading," *IEEE Transactions on Communications*, vol. 54, pp. 18 – 22, Jan. 2006.

[177] Z. Lin, E. Erkip, and M. Ghosh, "Rate adaptation for cooperative systems," in *IEEE Global Telecommunications Conference (GLOBECOM'06), San Francisco, CA, USA*, pp. 1 –5, Dec 2006.

[178] L. Yang, M. O. Hasna, and M.-S. Alouini, "Average outage duration of multihop communication systems with regenerative relays," *IEEE Transactions on Wireless Communications*, vol. 4, pp. 1366 – 1371, July 2005.

[179] J. Proakis, *Digital Communications, 4th ed.* McGraw-Hill, Apr. 2001.

[180] G. Golub and C. Loan, *Matrix Computations, 3rd ed.* The Johns Hopkins University Press, Apr. 1996.

[181] D. Bertsekas and R. G. Gallager, *Data Networks, 2nd ed.* Prentice-Hall, Apr. 1992.

[182] R. Horn and C. Johnson, *Matrix Analysis.* Cambridge University Press New York, NY, USA, Apr. 1986.

[183] C. Dong, L.-L. Yang, and L. Hanzo, "Multihop diversity for fading mitigation in multihop wireless networks," in *IEEE Vehicular Technology Conference (VTC'11-Fall), San Francisco, CA, USA*, pp. 1–5, Sept. 2011.

[184] L.-L. Yang, C. Dong, and L. Hanzo, "Multihop diversity-a precious source of fading mitigation in multihop wireless networks," in *IEEE Global Telecommunications Conference (Globecom'11), Houston, TX, USA*, pp. 1–5, Dec. 2011.

[185] M. Nakagami, "The m-distribution, a general formula of intensity of rapid fading," *Statistical Methods in Radio Wave Propagation: Proceedings of a Symposium*, vol. 47, pp. 3–36, June 1958.

[186] L. Hanzo, S. X. Ng, W. T. Webb, and T. Keller, *Quadrature Amplitude Modulation: From Basics to Adaptive Trellis-Coded, Turbo-Equalised and Space-Time Coded OFDM, CDMA and MC-CDMA Systems*. IEEE Press-John Wiley, September 2004.

[187] L.-L. Yang and L. Hanzo, "A recursive algorithm for the error probability evaluation of M-QAM," *IEEE Communications Letters*, vol. 4, pp. 304 –306, Oct. 2000.

[188] *http://functions.wolfram.com/*.

[189] G. Aniba and S. Aissa, "Cross-layer designed adaptive modulation algorithm with packet combining and truncated ARQ over MIMO Nakagami fading channels," *IEEE Transactions on Wireless Communications*, vol. 10, no. 4, pp. 1026–1031, 2011.

[190] T. Rapaport, *Wireless Communications: Principles and Practice*. Prentice Hall, Dec 2001.

[191] M. K. Simon and M.-S. Alouini, *Digital Communication over Fading Channels*. April 2005.

[192] C. Dong, L.-L. Yang, and L. Hanzo, "Multi-hop diversity aided multi-hop communications: A cumulative distribution function aware approach," *IEEE Transactions on Communications*, vol. 61, no. 11, pp. 4486–4499, 2013.

[193] A. Host-Madsen and J. Zhang, "Capacity bounds and power allocation for wireless relay channels," *IEEE Transactions on Information Theory*, vol. 51, no. 6, pp. 2020–2040, 2005.

[194] G. Farhadi and N. C. Beaulieu, "On the performance of amplify-and-forward cooperative systems with fixed gain relays," *IEEE Transactions on Wireless Communications*, vol. 7, no. 5, pp. 1851–1856, 2008.

[195] J. M. Torrance and L. Hanzo, "Upper bound performance of adaptive modulation in a slow Rayleigh fading channel," *Electronics Letters*, vol. 32, no. 8, pp. 718–719, 1996.

[196] A. Ikhlef, D. S. Michalopoulos, and R. Schober, "Max-max relay selection for relays with buffers," *IEEE Transactions on Wireless Communications*, vol. 11, pp. 1124 –1135, March 2012.

[197] A. Ikhlef, J. Kim, and R. Schober, "Mimicking full-duplex relaying using half-duplex relays with buffers," *IEEE Transactions on Vehicular Technology*, vol. 61, pp. 3025 –3037, Sept. 2012.

[198] N. Zlatanov and R. Schober, "Buffer-aided relaying with adaptive link selection-fixed and mixed rate transmission," *IEEE Transactions on Information Theory*, vol. 59, no. 5, pp. 2816–2840, 2013.

[199] H. Liu, B. Zhang, H. Mouftah, X. Shen, and J. Ma, "Opportunistic routing for wireless Ad Hoc and sensor networks: Present and future directions," *IEEE Communications Magazine*, vol. 47, no. 12, pp. 103–109, 2009.

[200] K. Zeng, Z. Yang, and W. Lou, "Location-aided opportunistic forwarding in multi-rate and multihop wireless networks," *IEEE Transactions on Vehicular Technology*, vol. 58, pp. 3032–3040, July 2009.

[201] J. Zuo, C. Dong, H. V. Nguyen, S. X. Ng, L.-l. Yang, and L. Hanzo, "Cross-layer aided energy-efficient opportunistic routing in ad hoc networks," *IEEE Transactions on Communications*, vol. 62, pp. 522–535, February 2014.

[202] J. Zuo, *Cross-Layer Aided Routing Design for Ad Hoc Networks*. PhD thesis, University of Southampton, June 2013.

Author Index

Index